Density (matrix) functional theory approach to quantum embedding for strongly correlated electrons

Sajanthan Sekaran

UNIVERSITÉ DE STRASBOURG

EDSC
École Doctorale des Sciences Chimiques

UNIVERSITÉ DE STRASBOURG

Institut de Chimie UMR 7177

THÈSE

présentée par :

Sajanthan SEKARAN

soutenue le : **16 septembre 2022**

pour obtenir le grade de : **Docteur de l'université de Strasbourg**

Discipline/ Spécialité : Chimie

Density (matrix) functional theory approach to quantum embedding for strongly correlated electrons.

SUPERVISEUR:

Pr. FROMAGER Emmanuel	Université de Strasbourg, France

RAPPORTEURS:

Dr. George BOOTH	King's College London, United Kingdom
Dr. Andre SEVERO PEREIRA GOMES	Université de Lille, France

EXAMINATEURS :

Pr. Neepa MAITRA	Rutgers University, United States of America
Dr. Eduard MATITO	Donostia Insitute Physics Center, Spain
Pr. Vincent ROBERT	Université de Strasbourg, France

Abstract

The present thesis aims at developing and implementing novel and *in-principle-exact* embedding methodologies at the interface between chemistry and physics. Towards an accurate description of strongly correlated molecules and materials, the quantum embedding will be applied to the *Hubbard model*, and then generalized to *Ab initio* molecular Hamiltonian. We will verify if *density matrix embedding theory* (DMET) can be made formally exact and systematically improvable while preserving a single-particle quantum partitioning picture. More precisely, we will rewrite the embedding as a functional of the density matrix, thus bypassing the Schmidt decomposition of the reference (correlated or not) full-system wave function. Then, we will clarify the connections between DMET and the *in-principle-exact* theories that are *density functional theory* (DFT) and *reduced density matrix functional theory* (RDMFT). On that basis, alternative flavors of DMET will be explored.

Résumé

L'objectif de cette thèse est le développement et l'implémentation de nouvelles méthodes dites d'embedding à l'intersection entre la chimie et la physique. Afin de pourvoir une description précise des molécules et matériaux fortement corrélés, l'embedding quantique sera appliqué au modèle d'Hubbard et généralisé à des Hamiltonien moléculaires *Ab initio*. Nous vérifierons si la *density matrix embedding theory* (DMET) peut être rendu formellement exacte et améliorée tout en préservant la nature orbitalaire de notre partitionnement quantique. Plus précisément, nous réécrirons notre approche d'embedding comme étant une fonctionnelle de la matrice densité à un corps, contournant ainsi la décomposition de Schmidt de la fonction d'onde de référence (corrélée ou non) décrivant le système dans son intégralité. Enfin, nous clarifierons les parallèles entre la DMET et les théories *en principe exactes* que sont la *density functional theory* (DFT) et la *reduced density matrix functional theory* (RDMFT). Sur cette base, plusieurs alternatives de la DMET seront explorées.

"Everything has its wonders, even darkness and silence, and I learn, whatever state I may be in, therein to be content."

Helen Keller

Acknowledgements

C'est avec une certaine appréhension que j'aborde cette page de remerciements tant de simples mots ne sauraient refléter ma gratitude envers toutes les personnes que j'ai eu l'honneur de rencontrer et qui, par leur être, ont pu modeler ma personne et m'ont poussé à faire émerger le meilleur de moi-même. Sachez que ni l'ordre, ni la quantité, ni la qualité de ces prochaines lignes n'ont pour volonté de définir une quelconque classification dans l'expression de ma reconnaissance.

Dans un premier temps, je tiens à remercier l'ensemble des membres du Laboratoire de Chimie Quantique (LCQ) de Strasbourg pour la liberté, l'enthousiasme et la soif de découverte qu'ils m'ont transmis. Bien que ces quelques qualificatifs ne sont qu'une goutte dans l'océan des sentiments partagés durant ces quelques années au sein du LCQ, je tiens à remercier l'ensemble des personnes ayant participé à promouvoir et à faire perpétuer ces nobles valeurs. Je tiens particulièrement à remercier Vincent, qui à mon humble avis, est le plus beau représentant de ces dernières. C'est avec joie et nostalgie que je repense à toutes nos discussions et c'est avec impatience que j'attends les prochaines à rêver d'un monde meilleur, un monde où les yum-yum sont au patrimoine mondial de l'Unesco.
Bien qu'ayant eu l'honneur d'avoir été considéré comme l'architecte de ce projet, rien de cet (humble) édifice n'aurait vu jour sans un maître d'oeuvre exceptionnel, Manu. Alors, merci d'avoir partagé avec moi les joies et les tristesses de cette thèse. Ta rigueur scientifique et ta patience m'ont permis de redéfinir ce qu'était la passion, j'espère qu'un jour, j'aurai également la chance de l'embrasser.
J'aimerais également remercier Matthieu pour son accompagnement et sa joie de vivre communicative. Enfin, que serait cette thèse sans cette joyeuse bande d'étudiants arpentant les couloirs du LCQ, alors un grand merci à Filip, Lucie, Oussama, Pablo et Saad, sans lesquels cette aventure aurait été moins magique tant sur le plan personnel que professionnel. Je retiendrai que même en science, "Happiness is only real when shared". Je tiens également à remercier les permanents du laboratoire: Chantal, Roberto, Etienne, Sylvie et Christophe pour leur contribution à l'épanouissement de l'équipe et des étudiants.

Ensuite, j'ai une pensée pour mes camarades m'ayant accompagné durant toutes ces années. Je garderai énormément de souvenirs de mon parcours d'étudiant, entre éclats de rire, bières, pleurs, whisky, danses frénétiques, une cafétéria qui devrait être interdite par l'organisation mondiale de la santé, des parties de Mario kart endiablées, des discussions nocturnes à refaire le monde,... Mais tout cela n'aurait pas été réalisable sans cette jolie bande de lurons, alors merci à vous de m'avoir fait tant vibrer et surtout aimer.

Pour conclure, j'aimerais remercier et honorer ma famille, ils sont et resteront ma plus grande source d'inspiration. J'ai la chance de m'épanouir à vos côtés et j'espère que je reflète votre bonté et votre amour du mieux possible.

p.s. : une pensée à toutes ces personnes travaillant dans l'ombre (ou non) sans lesquelles tout cela ne serait qu'un mirage.

Table of Contents

Résumé en français

Introduction **1**

1 Elements of theory **7**

1.1 Context 7

1.2 The orbital approximation 10

1.3 Second quantization 11

2 Standard methods in electronic structure theory **15**

2.1 Hartree-Fock theory 15

2.2 Post Hartree-Fock methods 18

2.3 Density Functional Theory 19

2.4 Reduced Density Matrix Functional Theory 25

3 Model Hamiltonians **29**

3.1 Hubbard model 29

3.2 Single Impurity Anderson Model 31

4 Review of quantum embedding approaches **35**

4.1 Real space partitioning 35

4.2 Orbital space partitioning 39

4.2.1 Dynamical Mean-Field Theory 40

4.2.2 Density Matrix Embedding Theory 42

5 Density matrix functional construction of a one-electron quantum bath **53**

5.1 Householder transformation 53
5.1.1 Geometrical interpretation 53
5.1.2 Householder transformation and density matrix embedding . . 55
5.1.3 Householder transformed density matrix 57
5.2 Block-Householder transformation 62
5.2.1 Construction of the Block-Householder transformation matrix 62
5.2.2 Properties of the Block-Householder representation and associated density matrix 66
5.3 Bath orbitals 71

6 Householder transformed density matrix functional embedding theory 77
6.1 Exact embedding in the non-interacting case 78
6.2 Approximate embedding in the interacting case 81
6.3 Summary of the embedding scheme 84
6.4 Results 85
6.4.1 Homogeneous 1D Hubbard model 85
6.4.2 Hydrogen ring 89

7 Local potential functional embedding theory 97
7.1 Non-interacting embedding Hamiltonian 98
7.2 Approximate interacting embedding 100
7.3 KS-DFT for uniform lattices 101
7.4 Density-functional interacting cluster 103
7.5 Local potential functional embedding theory 107
7.6 Comparison with SDE 110
7.7 LPFET algorithm 111
7.8 Results and discussion 113

8 Density matrix interpolation variational ansatz 119
8.1 Construction of the two-level interaction functional 119
8.2 Density matrix interpolation variational ansatz 122
8.3 Results 124

Conclusions **127**

Bibliography **131**

Papers

I. Sekaran, S.; Tsuchiizu, M.; Saubanère, M.; Fromager, E. Householder-transformed density matrix functional embedding theory. *Physical Review B* **2021**, *104, 035121*

II. Sekaran, S.; Saubanère, M.; Fromager, E. Local Potential Functional Embedding Theory: A Self-Consistent Flavor of Density Functional Theory for Lattices without Density Functionals. *Computation* **2022**, *10, 45*.

III. Yalouz, S.; Sekaran, S.; Saubanère, M. Quantum embedding of multi-orbital fragments using the block-Householder transformation. *The Journal of Chemical Physics* **2022**, *157, 214112*.

IV. Yalouz, S.; Gullin, M. F.; S. Sekaran. QuantNBody: a Python package for quantum chemistry and physics to build and manipulate many-body operators and wave functions. *submitted to the Journal of Open Source Software*.

V. Sekaran, S.; Bindech, O.; Fromager, E. Equivalence of Singular Value Decomposition and Block Householder Transformation in Density Matrix Embedding Theory, *in preparation*.

Acronyms

Acronyms	Meaning
1-RDM/2-RDM	one-/two- electron Reduced Density Matrix
BA	Bethe Ansatz
CASCI	Complete Active Space Configuration Interaction
CASPT2	Complete Active Space Perturbation Theory
CASSCF	Complete Active Space Self-Consistent Field
CI	Configuration Interaction
DET	Density Embedding Theory
DFT	Density Functional Theory
DMET	Density Matrix Embedding Theory
DMFT	Dynamical Mean-Field Theory
DIVA	Density matrix Interpolation Variational Ansatz
FCI	Full Configuration Interaction
HF	Hartree-Fock
HM	Hubbard Model
Ht DMFET	Householder transformed Density Matrix Functional Embedding Theory
KS DFT	Kohn-Sham Density Functional Theory
LPFET	Local Potential Functional Embedding Theory
MCSCF	Multi-Configurational Self-Consistent Field
NEVPT2	n-Electron Valence State Perturbation Theory
RDMFT	Reduced Density Matrix Functional Theory
SIAM	Single Impurity Anderson Model
SVD	Singular Value Decomposition
WFT	Wave Function Theory

Résumé en français

INTRODUCTION : En chimie quantique et en physique de la matière condensée, les systèmes dits fortement corrélés attirent l'attention tant en recherche fondamentale qu'en recherche appliquée. Bien qu'aucune définition mathématique exacte n'existe afin de décrire ce qu'est la corrélation forte, elle peut être vue comme une insuffisance du caractère mono-déterminantal de la fonction d'onde d'Hartree-Fock afin de reproduire la physique d'un système chimique possédant des orbitales moléculaires hautement occupées (quasi-) dégénérées. En chimie et en sciences de la matière, ces composés rassemblent une large gamme de molécules et de matériaux ayant des orbitales atomiques d and f partiellement remplies. Parmi ces derniers, les métaux de transition sont fréquemment utilisés pour la catalyse homogène[1,2,3] et inhomogène[4,5,6], mais jouent également un rôle prépondérant dans de nombreux processus biologiques[7,8,9]. En physique de la matière condensée, des interactions complexes entre les degrés de liberté de la charge, du spin, de l'orbitale et de la structure cristalline résultent de nombreuses propriétés physico-chimiques extraordinaires. Parmi elles, notons la supraconductivité à haute température découverte dans les nickelates[10,11] et les oxydes de cuivre[12,13,14], des effets de magnétorésistance colossale[15,16,17] ont été observés dans les oxydes de manganèse ou encore des transitions métal-isolant ont été répertoriées dans les oxydes de vanadium[18,19,20]. Ainsi, ces matériaux présentent un fort potentiel d'application dans le développement de nouvelles technologies. L'objectif de cette thèse est de développer de nouvelles méthodes afin de pouvoir traiter ces systèmes tant d'un point de vue de chimie quantique que celui de la physique de la matière condensée. Dans ce court résumé en français, nous présenterons les éléments de base permettant l'élaboration de ces méthodes et nous mettrons l'accent sur l'une d'entre elle : la *Householder transformed density matrix functional embedding*

theory (Ht-DMFET)[21]. Bien que ce résumé ne couvre pas l'ensemble du manuscrit de thèse, il permet d'avoir une première immersion dans le fascinant monde de l'embedding quantique.

En chimie quantique, le principal objectif est de décrire avec précision les propriétés et l'évolution dans le temps des systèmes atomiques et moléculaires. Dans sa formulation la plus simple et celle que nous adopterons, le système étudié est considéré dans le vide, à température nulle et sans influence d'un potentiel externe dépendant du temps (c.-à-d. champs électriques, magnétiques,...). Ainsi, l'accès aux propriétés d'un système s'obtient par la résolution de l'équation de Schrödinger (non relativistique) indépendante du temps (SE),

$$\hat{H} \left|\Psi_I\right\rangle = E_I \left|\Psi_I\right\rangle, \tag{1}$$

où E_I sont les différentes valeurs propres associées aux vecteurs propres $|\Psi_I\rangle$. Nous nous concentrerons dans cette thèse à l'état fondamental $|\Psi_0\rangle$. L'opérateur $\hat{H}$ représente l'Hamiltonian moléculaire et prend la forme suivante dans la base des coordonnées et en utilisant les unités atomiques,

$$\begin{aligned}\hat{H} &= \hat{T}_e + \hat{T}_N + \hat{V}_{NN} + \hat{V}_{Ne} + \hat{V}_{ee} \\ &= -\frac{1}{2}\sum_{i}^{N} \nabla_i^2 - \frac{1}{2}\sum_{A}^{M} \frac{\nabla_A^2}{M_A} + \frac{1}{2}\sum_{A}^{M}\sum_{B\neq A}^{M} \frac{Z_A Z_B}{r_{AB}} - \sum_{i}^{N}\sum_{A}^{M} \frac{Z_A}{r_{iA}} + \frac{1}{2}\sum_{i}^{N}\sum_{j\neq i}^{N} \frac{1}{r_{ij}}.\end{aligned} \tag{2}$$

Les deux premiers termes à droite sont les énergies cinétiques des électrons et des noyaux (dénotés respectivement par des lettres minuscules et majuscules). Les termes restants sont les interactions de Coulomb où Z_I correspond à la charge du noyau I et le dénominateur est la distance séparant les particules interagissantes. Les différentes sommations prennent en compte le nombre d'éléctrons N et de noyaux M.

Afin de résoudre l'équation de Schrödinger présentée à l'Éq. 1, plusieurs approches sont envisageables. Historiquement, les méthodes fonctions d'ondes dans lesquelles l'idée serait d'aller au-delà d'une description champ moyen en développant la fonction d'onde Hartree-Fock dans la base des configurations est avantageuse car elle permet d'avoir une description précise des systèmes fortement corrélés. Toutefois, ces méthodes nécessitent une forte capacité numérique et ne peuvent pas

être appliquées à de grandes molécules ou des systèmes périodiques. Afin de pallier ce problème, la théorie de la fonctionnelle de la densité (DFT)[22,23] se concentre sur une quantité réduite : la densité. Ainsi, elle contourne élégamment les problèmes rencontrés par les méthodes fonctions d'ondes. Toutefois, malgré les nombreuses approximations existantes pour déterminer une fonctionnelle de la densité, aucune n'est capable d'être systématiquement appliquée à des systèmes fortement corrélés. Une alternative aux difficultés rencontrées par ces deux approches est de développer des théories d'embedding. Ces dernières ont émergé ces dernières décennies comme une stratégie prometteuse afin de décrire avec précision la corrélation forte tant dans les molécules que dans les systèmes périodiques. Bien que toutes les approches d'embedding aient pour but de réduire la complexité et par la suite le temps de calcul, celle que nous utiliserons s'inscrit dans la catégorie des méthodes qui "divise pour mieux régner". La philosophie étant de remplacer un système dont la résolution complète serait numériquement coûteuse par une série de systèmes effectifs de petites tailles dont le coût de calcul de l'ensemble serait moindre. Appliquées à la chimie quantique, ces méthodes sont habituellement utilisées afin d'évaluer la structure électronique de systèmes complexes. Plus précisément, l'incapacité de résoudre l'équation de Schrödinger présentée à l'Éq. 1 est remplacée par une série d'équations de Schrödinger définie pour des fragments moléculaires ou "clusters" plus simples à décrire. Bien que la nomenclature varie selon les méthodes d'embedding, nous définirons le cluster comme étant un "fragment" moléculaire du système initial (composé d'une ou plusieurs orbitales localisées dénommées impuretées) et par un "bain" quantique dont le rôle est de reproduire de manière optimale l'environnement du fragment afin de décrire avec précision les interactions entre le fragment et le reste de la molécule.

La construction mathématique du bain dépend du choix de la variable prédominante dans l'embedding. Bien évidemment, ce choix n'est pas unique et cela se traduit par la diversité des méthodes d'embedding dans la littérature. Dans la *dynamical mean-field theory* (DMFT)[24,25], la variable principale est la fonction de Green locale qui est évaluée sur l'impureté (c.-à.-d. l'orbitale que l'on veut embedder dans le système original). Dans cette approche, les sites non interagissant

et éventuellement infinis du modèle d'Anderson représente le bain. Plus récemment, la *density matrix embedding theory* (DMET)[26,27] a attiré l'attention des chercheurs de par ses multiples avantages vis-à-vis de la DMFT. Cette approche, qui a été présentée comme une version indépendante de la DMFT, tire son épingle du jeu grâce à une réduction drastique de la dimension du bain, mais également par son abilité à pouvoir être appliqué à la fois aux molécules et aux systèmes périodiques. En DMET, le nombre d'orbitales du bain est, au maximum, égal au nombre d'orbitales contenues dans le fragment (ç.-à.-d. le nombre d'impuretés).

La présente thèse s'inscrit dans la lignée de ces prometteuses théories d'embedding. L'objectif étant de clarifier les connexions entre la DMET et les théories *en principe* exactes que sont la *density functional theory* (DFT) et la *reduced density matrix functional theory* (RDMFT)[28,29,28,30,31,32,33]. Plus précisément, nous étudierons si la DMET peut être rendu formellement exacte et si elle peut être améliorée systématiquement tout en préservant la nature orbitalaire et non pas *many-body* de notre partitionnement quantique. Ainsi, nous réécrirons notre partitionnement quantique comme une fonctionnelle de la matrice densité, évitant d'appliquer une décomposition de Schmidt sur la fonction d'onde de référence du système complet (corrélée ou non). Notons que nous utiliserons la transformation unitaire de (block) Householder afin de construire notre bain quantique. Dans ce résumé de thèse en français, nous analyserons seulement une des théories développées au cours de thèse : la *Householder transformed density matrix functional embedding theory*. Bien qu'ayant été appliquée à une chaîne d'hydrogène, nous nous concentrerons uniquement sur les résultats obtenus lors de son application au modèle d'Hubbard.

LE MODÉLE D'HUBBARD : En 1963, J. Hubbard introduisit le modèle de Hubbard (HM)[34] afin d'étudier la corrélation électronique des matériaux. De nos jours, il s'agit d'un modèle bien connu de la communauté de la physique de la matière condensée et fait état de référence afin de traiter les problèmes de corrélation forte. Les diverses applications connues du modèle d'Hubbard sont le fruit d'un équilibre entre la complexité du problème traitée et sa simple reformulation. En

effet, dans le cas le plus simple, le modèle de Fermi-Hubbard à une dimension (1D), les électrons sont représentés dans un espace discrétisé où chaque site équivaut à une orbitale extrêmement localisée. L'énergie cinétique est remplacée par un paramètre isotropique d'intensité t. De plus, dans l'approximation $tight-binding$, ce paramètre n'est défini qu'entre sites voisins,

$$\hat{T} \longrightarrow -t \sum_{\sigma=\uparrow,\downarrow} \sum_{i=0}^{L-1} \left(\hat{c}_{i\sigma}^{\dagger} \hat{c}_{(i+1)\sigma} + \text{H.c.} \right). \tag{3}$$

où L correspond au nombre de sites. L'opérateur de répulsion électronique est simplifié par un opérateur d'interaction local (sur site) et d'intensité U,

$$\hat{W}_{ee} \longrightarrow U \sum_{i=0}^{L-1} \hat{n}_{i\sigma} \hat{n}_{i\sigma'}, \tag{4}$$

où $\hat{n}_{i\sigma} = \hat{c}_{i\sigma}^{\dagger} \hat{c}_{i\sigma}$. Cette simplification tire son origine des orbitales de valence des métaux de transition et des terres rares. En effet, étant donné leur distribution radiale restreinte, il est présumé que pour ces éléments, les interactions électroniques intra-atomiques sont plus importantes que les inter-atomiques. Enfin, l'Hamiltonien d'Hubbard homogène à une dimension prend la forme suivante,

$$\hat{H}_{Hubbard} = -t \sum_{\sigma=\uparrow,\downarrow} \sum_{i=0}^{L-1} \left(\hat{c}_{i\sigma}^{\dagger} \hat{c}_{(i+1)\sigma} + \text{H.c.} \right) + U \sum_{i=0}^{L-1} \hat{n}_{i\sigma} \hat{n}_{i\sigma'}, \tag{5}$$

où $\hat{n}_i = \hat{n}_{i\sigma} + \hat{n}_{i\sigma'}$ est l'opérateur d'occupation sur le site i avec $\hat{n}_{i\sigma} = \hat{c}_{i\sigma}^{\dagger} \hat{c}_{i\sigma}$. Dans le modèle d'Hubbard, deux contributions énergétiques sont en compétition : l'énergie cinétique des électrons et leur répulsion électronique. Le modèle tente d'apprivoiser l'équilibre subtil entre les états délocalisés et localisés des composés. Ainsi, l'état fondamental du modèle d'Hubbard est gouverné par deux paramètres : l'intensité de corrélation U/t mais également la densité électronique $n = N/L$ où N est le nombre d'électrons.

En 1968, E. H. Lieb and F. Y. Wu ont trouvé les résultats analytiques de l'état fondamental du modèle de Hubbard à une dimension[35]. Parmi ces solutions, il a été prouvé que l'état fondamental dans le cas du demi-remplissage (c.-à.-d. N=L) est un isolant pour tout $U \neq 0$. Ce résultat important démontre que la nature isolante du modèle de Hubbard à demi-remplissage est entièrement due aux interactions entre electrons. Cette transition de phase (métal $\rightarrow$ isolant) est dénommée la

transition de Mott-Hubbard. Ainsi, malgré son apparente simplicité, le modèle de Hubbard est capable de capter un large spectre de phénomène physique et permet ainsi d'être utilisé comme une référence afin de tester de nouvelles théories et méthodes avant d'être appliquées à des systèmes plus complexes.

TRANSFORMATION DE (BLOCK) HOUSEHOLDER : Ayant le modèle d'Hubbard en main, nous pouvons nous concentrer sur le partitionnement quantique souhaité. Toutefois, il reste un dernier ingrédient à introduire, la transformation de Householder. En 1958, A. S. Householder développa la transformation unitaire de Householder (HH-t)[36]. D'un point de vue géométrique, il s'agit d'une réflexion, mais elle est principalement utilisée afin de tridiagonaliser une matrice ou d'y opérer une factorisation QR. Le point de vue géométrique est intéressant, car il permet d'avoir une première vision de cette transformation et introduit progressivement les différents éléments nécessaires à l'embedding. Pour un vecteur $\boldsymbol{X}$ de dimension $L \times 1$, on peut définir une réflexion à travers un plan ou un hyperplan $\mathbb{P}$ contenant l'origine de l'espace vectoriel. L'on dénotera le vecteur réfléchi $\boldsymbol{Y}$. La condition nécessaire et suffisante afin de construire cette transformation est d'avoir un vecteur unitaire $\boldsymbol{v}/(\boldsymbol{v}^\dagger\boldsymbol{v})$ orthogonal à $\mathbb{P}$. En observant la Fig. 1, on peut construire $\boldsymbol{Y}$,

$$\begin{aligned}\boldsymbol{Y} &= \boldsymbol{X} - 2\frac{(\boldsymbol{v}^\dagger\boldsymbol{X})\boldsymbol{v}}{\boldsymbol{v}^\dagger\boldsymbol{v}} \\ &= \boldsymbol{X} - 2\frac{\boldsymbol{v}(\boldsymbol{v}^\dagger\boldsymbol{X})}{\boldsymbol{v}^\dagger\boldsymbol{v}} \\ &= \left(\mathbf{1}_L - 2\frac{\boldsymbol{v}\boldsymbol{v}^\dagger}{\boldsymbol{v}^\dagger\boldsymbol{v}}\right)\boldsymbol{X} \\ &= \boldsymbol{R}(\boldsymbol{v})\boldsymbol{X}.\end{aligned} \tag{6}$$

où $\mathbf{1}_{\boldsymbol{L}}$ est la matrice identité. Ainsi, nous obtenons l'expression de la matrice de réflexion $\boldsymbol{R}(\boldsymbol{v})$ (c.-à.-d. matrice de Householder) à l'aide du vecteur unitaire $\boldsymbol{v}/(\boldsymbol{v}^\dagger\boldsymbol{v})$,

$$\boldsymbol{R}(\boldsymbol{v}) = \mathbf{1}_L - 2\frac{\boldsymbol{v}\boldsymbol{v}^\dagger}{\boldsymbol{v}^\dagger\boldsymbol{v}}. \tag{7}$$

Cette matrice est Hermitienne et unitaire,

$$\boldsymbol{R}^{-1}(\boldsymbol{v}) = \boldsymbol{R}(\boldsymbol{v}) = \boldsymbol{R}^\dagger(\boldsymbol{v}). \tag{8}$$

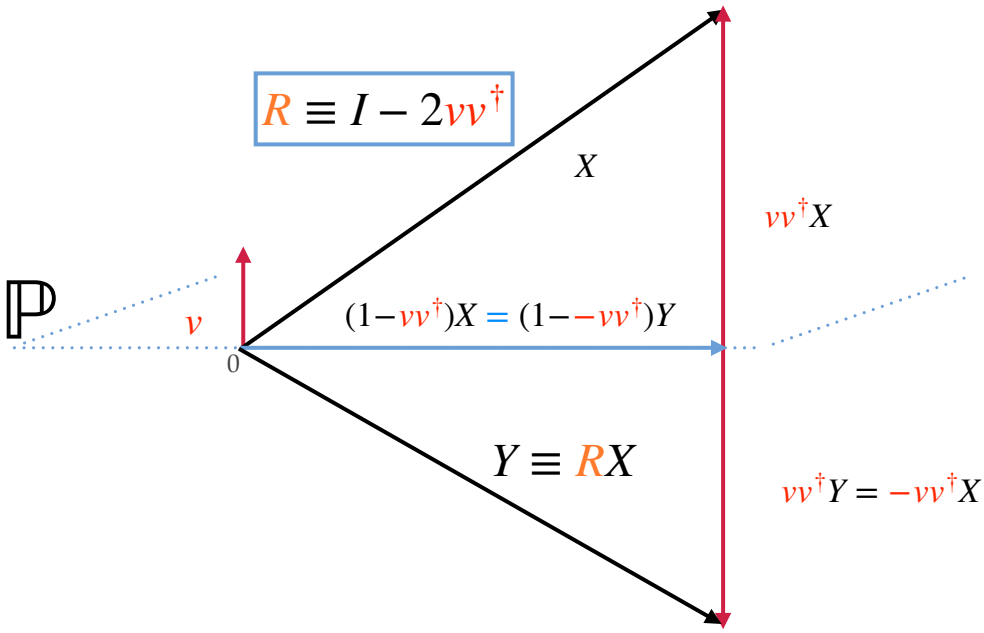

Figure 1: Interprétation géométrique de la transformation de Householder.

Afin de réaliser notre partitionnement, nous nous sommes inspirés de l'idée principale de la DMET qui est d'embedder une ou plusieurs orbitales qui seront seulement intriquées avec un nombre fini d'orbitales de bain. Etant donné le caractère local de la corrélation forte, il est avantageux de réécrire la matrice densité définie telle que,

$$\gamma_{ij} = \langle \Psi | \hat{c}_i^\dagger \hat{c}_j | \Psi \rangle \tag{9}$$

dans une base d'orbitale localisée, $\gamma_{ij}^{loc} \equiv \gamma_{ij} = \langle \Psi | \hat{c}_i^\dagger \hat{c}_j | \Psi \rangle$. Définissons l'orbitale 0 comme celle devant être embeddé (impureté), alors nous pouvons collecter tous les éléments de la matrice densité connectés à l'orbitale 0 dans le vecteur $\boldsymbol{X}$ mentionné ci-dessus,

$$\boldsymbol{X}^\dagger = [\gamma_{00}, \gamma_{10}, \ldots, \gamma_{i0}, \ldots] , \tag{10}$$

et dans la formulation la plus simple, nous pouvons changer de base afin d'imposer à l'impureté d'être seulement intriqué avec une seule orbitale : le bain,

$$\boldsymbol{X}^\dagger \xrightarrow{\boldsymbol{R}} \boldsymbol{Y}^\dagger = \boldsymbol{R}\boldsymbol{X}^\dagger = [\gamma_{00}, \xi, 0, 0, \ldots, 0, \ldots] , \tag{11}$$

Comme mentionné précédemment, à l'aide des vecteurs $\boldsymbol{X}$ et $\boldsymbol{Y}$, nous pouvons construire le vecteur $\boldsymbol{v}$ et ainsi la transformation $\boldsymbol{R}$ qui générera la réduction

d'intrication de l'impureté. Les détails menant aux formules finales sont détaillés dans le Chapitre 5,

$$R_{ij} = \delta_{ij} - 2v_i v_j, \tag{12}$$

où,

$$\begin{aligned} v_0 &= 0, \\ v_1 &= \frac{\gamma_{10} - \xi}{\sqrt{2\xi\left(\xi - \gamma_{10}\right)}}, \\ v_j &\overset{j\geq 2}{=} \frac{\gamma_{j0}}{\sqrt{2\xi\left(\xi - \gamma_{10}\right)}}, \end{aligned} \tag{13}$$

avec,

$$\xi = -\mathrm{sgn}\left(\gamma_{10}\right)\sqrt{\sum_{j>0}\gamma_{j0}^2}. \tag{14}$$

Ainsi, comme dépeint dans la Fig. 2, la matrice densité peut être réécrite dans la

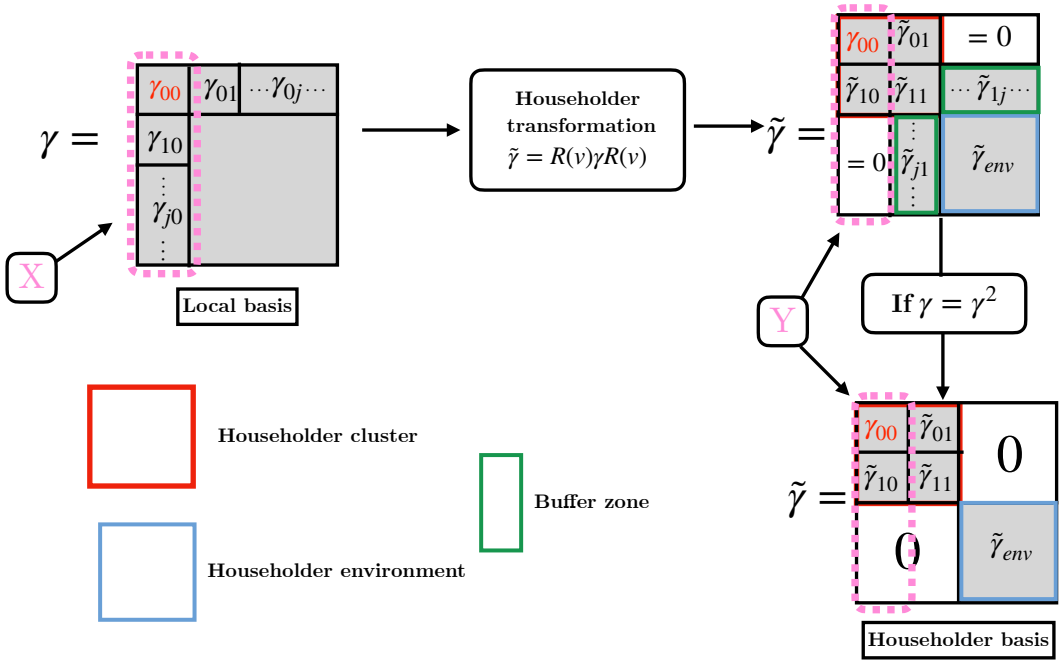

Figure 2: Schéma de la transformation de Householder appliqué à la matrice densité.

base de Householder,

$$\tilde{\boldsymbol{\gamma}} = \boldsymbol{R}^{\dagger}(\boldsymbol{v})\boldsymbol{\gamma}\boldsymbol{R}(\boldsymbol{v}) = \boldsymbol{R}(\boldsymbol{v})\boldsymbol{\gamma}\boldsymbol{R}(\boldsymbol{v}), \tag{15}$$

ou de manière équivalente,

$$\tilde{\gamma}_{ij} = \left\langle \hat{d}_{i\sigma}^{\dagger}\hat{d}_{j\sigma} \right\rangle, \tag{16}$$

où, selon les Eqs. (12), (13) and (14), les opérateurs de création (annihilation) sont des fonctionnelles de la matrice densité γ_{ij},

$$\begin{aligned} \hat{d}^\dagger_{i\sigma} &:= \sum_j R_{ij}\, \hat{c}^\dagger_{j\sigma} \\ &= \hat{c}^\dagger_{i\sigma} - 2v_i \sum_{j>0} v_j\, \hat{c}^\dagger_{j\sigma}. \end{aligned} \tag{17}$$

De nombreuses propriétés intéressantes découlent du changement de base. Premièrement, on observe que la transformation ne modifie pas l'opérateur de l'impureté inchangé,

$$\hat{d}^\dagger_{\mathrm{imp}} \equiv \hat{d}^\dagger_{0\sigma} = \hat{c}^\dagger_{0\sigma}, \tag{18}$$

Cette propriété est essentielle pour de futures applications. En effet, dans une optique d'embedding, si nous souhaitons séparer certaines orbitales d'intérêts tels que les orbitales d ou f d'un système chimique, il est dans notre intérêt de garder leur structure intacte. Le second point concerne l'orbitale de bain, de taille réduite, et dont le but est de représenter l'environnement du fragment de manière optimale. En dérivant les équations, nous nous retrouvons avec une orbitale de bain ayant la structure suivante,

$$\hat{d}^\dagger_{\mathrm{bath}} \equiv \hat{d}^\dagger_{1\sigma} = \left(1 - 2v_1^2\right) \hat{c}^\dagger_{1\sigma} - 2v_1 \sum_{j>1} v_j\, \hat{c}^\dagger_{j\sigma}. \tag{19}$$

où l'on constate que notre nouvelle orbitale "effective" du bain est explicitement construite à partir de l'environnement de l'impureté. De plus, en observant la structure de la matrice densité à la Fig. 2, on observe que l'orbitale de l'impureté est seulement intriquée avec celle du bain. Dans le cas général d'une description corrélée du système complet, l'orbitale du bain dans la représentation de Householder sera intriqué avec les orbitales restantes du reste du système comme observé par la buffer zone $\tilde{\gamma_{ji}}$. Toutefois, cette dernière est égale à zéro si la description initiale du système complet est réalisée à partir d'un calcul champ moyen. Ainsi, dans la nouvelle représentation, les orbitales de l'impureté et du bain sont seulement intriquées entre elles et pas avec le reste du système. De plus, le cluster (impureté + bain) contient exactement deux électrons.

Pour résumer cette partie, notons que nous avons introduit la transformation unitaire de Householder et l'avons connecté formellement au formalisme de la matrice

densité. Dans la nouvelle représentation, l'orbitale de l'impureté reste identique tandis que l'orbitale de bain est construite comme une combinaison linéaire des orbitales restantes. Nous avons également établi une connexion formelle avec l'orbitale de bain construire dans la DMET [Voir 5.3]. Parmi les différentes propriétés émergentes de notre transformation, celles obtenues lors d'une description champ moyen du système complet semblent être prometteuses afin d'appliquer des méthodes de structure électronique et de collecter plus de corrélation. En effet, il a été mentionné que si la transformation de Householder est appliquée à une matrice densité construire à partir d'un calcul champ moyen (matrice idempotente), les orbitales contenues dans le cluster sont strictement déconnectées du reste du système et contiennent un nombre entier d'électrons. Soulignons que toutes les méthodes d'embedding développées dans cette thèse auront pour point de départ ce calcul champ moyen et donc ces propriétés bien spécifiques. À ce niveau, un seul désavantage est à noter, bien que nous puissions fragmenter le système efficacement, le nombre d'orbitales à embedded est limité. Afin de contourner ce problème, nous utiliserons la transformation de block Householder.

Introduite en 1999 par F. Rotella et I. Zambettakis, la transformation de block Householder[37] généralise celle de Householder et l'étend aux formes block matricielles. Nous l'utiliserons afin d'augmenter le nombre d'orbitales d'impuretés à embedder. Cependant, par soucis de concision, nous ne détaillerons pas les dérivations mathématiques et prendrons comme acquis certaines propriétés découlant de cette transformation. Toutefois, ces informations peuvent être retrouvées au chapitre 5.2. Dans sa formulation la plus générale, la matrice de block Householder prend la forme suivante,

$$\boldsymbol{R}(\boldsymbol{V}) = \mathbf{1}_L - 2\boldsymbol{V}(\boldsymbol{V}^\dagger\boldsymbol{V})^{-1}\boldsymbol{V}^\dagger, \tag{20}$$

où $\mathbf{1}_L$ est la matrice identité et $\boldsymbol{V}$ est un non pas un vecteur, mais une matrice de dimension $L \times L_{frag}$ où L est le nombre total d'orbitales localisées du système et L_{frag} est le nombre d'orbitale composant le fragment (ç.-à.-d. le nombre d'impuretés). Il est intéressant de souligner que des similarités avec la fragmentation d'une seule impureté sont redécouvertes. En effet, les orbitales d'impuretés resteront inchangées dans la nouvelle représentation tandis que celles du bain seront une combinaison linéaire des orbitales restantes. De plus, dans le

cas d'une matrice densité idempotente, les orbitales du cluster seront totalement déconnectées du reste du système et ce même cluster contiendra deux fois le nombre de spin-orbitales d'impuretés. À nouveau, ces propriétés présentant des avantages techniques et conceptuelles seront à l'origine de la procédure d'embedding employée.

HOUSEHOLDER TRANSFORMED DENSITY MATRIX FUNCTIONAL EMBEDDING THEORY :[21] Dans cette stratégie d'embedding, l'objectif est d'avoir accès aux propriétés locales d'un système par l'évaluation de ses matrices densité réduite, mais non pas par la fonction d'onde décrivant l'intégralité du système, mais une fonction d'onde tronquée, celle du cluster,

$$\begin{aligned} \langle\Psi_0|\hat{c}^\dagger_{i\sigma}\hat{c}_{j\sigma}|\Psi_0\rangle &\approx \left\langle\Psi_0^{\mathcal{C}}\middle|\hat{c}^\dagger_{i\sigma}\hat{c}_{j\sigma}\middle|\Psi_0^{\mathcal{C}}\right\rangle, \\ \langle\Psi_0|\hat{c}^\dagger_{i\sigma}\hat{c}^\dagger_{j\sigma'}\hat{c}_{l\sigma'}\hat{c}_{k\sigma}|\Psi_0\rangle &\approx \left\langle\Psi_0^{\mathcal{C}}\middle|\hat{c}^\dagger_{i\sigma}\hat{c}^\dagger_{j\sigma'}\hat{c}_{l\sigma'}\hat{c}_{k\sigma}\middle|\Psi_0^{\mathcal{C}}\right\rangle, \end{aligned} \tag{21}$$

où $\Psi_0^{\mathcal{C}}$ est la fonction d'onde de l'état fondamental du cluster de Householder obtenu par notre procédure d'embedding.

Nous allons ci-dessous présenter les étapes déterminantes de notre approche, une description détaillée peut être retrouvée au chapitre 6.

Dans le cas non interagissant (U=0) qui est équivalent à l'approximation champ moyen dans le cas du modèle d'Hubbard uniforme, l'énergie par site de l'état fondamental est,

$$e^{\mathrm{NI}}(n) = -4t\gamma_{10}, \tag{22}$$

où l'on fixe le nombre d'électrons N dans la lattice et donc le remplissage uniforme $n = N/L = 2\gamma_{ii}$. En pratique, il suffit de diagonaliser la matrice de hopping $\boldsymbol{h} \equiv \{h_{ij}\}$ et de construire la matrice densité dans la base de la lattice à partir des spin-orbitales occupées $|\kappa_\sigma\rangle = \sum_i C_{i\kappa}|\phi_{i\sigma}\rangle$ comme suit,

$$\gamma_{ij} = \sum_{\kappa}^{\mathrm{occ.}} C_{i\kappa}C_{j\kappa}. \tag{23}$$

En appliquant la transformation de (block) Householder à cette matrice densité idempotente, nous obtenons la structure block diagonale illustrée à la Fig. 2. Étant donné que dans cette nouvelle représentation, la matrice densité est strictement

découplée en un block du cluster et celle de l'environnement, l'énergie du système complet non interagissant peut être séparée similairement,

$$E^{\mathrm{NI}} = E^{\mathrm{NI}}_{\mathcal{C}} + E^{\mathrm{NI}}_{\mathcal{E}}. \tag{24}$$

Similairement, la fonction d'onde du système complet peut être factorisée en une fonction d'onde du cluster et celle de son environnement,

$$|\Phi\rangle^{NI} = |\Phi\rangle^{NI}_{\mathcal{C}} \, |\Phi\rangle^{NI}_{\mathcal{E}} \, . \tag{25}$$

L'idée étant d'améliorer la description de la fonction d'onde du cluster afin d'en retirer le maximum de corrélation possible,

$$|\Phi\rangle^{NI}_{\mathcal{C}} \Longrightarrow |\Psi\rangle_{\mathcal{C}} \, , \tag{26}$$

Pour cela et tirant avantage de la taille réduite du cluster, nous pouvons appliquer des méthodes telles que les interactions de configuration. Notons que dans la méthode Ht-DMFET appliquée au modèle d'Hubbard, nous ne tiendrons pas en compte de la fonction d'onde décrivant l'environnement du cluster afin d'évaluer les propriétés locales des sites d'impuretés.
Afin d'évaluer l'énergie par site [Voir Éq. (22)],

$$\langle\Phi|\hat{t}_{01}|\Phi\rangle = -4t\gamma_{10}. \tag{27}$$

nous pouvons passer dans la représentation de Householder,

$$\begin{aligned}
\langle\Phi|\hat{t}_{01}|\Phi\rangle &= -4t \sum_{i} R_{1i}\tilde{\gamma}_{i0} \\
&= -4t \sum_{0\leq i\leq 1} R_{1i}\tilde{\gamma}_{i0} \\
&= -4t \sum_{0\leq i\leq 1} R_{1i} \left\langle \Phi^{\mathcal{C}} \middle| \hat{d}^{\dagger}_{i\sigma}\hat{d}_{0\sigma} \middle| \Phi^{\mathcal{C}} \right\rangle \\
&= -4t \sum_{i} R_{1i} \left\langle \Phi^{\mathcal{C}} \middle| \hat{d}^{\dagger}_{i\sigma}\hat{c}_{0\sigma} \middle| \Phi^{\mathcal{C}} \right\rangle ,
\end{aligned} \tag{28}$$

où l'on utilise l'Éq. (18) et le fait que $\hat{d}_{i\sigma}\left|\Phi^{\mathcal{C}}\right\rangle \overset{i\geq 1}{=} 0$, puisque $\Phi^{\mathcal{C}}$ est construit à partir du cluster. Finalement, on retrouve à partir de l'Éq. (28) l'égalité suivante,

$$\begin{aligned}
\langle\Phi|\hat{t}_{01}|\Phi\rangle &= -4t \left\langle \Phi^{\mathcal{C}} \middle| \hat{c}^{\dagger}_{1\sigma}\hat{c}_{0\sigma} \middle| \Phi^{\mathcal{C}} \right\rangle \\
&= \left\langle \Phi^{\mathcal{C}} \middle| \hat{t}_{01} \middle| \Phi^{\mathcal{C}} \right\rangle ,
\end{aligned} \tag{29}$$

qui simplifie drastiquement et de manière exacte l'évaluation des énergies par site pour les lattices.

Ainsi, selon l'Éq. (29), l'énergie non interagissante peut être directement évaluée à partir du cluster, ce qui est une simplification plus qu'importante du problème initial. Bien que cette description soit exacte, elle ne décrit que le cas non interagissant. Nous pouvons toutefois introduire la corrélation électronique dans le cluster. Désormais, la procédure est approximée et est l'analogue à la DMET[26] pour une lattice complète décrite à partir d'un calcul champ moyen. Par simplicité, nous conserverons le vecteur de Householder $\boldsymbol{v}$ obtenu à partir de la matrice densité non interagissante de l'Éq (23). Nous devons dans un premier temps réécrire l'opérateur local de répulsion électron dans la représentation de Householder,

$$U \sum_{i=0}^{L-1} \hat{n}_{i\sigma} \hat{n}_{i\sigma'} = \sum_{jklm} \tilde{U}_{jklm} \hat{d}^{\dagger}_{j\sigma} \hat{d}_{k\sigma} \hat{d}^{\dagger}_{l\sigma'} \hat{d}_{m\sigma'}, \tag{30}$$

où

$$\tilde{U}_{jklm} = U \sum_{i=0}^{L-1} R_{ij} R_{ik} R_{il} R_{im}. \tag{31}$$

Après projection dans le cluster, nous obtenons l'expression suivante pour l'Hamiltonien interagissant du cluster,:

$$\hat{\mathcal{H}}^{\mathcal{C}} = \hat{h}^{\mathcal{C}} + \sum_{j,k,l,m=0}^{2N_f} \tilde{U}_{jklm} \hat{d}^{\dagger}_{j\sigma} \hat{d}_{k\sigma} \hat{d}^{\dagger}_{l\sigma'} \hat{d}_{m\sigma'} \tag{32}$$

où,

$$\hat{h}^{\mathcal{C}} = \sum_{\sigma} \sum_{i,j=0}^{2N_f-1} \tilde{h}_{ij} \hat{d}^{\dagger}_{i\sigma} \hat{d}_{j\sigma}. \tag{33}$$

Dans la terminologie de la DMET[38,39], l'utilisation de l'Hamiltonien complet d'embedding Éq. (32) est nommée : embedding avec *bain interagissant* (IB). Dans ce cas, les interactions $\tilde{U}_{jklm}$ sur la totalité du cluster sont prises en compte. Il est à ce niveau important de souligner que dans ce travail, et tout comme en DMET, les orbitales de bain (qui sont décrites avec les opérateurs $\hat{d}^{\dagger}_{i\sigma}$ et $\hat{d}_{i\sigma}$ $(2N_f > i > N_f)$ sont déterminées à partir de la matrice densité non interagissante du système complet. Ainsi, l'acronyme IB ne doit pas être confondu avec le niveau

d'approximation utilisé pour le calcul des orbitales de bain. Dans l'approximation : *bain non interagissant* (NIB)[38,39], seules les interactions sur les sites d'impuretés sont conservées.

Retournons à l'Hamiltonien d'embedding obtenu à l'Éq. (32). On observe à la Fig. 3 que l'occupation de l'impureté dévie systématiquement du remplissage de la lattice n lorsque nous résolvons le problème interagissant du cluster. C'est pourquoi nous ajoutons, en complète analogie avec la DMET[39], un potentiel chimique $\tilde{\mu}_i^{\text{frag}}$ sur chaque site d'impureté (c.-à-d. une correction ad hoc) tel que la fonction d'onde du cluster,

$$\Psi^{\mathcal{C}} = \arg\min_{\Psi} \langle \Psi | \hat{\mathcal{H}}^{\mathcal{C}} - \tilde{\mu}_i^{\text{frag}} \sum_{\sigma} \sum_{i}^{N_f - 1} \hat{d}_{i\sigma}^{\dagger} \hat{d}_{i\sigma} | \Psi \rangle \,, \tag{34}$$

reproduit l'occupation n désirée, c.-à-d.

$$\left\langle \Psi^{\mathcal{C}} \middle| \sum_{\sigma} \hat{d}_{i\sigma}^{\dagger} \hat{d}_{i\sigma} \middle| \Psi^{\mathcal{C}} \right\rangle \stackrel{!}{=} n. \tag{35}$$

où l'indice i réfère à l'orbitale d'impureté nous intéressant. Une fois que la contrainte de l'Éq. (35) est respectée, une expression approximée pour l'énergie par site est obtenue,

$$e(n) \approx -4t \left\langle \hat{c}_{1\sigma}^{\dagger} \hat{c}_{0\sigma} \right\rangle_{\Psi^{\mathcal{C}}} + U \left\langle \hat{n}_{0\sigma} \hat{n}_{0\sigma'} \right\rangle_{\Psi^{\mathcal{C}}} , \tag{36}$$

Dans la terminologie de la DMET,[39], les Éqs. (34)–(36) décrivent un embedding *single-shot* ayant des conditions de mapping similaires à la *density embedding theory* (DET)[38,40].

RESULTATS SUR LE MODÈLE HOMOGÈNE D'HUBBARD À 1D : Pour un anneau homogène d'Hubbard ($L = 400$), le paramètre de hopping a été fixé à $t = 1$, des conditions périodiques/anti-périodiques ont été utilisées lorsque $\frac{N}{2}$ est impair/pair. Ces dernières sont utilisées afin d'enlever les dégénérescences pathologiques pouvant apparaître lors du calcul non interagissant du système à N-électrons. Des comparaisons sont effectuées avec les résultats Bethe Ansatz (BA) qui sont exacts dans la limite thermodynamique[35]. De plus, des calculs contenant un

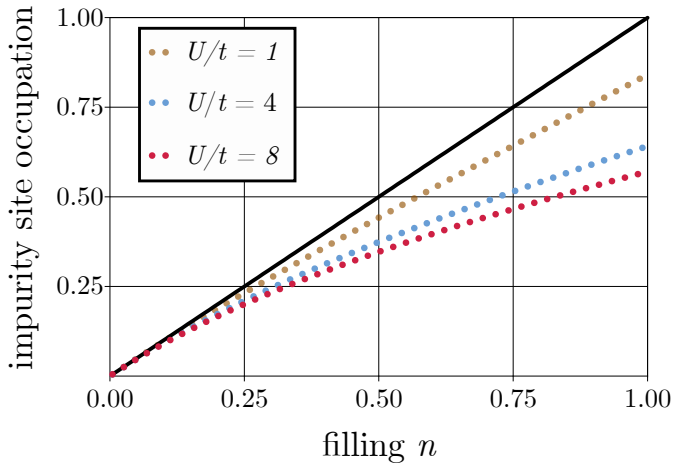

Figure 3: Courbe de l'occupation de l'orbitale d'impureté du cluster de Householder en fonction du remplissage n de la lattice pour plusieurs régimes de corrélation. Ces résultats sont obtenus dans le cas du bain non interagissant et avec $\tilde{\mu}^{\text{frag}} = 0$ [Voir Éq. (34)]. La ligne droite de référence en noir fait référence à la situation désirée (et qui est obtenu dans notre procédure en ajustant $\tilde{\mu}^{\text{frag}}$) lorsque l'occupation de l'impureté embeddé correspond au remplissage de la lattice.

embedding à multiple impureté ont été réalisé et le problème du cluster interagissant dans ce cas a été résoud numériquement à l'aide d'une méthode *full configuration interaction* développée dans le laboratoire.

Tout d'abord, nous discutons de l'importance d'avoir un potentiel chimique $\tilde{\mu}^{\text{frag}}$ permettant de restaurer l'occupation désirée du site d'impureté. Cette importance est illustrée par le calcul de l'énergie par site présenté à la Fig. 4 pour un cas simple, celui d'une unique impureté à demi-remplissage (n=1). Dès lors que la bonne valeur $\tilde{\mu}^{\text{frag}}$ a été utilisé (ce qui sera le cas dans le reste des discussions), elle assure que l'occupation de l'impureté correspond à celle du remplissage de la lattice, l'erreur devient substantiel dans le cas fortement corrélé seulement si l'interaction dans le bain est négligée. Nous remarquons que dans ce cas, nous reproduisons les résultats obtenus par la DMET dans la Ref.[26], comme attendu dans l'analyse fournie en Sec. 5.3. La correspondance des résultats avec ceux du BA sont quasiment parfaits dans tous les régimes de corrélation lorsque l'interaction est restaurée dans le bain. Ce succès peut être lié au fait que dans notre schéma

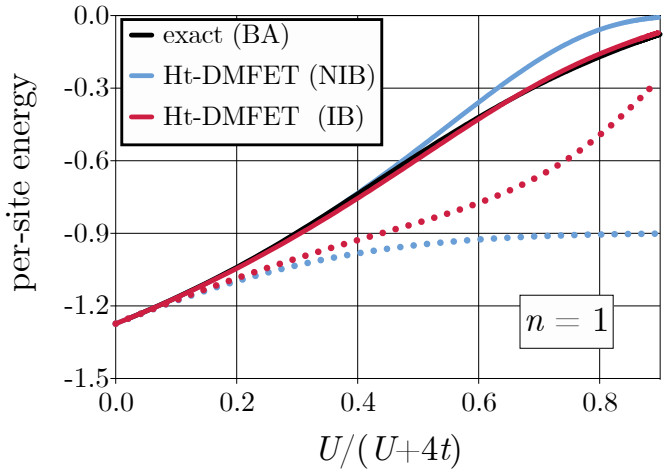

Figure 4: Courbe de l'énergie par site d'un calcul Ht-DMFET avec une seule impureté en fonction de l'intensité de la répulsion électronique à demi-remplissage ($n = 1$). Les résultats obtenus pour $\tilde{\mu}^{\text{frag}} = 0$ sont en lignes pointillées, ceux obtenus après ajustement du potential chimiques sont en lignes pleines. Les résultats avec l'interaction dans le bain ont été affichés à des fins de comparaisons. Enfin, les résultats exacts Bethe Ansatz (BA) sont affichés à des fins d'analyse.

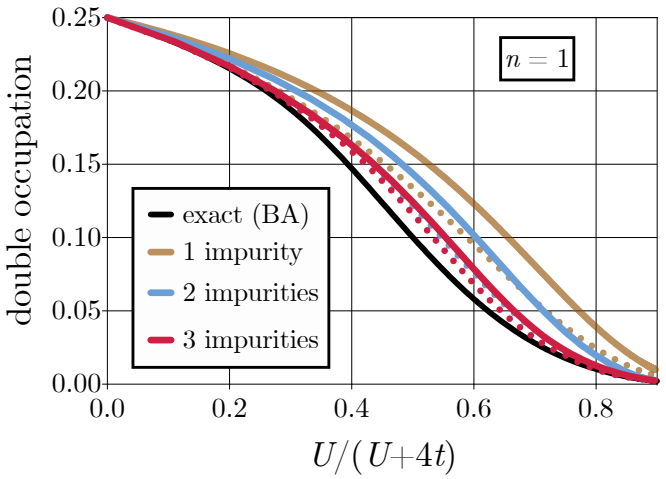

Figure 5: Courbe de la double occupation $\langle \hat{n}_{0\sigma}\hat{n}_{0\sigma'}\rangle_{\Psi^{\mathcal{C}}}$ d'une orbitale d'impureté lors d'un calcul Ht-DMFET en fonction de l'intensité de la répulsion électronique à demi-remplissage ($n = 1$). Les résultats avec l'interaction dans le bain ont été affichés à des fins de comparaisons. Enfin, les résultats exacts Bethe Ansatz (BA) sont affichés à des fins d'analyse.

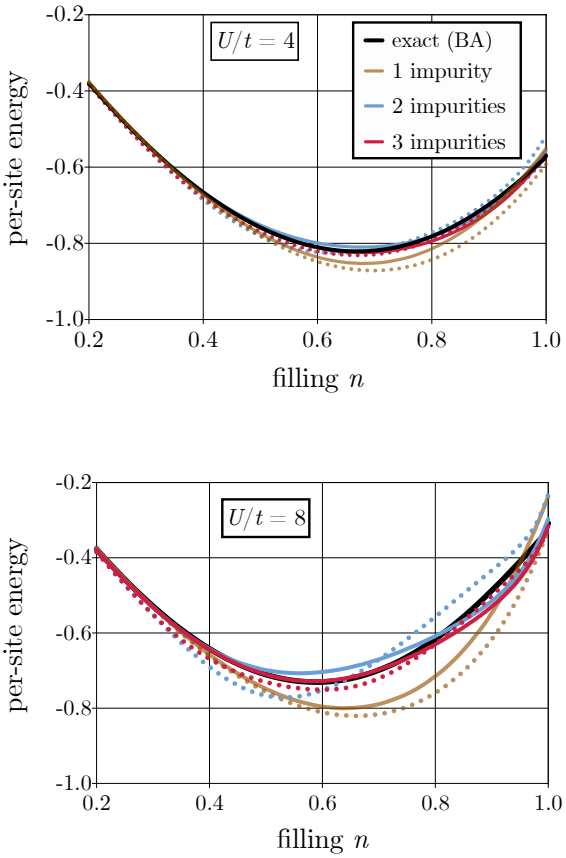

Figure 6: Courbe de l'énergie par site d'un calcul Ht-DMFET avec une en fonction du remplissage de la lattice n pour plusieurs régimes de corrélation $U/t = 4$ et $U/t = 8$. Les résultats obtenus pour une simple et multiple impureté sont en lignes pleines. Les lignes discontinues correspondent à l'approximation du bain non interagissant (NIB). Enfin, les résultats exacts Bethe Ansatz (BA) sont affichés à des fins d'analyse.

Ht-DMFET approximée, le cluster (corrélé) de Householder contient exactement deux électrons à demi-remplissage (conséquence de la symétrie trou-particule). Toutefois, bien que les interactions dans le bain améliorent la double occupation, les erreurs demeurent conséquentes dans le régime fortement corrélé, comme démontré dans la Fig. 5. Ainsi, le succès de Ht-DMFET dans le cas du demi-remplissage est également dû à des compensations d'erreurs dans le calcul de l'énergie par site.

En-dehors du demi-remplissage, la performance de Ht-DMFET se détériore lorsque U/t croît, comme démontré à la Fig. 6. Ceci est probablement lié au fait

que le nombre d'électrons dans notre cluster n'est pas autorisé à fluctuer. En effet, comme discuté dans la Sec. 5.1.3, en dehors du demi-remplissage, le cluster devient un système ouvert dès que U/t dévie de zéro. De manière intéressante, les résultats avec un bain non interagissant sont meilleurs dans ces régimes. De plus, comme attendu[26,38] et démontré dans le cadre du bas de la Fig. 6.4, les résultats obtenus sont de meilleures qualités lorsqu'on augmente la taille du fragment et donc du nombre d'impuretés à embedder,

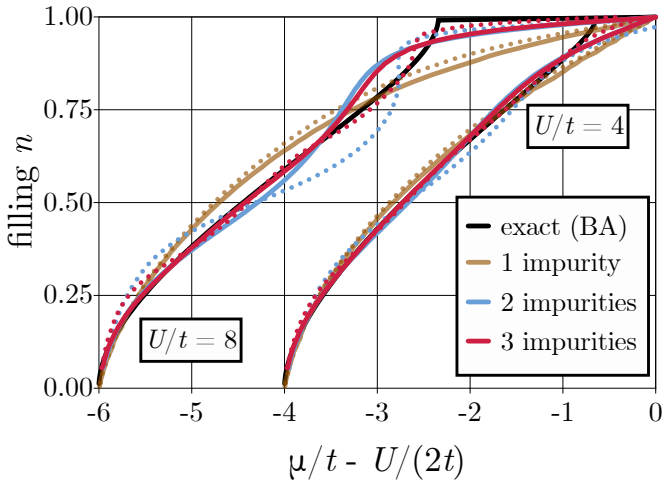

Figure 7: Courbe du remplissage de la lattice en fonction du potentiel chimique μ obtenu *via* la relation $\mu \equiv \mu(n) = \partial e(n)/\partial n$ pour différents régimes de corrélation. Les résultats en lignes continues correspondent aux résultats obtenus avec les bains non interagissants (NIB) tandis que les lignes discontinues représentent les résultats avec les bains interagissants (IB) Enfin, les résultats exacts Bethe Ansatz (BA) sont affichés à des fins d'analyse.

Finalement, on étudie à la Fig. 7, la transition de Mott-Hubbard *via* l'évaluation du potentiel chimique $\mu(n) = \partial e(n)/\partial n$ (fonctionnelle de la densité) à partir de l'expression de l'énergie par site introduite à l'Éq. (36). Comme attendu par la Réf.[26], embedder une seule impureté ne permet de décrire la transition de Mott-Hubbard tant dans l'approximation du bain interagissant que dans celle du non interagissant. Toutefois, embedder plusieurs impuretés améliorent substantiellement les résultats. On remarque notamment que si l'on rajoute l'interaction dans le

bain, les résultats obtenus pour trois impuretés sont presque totalement similaires aux résultats exacts. Ceci peut être expliqué par l'environnement de l'impureté qui tend vers une représentation plus exacte du système original.

Ainsi, nous observons que l'approche Ht-DMFET améliorent la description des propriétés locales quand le nombre d'impuretés dans le fragment est augmenté. Il est important de souligner que ces résultats ne sont pas reproductibles de manière systématique par des méthodes DFT. De plus, une description quasi correcte de la transition de Mott-Hubbard est prometteuse, car elle signifie que notre approche d'embedding est capable de capturer des phénomènes physiques non-communes.

CONCLUSION: Bien que dans ce court résumé, nous avons seulement présenté les éléments de construction d'une méthode d'embedding afin de traiter les systèmes fortement corrélés en chimie quantique et en physique de la matière condensée, plusieurs points importants ont émergé.

Pour commencer, nous avons observé que la transformation de (block) Householder jouait un rôle central. Le premier résultat important est relié à la construction du bain quantique. Nous avons observé qu'il a été construit analytiquement à partir de la matrice densité du système complet. Pour des raisons pragmatiques et des avantages numériques, nous avons décidé de décrire le système complet à partir d'une résolution avec des électrons non interagissants où avec une approximation dite de champ moyen. Ainsi, la matrice densité possède la propriété d'être idempotente et l'application de notre transformation unitaire permet d'avoir un découplage strict entre une partie nommée cluster de Householder et environnement de Householder. Plusieurs propriétés ont émergé de ce strict découplage. Premièrement, le nombre de spin-orbitales est fixé et le cluster contient un nombre fini d'électrons. Ainsi, cela permet de réaliser des calculs tels que le *Configuration Interaction* afin de restaurer la corrélation manquante dans le cluster de Householder.
Bien que non expliqués dans ce court résumé, nous avons également prouvé que les bains quantiques obtenus avec la DMET (utilisation de la décomposition en valeur singulière) vivaient dans le même espace vectoriel que ceux obtenus avec la

transformation de Householder. Ceci peut être retrouvé à la Sec. 5.3.

Similairement à l'esprit de la DMET, une version statique et à température nulle d'un embedding quantique a été formulé sous le nom de *Householder transformed density matrix functional embedding theory* (Ht-DMFET). Appliqué au modèle de Hubbard à 1D et à un Hamiltonian *Ab initio*, des résultats similaires à la DMET ont été obtenu. Comme attendu, ces résultats s'améliorent lorsque le fragment contient plusieurs impuretés. La transition de Mott-Hubbard a été correctement décrite et ce résultat est encourageant pour les futures applications. Notons que les conditions nécessaires à la description exacte de cette transition sont présentées à travers une méthode d'embedding dénommé *density matrix interpolation variational ansatz* (DIVA) présentée à la Sec. 8.

Pour conclure, de nouvelles idées et stratégies d'embedding ont été explorés afin de décrire avec précision les systèmes fortement corrélés. À travers des applications sur des Hamiltoniens modèles et *Ab initio*, des résultats encourageant ont été obtenus et ouvrent la porte à des études sur divers systèmes plus complexes. Ces extensions constituent un remarquable défi pour le futur.

Introduction

In quantum chemistry and condensed matter theory, strongly correlated systems have been attracting a lot of attention in both fundamental and applied research. Even though there is no clear mathematical definition of what strong correlation is, one of the most known definition of correlation was proposed by P. Löwdin[41] as the difference between the *Hartree-Fock*[42] (HF) and the exact energy. The strong electron correlation can be seen as the insufficiency of the single determinantal character of the HF wave function to reproduce the physics of a system with degenerate or nearly-degenerate highest occupied molecular orbitals.
In chemistry and material sciences, it gathers a large class of molecules and materials with partially filled *d*- and *f*-orbitals. Among them, the transition metal are widely used in homogeneous[1,2,3] and heterogeneous[4,5,6] catalysis but also play an essential role in many biological processes[7,8,9]. In condensed matter physics, a complex interplay between charge, spin, orbital and lattice degrees of freedom gives rise to numerous interesting physical and chemical properties. High-temperature superconductivity has been discovered in nickelates[10,11] or layered copper oxides[12,13,14], colossal magneto-resistance effects in manganese oxides[15,16,17], heavy fermion phenomena has been studied in lanthanide- or actinide-based metals[43,44,45] or metal-insulator transition has been observed in vanadium oxides[18,19,20]. Consequently, these materials present a high application potential in the development of new electronic devices. Current researches aim at rigorously understanding and predicting the behavior of this promising class of compounds.

To describe electronic correlation, different approaches can be used such as wave function based methods. In this context, the main idea is to go beyond the mean-field description provided by HF by expanding the molecular wave function

in the basis of configurations. Nevertheless, it faces the so-called exponential wall problem in practice and cannot be applied to large molecules and extended systems. Identifying an active space where a subset of spin-orbitals plays an important role in the description of electron correlation is a pragmatical approach to circumvent FCI limitations. From this idea, several standard approaches such as *multi-configurational self-consistent field + complete active space perturbation theory* (MCSCF + CASPT2)[46,47,48] or MCSCF + *n-electron valence state perturbation theory* (MSCSF + NEVPT2)[49,50] can *in-principle* describe accurately strongly correlated systems in a systematic way. Nevertheless, all these approaches have a high numerical cost and standard implementation cannot be used for modelling large molecules.

Density functional theory[22,23] (DFT) changes perspective and it focuses on the electronic density. Moreover, by the use of the Kohn-Sham scheme and the construction of an exchange-correlation functional, the high numerical cost of *wave function theories* (WFT) is elegantly bypassed. Numerous density functional approximations are available in the literature but none of them is able to properly describe strong correlation systematically. DFT has been successfully combined with lattice models to describe more precisely strongly correlated systems. In hybrid-like DFT+U[51,52,53,54,55] approach, the functional is improved by introducing the Hubbard parameter U which accounts for the localized character of electronic interaction in transition metals d and f open shells. Another approach is the DFT + *dynamical mean-field theory*[56,57,58] (DFT+DMFT) method where the main idea is to use the DFT Hamiltonian to define the one-body term of the Hubbard model and then supplement it by an exact Coulomb interaction for the correlated orbitals subset. While these approaches improve the quality of DFT calculations, they still suffer of neglecting the non-local correlation which can have an important role in many strongly correlated systems. Moreover, combining first-principles electronic structure theory and model Hamiltonian leads to difficulty to rigorously treat the double-counting correction.

One alternative to both *wave function* and *density functional theories* limitations is to develop embedding theories. Quantum embedding has emerged over

the last decades as a promising strategy for modelling quantum correlation in large and extended systems. In practice, the motivation of quantum embedding methods is driven by the will of reducing the computational costs of large numerical simulations. Many different approaches have been proposed including the so-called "divide and conquer" method. The philosophy of these methods is the following: starting with a large and complex system, one seeks to replace the expensive numerical resolution of a full-size problem by a series of effective smaller-size problems (where all calculations combined is numerically cheaper than solving the original problem). Applied to quantum chemistry, such methods have been usually used to evaluate the electronic structure of very large molecular systems. In this case, the expensive resolution of the electronic Schrödinger equation is replaced by the resolution of a series of Schrödinger equations for an embedded molecular fragments, or "*clusters*", which are easier to treat. Each cluster is composed by a given fragment (defined by a few localized orbitals from the original full system), which interacts with an associated auxiliary sub-system called "*bath*" whose role is to mimic the rest of the molecule and describe the interactions occurring between the associated local fragment and the rest of the molecule.

The mathematical construction of the bath depends on the choice of basic variable in the embedding procedure. Obviously, this choice is not unique, which explains the diversity of embedding schemes in the literature. In the well-established *dynamical mean-field theory*[24,25] (DMFT), the so-called local Green function, which is evaluated on the impurity (i.e. the site we want to embed in a large lattice), is the quantity of interest. In this case, the non-interacting, and possibly infinite, sites of the Anderson model (on which the Green function is mapped) represent the bath. Note that the fragmentation of a system, which is central in embedding calculations, allows for the combination of different electronic structure methods.

More recently, *density matrix embedding theory*[26,27] (DMET) has attracted an increasing attention as it drastically simplifies the bath (when compared to DMFT). This frequency-independent (and therefore formally simpler than DMFT) theory is not limited to system with high coordination number and is therefore ap-

plicable to both solids and molecules. In DMET, the number of bath sites equals (at most) the number of impurity sites within the fragment, the Schrödinger equation can be solved accurately (if not exactly) for the reduced-in-size "fragment+bath" system.

In the light of these promising embedding theories, one of the main objective of the present thesis is to clarify the connections between DMET and the *in-principle-exact* theories that are DFT and *reduced density matrix functional theory* (RDMFT). On that basis, alternative flavors of DMET will be explored.

First of all, the main transformation used in DMET is the *singular value decomposition* (SVD) which plays an important role in quantum information theory[59]. The SVD is in practice linked to the well-known Schmidt decomposition[60], which allows to compactify the wave function describing the quantum state of two interacting subsystems based on entanglement arguments. In DMET, it allows to drastically reduce the degrees of freedom of the bath. Consequently, it provides an advantageous starting point for quantum embedding. In standard implementations of DMET, the singular value decomposition is applied to a single Slater determinant Φ. In this case, the bath simply consists of effective sites (or orbitals) that can be determined numerically from the overlap matrix between the fragment and the occupied orbitals in Φ. The (one-electron reduced) density matrix comes into play in the optimization of Φ, through mapping constraints. The performance of DMET can in principle be improved systematically by incorporating correlation into the bath, which in the original formulation of the theory, means starting with a correlated wave function and leads ultimately to a bath described by *many-body* states. One objective of the present thesis is to verify if DMET can be made formally exact and systematically improvable while preserving a single-particle quantum partitioning picture. More precisely, we will rewrite the embedding as a functional of the density matrix, thus bypassing the Schmidt decomposition of the reference (correlated or not) full-system wave function. Note that while DMET uses the SVD in order to build the bath, we used a unitary (block) Householder transformation[36,37]. This transformation is at the very heart of the present thesis

and connection with SVD will be made.

We also investigate the mapping constraints proposed in DMET. We recall that in practice, the quantum partitioning in standard practical calculations is done at the single-particle level and the mapping constraints are upon the (one-electron reduced) density matrix. As pointed out in previous works[61,38], representability issues may arise in this context as it is impossible to exactly map a non idempotent matrix onto an idempotent one. In other words, a correlated density matrix is not non-interacting v-representable. Consequently, this leads to difficulties in the numerical robustness of the method. Note that relaxed constraints have been used, like in *density embedding theory* (DET)[38,40], where only site occupations (*i.e.*, the diagonal elements of the density matrix) are mapped. In this spirit, we developed a combination of DMET with KS-DFT which allows us to bypass the representability problems met in RDMFT and sticks to the well-established framework of DFT.

The present thesis aims at developing and implementing novel and *in-principle-exact* embedding methodologies at the interface between chemistry and physics. Towards an accurate description of strongly correlated molecules and materials, the quantum embedding will be applied to the *Hubbard model*, and then generalized to *Ab initio* molecular Hamiltonian. The thesis is organized as follows.

Chapter 1 presents the electronic problem we are interested in. After a general introduction to the electronic structure problem, we will briefly recap the second quantization formalism as it will be used to derive our different embedding scheme. Chapter 2 gives a brief state of the art of electronic structure in quantum chemistry. We will describe the advantages and inconvenients of standard methods to describe strongly correlated systems. In Chapter 3, we will briefly discuss two model Hamiltonians, namely the Hubbard model and the single impurity Anderson model as they both have been extensively used to provide an accurate approximation for real systems and especially strongly correlated ones. Then, we will present in a nutshell existing embedding methods in Chapter 4. From real space partitioning, we will move to orbital space partitioning and present DMFT and especially DMET which is central in the present thesis. Presentation of the works realized during this thesis starts in Chapter 5. We will introduce the Householder and block

Householder transformations which are used to construct one-electron quantum bath. One of the main results is presented in Section 5.3 where the connection between the *singular value decomposition* used in DMET and the *Householder transformation* applied to the density matrix will be discussed. In Chapter 6, the *Householder transformed density matrix functional embedding theory* (Ht-DMFET) is applied for the Hubbard model and then extended to an *Ab initio Hamiltonian*. In addition, in the *local potential functional embedding theory* (LPFET) of Chapter 7, a new paradigm for the embedding is proposed as it follows the framework of DFT. Finally, in Chapter 8, we briefly present an additional embedding scheme that we entitled the *density matrix interpolation variational ansatz* (DIVA). Although DIVA is very specific and have not been explored in great details, it provides an interesting proof of concept regarding the description of the density-driven Mott-Hubbard transition. Conclusions and perspectives are finally ending this work.

Chapter 1

Elements of theory

This section will settle the molecular and extended systems electronic structure problem that we are interested in. It provides in the first part a general introduction to the Schrödinger equation by analyzing the electronic Hamiltonian and its associated ground state wave function. Finally, a brief recap of the second quantization formalism is discussed as it will be widely used to derive our different embedding schemes.

1.1 Context

In quantum chemistry, one is interested in the properties and time evolution of atomic and molecular systems while in condensed matter physics the interest is aimed at extended systems. In its most simple formulation and the one we will adopt, the chemical system under study[1] is considered in the vacuum at zero temperature and no external time-dependent potential (*i.e.* electric, magnetic fields,...) is applied to the system. Thus, one can have access to the ground state electronic properties of any system by solving the (non-relavistic) time-independent Schrödinger equation (SE),

$$\hat{H} \left|\Psi_I\right\rangle = E_I \left|\Psi_I\right\rangle , \tag{1.1}$$

where E_I are the different eigenvalues and $\left|\Psi_I\right\rangle$ their associated eigenvectors. Note that we will focus our work on the ground state $\left|\Psi_0\right\rangle$ (the subscript 0 will be dropped

[1] In the following, for simplicity, "*the system*" will refer to the "*chemical system under study*".

for simplicity). The full molecular Hamiltonian operator $\hat{H}$ of the system takes the following form in the coordinate representation and using atomic units,

$$\begin{aligned}\hat{H} &= \hat{T}_e + \hat{T}_N + \hat{V}_{NN} + \hat{V}_{Ne} + \hat{V}_{ee} \\ &= -\frac{1}{2}\sum_i^N \nabla_i^2 - \frac{1}{2}\sum_A^M \frac{\nabla_A^2}{M_A} + \frac{1}{2}\sum_A^M \sum_{B\neq A}^M \frac{Z_A Z_B}{r_{AB}} - \sum_i^N \sum_A^M \frac{Z_A}{r_{iA}} + \frac{1}{2}\sum_i^N \sum_{j\neq i}^N \frac{1}{r_{ij}}.\end{aligned} \tag{1.2}$$

The two first terms of the right hand side (r.h.s) of the equation are the kinetic energies of the electrons and the nuclei which are denoted by lowercase and uppercase letters, respectively. The remaining terms are the usual Coulomb interactions where Z_I correspond to the charge of nucleus I and the denominator is the distance separating the interacting particles. Obviously, each summation runs over the number of particles (N electrons and M nuclei) present within the system.

In the eigenvalue integro-differential Eq. (1.1), one only has in hands the Hamiltonian describing interactions among the different particles of the system. Nevertheless, postulates of quantum mechanics are straightforward, solving the SE gives access to the ground state and excited states wave functions Ψ_I which are mathematical objects containing all the information about the system. Consequently, one can have access to any observable by taking the expectation value of any operator $\hat{O}$ with the given normalized wave function (*i.e.* $\langle\Psi|\Psi\rangle = 1$),

$$O[\Psi] = \langle\Psi|\hat{O}|\Psi\rangle\,. \tag{1.3}$$

Note that the exact observable value of Eq. (1.3) is only retrieved by the exact wave function associated with the system. Nevertheless, obtaining the exact wave function is an extremely complicated task as it describes the motion of $N + M$ interacting particles. In practice, analytical solutions for the SE can only be found for a few simple one-electron systems and approximations have to be made for more complex systems.

The Rayleigh-Ritz variational principle is of great use for building approximate wave function as it states that any approximate wave function $\left|\tilde{\Psi}_I\right\rangle$ will have an expectation value of the Hamiltonian which is always higher than the exact

ground state energy E_0,

$$\frac{\left\langle \tilde{\Psi}\middle|\hat{H}\middle|\tilde{\Psi}\right\rangle}{\left\langle \tilde{\Psi}\middle|\tilde{\Psi}\right\rangle} \geq E_0, \tag{1.4}$$

where the equality only holds for the exact ground state wave function. Thus, one could make use of the variation method in order to improve the description of a system,

$$E_0 = \min_{\Psi} \frac{\langle \Psi|\hat{H}|\Psi\rangle}{\langle \Psi|\Psi\rangle}. \tag{1.5}$$

One of the most famous approximations in order to simplify the electronic structure problem in Eq. (1.2) is the *Born-Oppenheimer approximation* (BO). M. Born and R. Oppenheimer assumed that the electronic 'relaxation' with respect to nuclear motion is instantaneous by considering the heavier mass of nuclei over electrons. Within this approximation, nuclei are considered as fixed charged points and thus their kinetic energy is neglected in a first step while the repulsion between nuclei is considered as a constant. It is therefore possible to separate the nuclear and electronic Hamiltonian as follows,

$$\begin{aligned}
\hat{H} &= \hat{H}_{Nuc} + \hat{H}_{el} \\
&= \left(\hat{T}_N + \hat{V}_{NN}\right) + \left(\hat{T}_e + \hat{V}_{Ne} + \hat{W}_{ee}\right) \\
&= \left(-\frac{1}{2}\sum_{A}^{M}\frac{\nabla_A^2}{M_A} + \frac{1}{2}\sum_{A}^{M}\sum_{B\neq A}^{M}\frac{Z_A Z_B}{r_{AB}}\right) + \left(-\frac{1}{2}\sum_{i}^{N}\nabla_i^2 - \sum_{i}^{N}\sum_{A}^{M}\frac{Z_A}{r_{iA}} + \frac{1}{2}\sum_{i}^{N}\sum_{j\neq i}^{N}\frac{1}{r_{ij}}\right),
\end{aligned} \tag{1.6}$$

and thus the wave function,

$$\Psi(\{\mathbf{x}_i\};\{\mathbf{x}_A\}) = \Psi_N(\{\mathbf{x}_A\})\Psi_{el}(\{\mathbf{x}_i\};\{\mathbf{x}_A\}), \tag{1.7}$$

where the electronic wave function $\Psi_{el}(\{\mathbf{x}_i\};\{\mathbf{x}_A\})$ is explicitly dependent on the electronic space and spin coordinates and parametrically on the nuclear ones. Note that the previous equality is exact in the so-called exact factorization formalism[62] and the expression becomes an approximation if the conditional is taken to be, for example, a Born-Oppenheimer wave function.

In electronic structure theory, focus is made on the resolution of the SE involving the electronic Hamiltonian,[2]

$$\hat{H}_{el} \equiv \hat{H}_{el}(\{\mathbf{x}_A\}), \tag{1.8}$$

[2]Note that for simplicity, we will drop the subscript for the kinetic energy.

which gives access the ground state electronic wave function,

$$\Psi_{0,el} = \Psi_{0,el}(\{\mathbf{x}_i\};\{\mathbf{x}_A\}), \tag{1.9}$$

which describes the motions of the electrons in the fixed nuclei field. Finally, the minimal energy E_0^{BO} of the system within the BO approximation is obtained by adding the constant nuclear repulsion,

$$E_0^{\mathrm{BO}} = E_{el}^{\mathrm{BO}} + \frac{1}{2}\sum_A \sum_{B\neq A} \frac{Z_A Z_B}{r_{AB}}. \tag{1.10}$$

Returning to the electronic Hamiltonian of Eq. (1.8), one can seek for further factorization of the electronic wave function,

$$\begin{aligned} \hat{H}_{el} &= \hat{T} + \hat{V}_{Ne} + \hat{W}_{ee} \\ &= -\frac{1}{2}\sum_i^N \nabla_i^2 - \sum_i^N \sum_A^M \frac{Z_A}{r_{iA}} + \frac{1}{2}\sum_i^N \sum_{j\neq i}^N \frac{1}{r_{ij}}. \end{aligned} \tag{1.11}$$

Nevertheless, this is not possible because of the electronic repulsion operator $\hat{W}_{ee}$. Thus, solving a many-body electronic problem ($N \geq 2$) requires to describe the coupled motion of two or more interacting electrons. This is the bottleneck in quantum chemistry as the eigenvector of Eq. (1.11) cannot be written in the form of a single product of one-electron wave functions. A general understanding and prediction of the electron correlation (*i.e.* interaction between electrons) in a system is at the very heart of the development of electronic structure theories. In quantum chemistry, the most popular ones can be classified in two families: the *wave function theories* (WFT) and the *density functional theories* (DFT). Both of them will be briefly introduced in Section 2. Despite the historical successes of WFT and DFT for describing and predicting the properties of many atomic and molecular systems, they both face limitations in order to describe the electronic correlation of many systems (*e.g.* strongly correlated ones). To circumvent their limitations, a third class of methods has become popular over the last decades and is at the heart of the present thesis, *embedding theories*.

1.2 The orbital approximation

To this point, we have presented the electronic SE and the complexity to describe the motion of N electrons simultaneously. Nevertheless, nothing has been said regarding

the mathematical structure of the wave function and how to build it in practice. A natural starting point is to assign a spatial distribution to each electron. This could be done by considering atoms localized orbitals. These functions are the so-called *atomic spin-orbitals* (AO) $\{\chi_\mu(\mathbf{x})\}$ and form an intuitive set of building blocks (*i.e.* basis set) for the construction of *molecular spin-orbitals* $\{\phi_p(\mathbf{x})\}$ (MO),

$$\phi_p(\mathbf{x}) = \sum_{\mu}^{K} C_{\mu p}\chi_\mu(\mathbf{x}), \tag{1.12}$$

where $C_{\mu p}$ is the MO coefficient associated with the contribution of the atomic spin-orbital $\chi_\mu(\mathbf{x})$ to the molecular spin-orbital $\phi_p(\mathbf{x})$. Note that while AOs are normalized and possibly non-orthogonal, MOs are orthonormalized,

$$\int d\mathbf{x}\phi_p^*(\mathbf{x})\phi_q(\mathbf{x}) = \delta_{pq}. \tag{1.13}$$

The N-electron wave functions Ψ can be approximated as a product of single-electron wave functions $\{\phi_p(\mathbf{x})\}$. Given the fermionic nature of electrons (*i.e.* particles that cannot occupy the same quantum state) and in virtue of the *Pauli exclusion principle*, the wave function should be anti-symmetric with respect to electron exchange. Thus, the structure and properties of determinants were first exploited by Slater[63] in order to construct electronic wave functions. For a N-electron system, the *Slater determinant* is defined as,

$$|\mathbf{\Phi}\rangle \equiv \Phi(\mathbf{x}_1, \mathbf{x}_2 ..., \mathbf{x}_N) = \frac{1}{\sqrt{N!}} \begin{vmatrix} \phi_1(\mathbf{x}_1) & \phi_2(\mathbf{x}_1) & . & . & . & \phi_N(\mathbf{x}_1) \\ \phi_1(\mathbf{x}_2) & \phi_2(\mathbf{x}_2) & . & . & . & \phi_N(\mathbf{x}_2) \\ . & . & . & . & . & \\ . & . & & . & & . \\ . & . & . & . & . & \\ \phi_1(\mathbf{x}_N) & \phi_2(\mathbf{x}_N) & . & . & . & \phi_N(\mathbf{x}_N) \end{vmatrix}. \tag{1.14}$$

Usually in quantum chemistry, Φ denotes a single determinant while Ψ refers to a linear combination of Slater determinants.

1.3 Second quantization

It is interesting to introduce the second quantization formalism as it provides a concise and simpler description of many-body states and especially correlated ones.

In this new representation, the Slater determinant in Eq. (1.14) is an occupation number vector belonging to the so-called Fock space,

$$|\mathbf{\Phi}\rangle \equiv |\phi_1\phi_2...\phi_N\rangle = \hat{c}^\dagger_{\phi_1}...\hat{c}^\dagger_{\phi_N}|vac\rangle\,, \tag{1.15}$$

where $|vac\rangle$ is the vacuum state and $\hat{c}^\dagger_{\phi_p}$ is a *creation operator* which creates an electron in the spin-orbital p. One can also define its hermitian conjugate, the *annihilation operator* $\hat{c}_{\phi_p}$ which destroys an electron in the spin-orbital p. Note that for simplicity, the label ϕ will be dropped. An interesting case is,

$$\hat{c}_p|vac\rangle = 0, \tag{1.16}$$

which means that we cannot remove an electron from the vacuum state (*i.e.* empty state) and therefore the latter is annihilated. Altogether, these operators fulfill the following anti-commutation relations,

$$\begin{aligned} \left[\hat{c}^\dagger_p, \hat{c}^\dagger_q\right]_+ &= 0, \\ \left[\hat{c}_p, \hat{c}_q\right]_+ &= 0, \\ \left[\hat{c}^\dagger_p, \hat{c}_q\right]_+ &= \delta_{pq}, \end{aligned} \tag{1.17}$$

which enforce the anti-symmetry of the Slater determinant by exchange of two electrons and the Pauli exclusion principle.

Note that within this formalism, the electronic Hamiltonian of Eq. 1.11 is represented as follows,

$$\hat{H}_{el} = \sum_{pq} h_{pq}\hat{c}^\dagger_p\hat{c}_q + \frac{1}{2}\sum_{pqrq} g_{pqrs}\hat{c}^\dagger_p\hat{c}^\dagger_q\hat{c}_s\hat{c}_r, \tag{1.18}$$

where h_{pq} and g_{pqrs} are the one- and two-electron integrals in a given one-electron MO basis. Taking the expectation value of Eq. (1.18) with any normalized wave function $|\Psi\rangle$ gives,

$$\begin{aligned} E = \langle\Psi|\hat{H}_{el}|\Psi\rangle &= \sum_{pq} h_{pq}\langle\Psi|\hat{c}^\dagger_p\hat{c}_q|\Psi\rangle + \frac{1}{2}\sum_{pqrq} g_{pqrs}\langle\Psi|\hat{c}^\dagger_p\hat{c}^\dagger_q\hat{c}_s\hat{c}_r|\Psi\rangle \\ &= \sum_{pq} h_{pq}\gamma_{pq} + \frac{1}{2}\sum_{pqrq} g_{pqrs}\Gamma_{pqsr}, \end{aligned} \tag{1.19}$$

where γ_{pq} and Γ_{prsq} are referred to as the *one-electron reduced density matrix*[3] and the *two-electron reduced density matrix*. The former will be the main variable in the

[3]For simplicity, we will refer to it as "density matrix"

present thesis and we will from now on denote it by $\boldsymbol{\gamma}$. The density matrix has the following properties: it is Hermitian,

$$\boldsymbol{\gamma}^\dagger = \boldsymbol{\gamma}, \tag{1.20}$$

the trace of the density matrix equals the number of electrons,

$$\mathrm{Tr}[\boldsymbol{\gamma}] = \mathrm{N}, \tag{1.21}$$

If $\boldsymbol{\gamma}$ is constructed from a single Slater determinant $\boldsymbol{\Phi}$, then,

$$\begin{aligned} \gamma_{pq} = & \langle \Phi | \hat{c}_p^\dagger \hat{c}_q | \Phi \rangle \\ = & \left(\sum_r^{occ\ in\ \boldsymbol{\Phi}} \delta_{rp} \right) \delta_{pq}. \end{aligned} \tag{1.22}$$

Therefore, the density matrix is diagonal in the molecular spin-orbitals representation and the diagonal elements are either one (occupied) or zero (unoccupied). Consequently, it is idempotent,

$$\boldsymbol{\gamma} = \boldsymbol{\gamma}^2. \tag{1.23}$$

As highlighted later on, this property is central in practical density matrix embedding calculations.

Chapter 2

Standard methods in electronic structure theory

In the present section, we will introduce the *Hartree-Fock theory* (HF), *configuration interaction* (CI) and *complete active space configuration interaction methods* (CASCI) which are electronic structure theories which tend to increasingly retrieve accurately electronic correlation. This choice has been made intentionally as in *density matrix embedding theory* (DMET) presented in Section 4.2.2, and which is at the heart of the present thesis, the original mean-field problem can be nearly transformed into a CASCI one. Moreover, sections are dedicated to *density functional theory* (DFT) and *reduced density matrix functional theory* (RDMFT) as they will play an essential role throughout the different embedding schemes developed.

2.1 Hartree-Fock theory

In the *Hartree-Fock* (HF) theory, the goal is to find the best set of molecular spin-orbitals at the single-determinant level of approximation. For this purpose, one apply the variational principle,

$$E_{HF} = \min_{\mathbf{\Phi} \equiv \hat{c}_1^\dagger \dots \hat{c}_N^\dagger |vac\rangle} \frac{\langle \mathbf{\Phi} | \hat{H}_{el} | \mathbf{\Phi} \rangle}{\langle \mathbf{\Phi} | \mathbf{\Phi} \rangle}, \tag{2.1}$$

and obtain the following one-electron-like HF equations,

$$\hat{f}(\mathbf{x}_i)\phi_p(\mathbf{x}_i) = \epsilon_p \phi_p(\mathbf{x}_i), \tag{2.2}$$

where $\hat{f}$ is the Fock operator and will be reviewed in details later. To achieve this, the electronic repulsion operator $\hat{W}_{ee}$ of the Hamiltonian in Eq. 1.11 is replaced by the Hartree-Fock potential operator $\hat{v}^{HF}$ which accounts for the average potential (or mean-field) experienced by the i-th electron from the $N-1$ remaining ones. This operator is decomposed into two bi-electronic operators, namely the local multiplicative Coulomb $\hat{J}$ operator and the non-local exchange $\hat{K}$ operator, which arises from the anti-symmetry of the wave function. The expectation value of the Coulomb operator applied on a electron i in spin-orbital ϕ_p results in the usual Coulomb repulsion between two charges densities,

$$\langle \phi_p(\mathbf{x}_i)|\hat{J}_q(\mathbf{x}_i)|\phi_p(\mathbf{x}_i)\rangle = \int d\mathbf{x}_i d\mathbf{x}_j \phi_p^*(\mathbf{x}_i)\phi_p(\mathbf{x}_i) r_{12}^{-1} \phi_q^*(\mathbf{x}_j)\phi_q(\mathbf{x}_j) = [pp \mid qq]. \quad (2.3)$$

In addition, the expectation value of the exchange operator results in a non-classical energy contribution from orbitals with the same spin,

$$\langle \phi_p(\mathbf{x}_i)|\hat{K}_q(\mathbf{x}_i)|\phi_p(\mathbf{x}_i)\rangle = \int d\mathbf{x}_i d\mathbf{x}_j \phi_p^*(\mathbf{x}_i)\phi_q(\mathbf{x}_i) r_{12}^{-1} \phi_q^*(\mathbf{x}_j)\phi_p(\mathbf{x}_j) = [pq \mid qp]. \quad (2.4)$$

Finally, the one-electron operator of Eq. (2.2) can then be rewritten as,

$$\begin{aligned} \hat{f}(\mathbf{x}_i) &= \hat{h}(\mathbf{x}_i) + \hat{v}^{HF}(\mathbf{x}_i) \\ &= \hat{h}(\mathbf{x}_i) + \sum_q \Big(\hat{J}_q(\mathbf{x}_i) - \hat{K}_q(\mathbf{x}_i) \Big), \end{aligned} \quad (2.5)$$

where the first term or the r.h.s. is composed of the kinetic energy and attractive potential energy operators of electron i [See Eq. (1.11)]. In the second term, one can perceive the mean-field description of the Fock operator $\hat{f}$ [See Eqs. (2.3) and (2.4)]. Solving the following set of Hartree-Fock equations,

$$\hat{f}(\mathbf{x}_i)\phi_p(\mathbf{x}_i) = \epsilon_p \phi_p(\mathbf{x}_i), \quad (2.6)$$

leads to the so-called canonical orbitals and their associated energies. Note that the Fock operator has a functional dependence on the solutions $\{\phi_p\}$ [See Eqs. (2.3),(2.4) and (2.6)]. Therefore, these pseudo-eigenvalue equations should be solved iteratively, hence the name: self-consistent field (SCF) method. These equations were originally solved by the Roothaan-Hall equations[64,65] who represented the Hartree-Fock equations in the atomic basis. At convergence, the ground-state Hartree-Fock energy of a N-electron system reads,

$$E_{HF} = \sum_p^{occ} h_{pp} + \frac{1}{2} \sum_{pq}^{occ} \Big(\langle pq|pq\rangle - \langle pq|qp\rangle \Big). \quad (2.7)$$

The density matrix is obtained by projecting the wave function within the subspace of occupied orbitals,

$$\{\gamma\} \equiv \gamma_{ij} = 2 \sum_{p}^{occ} C_{ip}^{*} C_{jp}. \tag{2.8}$$

Therefore, it fulfills the idempotency conditions of Eq. (1.23).

In summary, the Hartree-Fock method allows to find the best set of molecular spin-orbitals for a single Slater determinant by use of the variational principle. Therefore, the Hartree-Fock energy is an upper bound to the exact ground state energy and the difference between the true ground state energy E_0 and the one obtained with the self-consistent field procedure E_{HF} is defined as the correlation energy E_c,

$$-E_c = E_{HF} - E_0. \tag{2.9}$$

In quantum chemistry, the correlation energy is divided in two parts: the dynamical (weak) and static (or strong) correlations. While there is no clear mathematical definition of static correlation, physical insights can help to have a first distinction between them. In HF, each electron interact with an mean-field potential which is obviously a crude approximation of the physical reality. Weakly correlated systems corresponds to systems where the excited HF determinants energies are much higher as the reference one. The dynamical correlation is related to fluctuations and can be retrieved by the use of perturbation theory through second order. On the other hand, strong correlation reflects the insufficiency of a single determinant approach to describe qualitatively a system with (near-) degenerate frontier orbitals. This correlation is generally retrieved by the use of a multiconfigurational wave function. In the following section, we will concisely present two correlated theories, the *configuration interaction* and one of its extension, the *complete active space configuration interaction* (CASCI) which aim at retrieving the missing correlation of the HF approach.

2.2 Post Hartree-Fock methods

The *configuration interaction* (CI) idea is to build a wave function as a linear combination of HF Slater determinants (or configurations). For this, electrons from the occupied orbitals can be excited to virtual ones,

$$|\Psi(\boldsymbol{C})\rangle = c_0 |\Phi_0\rangle + \sum_{a,r} c_a^r |\Phi_a^r\rangle + \sum_{a<b} \sum_{r<s} c_{ab}^{rs} |\Phi_{ab}^{rs}\rangle + ..., \tag{2.10}$$

where a, b denotes occupied orbitals, r, s, virtual unoccupied ones and $\boldsymbol{C}$ is the so-called CI coefficient matrix. For simplicity, the previous equation can be rewritten in the following symbolic form,

$$|\Psi(\boldsymbol{C})\rangle = c_0 |\Phi_0\rangle + \sum_S \Big(c_S |S\rangle \Big) + \sum_D \Big(c_D |D\rangle \Big) + ..., \tag{2.11}$$

where $|S\rangle$, $|D\rangle$ denotes singly excited, doubly excited determinants, etc. Determination of the CI energy is obtained by variationally optimizing the CI expansion coefficients $\boldsymbol{C}$,

$$E_{CI} = \min_{\boldsymbol{C}} \frac{\langle \Psi(\boldsymbol{C}) | \hat{H} | \Psi(\boldsymbol{C}) \rangle}{\langle \Psi(\boldsymbol{C}) | \Psi(\boldsymbol{C}) \rangle}. \tag{2.12}$$

The minimization of the CI energy is equivalent to diagonalizing the so-called CI matrix,

$$\begin{array}{c} \\ \langle\Phi_0| \\ \langle S| \\ \langle D| \\ ... \end{array} \begin{array}{c} \begin{array}{cccc} |\Phi_0\rangle & |S\rangle & |D\rangle & ... \end{array} \\ \begin{bmatrix} \langle\Phi_0|\hat{H}|\Phi_0\rangle & 0 & \langle\Phi_0|\hat{H}|D\rangle & ... \\ 0 & \langle S|\hat{H}|S\rangle & \langle S|\hat{H}|D\rangle & ... \\ \langle D|\hat{H}|\Phi_0\rangle & \langle D|\hat{H}|S\rangle & \langle D|\hat{H}|D\rangle & ... \\ ... & ... & ... & ... \end{bmatrix} \end{array}. \tag{2.13}$$

One can already anticipate that the dimension of the matrix which depends on the number of n-tuple excitations can be substantial. Indeed, for a system of N electrons and a basis set composed of $2K$ spin-orbitals, there is $\mathrm{C}_{2\mathrm{K}}^{\mathrm{N}} = \binom{2\mathrm{K}}{\mathrm{N}}$

different ways of distributing the electrons. Building and solving this problem by taking into account all the excitations is referred to as the *full configuration interaction* (FCI) approach or exact diagonalization in physics. While FCI is exact for a given basis set, the number of configuration is growing extremely fast with the number of electron (*i.e.* the exponential wall problem). One way to circumvent the large number of configurations is to truncate the CI expansion of Eq. (2.10). In general, the singly- and doubly- excitated configuration are considered and this approximation is referred to as *CI singles and doubles* (CISD). Nonetheless, CISD remains a poor approximation and is not size-consistent.

One interesting approach to bypass these limitations consists in identifying the "active" subset of spin-orbitals which play an important role in the description of the electron correlation, while the remaining spin-orbitals are either occupied ("*core*" spin-orbitals) or empty ("*virtual*" spin-orbitals). The wave function can then be expanded by only taking into account configurations obtained with excitations within the "active space" leading to the *complete active space configuration interaction* (CASCI) method. In other words, one applies a FCI calculation in the active space. On top of that, one can simultaneously optimize the orbitals in order to further minimize the energy, resulting in the *complete active space self-consistent field* method (CASSCF). Nevertheless, while these methods could accurately describe strongly correlated systems, they are still facing a high numerical cost. Development of new algorithms to circumvent this problem is an active field of research but we will now focus on a different paradigm where the exact ground state properties could be *in-principle* retrieved with a single determinant wave function, the well-known *density functional theory* (DFT).

2.3 Density Functional Theory

DFT is the most widespread method to determine electronic properties of molecules and solids from first principles. Triggered by its early availability in quantum chemistry programs such as Gaussian70 and the emergence of hybrid functionals, its successes can be explained by its low computational cost and a relative good

accuracy. Note that W. Kohn and J. Pople shared the Nobel prize in 1998 *"for his development of the density-functional theory"* and *"for his development of computational methods in quantum chemistry"*, respectively. We will in the following derive the key equations of DFT. Starting from the general ideas, we will dive, step by step, into the Kohn-Sham formalism which is at the origin of the extensive use of DFT.

In the electronic Hamiltonian of Eq. (1.11), the operators $\hat{T}$ and $\hat{W}_{ee}$ are system independent (*i.e.* universal) while the external potential operator $\hat{V}_{ext}$ (which would correspond to the nuclear potential $\hat{V}_{Ne}$ in a conventional quantum chemical calculation) depends on the structure of nuclei. In the first theorem of Hohenberg and Kohn (HK)[66], a one-to-one correspondence of the external potential v_{ne} with the ground state electronic density $n(\boldsymbol{r})$ has been demonstrated. Thus, the knowledge of the ground state electronic density allows, *in principle*, to build the electronic Hamiltonian and therefore gives access to all the ground and exited states properties of a given system.
Consequently, observables are functionals of the density. Integrating over the spin variables, the latter is defined as,

$$n(\boldsymbol{r}) = N \sum_{\sigma_1} \int d^3\mathbf{x}_2 \int ... \int d^3\mathbf{x}_N \Psi^*(\boldsymbol{r}\sigma_1, \mathbf{x}_2, ..., \boldsymbol{r}_N)\Psi(\boldsymbol{r}\sigma_1, \mathbf{x}_2, ..., \mathbf{x}_N), \quad (2.14)$$

which normalizes to the number of electrons N [See also Eq. (1.21)],

$$\int d^3\boldsymbol{r} n(\boldsymbol{r}) = N. \quad (2.15)$$

Thus, the ground state wave function is a functional of the density $\Psi[n]$ and so is the expectation value of the kinetic and the electronic repulsion operators. They define the so-called HK universal functional,

$$F[n] = \langle \Psi[n] | \hat{T} + \hat{W}_{ee} | \Psi[n] \rangle . \quad (2.16)$$

Valid for any integer number of particles, it can be used to define the total electronic energy functional,

$$E[n] = F[n] + \int d^3\boldsymbol{r} v_{ne}(\boldsymbol{r}) n(\boldsymbol{r}). \quad (2.17)$$

The second HK theorem establishes a variational principle[66] where the ground state energy E_0 is obtained by minimizing this energy functional with respect to N-electron densities n,

$$E_0 = \min_{n \to N} \Big\{ F[n] + \int d^3\boldsymbol{r} v_{ne}(\boldsymbol{r}) n(\boldsymbol{r}) \Big\}. \tag{2.18}$$

The minimum being reached for the ground state density $n_0(\boldsymbol{r})$ corresponding to the potential $v_{ne}(\boldsymbol{r})$. One theoretical drawback is the v-representability problem, *i.e.* making sure that the ground state density $n_0(\boldsymbol{r})$ corresponds to a physical external potential $v_{ne}(\boldsymbol{r})$. By definition, $n_0(\boldsymbol{r})$ is v-representable but the problem is to know if, for a given density n, the wave function $\Psi[n]$ exists. Unfortunately the v-representability conditions are not known, but this problem could be circumvented by Levy-Lieb constraint-search formulation[31,67],

$$F_{LL}[n] = \min_{\Psi \to n} \langle \Psi | \hat{T} + \hat{W}_{ee} | \Psi \rangle \,, \tag{2.19}$$

where the minimization is done over normalized N-electron anti-symmetric wave functions Ψ yielding the density n [See Eq. (2.14)], known as the N-representability condition. Unlike the v-representability conditions, the pure-state N-representability conditions are known explicitely[68,69]. Therefore, a new variational principle can then be applied,

$$E_0 = \min_{n} \Big\{ F_{LL}[n] + \int d^3\boldsymbol{r} v_{ne}(\boldsymbol{r}) n(\boldsymbol{r}) \Big\}. \tag{2.20}$$

Even though in theory, replacing the wave function by a universal functional depending only on the density (*i.e.* orbital-free formulation) is a drastic simplification, an explicit analytical form of the universal functional $F[n]$ as a functional of the density is not known in practice. One illustrative way to understand this complexity is to think of the vague relation between the velocity of electrons with its spatial distribution.

One has to wait until 1965 and the formalism[23] proposed by W. Kohn and L. J. Sham to establish the foundations of an efficient and robust theoretical framework to study electronic structures of materials and molecules. Knowing that the ground state density $n_0(\boldsymbol{r})$ is the key variable in DFT, they mapped the interacting problem onto an effective non-interacting one with the constraint that the auxiliary system (*i.e.* non-interacting) has the density of the physical one. Thus, similarly

to the Hartree-Fock theory [See Section 2.1], the non-interacting system could be described by a single determinant $\Phi(\phi_1, ..., \phi_N)$. Within this formalism, the density is simply expressed in terms of the N occupied spin-orbitals,

$$n(\boldsymbol{r}) = \sum_{p=1}^{N} |\phi_p(\boldsymbol{r})|^2. \tag{2.21}$$

In *Kohn-Sham DFT* (KS-DFT), the universal functional $F[n]$ in Eq. 2.16 is decomposed as follows,

$$F[n] = T_s[n] + E_{Hxc}[n], \tag{2.22}$$

where $T_s[n]$ is the non-interacting kinetic energy which can be defined through the constrained-search formalism[31] as follow,

$$\begin{aligned} T_s[n] &= \min_{\Phi \to n} \langle \Phi | \hat{T} | \Phi \rangle \\ &= \langle \Phi[n] | \hat{T} | \Phi[n] \rangle \\ &= -\frac{1}{2} \sum_{p} \langle \phi_p[n] | \nabla^2 | \phi_p[n] \rangle \,, \end{aligned} \tag{2.23}$$

where the minimization is done over all normalized N-electron anti-symmetric mono-determinantal wave functions Φ yielding the density n. Thus, orbitals have been re-introduced in order to circumvent the difficulty to construct an explicit functional of the density for the kinetic energy.

$$T_s[n] \to T_s[\{\phi_p[n]\}]. \tag{2.24}$$

The remaining part is the Hartree-exchange-correlation functional which can be decomposed into its Hartree and exchange-correlation contributions,

$$E_{Hxc}[n] = E_H[n] + E_{xc}[n]. \tag{2.25}$$

The former reads just as in the Hartree-Fock theory [See Eq. 2.3],

$$E_H[n] = \frac{1}{2} \int d^3\boldsymbol{r} \int d^3\boldsymbol{r'} \frac{n(\boldsymbol{r}) n(\boldsymbol{r'})}{|\boldsymbol{r} - \boldsymbol{r'}|}, \tag{2.26}$$

while the exchange part [See Eq. 2.4] can be extracted by the following difference,

$$E_x[n] = \langle \Phi[n] | \hat{W}_{ee} | \Phi[n] \rangle - E_H[n], \tag{2.27}$$

and finally, the correlation energy contains all contributions which are not coming from the mean-field approximation,

$$\begin{aligned} E_c[n] &= F[n] - T_s[n] - E_H[n] - E_x[n] \\ &= \Big[\langle \Psi[n] | \hat{T} | \Psi[n] \rangle - \langle \Phi[n] | \hat{T} | \Phi[n] \rangle \Big] \\ &+ \Big[\langle \Psi[n] | \hat{W}_{ee} | \Psi[n] \rangle - \langle \Phi[n] | \hat{W}_{ee} | \Phi[n] \rangle \Big] \\ &= T_c[n] + U_c[n]. \end{aligned} \tag{2.28}$$

The explicit form in terms of the density of the exchange-correlation functional is analytically unknown and has to be approximated. In addition to the Hxc functional, W. Kohn and L. J. Sham reformulate the variational property of Eq. (2.20) in terms of single-determinant as,

$$E_0 = \min_{\Phi} \Big\{ \langle \Phi | \hat{T} + \hat{V}_{Ne} | \Phi \rangle + E_{Hxc}[n_\Phi] \Big\}. \tag{2.29}$$

The main advantage of this form is that all the contributions are either treated at the single-determinant level or is a functional of the density which provides tremendous simplification compared to Eq. (2.20). Similarly to the HF equation, rewriting the density of Eq. (2.29) in terms of spin-orbitals and integrating over the spin variables, one obtains,

$$E_0 \left[\{\phi_p\} \right] = \sum_{p=1}^{N} \int d\boldsymbol{r} \phi_p^*(\boldsymbol{r}) \left(-\frac{1}{2}\nabla^2 + v_{ne}(\boldsymbol{r}) \right) \phi_p(\boldsymbol{r}) + E_{Hxc}[n_0], \tag{2.30}$$

where,

$$n_0(\boldsymbol{r}) = \sum_{p=1}^{N} |\phi_p(\boldsymbol{r})|^2. \tag{2.31}$$

By using the variational principle, one ends up with the one-electron-like Kohn-Sham equations,

$$\left(-\frac{1}{2}\nabla^2 + v_s(\boldsymbol{r}) \right) \phi_p(\boldsymbol{r}) \quad = \epsilon_p \phi_p(\boldsymbol{r}), \tag{2.32}$$

where

$$v_s(\boldsymbol{r}) = v_{ne}(\boldsymbol{r}) + v_{Hxc}[n_0], \tag{2.33}$$

is the KS potential and contains two contributions, the external potential v_{ne} and the so-called Hartree-exchange-correlation potential v_{Hxc}. Note that,

$$v_{Hxc}[n] = \frac{\delta E_{Hxc}[n]}{\delta n(\boldsymbol{r})}. \tag{2.34}$$

The eigenfunctions of the one-electron-like KS Hamiltonian of Eq. 2.32 are referred to as the KS orbitals. As in the HF theory, the previous KS equations have to be solved self-consistently as $v_{Hxc}[n_0]$ of Eqs. (2.32), (2.33) and (2.34) is dependent on the orbitals through the density [See Eq. 2.21].

Despite the elegance and the success of regular KS-DFT in countless applications, the exact $E_{xc}[n]$ is unknown and results depend on the available approximations. The problem being that there is no general strategy to build density functional approximations for strongly correlated systems. Nevertheless, KS-DFT limitations can be circumvent by the use of different strategies.

In DFT+U[51,52,53,54,55], the idea is to bypass the inadequate treatment of the local Coulomb interaction by the approximated xc functionals by improving the KS potential of Eq. (2.33). To this purpose, the KS Hamiltonian is corrected by a local Hubbard-like local electronic repulsion operator $\hat{U}$ [See Section 3.1]. For simplicity, this interaction, which takes the form of an effective single-electron operator, can be added on electrons belonging to $d-$ or $f-$ orbitals in order to shift their energy. While this approach well describes the magnetic ground state of correlated materials, it is not suitable for metal-insulator transition. Apart from DFT+U, there exist other attemps to circumvent the limitations of regular DFT by correcting the functional: the self-interaction-correction approach[70,71] or the hybrid functional method[72,73,74,75,76] are two examples. Alongside, alternative KS schemes are constructed such as the strictly-correlated electron approach[77].

Finally, despite the original limitation of DFT to describe strongly correlated systems, many approaches are developed to circumvent them. However, using the one-electron reduced density matrix instead of the spatial density allows for fractional occupation numbers and seems to be more suitable for the description of strongly correlated systems. In the following section, we will provide the main ingredients of *reduced density matrix functional theory* (RDMFT).

2.4 Reduced Density Matrix Functional Theory

Given a N-electron wave function Ψ, the one-electron reduced density matrix which was initially introduced in the present thesis within the second quantization formalism [See Eq. (1.19)] could be rewritten as,

$$\gamma(\mathbf{x},\mathbf{x}') = N \int d\mathbf{x}_2 ... \int d\mathbf{x}_N \Psi^*(\mathbf{x},\mathbf{x}_2,...,\mathbf{x}_N)\Psi(\mathbf{x}',\mathbf{x}_2,...,\mathbf{x}_N). \tag{2.35}$$

One great advantage of *reduced density matrix functional theory* (RDMFT) is the explicit expression of the kinetic energy as a functional of the density matrix,

$$\left\langle \hat{T} \right\rangle = \sum_{\sigma} \int d^3\mathbf{r} \int d^3\mathbf{r}' \delta(\mathbf{r}-\mathbf{r}') \left(-\frac{\nabla^2_{\mathbf{r}}}{2} \right) \gamma(\mathbf{r}'\sigma, \mathbf{r}\sigma), \tag{2.36}$$

thus circumventing the problem observed in orbital-free formulation of DFT. Moreover, in RDMFT the orbitals are fractionally occupied and the theory is more appropriate to account for static correlation. Thus, it should in-principle provide a better description than those of density functional approximations.

In the following, we will briefly discuss the theoretical foundations of RMDFT by following the approach proposed by K. Pernal and K.J.H. Giesbertz[78].
The self-adjointness character of the density matrix in Eq. (2.35) allows its spectral decomposition,

$$\gamma(\mathbf{x},\mathbf{x}') = \sum_{p} n_p \phi^*_p(\mathbf{x})\phi_p(\mathbf{x}'), \tag{2.37}$$

where the set of eigenvectors $\{\phi_p\}$ and associated eigenvalues $\{n_p\}$ are referred to as the natural spin-orbitals and natural occupation numbers, respectively. A set of conditions regarding these quantities lay down the foundations of RDMFT. From the self-adjointness of the density matrix one has,

$$\forall p,q \qquad \int d\mathbf{x} \phi^*_p(\mathbf{x})\phi_q(\mathbf{x}) = \delta_{pq}. \tag{2.38}$$

Moreover, the natural occupancies n_p are bounded[28,29] by virtue of the Pauli exclusion principle,

$$\forall p \qquad 0 \leq n_p \leq 1. \tag{2.39}$$

and finally the occupancies sum up to the total number of electrons N,

$$\sum_p n_p = N. \tag{2.40}$$

These ensemble N-representability conditions are of prior importance since Coleman proved in 1963 that if an "*Hermitian 1-RDM satisfies these sufficient and necessary conditions, there exists an ensemble of N-electron anti-symmetric wave functions that yield γ*"[28]. Similarly, the conditions to have an 1-RDM which is representable by a pure N-electron wave function or more precisely derivable from an N-electron pure density matrix implies supplementary restrictions on the 1-RDM. Those constraints which go beyond Pauli constraints are referred to as pure N-representability conditions or generalized Pauli constraints. Nonetheless, the number and complexity of constraints increase dramatically with the number of electrons and the size of basis[79].

The applicability of RDMFT finds its roots in the work of T. L. Gilbert[30] who extended the Hohenberg-Kohn theorem to nonlocal potentials. Similarly to regular DFT, it establishes the existence of a 1-RDM functional for the energy of any system,

$$E[\gamma] = \mathrm{Tr}[\hat{\mathrm{h}}\gamma] + \langle\Psi[\gamma]|\hat{W}_{ee}|\Psi[\gamma]\rangle\,, \tag{2.41}$$

with,

$$\hat{h} = -\frac{\nabla^2}{2} + \hat{v}, \tag{2.42}$$

and where $\Psi[\gamma]$ is the ground state wave function associated with a v-representable density matrix γ. In addition, a variational principle has been proven,

$$\forall\gamma \in v-rep \quad E_v[\gamma] \geq E_0, \tag{2.43}$$

where v-rep denotes a set of pure-state v-representable 1-RDMs. Levy's constrained search formulation[31] also contains an extension of the density matrix functional domain to all pure-state N-representable 1-RDMs by defining the electronic repulsion functional,

$$\hat{W}^L_{ee}[\gamma] = \min_{\Psi\to\gamma} \langle\Psi|\hat{W}_{ee}|\Psi\rangle\,. \tag{2.44}$$

But, the decisive outbreak arises in 1980 from the extension of Levy's constrained search formulation to ensemble N-representable 1-RDMs by S.M. Valone[32,33],

$$\hat{W}_{ee}^{V} = \min_{\hat{\Gamma}\to\gamma} \mathrm{Tr}[\hat{\mathrm{W}}_{\mathrm{ee}}\hat{\Gamma}]. \tag{2.45}$$

The minimization in Eq. (2.45) is performed over a grand-canonical ensemble density matrix operators $\hat{\Gamma}^{(N)} = \sum_I \lambda_I \left|\Psi_I^{(N)}\right\rangle \left\langle\Psi_I^{(N)}\right|$ that reproduces a density matrix γ respecting the ensemble N-representability conditions of Eqs. (2.38),(2.39) and (2.40),

$$\gamma_{\Gamma^{(\hat{N})}} = \sum_I \lambda_I \gamma_{\Psi_I}. \tag{2.46}$$

Thus, the ensemble N-representability conditions accompanied with Eq. (2.45) are the RDMFT foundations.

Chapter 3

Model Hamiltonians

The complexity of the molecular Hamiltonian [See Eq. 1.2] is related to the presence of the electron-electron repulsion operator. Consequently, it is far from trivial to solve the associated Schrödinger equation. Although numerous development have been proposed to provide an accurate numerical solution with a reasonable computation cost, it is sometimes preferable to reformulate the original complex problem into a simpler and solvable one. Despite their apparent simplicity, model Hamiltonians can capture many physical effects of interest and provide an accurate approximation for real systems. If the exact results are known, they can also provide a testing ground for the development of new theories or methodologies. We will in the following, describe two of them, the *Hubbard model* (HM) and the *single impurity Anderson model* (SIAM).

3.1 Hubbard model

The success of band theory can be explained by its simple classification of metals within different classes such as conductors, semiconductors and insulators and thus was at the origin of the growth of the entire microelectronics industry. Nevertheless, its independent particle picture has failed to describe the electron conduction, metallic behavior and other physical properties of many of the transition and rare-earth metals. This class of compounds are referred to as *strongly-correlated* materials and possess peculiar electronic or magnetic properties such as high-temperature superconductivity, metal-insulator transition or colossal magnetoresistance. These

properties emerge from a subtle interplay between lattice structure, atomic orbitals, charge and spin degrees of freedom. In 1963, J. Hubbard proposed the *Hubbard model*[34] (HM) in order to study electronic correlation of these materials. Nowadays, this model is widely used and became a well-known reference model in order to treat strongly correlated electronic systems. The countless applications of the Hubbard model can be explained by the balance between the complexity of the problem and its simple reformulation. Indeed, in the simplest case of the one-dimensional Fermi-Hubbard model, a static lattice of L sites (*i.e.* localized orbitals) is the playground for correlated electrons. The kinetic energy is replaced by an isotropic hopping parameter of strength t. Moreover, within the *tight-binding approximation*, the latter is only defined in-between nearest neighbours,

$$\hat{T} \longrightarrow -t \sum_{\sigma=\uparrow,\downarrow} \sum_{i=0}^{L-1} \left(\hat{c}_{i\sigma}^{\dagger} \hat{c}_{(i+1)\sigma} + \text{H.c.} \right). \tag{3.1}$$

The electronic repulsion operator is simplified by a local on-site bi-electronic interaction operator and its strength parameter U,

$$\hat{W}_{ee} \longrightarrow U \sum_{i=0}^{L-1} \hat{n}_{i\sigma} \hat{n}_{i\sigma'}, \tag{3.2}$$

where $\hat{n}_{i\sigma} = \hat{c}_{i\sigma}^{\dagger} \hat{c}_{i\sigma}$. This simplification originates from the valence orbitals of transition and metal earth atoms. Given their narrow spatial distribution, it is presumed that the intra-atomic electronic interaction is larger than the inter-atomic one for solids composed of these elements. Altogether, the homogeneous (*i.e.* all sites are identical) one-dimensional Hubbard Hamiltonian takes the following form,

$$\hat{H}_{Hubbard} = -t \sum_{\sigma=\uparrow,\downarrow} \sum_{i=0}^{L-1} \left(\hat{c}_{i\sigma}^{\dagger} \hat{c}_{(i+1)\sigma} + \text{H.c.} \right) + U \sum_{i=0}^{L-1} \hat{n}_{i\sigma} \hat{n}_{i\sigma'} - \mu \sum_{i} \hat{n}_{i}, \tag{3.3}$$

where $\hat{n}_i = \hat{n}_{i\sigma} + \hat{n}_{i\sigma'}$ is the occupation operator on site i with $\hat{n}_{i\sigma} = \hat{c}_{i\sigma}^{\dagger} \hat{c}_{i\sigma}$ and μ is the chemical potential which controls the electron filling in the system. It is considered for grand canonical calculations, and omitted otherwise. In the HM, two energy contributions are competing: the kinetic and electron interaction energies. The model aims at understanding the subtle balance between the delocalized and localized states of these compounds. Thus, the ground state behavior of the HM is governed by two parameters: the correlation strength parameter U/t but also the

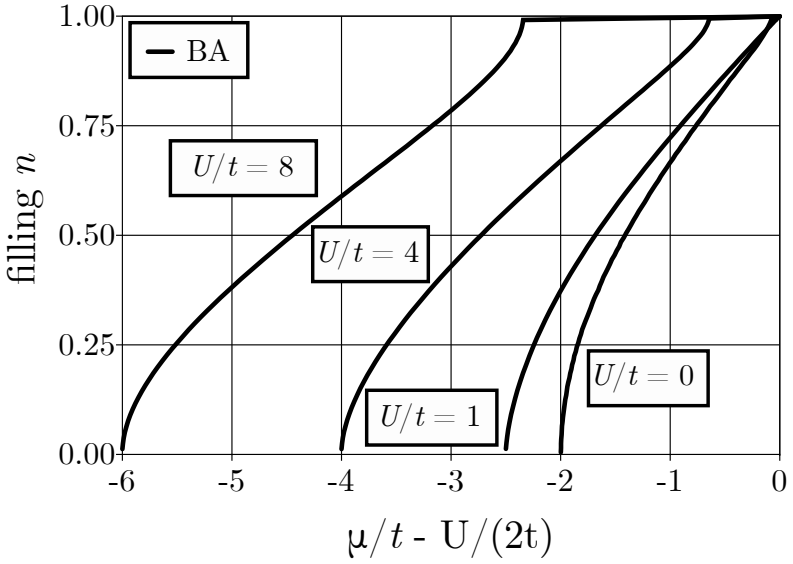

Figure 3.1: Exact ground state lattice filling n as a function of the chemical potential μ obtained by E. H. Lieb and F. Y. Wu (*Bethe Ansatz*). At half-filling, the ground state in insulating for any nonzero U and conducting for U=0.

electron density $n = N/L$.

In 1968, E. H. Lieb and F. Y. Wu provided exact results for the ground state[35] of the one-dimensional Hubbard model described by the Eq. (3.3). Among them, they have shown that the ground state for the half-filled case (*i.e.* N=L) is insulating for any nonzero U which demonstrates that the insulating nature of the half-filled 1D Hubbard lattice is driven entirely by electron-electron interactions. The phase transition from the metallic phase (U=0) to the Mott insulating state is referred to as the *Mott-Hubbard transition* and is of unconventional nature. Therefore, despite its apparent simplicity, the HM is able to catch a large spectrum of physical phenomena and convey the possibility to use the Hubbard model as a benchmark for the development of new methods including quantum chemical ones.

3.2 Single Impurity Anderson Model

In its simplest form, the single impurity Anderson model[80] (SIAM) was developed in order to model the interplay between charge and spin fluctuations of a local-

ized interacting impurity within a non-interacting metallic environment. In such a system, the interaction between the conduction electrons with the impurity can lead to anomalous change of electrical resistivity with temperature, known as the Kondo effect.[81] Nonetheless, its presentation here is related to the major role it plays in quantum embedding. In the well-established *dynamical mean-field theory* (DMFT) [See Section 4.2.1], the Hubbard Hamiltonian [See Section 3.1] is mapped onto a SIAM Hamiltonian one in order to retrieve properties of strongly correlated extended systems. The SIAM[80] Hamiltonian reads [See Figure 3.2],

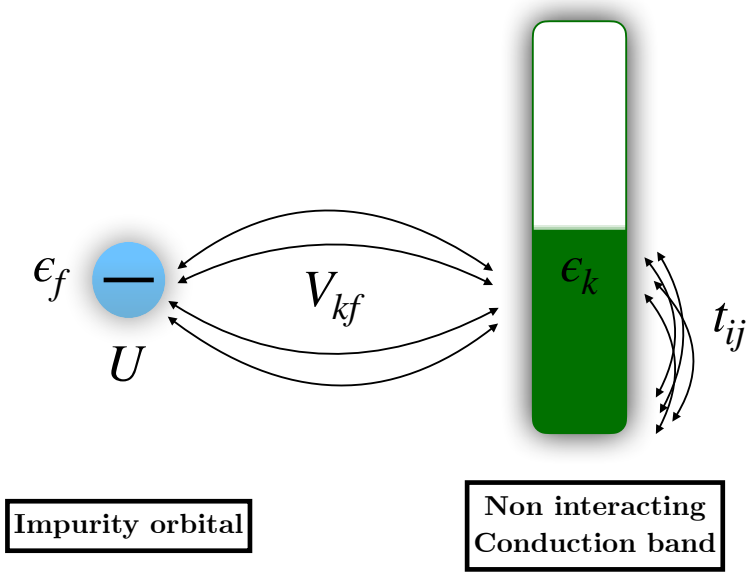

Figure 3.2: Schematic representation of the single impurity Anderson model.

$$\hat{H}_{SIAM} = \hat{H}_{cond} + \hat{H}_{imp} + \hat{W}_{ee}. \tag{3.4}$$

The first term on the r.h.s. is the energy of the free-electron medium which represents the single-particle electronic structure of the relevant valence electrons in the host metal (*i.e.* conduction band). In its most simple form, one can consider this delocalized medium as a collection of non-interacting atomic orbitals,

$$\begin{aligned} \hat{H}_{cond} &= \sum_{k\sigma} \epsilon_k \hat{c}^{\dagger}_{k\sigma} \hat{c}_{k\sigma} \\ &= \sum_{\langle i,j \rangle \sigma} \epsilon^s_i \hat{a}^{\dagger}_{i\sigma} \hat{a}_{i\sigma} + t_{ij} \hat{a}^{\dagger}_{i\sigma} \hat{a}_{j\sigma}, \end{aligned} \tag{3.5}$$

where each electrons on site i has the energy level ϵ^s_i and can move to one of its nearest-neighbor (NN) thanks to the hopping parameter t_{ij}. The second term on the

r.h.s. of Eq. (3.4) is the interaction between the impurity and the metal contribution,

$$\hat{H}_{imp} = \sum_{\sigma} \epsilon_f \hat{f}^{\dagger}_{\sigma} \hat{f}_{\sigma} + \sum_{k\sigma} V_{kf} \left(\hat{c}^{\dagger}_{k\sigma} \hat{f}_{\sigma} + \hat{f}^{\dagger}_{\sigma} \hat{c}_{k\sigma} \right). \tag{3.6}$$

The localized impurity f orbital has an energy ϵ_f and an hybridization energy term V_{kf} which couples the medium to the impurity orbital. Finally, the last term in Eq. (3.4) is the Coulomb interaction between two electrons occupying the localized f orbital,

$$\hat{W}_{ee} = U \hat{n}_{f\sigma} \hat{n}_{f\sigma'}. \tag{3.7}$$

Among the various applications of the SIAM, it is used for instance to model impurities in semiconductor[82], molecular junction[83,84,85] or single-electron transistor[86]. The challenge here is to tackle the "bath" which can consist of an infinite number of orbitals. Many approaches exist in order to solve the SIAM Hamiltonian, among them we can refer to[1]: *exact diagonalization*[87], *CISD*[88], *quantum monte carlo* (QMC)[89,90,91,92,93], *density matrix renormalization group* (DMRG)[94,95] or *iterative perturbation theory* (IPT)[24].

[1] cited articles are related to the resolution of SIAM within the DMFT context.

Chapter 4

Review of quantum embedding approaches

Despite the increasing computational power available, applying *full configuration interaction* (FCI) calculations for large molecular systems or extended systems remain intractable (*i.e.* exponential wall problem [See Section 2.2]). Among the various ideas to overcome these shortcomings, embedding theories have shown to be highly effective in a large variety of applications. The philosophy of embedding is to divide a molecule or a solid into smaller and less-costly subsystems (*i.e.* fragments). Each of these fragments is embedded into a bath, which is a simplification of the true environment. An accurate description of the fragment is only possible by taking into account in a simpler way its interaction with the environment. Obviously, there is no unique definition of the quantum bath. Moreover, the targeted quantity in the fragment (density, the density matrix, the Green's function,...) explains the large number of embedding scheme in the literature. In this section, two popular partitioning approach will be presented, real space and orbital space partitioning.

4.1 Real space partitioning

We would like here to introduce some embedding methods where the partition occurs in real space. Note that this description follows an historical approach and is far from being exhaustive. One of the first ideas was to manipulate the key ingredient of DFT, the density $n(\boldsymbol{r})$. Partitioning a system by using a measurable real-space

quantity seems quite intuitive and on top of that, it offers the possibility to follow chemical intuitions. Back in 1972, R. G. Gordon and Y. S. Kim proposed a simple embedding model to calculate forces between closed-shell atoms and molecules[96]. Under the assumption that there is no distortion of the atomic electronic densities, the total electron density of two interacting atoms A and B is taken as the sum of the two atomic densities,

$$n(\boldsymbol{r}) = n^{(A)}(\boldsymbol{r}) + n^{(B)}(\boldsymbol{r}). \tag{4.1}$$

Coulombic interactions are calculated using this assumption and remaining contributions including kinetic energy, electron exchange and correlation are evaluated from the *local density approximation* (LDA) functional. It is worth mentioning that the authors were already enthusiastic to perform calculations that "take very little computer time" (*i.e.* 4 to 8 seconds to calculate the interaction potential at one internuclear separation). While this simple approach allows to effectively reduce the computational cost, it still contained limitations. For example, the full potential energy surface was only described by inclusion of long-range induction and dispersion forces[97,98]. This approach was further improved by the construction of several self-consistent density-functional formulations[99,100,101] which led to the development of *subsystem density functional theory*[99] and *frozen-density embedding* (FDE)[101]. Note that both of these methods have been recently reviewed by C. R. Jacob, J. Neugebauer[102] and A. S. P. Gomes[103].

In *subsystem DFT*, the full system is split into subsystems I and their densities $n^{(I)}(\boldsymbol{r})$ should add up to the total density $n_{tot}(\boldsymbol{r})$.

$$n_{tot}(\boldsymbol{r}) = n(\boldsymbol{r}) = \sum_I n^{(I)}(\boldsymbol{r}), \tag{4.2}$$

Following the KS strategy, each subsystem is represented by a fictitious subsystem of non-interacting particles and its density takes the following form [See Eq. 2.21],

$$n^{(I)}(\boldsymbol{r}) = \sum_{i_I}^{N_I} |\phi_{i_I}(\boldsymbol{r})|^2, \tag{4.3}$$

where the summation runs over each orbital i_I of the corresponding subsystem I. Note that it can be generalized to subsystems with fractional electron numbers[104]. In

the most simple case, the total density is partitioned into the electron densities of the active subsystem $n^{(I)}(\boldsymbol{r})$, *i.e* a specific subsystem of interest, and the environment density $n^{(II)}(\boldsymbol{r})$. This allows to decompose the total energy of DFT into three terms,

$$E_{tot} = E[n^{(I)}, n^{(II)}] = E^{(I)} + E^{(II)} + E^{(int)}, \tag{4.4}$$

where the first two terms on the r.h.s. account for the energy contribution of each subsystems. More precisely, for (j= I, II),

$$E^{(j)} = E^{(j)}_{NN} + \int d^3\boldsymbol{r} n^{(j)}(\boldsymbol{r}) v^{(j)}_{ne}(\boldsymbol{r}) + \frac{1}{2}\int d^3\boldsymbol{r} d^3\boldsymbol{r}' \frac{n^{(j)}(\boldsymbol{r}) n^{(j)}(\boldsymbol{r}')}{|\boldsymbol{r}-\boldsymbol{r}'|} + E_{xc}[n^{(j)}] + T_s[n^{(j)}], \tag{4.5}$$

where $E^{(j)}_{NN}$ is the repulsion energy between nuclei and the last term on the r.h.s. of Eq. (4.4) corresponds to the interaction energy,

$$\begin{aligned} E_{int} = E_{int}[n^{(I)}, n^{(II)}] = E^{(int)}_{NN} &+ \int d^3\boldsymbol{r} n^{(I)}(\boldsymbol{r}) v^{(II)}_{ne}(\boldsymbol{r}) \\ &+ \int d^3\boldsymbol{r} n^{(II)}(\boldsymbol{r}) v^{(I)}_{ne}(\boldsymbol{r}) + \int d^3\boldsymbol{r} d^3\boldsymbol{r}' \frac{n^{(I)}(\boldsymbol{r}) n^{(II)}(\boldsymbol{r}')}{|\boldsymbol{r}-\boldsymbol{r}'|} \\ &+ T^{nad}_s[n^{(I)}, n^{(II)}] + E^{nad}_{xc}[n^{(I)}, n^{(II)}], \end{aligned} \tag{4.6}$$

The first four terms correspond to all remaining classical electrostatic interactions in-between the two subsystems and the last two terms are referred to as the non-additive non-interacting kinetic energy and exchange-correlation functionals. They originate from the approximation made in Eq. (4.5) that the total non-interacting kinetic energy functional can be decomposed into the sum of the subsystem kinetic energies,

$$T_s[n] \approx \sum_j T_s[\{n^{(j)}\}]. \tag{4.7}$$

This decomposition can be made formally exact by adding the missing complementary term, *i.e.* the non-additive term (*nad*),

$$T^{nad}_s[n^{(I)}, n^{(II)}] = T_s[n] - \sum_j T_s[\{n^{(j)}\}]. \tag{4.8}$$

Note that this decomposition is in principle exact. The evaluation of the energy is realized by minimizing the energy expression with respect to orbitals of the chosen subsystem j while keeping frozen the densities of the other subsystems, *i.e. Kohn-Sham equations with constrained electron density* (KSCED),

$$\left(-\frac{\boldsymbol{\nabla}^2}{2} + v^{(j)}_{eff}[n^{(j)}](\boldsymbol{r}) + v^{(j)}_{emb}[n^{(j)}, n_{tot}](\boldsymbol{r})\right)\phi_{i_j}(\boldsymbol{r}) = \epsilon_{i_j}\phi_{i_j}(\boldsymbol{r}), \tag{4.9}$$

where $v_{eff}^{(j)}[n^{(j)}](\boldsymbol{r})$ contains all the terms that are present in a KS-DFT calculation for the subsystem j,

$$v_{eff}^{(j)}[n^{(j)}](\boldsymbol{r}) = v_{ne}^{(j)}(\boldsymbol{r}) + v_H[n^{(j)}](\boldsymbol{r}) + v_{xc}[n^{(j)}](\boldsymbol{r}), \tag{4.10}$$

and $v_{ne}^{(j)}(\boldsymbol{r})$ contains all nuclei assigned to the subsystem j. The additional embedding potential for the system j is given by,

$$\begin{aligned} v_{emb}^{(j)}[n^{(j)}, n_{tot}](\boldsymbol{r}) = &\sum_{I \neq j} v_{ne}^{(I)}(\boldsymbol{r}) + v_H[n_{tot} - n^{(j)}](\boldsymbol{r}) \\ &+ v_{xc}^{nad}[n^{(j)}, n_{tot}](\boldsymbol{r}) + v_{kin}^{nad}[n^{(j)}, n_{tot}](\boldsymbol{r}). \end{aligned} \tag{4.11}$$

In these equations there are terms coupling the constrained and the non-constrained electrons densities which are not present in regular KS-DFT, namely the non-additive exchange-correlation and non-additive kinetic energy functionals. Their role is to describe all the effects that are not present in the study of a chosen subsystem. Hence, in *subsytem DFT*, the densities of all fragments are self-consistently optimized.

Frozen density embedding (FDE) is an approximation of subsystem DFT where one particular subsystem is considered to be embedded in an effective environment potential. In FDE, the electron density is partitioned into an active subsystem and a frozen environment part. The total density reads,

$$n_{tot}(\boldsymbol{r}) = n_{active}(\boldsymbol{r}) + n_{environment}(\boldsymbol{r}). \tag{4.12}$$

In FDE, only the density of the active subsystem is optimized. It has been observed that the assumption to keep the environment density frozen was not valid. Indeed, both the active and the environment densities change when taking different geometries of molecular complex. Thus, the so called *free-and-thaw* was introduced[105] in order to alternatively freeze the active and environment part until self-consistency is reached. The non-uniqueness of the density partitioning was solved by A. Wasserman in *partition density functional theory* (PDFT)[106,104] followed by E. A. Carter[107,108] by using a unique embedding potential for all subsystems. This common potential could be seen as an interaction potential between them.

In order to treat systems for which DFT fails (*e.g.* strongly correlated systems), a strict formal derivation of WFT-in-DFT embedding within the theoretical framework of DFT has been given by T. A. Wesolowksi[109]. WFT-in-DFT embedding scheme based on subsystem-DFT have been first proposed by E. A. Carter[110,111,112,113]. Projected-based WFT-in-DFT[114,115,116] embedding has also recently gain popularity and has been applied to the study of transition-metal catalysis[117], enzyme reactivity[118], and battery electrolyte decomposition[119].

Applying DFT-in-DFT of WTF-in-DFT embedding schemes offer the possibility to treat large systems and the number of applications is increasing[112,120,121,103]. Nevertheless, despite its conceptual simplicity, these approaches inherit limitations intrinsic to all combinations of wave functions with density functional approximations which could result with the so-called "double counting" problem. Another disadvantage of DFT embedding is the lack, by definition, of off-diagonal density matrix correlations (*i.e.* coherence and entanglement). An alternative is to use embedding theories of richer quantum variables with off-diagonal correlations, such as the single-particle Green's function or the density matrix. These quantities are often the central variables in the orbital space partitioning and will be the subject of the next section.

4.2 Orbital space partitioning

In condensed matter physics, several theoretical approaches to study strongly correlated systems start from Hamiltonians on discrete lattices such as the *Hubbard* [See Section 3.1] and the *Anderson models* [See Section 3.2] and investigate the localized character of electronic states by means of a local Coulomb repulsion. In the following, we will present two popular approaches, the *dynamical mean-field theory* and (DMFT) and the *density matrix embedding theory* (DMET).

4.2.1 Dynamical Mean-Field Theory

Dynamical mean-Field theory (DMFT)[24,25,122,123,88] has been successfully able to catch many physical properties of strongly correlated materials. The purpose of this section is to provide the reader a simple introduction to the basic ingredients of DMFT.

The main variable of DMFT is the (zero temperature, for simplicity) single-particle Green's function (GF) which reads,

$$G(\mathbf{x}, t_1; \mathbf{x}', t_2) \overset{t_1 \geq t_2}{=} -i \langle \Psi_0 | \hat{\Psi}(\mathbf{x}, t_1) \hat{\Psi}^\dagger(\mathbf{x}', t_2) | \Psi_0 \rangle , \tag{4.13}$$

and,

$$G(\mathbf{x}, t_1; \mathbf{x}', t_2) \overset{t_2 \geq t_1}{=} i \langle \Psi_0 | \hat{\Psi}^\dagger(\mathbf{x}', t_2) \hat{\Psi}(\mathbf{x}, t_1) | \Psi_0 \rangle , \tag{4.14}$$

where $|\Psi_0\rangle$ is a N-electron ground state wave function and $\hat{\Psi}(\mathbf{x}, t_i)$ ($\hat{\Psi}^\dagger(\mathbf{x}, t_i)$) are field operators which annihilate (create) an electron at a position/spin $\mathbf{x}$ and at time t_i, respectively. Therefore, depending on the time ordering, the GF contains information on one-electron photoemission spectrum (*i.e.* electron affinity and ionization). Note that this quantity is a time dependent extension of the density matrix. For $t_2 \to t_1^+$,

$$G(\mathbf{x}, t_1; \mathbf{x}', t_2) \overset{t_2 \to t_1^+}{=} i \langle \Psi_0 | \hat{\Psi}^\dagger(\mathbf{x}', t_1) \hat{\Psi}(\mathbf{x}, t_1) | \Psi_0 \rangle = i\gamma(\mathbf{x}', \mathbf{x}). \tag{4.15}$$

The idea behing DMFT is to map the full unsolvable many-body lattice problem onto an impurity problem that can be solved numerically. For that purpose, one selects a single site from the original lattice and model it by a SIAM [See Section 3.2 and Eq. (3.4)]. First considering the non-interacting case, one can construct the Fourier transform of its associated non-interacting GF for the impurity site,

$$\mathcal{G}_0(\omega) = \frac{1}{\omega - \epsilon_0 - \Delta(\omega)}, \tag{4.16}$$

where $\mathcal{G}_0(\omega)$ is now explicitely frequency-dependent and $\Delta(\omega)$ is referred to as the hybridization function which reads,

$$\Delta(\omega) = \sum_k \frac{|V_{k0}|^2}{\omega - \epsilon_k}. \tag{4.17}$$

The hybridization function is the important quantity in DMFT and allows for the electron fluctuations on the impurity (*i.e.* exchange of electrons between the impurity and the bath). Note that it plays the role of the mean-field and is frequency dependent, hence the name d*ynamical mean-field theory*. Its description should correspond to the one of the lattice as the ultimate goal in DMFT is for the interacting impurity GF to be equal to the local GF. Note that the hybridization function has to be determined self-consistently.

Once the non-interacting GF has been calculated, one can estimate the GF associated to the interacting single impurity as follows,

$$G_{imp}(\omega) = \frac{1}{\omega - \epsilon_0 - \Delta(\omega) - \Sigma(\omega)}. \tag{4.18}$$

Evaluating $G_{imp}(\omega)$ will give access to the self-energy $\Sigma(\omega)$, which contains all the many-body effects, thanks to the Dyson equation,

$$\Sigma(\omega) = \mathcal{G}_0^{-1}(\omega) - G_{imp}^{-1}(\omega). \tag{4.19}$$

Note that the true interacting Hubbard lattice self-energy $\Sigma^{\text{lattice}}(k, \omega)$ has no reason to be momentum independent but this approximation is made in DMFT,

$$\Sigma^{\text{lattice}}(k, \omega) \approx \Sigma(\omega). \tag{4.20}$$

where the self-energy on the r.h.s. is obtained from the SIAM according to Eq. (4.19). Using the self-energy approximated with the impurity model, one can calculate the local Green's function in the original lattice,

$$G_{loc}(\omega) = \frac{1}{L} \sum_k \frac{1}{\omega - \epsilon_k - \Sigma(\omega)}. \tag{4.21}$$

Finally, as mentioned earlier, the self-consistency condition in DMFT requires the local Green's function of the lattice to be equal to the one of the impurity,

$$\begin{aligned} & G_{loc}(\omega) = G_{imp}(\omega) \\ \Leftrightarrow & \frac{1}{L} \sum_k \frac{1}{\omega - \epsilon_k - \Sigma(\omega)} = \frac{1}{\omega - \epsilon_0 - \Delta(\omega) - \Sigma(\omega)}. \end{aligned} \tag{4.22}$$

Solving this equation gives access to a new hybridization function $\Delta(\omega)$. Introducing the latter into the SIAM will provide a new interacting Green's function $G_{imp}(\omega)$ that has to be evaluated, thus leading to a new self-energy $\Sigma(\omega)$ according

to Eq. (4.19) and the self-consistent loop continues until convergence.

DMFT is the state-of-the-art method to study strongly correlated extended systems. Several extensions to a cluster version were developed in order to retrieve non-local and short-range correlations. Among them, *dynamical cluster approximation* (DCA)[124], *cellular dynamical mean-field theory* (C-DMFT)[125] and its simplified version *variational cluster approach* (VCA)[126]. DMFT concepts and techniques have been applied, among others, to study manganites, ruthenates, vanadates, actinides, lanthanides, fullerenes, quantum criticality in heavy fermion systems or magnetic semiconductors[122].

Another method of choice to describe strongly correlated systems is the DFT+DMFT method where the main idea is to use the DFT Hamiltonian to define the one body term of the Hubbard model and then supplement it by an exact Coulomb interaction for the correlated orbitals subset. Along the years, this method has provided good agreement to describe a lot of strongly correlated systems properties such as the phase transition[127,128], total energies and phonons[129,130], superconductivity[131,132,133,134,135,136] or spin-orbit effects[137,138,139]. Nevertheless, while DMFT+DFT has proven to be a successful route towards the description of strongly correlated materials, it still suffers of computationally expensive solution for multi-orbital impurity problems. Moreover, as briefly mentioned before, the DMFT works better with high coordination number. While this is not a drastic approximation for extended systems ($\neq$ 1D), it is for molecules. This brings us to the main topic of this thesis, an alternative and simpler formulation of DMFT which can be applied to both strongly correlated materials and molecules, namely the *density matrix embedding theory*[26].

4.2.2 Density Matrix Embedding Theory

Following the ideas of quantum embedding, *density matrix embedding theory* (DMET)[26,27] which has been introduced by G. Chan and K. Knizia, can be seen as a frequency-independent simplification of DMFT. While the latter is an embedding theory for lattices, DMET originally constitutes a possible route towards

static properties of both extended and chemical systems, giving the possibility of using wave function based quantum chemical methods in order to solve quantum many-body problems which are, in general, out of reach.

While in the original DMFT formulation, the interacting lattice problem is mapped onto a single-impurity Anderson problem where the bath consists of an infinite number of orbitals, one considerable advantage of DMET over DMFT is the dractic reduction of the bath's dimension. Note that the nature of the DMET bath has not been defined yet as it could take different forms depending on the level of description of the full system. This will be clarified in the following. We will focus on the ground state theory but extensions to finite temperatures[140], non-equilbrium regimes[141], excited states[142,143] and spin-systems[144,145] have been studied.

Before turning to the construction of the bath in DMET, it is important to review the main properties of the *singular value decomposition* (SVD) as it is the main transformation used in DMET to build the bath.

Singular Value decomposition

The singular value decomposition is the generalization of the eigendecomposition to non-square matrices. Given a matrix $\boldsymbol{A}_{m\times n}$, it takes the following form,

$$\boldsymbol{A} = \boldsymbol{U}\boldsymbol{\Sigma}\boldsymbol{V}^{\dagger}, \tag{4.23}$$

where $\boldsymbol{U}_{m\times m}$ and $\boldsymbol{V}_{n\times n}$ are unitary matrices, $\boldsymbol{\Sigma}_{m\times n}$ only contains diagonal elements σ_i and $\sigma_i > 0$ for $1 \leq i \leq r$ where $r = min(m, n)$.

Columns of $\boldsymbol{U}$ and rows of $\boldsymbol{V}$ are referred to as left and right singular vectors respectively, while the σ_i are the singular values. Given that $\boldsymbol{U}$ and $\boldsymbol{V}$ are nonsingular, Rank($\boldsymbol{A}$) = rank($\boldsymbol{\Sigma}$) = r where r corresponds to the number of non-zero singular values.

For embedding purposes, the orthonormal basis of $\boldsymbol{U}$ and $\boldsymbol{V}$ will be of great

importance. One can relate SVD to eigenvalue decomposition as follows,

$$\begin{aligned} \boldsymbol{A}\boldsymbol{A}^{\dagger} &= \boldsymbol{U}\boldsymbol{\Sigma}\boldsymbol{V}^{\dagger}\boldsymbol{V}\boldsymbol{\Sigma}^{\dagger}\boldsymbol{U}^{\dagger} \\ &= \boldsymbol{U}(\boldsymbol{\Sigma}\boldsymbol{\Sigma}^{\dagger})\boldsymbol{U}^{\dagger} \end{aligned} \tag{4.24}$$

where the non zero diagonal elements of $\boldsymbol{\Sigma}\boldsymbol{\Sigma}^{\dagger}$ read,

$$\boldsymbol{\mathcal{D}} \equiv \left\{\delta_{ii'}\sigma_i^2\right\}. \tag{4.25}$$

Consequently we can split the columns of $\boldsymbol{U}$ as follows,

$$\boldsymbol{U} \equiv (\boldsymbol{U}_1, \boldsymbol{U}_2) = (\boldsymbol{u}_1, ..., \boldsymbol{u}_r, \boldsymbol{u}_{r+1}, ..., \boldsymbol{u}_m), \tag{4.26}$$

and $\boldsymbol{U}_1$ are the eigenvectors of $\boldsymbol{A}\boldsymbol{A}^{\dagger}$ while $\boldsymbol{U}_2$ span the Null space of $\boldsymbol{A}^{\dagger}$. Using the fact that Rank($\boldsymbol{A}$)=r of the matrix $\boldsymbol{A}$ and rewriting Eq. 4.24, one obtains,

$$\boldsymbol{A}\boldsymbol{A}^{\dagger}\boldsymbol{U}_1 = \boldsymbol{U}_1\boldsymbol{\mathcal{D}}, \tag{4.27}$$

and

$$\boldsymbol{A}^{\dagger}\boldsymbol{U}_2 = \boldsymbol{0}. \tag{4.28}$$

Note that Eqs. (4.27) and (4.28) will be of great importance in the construction of the bath and environment orbitals in DMET.

Density Matrix Embedding Theory

The general idea of DMET is to divide a system in two parts, the fragment A and its environment B. The wave function $|\Psi\rangle$ can be expressed in the Hilbert space of their respective states $\{|A_i\rangle\}$ and $\{|B_j\rangle\}$,

$$|\Psi\rangle = \sum_{i}^{N_A}\sum_{j}^{N_B}\Psi_{ij}\,|A_i\rangle\,|B_j\rangle\,, \tag{4.29}$$

where N_A and N_B are the number of many-body states for the fragment $\{|A_i\rangle\}$ and the environment $\{|B_j\rangle\}$, respectively. If $|\Psi\rangle$ is known, one can circumvent the high dimensional problem by taking advantage of the Schmidt Decomposition applied to the coefficient matrix Ψ_{ij},

$$\Psi_{ij} = \sum_{\alpha}^{min(N_A,N_B)} U_{i\alpha}\sigma_{\alpha}V_{\alpha j}^{\dagger}, \tag{4.30}$$

where U and V are unitary matrices and $\{\sigma_\alpha\}$ are the singular values. Let's suppose that the number of states of fragment A is $N_A < N_B$, replacing the coefficient matrix of Eq. (4.29) by the previous decomposition leads to,

$$\begin{aligned} |\Psi\rangle &= \sum_{i}^{N_A}\sum_{j}^{N_B}\sum_{\alpha}^{N_A} U_{i\alpha}\sigma_\alpha V^\dagger_{\alpha j}\,|A_i\rangle\,|B_j\rangle \\ &= \sum_{\alpha}^{N_A}\sigma_\alpha \sum_{i}^{N_A} U_{i\alpha}\,|A_i\rangle \sum_{j}^{N_B} V^\dagger_{\alpha j}\,|B_j\rangle \\ &= \sum_{\alpha}^{N_A}\sigma_\alpha \left|\tilde{A}_\alpha\right\rangle \left|\tilde{B}_\alpha\right\rangle, \end{aligned} \tag{4.31}$$

where the many-body states $\{|A_i\rangle\}$ and $\{|B_j\rangle\}$ have been separately transformed. Most importantly, the number of many-body states describing the environment B has been reduced to those of the fragment A. In this context, the collection of many-body states $\{\tilde{B}_\alpha\}$ is the bath. A new embedded Hamiltonian $\hat{H}^{emb}$ can be constructed by projecting the original full Hamiltonian $\hat{H}$ onto the many-body states of the fragment $\left|\tilde{A}_\alpha\right\rangle$ and the bath $\left|\tilde{B}_\alpha\right\rangle$,

$$\hat{H}_{emb} = \hat{P}\hat{H}\hat{P}, \tag{4.32}$$

where

$$\hat{P} = \sum_{\alpha\beta}\left|\tilde{A}_\alpha\tilde{B}_\beta\right\rangle\left\langle\tilde{A}_\alpha\tilde{B}_\beta\right|. \tag{4.33}$$

Nevertheless, the construction is based upon the assumption that the exact ground state wave function $|\Psi\rangle$ is known, which is obviously not the case, otherwise there would be no point in performing an embedding.

In practical DMET calculations, the general idea is to treat the full system with a computationally affordable method such as *Hartree-Fock* method or *density functional theory* and self-consistently improve the description of each fragment of the partition with an exact diagonalization of the embedded Hamiltonian. The main advantage of this approximation is that the fragment and the bath are now defined as single-particle basis. Moreover, due to the local character of strong correlations, the full problem is nearly transformed into a CASCI one where the fragment orbitals (the so-called impurities) and the bath ones are part of the active

orbital space [See Section 2.2] which can be treated with high accuracy quantum chemistry methods.

The first goal of DMET is to identify a subsystem (consisting of the fragment and one-electron quantum bath subspace) that is, ideally, strictly disentangled from its environment. To this point, we will not follow the original derivations of DMET where the SVD is applied to the coefficient matrix between the occupied molecular spin-orbitals and the localized fragment ones[39] but we will exclusively work in the localized spin-orbitals basis. The purpose is to avoid the construction of bath spin-orbitals directly from the wave function but use the reduced density matrix functional theory formalism. Therefore, the bath is a simple (as explicit as possible) functional of the density matrix (written in the localized basis). This allows the use of correlated density matrices which could be used in the future to connect DMET to RDMFT. This choice is interesting as it will allow us to connect DMET bath orbitals to the ones obtained by means of the *Householder transformation*[36,37] in the new embedding scheme proposed by the author and its collaborators [See Section 5.3].

Quantum bath from the singular value decomposition of density matrix blocks

Our key ingredient is the density matrix of the full system written in the lattice (or localized molecular spin-orbital) representation,

$$\boldsymbol{\gamma} \equiv \left\{ \gamma_{ij} = \left\langle \hat{c}_i^\dagger \hat{c}_j \right\rangle \right\}_{1 \leq i,j \leq L}, \tag{4.34}$$

that we write in blocks as follows, for convenience,

$$\boldsymbol{\gamma} = \begin{bmatrix} \boldsymbol{\gamma}_{ff} & \boldsymbol{\gamma}_{ef}^\dagger \\ \boldsymbol{\gamma}_{ef} & \boldsymbol{\gamma}_{ee} \end{bmatrix}. \tag{4.35}$$

where $\boldsymbol{\gamma}_{ff} \equiv \{\gamma_{ij}\}_{1 \leq i,j \leq L_{frag}}$ is the fragment block that describes the to-be-embedded L_{frag} spin-orbitals. The latter are usually referred to as the *impurities*.

Note that the indices f and e in Eq. (4.35) do not refer to specific matrix elements. They have been introduced in order to easily identify the matrix blocks

(in bold) and their dimensions. For example, the environment-fragment block reads $\boldsymbol{\gamma}_{ef} \equiv \{\gamma_{ij}\}_{L_{\text{frag}}<i\leq L, 1\leq j\leq L_{\text{frag}}}$. The fact that it is non-zero obviously prevents us from treating the fragment as a separate subsystem. Nevertheless, we can identify a one-electron subspace which corresponds to the bath to which the fragment will, ultimately, be exclusively entangled. For that purpose, we consider the SVD of $\boldsymbol{\gamma}_{ef}$,

$$\boldsymbol{\gamma}_{ef} = \boldsymbol{U}_{ee}\boldsymbol{\sigma}_{eb}\boldsymbol{V}^{\dagger}_{fb}, \tag{4.36}$$

where

$$\boldsymbol{\sigma}_{eb} = \begin{bmatrix} \boldsymbol{\mathcal{D}}^{\frac{1}{2}} \\ \mathbf{0}_{\mathcal{E}b} \end{bmatrix}, \tag{4.37}$$

and

$$\boldsymbol{\mathcal{D}} \equiv \left\{\delta_{bb'}\sigma_b^2\right\}, \tag{4.38}$$

is the $L_{\text{frag}} \times L_{\text{frag}}$ diagonal matrix of the (nonzero) squared singular values. We implicitly assumed in Eq. (4.36) that the dimension of the fragment is (significantly in practice) smaller than the one of its environment, *i.e.*, $L_{\text{frag}} < L - L_{\text{frag}}$ or, equivalently, $L_{\text{frag}} < \frac{L}{2}$. This is always the case in practical calculations where L_{frag} is taken as small as possible in order to reduce the computational cost of the embedding calculation. Note that $\sigma_b > 0$, is obtained by diagonalizing the Hermitian $L_{frag} \times L_{frag}$ matrix $\boldsymbol{\gamma}^{\dagger}_{ef}\boldsymbol{\gamma}_{ef}$ [See Eq. (4.24)], *i.e.*,

$$\boldsymbol{U}^{\dagger}\boldsymbol{\gamma}^{\dagger}_{ef}\boldsymbol{\gamma}_{ef}\boldsymbol{U} = \boldsymbol{\mathcal{D}}, \tag{4.39}$$

with $\boldsymbol{U}^{\dagger}\boldsymbol{U} = \boldsymbol{U}\boldsymbol{U}^{\dagger} = \mathbf{1}_f$.

The column vectors of $\boldsymbol{U}$ can be decomposed as [See Eq. (4.26)],

$$\boldsymbol{U}_{ee} = \begin{bmatrix} \boldsymbol{U}_{eb} & \boldsymbol{U}_{e\mathcal{E}} \end{bmatrix}. \tag{4.40}$$

From this expression, we will construct the quantum bath. Starting from Eq. (4.39) one has,

$$\begin{aligned} \boldsymbol{\gamma}^{\dagger}_{ef}\boldsymbol{\gamma}_{ef} &= \boldsymbol{U}\boldsymbol{\mathcal{D}}\boldsymbol{U}^{\dagger} \\ \boldsymbol{\gamma}_{ef}\boldsymbol{\gamma}^{\dagger}_{ef}\boldsymbol{\gamma}_{ef} &= \boldsymbol{\gamma}_{ef}\boldsymbol{U}\boldsymbol{\mathcal{D}}\boldsymbol{U}^{\dagger}, \end{aligned} \tag{4.41}$$

or equivalently,

$$\boldsymbol{\gamma}_{ef}\boldsymbol{\gamma}^{\dagger}_{ef}(\boldsymbol{\gamma}_{ef}\boldsymbol{U}) = (\boldsymbol{\gamma}_{ef}\boldsymbol{U})\boldsymbol{\mathcal{D}}, \tag{4.42}$$

which has the form of an eigenvalue equation with $\boldsymbol{\mathcal{D}}$ the eigenvalues and $\boldsymbol{\gamma}_{ef}\boldsymbol{U}$ their associated eigenvectors. Note the latter are not orthonormalized,

$$\boldsymbol{U}^\dagger\boldsymbol{\gamma}_{ef}^\dagger\boldsymbol{\gamma}_{ef}\boldsymbol{U} = \boldsymbol{U}^\dagger\boldsymbol{U}\boldsymbol{\mathcal{D}}\boldsymbol{U}^\dagger\boldsymbol{U} = \boldsymbol{\mathcal{D}}. \tag{4.43}$$

Consequently, one can rewrite Eq. (4.42) as,

$$\begin{aligned}
\boldsymbol{\gamma}_{ef}\boldsymbol{\gamma}_{ef}^\dagger(\boldsymbol{\gamma}_{ef}\boldsymbol{U}) &= (\boldsymbol{\gamma}_{ef}\boldsymbol{U})\boldsymbol{\mathcal{D}} \\
\boldsymbol{\gamma}_{ef}\boldsymbol{\gamma}_{ef}^\dagger(\boldsymbol{\gamma}_{ef}\boldsymbol{U})\boldsymbol{\mathcal{D}}^{-\frac{1}{2}} &= (\boldsymbol{\gamma}_{ef}\boldsymbol{U})\boldsymbol{\mathcal{D}}\boldsymbol{\mathcal{D}}^{-\frac{1}{2}} \\
\boldsymbol{\gamma}_{ef}\boldsymbol{\gamma}_{ef}^\dagger(\boldsymbol{\gamma}_{ef}\boldsymbol{U}\boldsymbol{\mathcal{D}}^{-\frac{1}{2}}) &= (\boldsymbol{\gamma}_{ef}\boldsymbol{U}\boldsymbol{\mathcal{D}}^{-\frac{1}{2}})\boldsymbol{\mathcal{D}},
\end{aligned} \tag{4.44}$$

where according to Eq. (4.27), the orthonormalized quantum bath is defined as,

$$\boldsymbol{U}_{eb} = \boldsymbol{\gamma}_{ef}\boldsymbol{\mathcal{U}}\boldsymbol{\mathcal{D}}^{-\frac{1}{2}}. \tag{4.45}$$

Note that by construction,

$$\boldsymbol{U}_{eb}^\dagger\boldsymbol{U}_{eb} = \boldsymbol{\mathcal{D}}^{-\frac{1}{2}}\boldsymbol{\mathcal{U}}^\dagger\boldsymbol{\gamma}_{ef}^\dagger\boldsymbol{\gamma}_{ef}\boldsymbol{\mathcal{U}}\boldsymbol{\mathcal{D}}^{-\frac{1}{2}} = \mathbf{1}_{ff}. \tag{4.46}$$

The cluster's environment could also be build from $\boldsymbol{\gamma}_{ef}$ following Eq. (4.28),

$$\boldsymbol{\gamma}_{ef}^\dagger\boldsymbol{U}_{e\mathcal{E}} = \mathbf{0}_{f\mathcal{E}}. \tag{4.47}$$

The above orthogonality constraint is central. It separates the environment (e) of the fragment into bath (b) and cluster's environment ($\mathcal{E}$) spin-orbital subspaces. For convenience, we consider the basis used for $\mathcal{E}$, which is implicitly defined *via* the orthogonality constraint of Eq. (4.47), to be orthonormal, *i.e.*,

$$\boldsymbol{U}_{e\mathcal{E}}^\dagger\boldsymbol{U}_{e\mathcal{E}} = \mathbf{1}_{\mathcal{E}}. \tag{4.48}$$

Note that, since

$$\boldsymbol{\gamma}_{ef}\boldsymbol{\gamma}_{ef}^\dagger\boldsymbol{U}_{eb} = \boldsymbol{U}_{eb}\boldsymbol{\mathcal{D}}, \tag{4.49}$$

it comes

$$\begin{aligned}
\boldsymbol{U}_{e\mathcal{E}}^\dagger\boldsymbol{\gamma}_{ef}\boldsymbol{\gamma}_{ef}^\dagger\boldsymbol{U}_{eb} &= \boldsymbol{U}_{e\mathcal{E}}^\dagger\boldsymbol{U}_{eb}\boldsymbol{\mathcal{D}} \\
&= \left(\boldsymbol{\gamma}_{ef}^\dagger\boldsymbol{U}_{e\mathcal{E}}\right)^\dagger\boldsymbol{\gamma}_{ef}^\dagger\boldsymbol{U}_{eb} \\
&= \mathbf{0}_{\mathcal{E}b},
\end{aligned} \tag{4.50}$$

according to Eq. (4.47) thus leading to

$$\boldsymbol{U}_{e\mathcal{E}}^{\dagger}\boldsymbol{U}_{eb} = \mathbf{0}_{\mathcal{E}b}, \tag{4.51}$$

which implies with Eqs. (4.46) and (4.48) that $\boldsymbol{U}_{ee}$ is unitary, as expected.

To resume, we observed that in DMET, once we have defined the fragment to embed, two set of spin-orbitals can be constructed from the environment-fragment density matrix block $\boldsymbol{\gamma}_{ef}$. The fragment will only be entangled to the bath but the latter, in general, can be entangled with the cluster's environment. The structure of the density matrix in the new representation strongly depends on the level of description of the full system under study. In the following, we will articulate several interesting properties which will be derived in details in Section 5.2.2. More precisely, in the standard approach, the description of the full system is at the mean-field level (*i.e.* $|\Psi\rangle \approx |\Phi\rangle$ (single determinant)) where the associated density matrix is idempotent in the new (embedding) representation (*i.e.* $\tilde{\boldsymbol{\gamma}} = \tilde{\boldsymbol{\gamma}}^2$). In this case, the resulting density matrix in the new representation will be composed of two strictly disentangled blocks [See Figure 5.4]. The first block is half-filled and composed of the fragment and bath orbitals and is generally referred to as the cluster. The second block is referred to as the cluster's environment and is composed of the remaining occupied and unoccupied orbitals. The decoupling is exact for an idempotent density matrix and therefore for non-interacting (or mean-field) electrons and will be largely discussed in Section 5.2.2. Introduction of electronic interaction within the cluster leads to a partitioning similar to a CAS-CI calculations [See Section 2.2 and Fig. 4.1] where the active space is composed of the fragment and bath spin-orbitals, the core spin-orbitals are those which are occupied in the cluster's environment while the virtual spin-orbitals are the unoccupied.
The separation of a set of spin-orbitals from the rest of the system allows to apply high accuracy quantum chemistry electronic structure methods within a reduced-in-size block of the full size original system. These calculations consist in improving the original mean-field description of the full system and bring us to the second most important aspect of DMET, the self-consistency.

In DMET, we have seen that there is an original mean-field description of

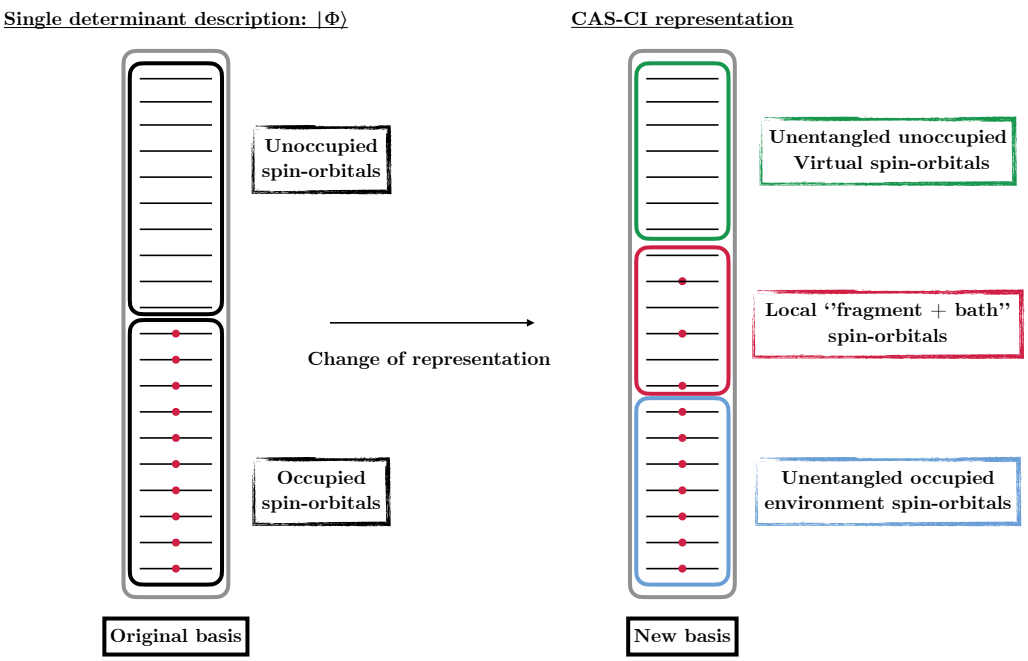

Figure 4.1: Schematic representation of the transformation of the original problem into a CAS-CI one. Inspired by S. Wouters *et al.*[39].

the full lattice corresponding to a given Hamiltonian $\hat{h}$ and its associated ground state wave function $|\Phi\rangle$. On the other hand, taking another representation allows to embed the fragment spin-orbitals within bath ones and both of them are totally decoupled from the cluster's environment. This subsystem, denoted x, is described by an interacting embedding Hamiltonian $\hat{H}_x$,

$$\hat{H}^x = \sum_{ij}^{L_{A_x}+L_{B_x}} \tilde{h}^x_{ij} \hat{d}^\dagger_i \hat{d}_j + \frac{1}{2} \sum_{ijkl}^{L_{A_x}} \tilde{g}^x_{ijkl} \hat{d}^\dagger_i \hat{d}^\dagger_j \hat{d}_l \hat{d}_k, \tag{4.52}$$

where L_{A_x} (L_{B_x}) denotes the number of spin-orbitals within the fragment (associated bath) x. It is treated with high accuracy methods such as FCI resulting in its associated ground state wave function $|\Psi_x\rangle$. The purpose of DMET is to self-consistently improve the original mean-field description $|\Phi\rangle$. To this point, both Hamiltonians are connected by a correlation potential (CF) $\hat{C}_x$,

$$\hat{H}^x = \hat{h} + \hat{C}_x, \tag{4.53}$$

where $\hat{h}$ is the original mean-field Hamiltonian and $\hat{C}_x$ reads,

$$\hat{C}_x = \sum_{ij \in A_x} u^x_{ij} \hat{c}^\dagger_i \hat{c}_j. \tag{4.54}$$

The matrix elements u_{ij}^{x} are adjusted such that the density matrix of $|\Phi\rangle$ matches the one associated with $|\Psi_x\rangle$. In other words, the correlation potential mimics the effect of the two-electron repulsion in the cluster x on the density matrix associated with the mean-field like description. It is thought as a non-local version of the KS potential which of course raises fundamental questions related to representability [See Section 2.4] as it is not possible to map a non-idempotent density matrix obtained from a correlated wave function onto an idempotent one extracted from a mean-field wave function.

In the DMET self-consistent procedure, the correlation potential can take several forms. In the original formulation of DMET, a cost function CF is built such that the density matrices match to the maximum extent,

$$CF_{mat}(u) = \min_{u} \sum_{x}^{fragments} \sum_{ij \in x} (\gamma_{ij}^{x} - \gamma_{ij}^{mf})^2, \tag{4.55}$$

while in the density embedding theory[38,40], Bulik *et al.* decided to map only the densities (*i.e.* diagonal elements of the density matrix),

$$CF_{dens}(u) = \min_{u} \sum_{x}^{fragments} \sum_{i \in x} (\gamma_{ii}^{x} - \gamma_{ii}^{mf})^2. \tag{4.56}$$

Interestingly, these CFs and their associated minimizing matrix elements u_{ij}^{x} in Eq. (4.54) will determine at each step the new mean-field description $|\Phi\rangle$ and consequently the density matrix elements γ_{ij}^{mf} but also the construction of the new bath spin-orbitals and therefore the correlated density matrix γ_{ij}^{x}. At convergence, the one- and two-electron reduced density matrices of each local fragments are evaluated and collected,

$$\begin{aligned} \left\langle \hat{c}_i^{\dagger} \hat{c}_j \right\rangle_{\{i,j\} \in x} &= \gamma_{ij}^{x}, \\ \left\langle \hat{c}_i^{\dagger} \hat{c}_j^{\dagger} \hat{c}_l \hat{c}_k \right\rangle_{\{i,j,k,l\} \in x} &= \Gamma_{ijkl}^{x}, \end{aligned} \tag{4.57}$$

in order to evaluate the total energy by summation over the fragments, in the so-called "democratic" way[39].

Note that while we described the original framework of DMET, many different flavors exist. For instance, the mean-field description of the full system can

be done with a non-interacting Hamiltonian and explicit connection with DFT can be made [See Section 7]. Moreover, the accurate description of the local fragment can be done within the so-called interacting or non-interacting bath formulation but this is discussed later [See Section 6.2]. We can also incorporate quantum fluctuations through a (truncated) description of the effective dynamics[146].

To conclude, DMET provides a simple and efficient way to construct bath spin-orbitals allowing the use of the existing quantum chemistry many-body solvers. Moreover, it also provides many ways to perform the self-consistent loop necessary to the improvement of the mean-field description of the full system. In the next chapter, we will focus on these two aspects. First we will discuss another way to construct the bath and clarify their connections with the SVD. Then we will focus on how we may circumvent the ill-defined self-consistent procedure, for example, by making exact the *density embedding theory* in the context of DFT.

Chapter 5

Density matrix functional construction of a one-electron quantum bath

In this section, we will successively present the *Householder* and *block-Householder transformations* which are at the core of the different embedding scheme introduced in Sections 6,7 and 8. These transformations allow to build single or multiple orbitals quantum bath for the selected fragment(s). A first insight will be provided by a geometrical interpretation of these transformations. Then, connection with the density matrix and some interesting properties will be discussed. Note that this section is greatly inspired by the work published by the author and collaborators.[21]

5.1 Householder transformation

In 1958, A. S. Householder developed the *Householder transformation*[36] (HH-t) which is an unitary transformation, and more precisely a reflection. It is mainly used for tridiagonalization or QR decomposition and presents the advantage of requiring less arithmetic operations than the Givens rotation method[147].

5.1.1 Geometrical interpretation

The geometrical point of view will provide us the general framework to build the different components of the HH-t. Given a vector $\boldsymbol{X}$ of dimension $L\times 1$, denoted L

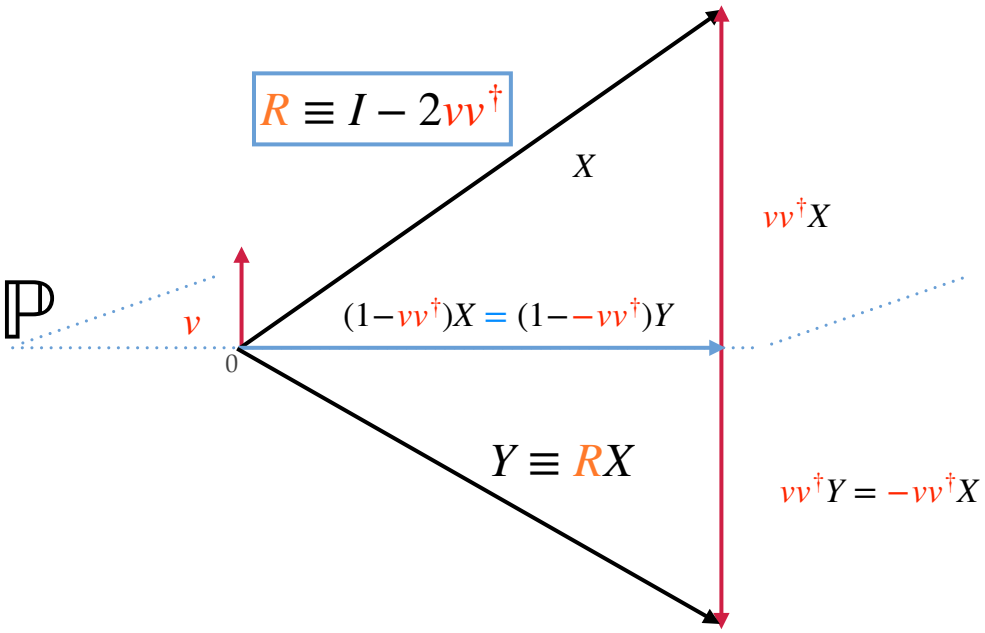

Figure 5.1: Geometrical interpretation of the Householder transformation.

for simplicity, one can define its reflection through the plane or the hyperplane $\mathbb{P}$ that contains the origin. The reflected vector will be denoted as $\boldsymbol{Y}$. The necessary and sufficient condition is to have a unit vector $\boldsymbol{v}/(\boldsymbol{v}^\dagger\boldsymbol{v})$ which is orthogonal to $\mathbb{P}$. Then, as observed in Fig. 5.1, one can build the component of $\boldsymbol{X}$ in direction of $\boldsymbol{v}$ using the following dot product $\boldsymbol{v}(\boldsymbol{v}^\dagger.\boldsymbol{X})$. Consequently, $\boldsymbol{Y}$ is constructed as,

$$\begin{aligned}\boldsymbol{Y} &= \boldsymbol{X} - 2\frac{(\boldsymbol{v}^\dagger\boldsymbol{X})\boldsymbol{v}}{\boldsymbol{v}^\dagger\boldsymbol{v}} \\ &= \boldsymbol{X} - 2\frac{\boldsymbol{v}(\boldsymbol{v}^\dagger\boldsymbol{X})}{\boldsymbol{v}^\dagger\boldsymbol{v}} \\ &= \left(\mathbf{1}_L - 2\frac{\boldsymbol{v}\boldsymbol{v}^\dagger}{\boldsymbol{v}^\dagger\boldsymbol{v}}\right)\boldsymbol{X} \\ &= \boldsymbol{R}(\boldsymbol{v})\boldsymbol{X}.\end{aligned} \tag{5.1}$$

where $\mathbf{1}_{\boldsymbol{L}}$ is the identity matrix. Thus, we obtain the expression of the reflection matrix $\boldsymbol{R}(\boldsymbol{v})$ (*i.e.* Householder matrix) in terms of the unit vector $\boldsymbol{v}/(\boldsymbol{v}^\dagger\boldsymbol{v})$,

$$\boldsymbol{R}(\boldsymbol{v}) = \mathbf{1}_L - 2\frac{\boldsymbol{v}\boldsymbol{v}^\dagger}{\boldsymbol{v}^\dagger\boldsymbol{v}}. \tag{5.2}$$

Note that the latter is Hermitian,

$$\begin{aligned}\boldsymbol{R}(\boldsymbol{v})^\dagger &= \left(\mathbf{1}_L - 2\frac{\boldsymbol{v}\boldsymbol{v}^\dagger}{\boldsymbol{v}^\dagger\boldsymbol{v}}\right)^\dagger \\ &= \mathbf{1}_L^\dagger - 2\left(\frac{\boldsymbol{v}\boldsymbol{v}^\dagger}{\boldsymbol{v}^\dagger\boldsymbol{v}}\right)^\dagger \\ &= \mathbf{1}_L - 2\frac{\boldsymbol{v}\boldsymbol{v}^\dagger}{\boldsymbol{v}^\dagger\boldsymbol{v}} \\ &= \boldsymbol{R}(\boldsymbol{v}),\end{aligned} \tag{5.3}$$

and unitary (real algebra is used).

$$\begin{aligned}\boldsymbol{R}(\boldsymbol{v})\boldsymbol{R}(\boldsymbol{v}) &= \left(\mathbf{1}_L - 2\frac{\boldsymbol{v}\boldsymbol{v}^\dagger}{\boldsymbol{v}^\dagger\boldsymbol{v}}\right)\left(\mathbf{1}_L - 2\frac{\boldsymbol{v}\boldsymbol{v}^\dagger}{\boldsymbol{v}^\dagger\boldsymbol{v}}\right) \\ &= \mathbf{1}_L - 4\frac{\boldsymbol{v}\boldsymbol{v}^\dagger}{\boldsymbol{v}^\dagger\boldsymbol{v}} + 4\frac{(\boldsymbol{v}\boldsymbol{v}^\dagger)(\boldsymbol{v}\boldsymbol{v}^\dagger)}{(\boldsymbol{v}^\dagger\boldsymbol{v})^2} \\ &= \mathbf{1}_L - 4\frac{\boldsymbol{v}\boldsymbol{v}^\dagger}{\boldsymbol{v}^\dagger\boldsymbol{v}} + 4\frac{\boldsymbol{v}(\boldsymbol{v}^\dagger\boldsymbol{v})\boldsymbol{v}^\dagger}{(\boldsymbol{v}^\dagger\boldsymbol{v})^2} \\ &= \mathbf{1}_L,\end{aligned} \tag{5.4}$$

thus,

$$\boldsymbol{R}^{-1}(\boldsymbol{v}) = \boldsymbol{R}(\boldsymbol{v}) = \boldsymbol{R}^\dagger(\boldsymbol{v}). \tag{5.5}$$

Observing that the Householder transformation is $\boldsymbol{v}$-dependent and given two vectors $\boldsymbol{X}$ and $\boldsymbol{Y}$ with the same norm,

$$|\boldsymbol{X}| = \sqrt{\boldsymbol{X}^\dagger\boldsymbol{X}} = \sqrt{\boldsymbol{Y}^\dagger\boldsymbol{Y}} = |\boldsymbol{Y}|, \tag{5.6}$$

one can construct the unitary vector $\boldsymbol{v}/(\boldsymbol{v}^\dagger\boldsymbol{v})$ as following [See Figure 5.1],

$$\boldsymbol{v} = \boldsymbol{v}/(\boldsymbol{v}^\dagger\boldsymbol{v}) = \frac{\boldsymbol{X}-\boldsymbol{Y}}{|\boldsymbol{X}-\boldsymbol{Y}|}. \tag{5.7}$$

For simplicity, we will from now on denote the unit vector $\boldsymbol{v}/(\boldsymbol{v}^\dagger\boldsymbol{v})$ as $\boldsymbol{v}$.

5.1.2 Householder transformation and density matrix embedding

Similarly as in DMET, the main idea of our embedding scheme is to embed a fragment which will be exclusively entangled with the so-called *bath* orbital. Given the *local* character of strong correlation, it is advantageous to rewrite the density

matrix in a localized orbital representation, $\boldsymbol{\gamma}_{ij}^{loc} \equiv \boldsymbol{\gamma}_{ij}$. From this starting point, we will construct an appropriate HH-t to achieve our goal.

In the following, we will define the different phases to embed a given fragment (referred to as site/orbital 0). Given that we are only interested in the singlet ground state, the (spin) density matrix are denoted without spin indices,

$$\boldsymbol{\gamma}_{ij} = \langle \hat{c}_{i\sigma}^{\dagger} \hat{c}_{j\sigma} \rangle = \langle \hat{c}_{i\sigma'}^{\dagger} \hat{c}_{j\sigma'} \rangle. \tag{5.8}$$

All its elements connected to site 0 are collected into the above-mentioned column $\boldsymbol{X}$ [See Figure 5.2], *i.e.*,

$$\boldsymbol{X}^{\dagger} = [\gamma_{00}, \gamma_{10}, \ldots, \gamma_{i0}, \ldots] , \tag{5.9}$$

and in the most simple case, we impose the fragment to be entangled with a single bath orbital in the new representation,

$$\boldsymbol{X}^{\dagger} \xrightarrow{\boldsymbol{R}} \boldsymbol{Y}^{\dagger} = \boldsymbol{R}\boldsymbol{X}^{\dagger} = [\gamma_{00}, \xi, 0, 0, \ldots, 0, \ldots] , \tag{5.10}$$

where all but the first two rows of $\boldsymbol{Y}$ are set to zero.

As observed in the previous section, given $\boldsymbol{X}$ and $\boldsymbol{Y}$ one can build $\boldsymbol{v}$ and thus the transformation $\boldsymbol{R}$ which will generate the connectivity reduction. First of all, the norm constraint of Eq. (5.6) reads,

$$\xi^2 = \sum_{j>0} \gamma_{j0}^2. \tag{5.11}$$

As a result,

$$\begin{aligned} |\boldsymbol{X} - \boldsymbol{Y}|^2 &= (\gamma_{10} - \xi)^2 + \sum_{j>1} \gamma_{j0}^2 \\ &= (\gamma_{10} - \xi)^2 + \xi^2 - \gamma_{10}^2, \\ &= 2\xi \left(\xi - \gamma_{10}\right). \end{aligned} \tag{5.12}$$

Obviously, if $\xi = 0$ then the fragment would be isolated from the rest of the lattice [See Equation (5.10)] in the Householder representation. This case makes no sense in our approach as we could not retrieve any entanglement from the environment of the

selected fragment. Moreover, if the fragment orbital in the real space representation reads,

$$\boldsymbol{X}^\dagger = [\gamma_{00}, \gamma_{10}, 0, \ldots, 0]\,, \tag{5.13}$$

meaning that the fragment is only connected to one orbital, the HH-t should still be defined, meaning that $|\boldsymbol{X} - \boldsymbol{Y}|$ should never vanish [See Eq. (5.7)] and thus fixes the sign of ξ [See Equation (5.12)] for the case of one connected bath orbital,

$$\xi = -\mathrm{sgn}\,(\gamma_{10}) \sqrt{\sum_{j>0} \gamma_{j0}^2}. \tag{5.14}$$

Thus, thanks to Eqs. (5.2), (5.7), (5.9), and (5.10), one can define the final expressions:

$$R_{ij} = \delta_{ij} - 2 v_i v_j, \tag{5.15}$$

where

$$\begin{aligned} v_0 &= 0, \\ v_1 &= \frac{\gamma_{10} - \xi}{\sqrt{2\xi\,(\xi - \gamma_{10})}}, \\ v_j &\overset{j\geq 2}{=} \frac{\gamma_{j0}}{\sqrt{2\xi\,(\xi - \gamma_{10})}}, \end{aligned} \tag{5.16}$$

5.1.3 Householder transformed density matrix

As sketched in Fig. 5.2, the Householder transformed density matrix can now be evaluated as follows,

$$\tilde{\boldsymbol{\gamma}} = \boldsymbol{R}^\dagger(\boldsymbol{v})\boldsymbol{\gamma}\boldsymbol{R}(\boldsymbol{v}) = \boldsymbol{R}(\boldsymbol{v})\boldsymbol{\gamma}\boldsymbol{R}(\boldsymbol{v}), \tag{5.17}$$

or, equivalently,

$$\tilde{\gamma}_{ij} = \left\langle \hat{d}_{i\sigma}^\dagger \hat{d}_{j\sigma} \right\rangle, \tag{5.18}$$

where, according to Eqs. (5.15), (5.16), and (5.14), the Householder transformed creation (annihilation) operators are functionals of the density matrix elements γ_{ij},

$$\begin{aligned} \hat{d}_{i\sigma}^\dagger &:= \sum_j R_{ij}\, \hat{c}_{j\sigma}^\dagger \\ &= \hat{c}_{i\sigma}^\dagger - 2 v_i \sum_{j>0} v_j\, \hat{c}_{j\sigma}^\dagger. \end{aligned} \tag{5.19}$$

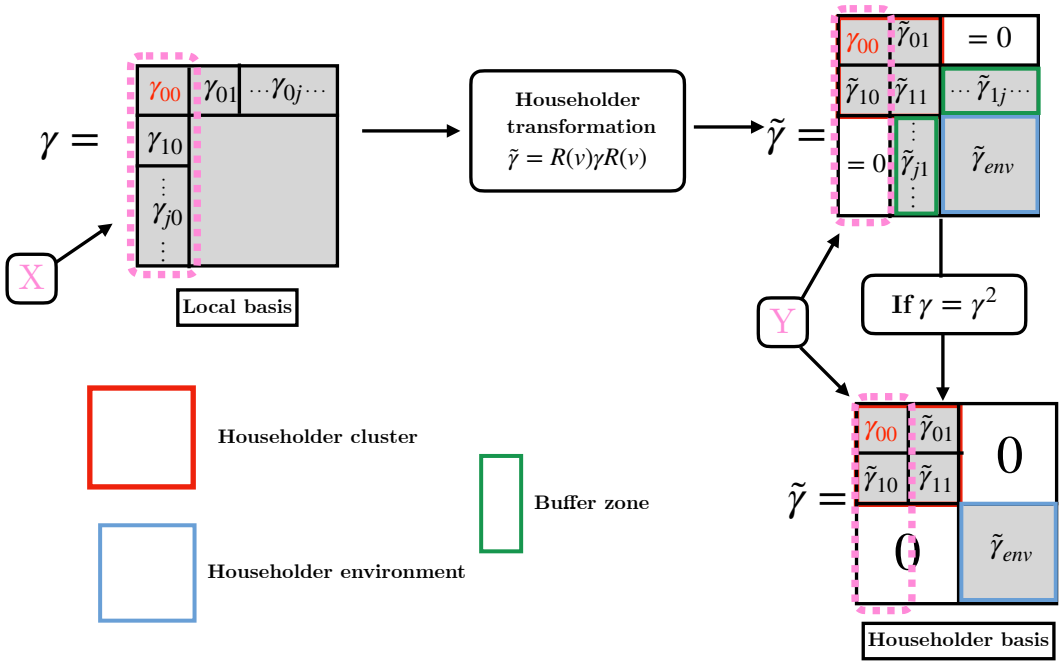

Figure 5.2: Schematics of the Householder transformation applied to the density matrix.

The unitary character of $\boldsymbol{R}$ allows the inverse transformation (from the Householder representation to the lattice one) which simply reads,

$$\sum_i R_{ki}\hat{d}^\dagger_{i\sigma} = \sum_{ij} R_{ki}R_{ij}\hat{c}^\dagger_{j\sigma} = \sum_j \delta_{kj}\hat{c}^\dagger_{j\sigma} = \hat{c}^\dagger_{k\sigma}, \tag{5.20}$$

or, equivalently,

$$\hat{c}^\dagger_{k\sigma} = \hat{d}^\dagger_{k\sigma} - 2v_k \sum_{i>0} v_i \hat{d}^\dagger_{i\sigma}. \tag{5.21}$$

Two main features of the Householder transformation applied on the density matrix are at the core of the proposed embedding schemes. To begin, we observe that the transformation leaves the fragment operator unchanged,

$$\hat{d}^\dagger_{\text{imp}} \equiv \hat{d}^\dagger_{0\sigma} = \hat{c}^\dagger_{0\sigma}. \tag{5.22}$$

It is worth mentioning that in future application, in an embedding purpose where one would like to separate some orbitals of interest (*i.e.* *d*- or *f*-orbitals) from the rest of the system, it is in our interest to keep their structure not altered. At the same time, the bath orbital is constructed explicitly from the environment (in the

lattice) of the fragment as follows,

$$\hat{d}^{\dagger}_{\text{bath}} \equiv \hat{d}^{\dagger}_{1\sigma} = \left(1 - 2v_1^2\right) \hat{c}^{\dagger}_{1\sigma} - 2v_1 \sum_{j>1} v_j \, \hat{c}^{\dagger}_{j\sigma}. \tag{5.23}$$

and thus become an "effective" orbital which try to mimic the behavior of the rest of the system. A further examination of the bath orbital(s) and their connection with those of DMET will be presented in Section 5.3. Then, the second point of importance is the entanglement among the orbitals in the Householder representation. We have already observed that by construction, the fragment is only entangled with the bath orbital (*i.e.* the first column (row) of the Householder transformed density matrix equals zero outside the cluster) [See Eq. (5.10) and Fig. 5.2]. Indeed, according to Eqs. (5.10) and (5.16),

$$\begin{aligned} \tilde{\gamma}_{j0} &= \sum_{kl} R_{jk} \gamma_{kl} R_{l0} \\ &= \sum_{k} R_{jk} \gamma_{k0} \\ &= \left[\boldsymbol{RX}\right]_j \\ &= Y_j \overset{j\geq 2}{=} 0. \end{aligned} \tag{5.24}$$

Similarly, one can evaluate the entanglement of the bath orbital with the remaining environment orbitals,

$$\begin{aligned} \tilde{\gamma}_{j1} &= \sum_{kl} R_{jk} \gamma_{kl} R_{l1} \\ &= \sum_{kl} R_{jk} \gamma_{kl} (\delta_{l1} - 2v_l v_1) \\ &= \sum_{k} (R_{jk} \gamma_{k1} - 2v_1 \sum_{l} v_l R_{jk} \gamma_{kl}) \\ &\neq 0. \end{aligned} \tag{5.25}$$

Thus, in the general (interacting) case, the exact Householder cluster is *not* disconnected from its environment. This tendency is shown in Fig. 5.3 for small Hubbard rings, the Householder transformed (ground state) density matrix has a nonzero buffer sector $\{\tilde{\gamma}_{j1}\}_{j\geq 2}$, which is a signature of the cluster's entanglement with its environment. The buffer zone is represented by the green area in Fig. 5.2 and is, in this case, a vector of dimension $(L-2)\times 1$. The first observation is the invariance under the Householder transformation of the occupation of the fragment [See top

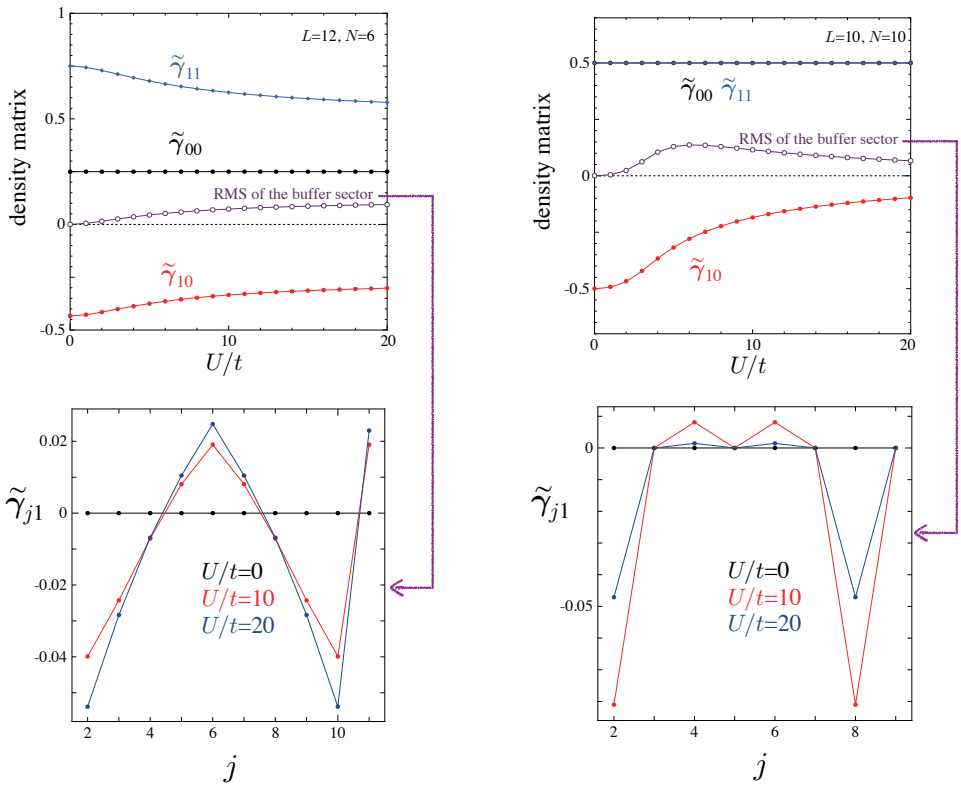

Figure 5.3: Left panel: (Top) Exact (ground state) Householder transformed density matrix elements in the cluster sector and root mean square (RMS) of the elements in the buffer sector, both plotted as functions of U/t for a quarter-filled 12-site Hubbard ring. (Bottom) Individual elements in the buffer sector for various U/t values. Right panel: Same as left panel for a half-filled 10-site Hubbard ring.

panels of Fig. 5.3],

$$\tilde{\gamma}_{00} = \sum_{kl} R_{0k}\gamma_{kl}R_{l0} = \gamma_{00}. \tag{5.26}$$

Moreover, the existence of such a buffer can be related to the deviation of the density matrix from idempotency. Indeed, according to Eq. (5.24),

$$\begin{aligned}\left[\tilde{\gamma}^2\right]_{j0} = \sum_{k} \tilde{\gamma}_{jk}\tilde{\gamma}_{k0} &= \tilde{\gamma}_{j0}\tilde{\gamma}_{00} + \tilde{\gamma}_{j1}\tilde{\gamma}_{10} \\ &\overset{j\geqq 2}{=} \tilde{\gamma}_{j1}\tilde{\gamma}_{10},\end{aligned} \tag{5.27}$$

thus leading to [See Equation(5.10)]

$$\tilde{\gamma}_{j1} \overset{j\geqq 2}{=} \frac{[\tilde{\gamma}^2]_{j0}}{\tilde{\gamma}_{10}} = \frac{[\tilde{\gamma}^2]_{j0}}{\xi}, \tag{5.28}$$

or, equivalently,

$$\tilde{\gamma}_{j1} \overset{j\geq 2}{=} \frac{[\tilde{\boldsymbol{\gamma}}^2 - \tilde{\boldsymbol{\gamma}}]_{j0}}{\xi}. \tag{5.29}$$

where we made use of Eq. (5.9) and that $\tilde{\gamma}_{j0} = 0$ for all $j \geq 2$. Consequently, applying the HH-t to an idempotent matrix will strictly disentangled the Householder cluster from its environment. On top of that, we observe that the Householder cluster is, in general, an *open* subsystem [see top left panel of Fig. 5.3 where $\tilde{\gamma}_{00}+\tilde{\gamma}_{11} \neq constant$]. This again can be related to the deviation from idempotency. Indeed, by considering the particular case $j = 1$ on the first line of Eq. (5.27), it comes

$$\frac{\mathcal{N}^{\mathcal{C}}}{2} := \tilde{\gamma}_{00} + \tilde{\gamma}_{11} = \frac{[\tilde{\boldsymbol{\gamma}}^2]_{10}}{[\tilde{\boldsymbol{\gamma}}]_{10}}, \tag{5.30}$$

where $\mathcal{N}^{\mathcal{C}}$ is the total (spin-summed) number of electrons in the cluster. Interestingly, when the interacting lattice is half-filled, the fluctuations in the number of electrons within the Householder cluster vanish and the latter contains exactly two electrons for all U/t values [see Fig. 5.3]. Moreover, in the buffer sector of the density matrix, elements with odd row (column) indices are zero [see the bottom right panel of Fig. 5.3]. Nevertheless, even in this particular case, the cluster remains connected to its Householder environment as long as the lattice is interacting ($U/t \neq 0$). As proved analytically[21], these properties originate from the hole-particle symmetry of the Hubbard Hamiltonian.

To conclude this section, note that we have introduce the unitary HH-t and made a formal connection with the one-electron reduced density matrix. In the new representation, the fragment orbital remains identical while an effective bath orbital is constructed as linear combination of remaining sites. Note that further investigation on the bath orbital will be done and a formal connection could be made with density matrix embedding theory (DMET) [See Section 5.3]. Moreover, among the different features retrieved by the HH-t, interesting ones originate from applying it to an idempotent density matrix. We have proved the strict disentanglement between the Householder cluster and its environment and highlighted the fixed number of electrons within the cluster. It is worth saying that these feature will be central in the embedding schemes proposed in Sections 6, 7 and 8. Moreover, the single-orbital picture allows us to take advantage of the existing

quantum chemistry methods in order to retrieve more electronic correlation [See Section. 2.2]. Nevertheless, this appealing transformation has one major drawback. While it offers a simple way to fragment the system within different parts, it is still limited by the number of orbitals composing the cluster. This issue has been overcome thanks to the block Householder transformation.

5.2 Block-Householder transformation

In 1999, F. Rotella and I. Zambettakis introduced the *block Householder transformation*[37] which generalizes the HH-t and extend it to a block matricial form. We will make use of the block HH-t in order to increase the number of orbitals to embed. To this point, the main equations leading to the block structure of a given matrix are first derived, then we will demonstrate that similar properties as the original HH-t can be retrieved if we apply the block HH-t to an idempotent density matrix. Note that this work is in preparation in order to be submitted.

5.2.1 Construction of the Block-Householder transformation matrix

The following section which demonstrates the general construction of the block HH-t matrix is greatly inspired by the book of F. Rottela and P. Borne, "Théorie et pratique du calcul matriciel"[148]. The reader can skip this part if not interested by the demonstration.

Starting with a matrix $\boldsymbol{V}$ of dimension $L\times\ L_{frag}$ where L is the total number of local orbitals in a system and L_{frag} the number of orbital in a reference fragment (*i.e.* impurities). We assume here that all the columns of $\boldsymbol{V}$ are are linearly independent, *i.e.* $\boldsymbol{Rank}(\boldsymbol{V}) = L_{frag}$ and $L_{frag} \leq L$, then the transformation matrix could be written as follows,

$$\boldsymbol{R}(\boldsymbol{V}) = \mathbf{1}_L - 2\boldsymbol{V}(\boldsymbol{V}^\dagger\boldsymbol{V})^{-1}\boldsymbol{V}^\dagger, \tag{5.31}$$

where $\mathbf{1}_L$ is the identity matrix. For simplicity, $(\boldsymbol{V}^\dagger\boldsymbol{V})^{-1}\boldsymbol{V}^\dagger$ which is the Moore-Penrose pseudo-inverse of $\boldsymbol{V}$ will be rewritten as $\boldsymbol{V}^+$. Therefore, Eq. (5.31) becomes

$$\boldsymbol{R}(\boldsymbol{V}) = \mathbf{1}_L - 2\boldsymbol{V}\boldsymbol{V}^+. \tag{5.32}$$

The uniqueness of the pseudo-inverse (Moore-Penrose pseudo-inverse) is only obtained when the four following properties are obeyed:

$$\begin{aligned} &P1 : \boldsymbol{V}\boldsymbol{V}^+\boldsymbol{V} = \boldsymbol{V}, \\ &P2 : \boldsymbol{V}^+\boldsymbol{V}\boldsymbol{V}^+ = \boldsymbol{V}^+, \\ &P3 : (\boldsymbol{V}\boldsymbol{V}^+)^\dagger = \boldsymbol{V}\boldsymbol{V}^+, \\ &P4 : (\boldsymbol{V}^+\boldsymbol{V})^\dagger = \boldsymbol{V}^+\boldsymbol{V}. \end{aligned} \tag{5.33}$$

In particular, when $\boldsymbol{V}$ has linearly independent columns (and thus $\boldsymbol{V}^\dagger\boldsymbol{V}$ is invertible), $\boldsymbol{V}^+$ can be computed as,

$$\boldsymbol{V}^+ = (\boldsymbol{V}^\dagger\boldsymbol{V})^{-1}\boldsymbol{V}^\dagger \tag{5.34}$$

From a geometrical point of view, it should be seen as a reflection that transforms the L_{frag} L-row (column) vectors collected in $\boldsymbol{V}$ into their opposite [See Eq. (5.32) and *P1* in Eq. 5.33],

$$\boldsymbol{R}\boldsymbol{V} = -\boldsymbol{V}. \tag{5.35}$$

Let's now consider a block matrix $\boldsymbol{X}$ of dimensions $L \times L_{frag}$ with the following form

$$\boldsymbol{X} = \begin{bmatrix} \boldsymbol{\gamma}_{FF} \\ \boldsymbol{\gamma}_{e_1 f} \\ \boldsymbol{\gamma}_{e_2 f} \end{bmatrix}, \tag{5.36}$$

where both γ_{FF} and $\gamma_{e_1 f}$ are of same dimensions $L_{frag} \times L_{frag}$ and $\gamma_{e_2 f}$ is of dimension $(L - 2 \times L_{frag}) \times L_{frag}$. Note here that $\gamma_{e_1 f}$ is assumed to be non-singular and thus invertible. From a physical point of view, these properties can be met when the chosen fragment orbitals are not disconnected from its environment. In which case, the embedding would be unnecessary. Two other matrices of same dimension will be needed in the following,

$$\bar{\boldsymbol{X}} = \begin{bmatrix} 0 \\ \boldsymbol{\gamma}_{e_1 f} \\ \boldsymbol{\gamma}_{e_2 f} \end{bmatrix}, \tag{5.37}$$

and

$$\boldsymbol{V} = \begin{bmatrix} 0 \\ \boldsymbol{\gamma}_{e_1 f} + \boldsymbol{W} \\ \boldsymbol{\gamma}_{e_2 f} \end{bmatrix}. \tag{5.38}$$

We finally obtain,

$$\begin{aligned} \boldsymbol{R}(\boldsymbol{V})\boldsymbol{X} &= \boldsymbol{X} - 2\boldsymbol{V}(\boldsymbol{V}^\dagger \boldsymbol{V})^{-1}\boldsymbol{V}^\dagger \boldsymbol{X} \\ &= \boldsymbol{X} - 2\boldsymbol{V}\boldsymbol{V}^+ \boldsymbol{X}. \end{aligned} \tag{5.39}$$

Some elements of Eq. (5.39) will be useful later under the following decomposition,

$$\begin{aligned} \boldsymbol{V}^\dagger \boldsymbol{V} &= (\boldsymbol{\gamma}_{e_1 f} + \boldsymbol{W})^\dagger (\boldsymbol{\gamma}_{e_1 f} + \boldsymbol{W}) + \boldsymbol{\gamma}_{e_2 f}^\dagger \boldsymbol{\gamma}_{e_2 f} \\ &= \boldsymbol{\gamma}_{e_1 f}^\dagger \boldsymbol{\gamma}_{e_1 f} + \boldsymbol{W}^\dagger \boldsymbol{\gamma}_{e_1 f} + \boldsymbol{\gamma}_{e_1 f}^\dagger \boldsymbol{W} + \boldsymbol{W}^\dagger \boldsymbol{W} + \boldsymbol{\gamma}_{e_2 f}^\dagger \boldsymbol{\gamma}_{e_2 f} \\ \boldsymbol{V}^\dagger \boldsymbol{X} &= (\boldsymbol{\gamma}_{e_1 f} + \boldsymbol{W})^\dagger \boldsymbol{\gamma}_{e_1 f} + \boldsymbol{\gamma}_{e_2 f}^\dagger \boldsymbol{\gamma}_{e_2 f} \\ &= \boldsymbol{\gamma}_{e_1 f}^\dagger \boldsymbol{\gamma}_{e_1 f} + \boldsymbol{W}^\dagger \boldsymbol{\gamma}_{e_1 f} + \boldsymbol{\gamma}_{e_2 f}^\dagger \boldsymbol{\gamma}_{e_2 f}. \end{aligned} \tag{5.40}$$

In the new representation, the transformation of the $\boldsymbol{X}$ block matrix leads to

$$\boldsymbol{R}(\boldsymbol{V})\boldsymbol{X} = \begin{bmatrix} \boldsymbol{\gamma}_{FF} \\ \boldsymbol{Z}_1 \\ \boldsymbol{Z}_2 \end{bmatrix} = \begin{bmatrix} \boldsymbol{\gamma}_{FF} \\ \tilde{\boldsymbol{\gamma}}_{e_1 f} \\ \tilde{\boldsymbol{\gamma}}_{e_2 f} \end{bmatrix}, \tag{5.41}$$

where the goal of this transformation is to set $\boldsymbol{Z}_2$ (*i.e.* $\tilde{\boldsymbol{\gamma}}_{e_2 f}$) to 0. Note that one can verify thanks to Eqs. (5.31), (5.38) and (5.39) that the first block of the matrix $\boldsymbol{X}$ is unchanged.

From now on, we'll see how one could choose the appropriate $\boldsymbol{W}$ in Eq. (5.38) in order to have $\boldsymbol{Z}_2 = 0$,

$$\begin{aligned} \boldsymbol{Z}_2 &= \gamma_{e_2 f} - 2\gamma_{e_2 f}(\boldsymbol{V}^\dagger \boldsymbol{V})^{-1}\boldsymbol{V}^\dagger \boldsymbol{X} \\ &= \gamma_{e_2 f}(\boldsymbol{V}^\dagger \boldsymbol{V})^{-1}\left[\boldsymbol{V}^\dagger \boldsymbol{V} - 2\boldsymbol{V}^\dagger \boldsymbol{X}\right]. \end{aligned} \tag{5.42}$$

Therefore

$$\boldsymbol{Z}_2 = \boldsymbol{0} \Leftrightarrow \boldsymbol{V}^\dagger \boldsymbol{V} = 2\boldsymbol{V}^\dagger \boldsymbol{X}. \tag{5.43}$$

Using both decompositions of Eq. (5.40), we can rewrite Eq. (5.43),

$$\begin{aligned} &\boldsymbol{V}^\dagger\boldsymbol{V} = 2\boldsymbol{V}^\dagger\boldsymbol{X} \\ \Leftrightarrow&\boldsymbol{\gamma}_{e_1f}^\dagger\boldsymbol{\gamma}_{e_1f} + \boldsymbol{W}^\dagger\boldsymbol{\gamma}_{e_1f} + \boldsymbol{\gamma}_{e_1f}^\dagger\boldsymbol{W} + \boldsymbol{W}^\dagger\boldsymbol{W} + \boldsymbol{\gamma}_{e_2f}^\dagger\boldsymbol{\gamma}_{e_2f} \\ =&2\boldsymbol{\gamma}_{e_1f}^\dagger\boldsymbol{\gamma}_{e_1f} + 2\boldsymbol{W}^\dagger\boldsymbol{\gamma}_{e_1f} + 2\boldsymbol{\gamma}_{e_2f}^\dagger\boldsymbol{\gamma}_{e_2f}, \end{aligned} \tag{5.44}$$

which can be rewritten as,

$$\boldsymbol{W}^\dagger\boldsymbol{W} + \boldsymbol{\gamma}_{e_1f}^\dagger\boldsymbol{W} - \boldsymbol{W}^\dagger\boldsymbol{\gamma}_{e_1f} = \boldsymbol{\gamma}_{e_1f}^\dagger\boldsymbol{\gamma}_{e_1f} + \boldsymbol{\gamma}_{e_2f}^\dagger\boldsymbol{\gamma}_{e_2f}. \tag{5.45}$$

Once factorized,

$$(\boldsymbol{W} + \boldsymbol{\gamma}_{e_1f})^\dagger(\boldsymbol{W} - \boldsymbol{\gamma}_{e_1f}) = \boldsymbol{\gamma}_{e_2f}^\dagger\boldsymbol{\gamma}_{e_2f}. \tag{5.46}$$

From the property that $\boldsymbol{A}^\dagger A$ is symmetric for any matrix $\boldsymbol{A}$, one can deduce that $(\boldsymbol{W} + \boldsymbol{\gamma}_{e_1f})^\dagger(\boldsymbol{W} - \boldsymbol{\gamma}_{e_1f})$ should be symmetric, thus,

$$(\boldsymbol{W} + \boldsymbol{\gamma}_{e_1f})^\dagger(\boldsymbol{W} - \boldsymbol{\gamma}_{e_1f}) = (\boldsymbol{W} - \boldsymbol{\gamma}_{e_1f})^\dagger(\boldsymbol{W} + \boldsymbol{\gamma}_{e_1f}), \tag{5.47}$$

which finally gives,

$$\boldsymbol{\gamma}_{e_1f}^\dagger\boldsymbol{W} = \boldsymbol{W}^\dagger\boldsymbol{\gamma}_{e_1f}. \tag{5.48}$$

Finally, we can simplify Eq. (5.45) and we obtain the equation that $\boldsymbol{W}$ should verify:

$$\boldsymbol{W}^\dagger\boldsymbol{W} = \boldsymbol{\gamma}_{e_1f}^\dagger\boldsymbol{\gamma}_{e_1f} + \boldsymbol{\gamma}_{e_2f}^\dagger\boldsymbol{\gamma}_{e_2f} = \tilde{\boldsymbol{X}}^\dagger\tilde{\boldsymbol{X}}, \tag{5.49}$$

where the last equality is easily recovered from Eq. (5.37) and $\boldsymbol{W}$ is taken such as $\boldsymbol{\gamma}_{e_1f}^\dagger\boldsymbol{W}$ is symmetric [See Equation 5.48]. Rewritting this equation leads to,

$$\boldsymbol{\gamma}_{e_1f}^{-\dagger}\boldsymbol{W}^\dagger\boldsymbol{W}\boldsymbol{\gamma}_{e_1f}^{-1} = \mathbf{1}_{L_f} + \boldsymbol{\gamma}_{e_1f}^{-\dagger}\boldsymbol{\gamma}_{e_2f}^\dagger\boldsymbol{\gamma}_{e_2f}\boldsymbol{\gamma}_{e_1f}^{-1}. \tag{5.50}$$

If one rewrite Eq. (5.48) into the following form,

$$\boldsymbol{W}\boldsymbol{\gamma}_{e_1f}^{-1} = \boldsymbol{\gamma}_{e_1f}^{-\dagger}\boldsymbol{W}^\dagger, \tag{5.51}$$

and consider $\boldsymbol{M} = \boldsymbol{W}{\boldsymbol{\gamma}_{e_1f}}^{-1}$, Eq. (5.50) can be rewritten as

$$\boldsymbol{M}^2 = \mathbf{1}_{L_f} + \boldsymbol{\Lambda}^\dagger\boldsymbol{\Lambda}, \tag{5.52}$$

where

$$\boldsymbol{\Lambda} = \boldsymbol{\gamma}_{e_2f}\boldsymbol{\gamma}_{e_1f}^{-1}. \tag{5.53}$$

Given that $\mathbf{1}_{L_f} + \mathbf{\Lambda}^\dagger\mathbf{\Lambda}$ is a positive definite matrix, we look for its square root $\boldsymbol{Z}$. Using the Jordan form of $\mathbf{1}_{L_f} + \mathbf{\Lambda}^\dagger\mathbf{\Lambda}$, one can rewrite Eq. (5.52) as a diagonalization problem,

$$\mathbf{1}_{L_f} + \mathbf{\Lambda}^\dagger\mathbf{\Lambda} = \tilde{\boldsymbol{U}}\boldsymbol{D}\tilde{\boldsymbol{U}}^\dagger, \tag{5.54}$$

where $\tilde{\boldsymbol{U}}$ is a unitary matrix and

$$\boldsymbol{D} = \mathrm{diag}_{i=1}^{N_{total}}\{\sigma_i\}, \tag{5.55}$$

with the scalar values $\sigma_i > 0$. Finally, one reads $\boldsymbol{Z}$, the square root of $\boldsymbol{M}^2$ as,

$$\boldsymbol{Z} = \tilde{\boldsymbol{U}}\sqrt{\boldsymbol{D}}\tilde{\boldsymbol{U}}^\dagger, \tag{5.56}$$

where $\sqrt{\boldsymbol{D}} = \mathrm{diag}_{i=1}^{N_{total}}\{\sqrt{\sigma_i}\}$. Finally, one obtains from $\boldsymbol{M} = \boldsymbol{W}\boldsymbol{\gamma}_{e_1f}^{-1}$, Eq. (5.52), (5.54) and (5.56),

$$\boldsymbol{W} = \tilde{\boldsymbol{U}}\sqrt{\boldsymbol{D}}\tilde{\boldsymbol{U}}^\dagger\boldsymbol{\gamma}_{e_1f}, \tag{5.57}$$

leading to $\boldsymbol{Z}_2 = 0$. Indeed, we know that $\boldsymbol{W}$ should verify Eq. (5.49).

$$\begin{aligned}
\boldsymbol{W}^\dagger\boldsymbol{W} &= (\tilde{\boldsymbol{U}}\sqrt{\boldsymbol{D}}\tilde{\boldsymbol{U}}^\dagger\boldsymbol{\gamma}_{e_1f})^\dagger(\tilde{\boldsymbol{U}}\sqrt{\boldsymbol{D}}\tilde{\boldsymbol{U}}^\dagger\boldsymbol{\gamma}_{e_1f}) \\
&= \boldsymbol{\gamma}_{e_1f}^\dagger\tilde{\boldsymbol{U}}\sqrt{\boldsymbol{D}}\tilde{\boldsymbol{U}}^\dagger\tilde{\boldsymbol{U}}\sqrt{\boldsymbol{D}}\tilde{\boldsymbol{U}}^\dagger\boldsymbol{\gamma}_{e_1f} \\
&= \boldsymbol{\gamma}_{e_1f}^\dagger\tilde{\boldsymbol{U}}\sqrt{\boldsymbol{D}}\sqrt{\boldsymbol{D}}\tilde{\boldsymbol{U}}^\dagger\boldsymbol{\gamma}_{e_1f} \\
&= \boldsymbol{\gamma}_{e_1f}^\dagger\tilde{\boldsymbol{U}}\boldsymbol{D}\tilde{\boldsymbol{U}}^\dagger\boldsymbol{\gamma}_{e_1f} \\
&= \boldsymbol{\gamma}_{e_1f}^\dagger(\mathbf{1}_{L_f} + \mathbf{\Lambda}^\dagger\mathbf{\Lambda})\boldsymbol{\gamma}_{e_1f} \\
&= \boldsymbol{\gamma}_{e_1f}^\dagger\boldsymbol{\gamma}_{e_1f} + \boldsymbol{\gamma}_{e_1f}^\dagger(\boldsymbol{\gamma}_{e_2f}\boldsymbol{\gamma}_{e_1f}^{-1})^\dagger(\boldsymbol{\gamma}_{e_2f}\boldsymbol{\gamma}_{e_1f}^{-1})\boldsymbol{\gamma}_{e_1f} \\
&= \boldsymbol{\gamma}_{e_1f}^\dagger\boldsymbol{\gamma}_{e_1f} + \boldsymbol{\gamma}_{e_1f}^\dagger\boldsymbol{\gamma}_{e_1f}^{-\dagger}\boldsymbol{\gamma}_{e_2f}^\dagger\boldsymbol{\gamma}_{e_2f}\boldsymbol{\gamma}_{e_1f}^{-1}\boldsymbol{\gamma}_{e_1f} \\
&= \boldsymbol{\gamma}_{e_1f}^\dagger\boldsymbol{\gamma}_{e_1f} + \boldsymbol{\gamma}_{e_2f}^\dagger\boldsymbol{\gamma}_{e_2f} \\
&= \tilde{\boldsymbol{X}}^\dagger\tilde{\boldsymbol{X}}.
\end{aligned} \tag{5.58}$$

5.2.2 Properties of the Block-Householder representation and associated density matrix

In this section, we demonstrate that the block-Householder transformed 1-RDM

$$\tilde{\boldsymbol{\gamma}} = \boldsymbol{R}(\boldsymbol{V})\boldsymbol{\gamma}\boldsymbol{R}(\boldsymbol{V}), \tag{5.59}$$

presents a pure block-diagonal form when starting with an idempotent matrix $\boldsymbol{\gamma} = \boldsymbol{\gamma}^2$. The two blocks are referred to as the Householder cluster and the Householder environment. Starting with the block HH-t,

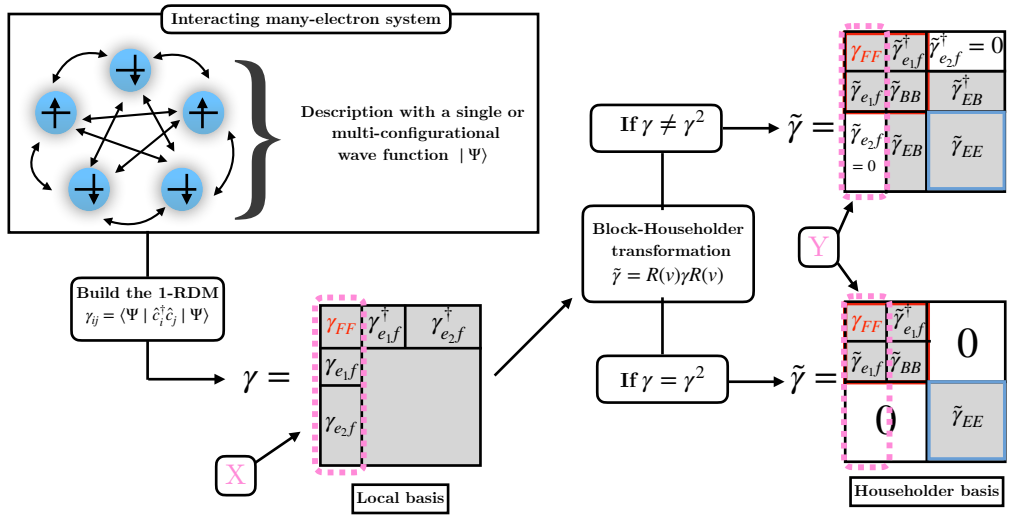

Figure 5.4: Steps realized to partition a system's 1-RDM with the block Householder transformation.

$$\boldsymbol{R}(\boldsymbol{V}) = \mathbf{1}_L - 2\boldsymbol{V}(\boldsymbol{V}^\dagger\boldsymbol{V})^{-1}\boldsymbol{V}^\dagger. \tag{5.60}$$

Its hermitian character ($\boldsymbol{R}(\boldsymbol{V}) = \boldsymbol{R}(\boldsymbol{V})^\dagger$) is straightforward. Moreover,

$$\begin{aligned}
\boldsymbol{R}(\boldsymbol{V})\boldsymbol{R}(\boldsymbol{V}) &= \left(\mathbf{1}_L - 2\boldsymbol{V}(\boldsymbol{V}^\dagger\boldsymbol{V})^{-1}\boldsymbol{V}^\dagger\right)\left(\mathbf{1}_L - 2\boldsymbol{V}(\boldsymbol{V}^\dagger\boldsymbol{V})^{-1}\boldsymbol{V}^\dagger\right) \\
&= \mathbf{1}_L - 4\boldsymbol{V}(\boldsymbol{V}^\dagger\boldsymbol{V})^{-1}\boldsymbol{V}^\dagger + 4\boldsymbol{V}(\boldsymbol{V}^\dagger\boldsymbol{V})^{-1}\left(\boldsymbol{V}^\dagger\boldsymbol{V}(\boldsymbol{V}^\dagger\boldsymbol{V})^{-1}\right)\boldsymbol{V}^\dagger \\
&= \mathbf{1}_L - 4\boldsymbol{V}(\boldsymbol{V}^\dagger\boldsymbol{V})^{-1}\boldsymbol{V}^\dagger + 4\boldsymbol{V}(\boldsymbol{V}^\dagger\boldsymbol{V})^{-1}\boldsymbol{V}^\dagger \\
&= \mathbf{1}_L,
\end{aligned} \tag{5.61}$$

which proves that $\boldsymbol{R}(\boldsymbol{V})$ is unitary.

As a result, one can show that the original idempotency of $\boldsymbol{\gamma}$ is a property that is communicated to the transformed 1-RDM as shown below

$$\begin{aligned}
\tilde{\gamma}^2 &= \boldsymbol{R}(\boldsymbol{V})\gamma\boldsymbol{R}(\boldsymbol{V})\boldsymbol{R}(\boldsymbol{V})\gamma\boldsymbol{R}(\boldsymbol{V}) \\
&= \boldsymbol{R}(\boldsymbol{V})\gamma^2\boldsymbol{R}(\boldsymbol{V}) \\
&= \boldsymbol{R}(\boldsymbol{V})\gamma\boldsymbol{R}(\boldsymbol{V}) \\
&= \tilde{\gamma}.
\end{aligned} \tag{5.62}$$

This idempotency can be used to define a set of equalities between the different blocks of the matrices γ and γ^2. For simplicity, the notation of Fig. 5.5 will be used for this section,

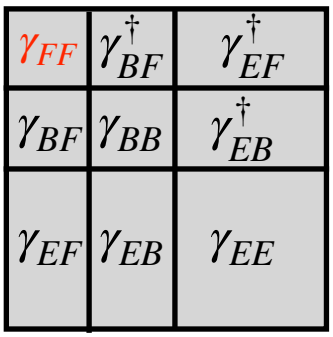

Figure 5.5: Simplified block notation for the density matrix where F, B and E refer to the fragment, bath and environment, respectively.

$$
\begin{aligned}
\gamma_{FF} &= \gamma_{FF}^2 + \gamma_{BF}^{\dagger}\gamma_{BF} + \gamma_{EF}^{\dagger}\gamma_{EF}, \\
\gamma_{BF} &= \gamma_{BF}\gamma_{FF} + \gamma_{BB}\gamma_{BF} + \gamma_{EB}^{\dagger}\gamma_{EF}, \\
\gamma_{EF} &= \gamma_{EF}\gamma_{FF} + \gamma_{EB}\gamma_{BF} + \gamma_{EE}\gamma_{EF}, \\
\gamma_{FB} &= \gamma_{BF}^{\dagger}, \\
\gamma_{FE} &= \gamma_{EF}^{\dagger}, \\
\gamma_{BB} &= \gamma_{BF}\gamma_{BF}^{\dagger} + \gamma_{BB}^2 + \gamma_{EB}^{\dagger}\gamma_{EB}, \\
\gamma_{EB} &= \gamma_{EF}\gamma_{BF}^{\dagger} + \gamma_{EB}\gamma_{BB} + \gamma_{EE}\gamma_{EB}, \\
\gamma_{BE} &= \gamma_{EB}^{\dagger}.
\end{aligned}
\tag{5.63}
$$

By construction, we know that the block $\tilde{\gamma}_{EF} = 0$ in the Householder representation. This means that

$$
\begin{aligned}
\tilde{\gamma}_{EF}\tilde{\gamma}_{FF} + \tilde{\gamma}_{EB}\tilde{\gamma}_{BF} + \tilde{\gamma}_{EE}\tilde{\gamma}_{EF} &= 0 \\
\tilde{\gamma}_{EB}\tilde{\gamma}_{BF} &= 0.
\end{aligned}
\tag{5.64}
$$

Assuming that, $\tilde{\gamma}_{BF}$ is invertible, we end up with

$$
\tilde{\gamma}_{EB} = 0. \tag{5.65}
$$

These results shows that starting from an idempotent (mean-field) density matrix, no off-diagonal terms can connect the cluster to the environement block in $\tilde{\gamma}$. As a consequence, the transformed 1-RDM becomes purely block-diagonal with two perfectly disentangled Householder cluster and environment sub-spaces.

In order to demonstrate the number of electrons within the cluster in the idempotent case, one will rely on the estimation of the rank of matrices. In practice, the rank describe the number of independent vectors used to built a representation of a given reference matrix. As an illustration, we know that the rank $\boldsymbol{Rank}(\boldsymbol{\gamma})$ of the full 1-RDM is,

$$\boldsymbol{Rank}(\boldsymbol{\gamma}) = \boldsymbol{Rank}\left(\sum_{i}^{N_{elec}/2} |\phi_i\rangle\langle\phi_i|\right) = \frac{N_{elec}}{2}, \tag{5.66}$$

as the matrix $\boldsymbol{\gamma}$ is built from N_{elec} occupied spin-orbitals (noted $|\phi_i\rangle$) which are independent and orthogonal. As a result, we see here that the effective number of electrons contained in a given orbital subspace can be directly related to the rank of the matrix built from the same orbitals.

Based on this observation, to determine the number of electrons contained in the cluster subspace (and by completion the number of electrons in the environment), we will here evaluate the rank of the Householder cluster block matrix. The targeted block is composed of four sub-matrices [See Figure 5.4] which makes the evaluation of the rank as follows,

$$\begin{aligned}\boldsymbol{Rank}\begin{pmatrix}\boldsymbol{\gamma}_{FF} & \tilde{\boldsymbol{\gamma}}_{BF}^{\dagger} \\ \tilde{\boldsymbol{\gamma}}_{BF} & \tilde{\boldsymbol{\gamma}}_{BB}\end{pmatrix} &= \boldsymbol{Rank}(\boldsymbol{\gamma}_{FF}) \\ &\quad + \boldsymbol{Rank}(\tilde{\boldsymbol{\gamma}}_{BB} - \tilde{\boldsymbol{\gamma}}_{BF}(\tilde{\boldsymbol{\gamma}}_{FF})^{-1}\tilde{\boldsymbol{\gamma}}_{BF}^{\dagger}).\end{aligned} \tag{5.67}$$

In order to evaluate this rank, one needs several ingredients. First, from the second line in Eq. (5.63) we know that the following equations holds for the $\tilde{\boldsymbol{\gamma}}_{BF}$ term,

$$\tilde{\boldsymbol{\gamma}}_{BF} = \tilde{\boldsymbol{\gamma}}_{BF}\boldsymbol{\gamma}_{FF} + \tilde{\boldsymbol{\gamma}}_{BB}\tilde{\boldsymbol{\gamma}}_{BF} + \tilde{\boldsymbol{\gamma}}_{EB}^{\dagger}\tilde{\boldsymbol{\gamma}}_{EF}, \tag{5.68}$$

which gives after some manipulations (and invoking the fact that $\tilde{\boldsymbol{\gamma}}_{EB} = 0$ in the idempotent case) the following relation,

$$\mathbf{1}_L - \boldsymbol{\gamma}_{FF} = \tilde{\boldsymbol{\gamma}}_{BF}^{-1}\tilde{\boldsymbol{\gamma}}_{BB}\tilde{\boldsymbol{\gamma}}_{BF}. \tag{5.69}$$

In a similar fashion, one knows from Eq. (5.63) that

$$\tilde{\boldsymbol{\gamma}}_{BF}^{\dagger} = \boldsymbol{\gamma}_{FF}\tilde{\boldsymbol{\gamma}}_{BF}^{\dagger} + \tilde{\boldsymbol{\gamma}}_{BF}^{\dagger}\tilde{\boldsymbol{\gamma}}_{BB} + \tilde{\boldsymbol{\gamma}}_{EF}^{\dagger}\tilde{\boldsymbol{\gamma}}_{EB}, \tag{5.70}$$

which yields the following definition for the $\tilde{\boldsymbol{\gamma}}_{BB}$ sub-block,

$$\tilde{\boldsymbol{\gamma}}_{BB} = \mathbf{1}_L - \tilde{\boldsymbol{\gamma}}_{BF}\boldsymbol{\gamma}_{FF}\tilde{\boldsymbol{\gamma}}_{BF}^{\dagger}. \tag{5.71}$$

Then by multiplying the second line in Eqs. (5.63) on the right side by $\boldsymbol{\gamma}_{FF}$ on obtains,

$$\begin{aligned} \tilde{\boldsymbol{\gamma}}_{BF}\boldsymbol{\gamma}_{FF} &= \tilde{\boldsymbol{\gamma}}_{BF}\boldsymbol{\gamma}_{FF}^2 + \tilde{\boldsymbol{\gamma}}_{BB}\tilde{\boldsymbol{\gamma}}_{BF}\boldsymbol{\gamma}_{FF} + \tilde{\boldsymbol{\gamma}}_{EB}^{\dagger}\tilde{\boldsymbol{\gamma}}_{EF}\boldsymbol{\gamma}_{FF} \\ &= \tilde{\boldsymbol{\gamma}}_{BF}\left(\boldsymbol{\gamma}_{FF} - \tilde{\boldsymbol{\gamma}}_{BF}^{\dagger}\tilde{\boldsymbol{\gamma}}_{BF}\right) + \tilde{\boldsymbol{\gamma}}_{BB}\tilde{\boldsymbol{\gamma}}_{BF}\boldsymbol{\gamma}_{FF}, \end{aligned} \tag{5.72}$$

where we injected the definition of $\boldsymbol{\gamma}_{FF}^2$ obtained from the right side of the first line in Eq. 5.63. After manipulating this equation one can isolate $\boldsymbol{\gamma}_{FF}$ and find its inverse which is,

$$\boldsymbol{\gamma}_{FF}^{-1} = \tilde{\boldsymbol{\gamma}}_{BF}^{-1}\tilde{\boldsymbol{\gamma}}_{BF}^{-\dagger}\tilde{\boldsymbol{\gamma}}_{BF}^{-1}\tilde{\boldsymbol{\gamma}}_{BB}\tilde{\boldsymbol{\gamma}}_{BF}. \tag{5.73}$$

Based on this last equation, one can reconstruct the last term of Eq. (5.67),

$$\begin{aligned} \tilde{\boldsymbol{\gamma}}_{BF}\boldsymbol{\gamma}_{FF}^{-1}\tilde{\boldsymbol{\gamma}}_{BF}^{\dagger} &= \tilde{\boldsymbol{\gamma}}_{BF}\left(\tilde{\boldsymbol{\gamma}}_{BF}^{-1}\tilde{\boldsymbol{\gamma}}_{BF}^{-\dagger}\tilde{\boldsymbol{\gamma}}_{BF}^{-1}\tilde{\boldsymbol{\gamma}}_{BB}\tilde{\boldsymbol{\gamma}}_{BF}\right)\tilde{\boldsymbol{\gamma}}_{BF}^{\dagger} \\ &= \tilde{\boldsymbol{\gamma}}_{BF}^{-\dagger}\tilde{\boldsymbol{\gamma}}_{BF}^{-1}\tilde{\boldsymbol{\gamma}}_{BB}\tilde{\boldsymbol{\gamma}}_{BF}\tilde{\boldsymbol{\gamma}}_{BF}^{\dagger}. \end{aligned} \tag{5.74}$$

Then, using both Eq. (5.69) and Eq. (5.71), one ends up with the following relation,

$$\begin{aligned} \tilde{\boldsymbol{\gamma}}_{BF}\boldsymbol{\gamma}_{FF}^{-1}\tilde{\boldsymbol{\gamma}}_{BF}^{\dagger} &= \tilde{\boldsymbol{\gamma}}_{BF}^{-\dagger}\left(\mathbf{1}_L - \boldsymbol{\gamma}_{FF}\right)\tilde{\boldsymbol{\gamma}}_{BF}^{\dagger} \\ &= \mathbf{1}_L - \tilde{\boldsymbol{\gamma}}_{BF}^{-\dagger}\boldsymbol{\gamma}_{FF}\tilde{\boldsymbol{\gamma}}_{BF}^{\dagger} \\ &= \tilde{\boldsymbol{\gamma}}_{BB}. \end{aligned} \tag{5.75}$$

Consequently, by injecting this relation into the second term of the original definition of the rank of the cluster matrix Eq. (5.67), one can show that this quantity reduces to the following simpler form,

$$\boldsymbol{Rank}\begin{pmatrix} \boldsymbol{\gamma}_{FF} & \tilde{\boldsymbol{\gamma}}_{BF}^{\dagger} \\ \tilde{\boldsymbol{\gamma}}_{BF} & \tilde{\boldsymbol{\gamma}}_{BB} \end{pmatrix} = \boldsymbol{Rank}(\boldsymbol{\gamma}_{FF}). \tag{5.76}$$

Therefore, we demonstrate here that the Householder cluster's rank confounds with the rank of the fragment sub-block $\boldsymbol{\gamma}_{FF}$. Considering that $\boldsymbol{\gamma}_{FF}$ is invertible, the associated matrix is then by definition full rank $\boldsymbol{Rank}(\tilde{\boldsymbol{\gamma}}_{FF}) = \boldsymbol{dim}(\tilde{\boldsymbol{\gamma}}_{FF}) = L_{frag}$. Here, L_{frag} is the number of local spin-orbitals considered as belonging to the

fragment. We then know that the total number of electrons contained in the cluster subspace is exactly $2L_{frag}$ if we refer to spatial orbitals.

Finally, using the block extension of the HH-t led us to similar conclusions as in Section 5.1. Starting with an mean-field description of the system (*i.e.* idempotent density matrix), one can strictly separate the Householder cluster and its environment. Moreover, the cluster is composed of a fixed number of spin-orbitals. Among them, the fragment orbitals are unchanged. Note that starting with a correlated description of the system (*i.e.* non-idempotent density matrix) leads to sub-blocks of the density matrix in the Householder representation which are not strictly disconnected [See $\tilde{\gamma}_{EB}$ in Fig. 5.4]. In this case, the buffer zone is of size $(L - 2 \times L_{frag}) \times L_{frag}$ and the Householder cluster does not contain an integer number of electrons. Consequently, the cornerstone of our embedding schemes will be the mean-field description of the original system as it provides a more comfortable starting point. Another interesting question is now appearing, "*what is the nature of the bath orbitals ?*". In the next section, this question will be addressed and we will make an interesting connection with density matrix embedding theory.

5.3 Bath orbitals

In this section, we will develop in details the construction of bath spin-orbitals by the use of the block HH-t. Interestingly, a connection with bath spin-orbitals constructed with the use of singular value decomposition (*i.e.* such as in DMET) will be made. Note that this work has not been published and is still under investigation.

As discussed further in the following, a substantial difference between the SVD and block Householder constructions of the quantum bath lies in the fact that, in the latter, the following sub-block structure is introduced for describing the coupling between the fragment and its environment [See sub-block in Eq. (4.35)],

$$\boldsymbol{\gamma}_{ef} = \begin{bmatrix} \boldsymbol{\gamma}_{e_1 f} \\ \boldsymbol{\gamma}_{e_2 f} \end{bmatrix}, \tag{5.77}$$

where the square matrix $\boldsymbol{\gamma}_{e_1 f} \equiv \{\gamma_{ij}\}_{L_{frag}+1\leq i\leq 2L_{frag}, 1\leq j\leq L_{frag}}$ is assumed to be *invertible* and e_1 denotes an orthonormal spin-orbital space of dimension $L_{e_1} = L_{frag}$ with which the fragment is entangled. The rest of the environment, which is of dimension $L_{e_2} = L - 2L_{frag}$ and is orthogonal to both f and e_1 spin-orbital spaces, is denoted e_2. There is definitely some arbitrariness in the choice of e_1 or, equivalently, in the numbering of the spin-orbitals in the environment. We will see that the choice of e_1 has no impact on the construction of the bath spin-orbital space, as long as $\boldsymbol{\gamma}_{e_1 f}^{-1}$ exists.

We recall the block Householder unitary (and Hermitian) transformation that applies to the full spin-orbital space is defined as follows in the lattice representation,

$$\boldsymbol{R} \equiv \boldsymbol{R}[\boldsymbol{\gamma}] = \mathbf{1}_L - 2\boldsymbol{V}\left(\boldsymbol{V}^\dagger \boldsymbol{V}\right)^{-1} \boldsymbol{V}^\dagger, \tag{5.78}$$

where $\mathbf{1}_L$ is the identity matrix. From Eqs. (5.38) and (5.57), on can decompose further the $\boldsymbol{V}$ matrix,

$$\boldsymbol{V} = \begin{bmatrix} \mathbf{0}_{L_{frag}} \\ \left(\mathbf{1}_{L_{frag}} + \tilde{\boldsymbol{U}}\tilde{\boldsymbol{D}}^{\frac{1}{2}}\tilde{\boldsymbol{U}}^\dagger\right)\boldsymbol{\gamma}_{e_1 f} \\ \boldsymbol{\gamma}_{e_2 f} \end{bmatrix}, \tag{5.79}$$

$\mathbf{1}_{L_{frag}}$ and $\mathbf{0}_{L_{frag}}$ are the $L_{frag} \times L_{frag}$ identity and zero matrices, respectively. The $L_{frag} \times L_{frag}$ unitary $\tilde{\boldsymbol{U}}$ and diagonal $\tilde{\boldsymbol{D}} \equiv \mathrm{diag}\left\{\tilde{\sigma}_{\tilde{b}}\right\}_{1\leq \tilde{b}\leq L_{frag}}$ matrices are determined from the following diagonalization problem [See Eqs. (5.53) and (5.54)],

$$\mathbf{1}_{L_{frag}} + \left[\boldsymbol{\gamma}_{e_2 f}\boldsymbol{\gamma}_{e_1 f}^{-1}\right]^\dagger \boldsymbol{\gamma}_{e_2 f}\boldsymbol{\gamma}_{e_1 f}^{-1} = \tilde{\boldsymbol{U}}\tilde{\boldsymbol{D}}\tilde{\boldsymbol{U}}^\dagger, \tag{5.80}$$

where, as readily seen, $\tilde{d}_i \geq 1$, for $1 \leq i \leq L_{frag}$. As a result, the determinant of $\tilde{\boldsymbol{D}}$ is strictly positive and both $\tilde{\boldsymbol{D}}^{\frac{1}{2}} \equiv \mathrm{diag}\left\{\sqrt{\tilde{d}_i}\right\}_{1\leq i\leq L_{frag}}$ and $\tilde{\boldsymbol{D}}^{-1} \equiv \mathrm{diag}\left\{1/\tilde{d}_i\right\}_{1\leq i\leq L_{frag}}$ are well defined. According to Eqs. (5.38) and (5.79), the to-be-inverted $\boldsymbol{V}^\dagger\boldsymbol{V}$ matrix can be expressed more explicitly as follows,

$$\begin{aligned} \boldsymbol{V}^\dagger\boldsymbol{V} &= \boldsymbol{\gamma}_{e_1 f}^\dagger \left(\mathbf{1}_{L_{frag}} + \tilde{\boldsymbol{U}}\tilde{\boldsymbol{D}}^{\frac{1}{2}}\tilde{\boldsymbol{U}}^\dagger\right)\left(\mathbf{1}_{L_{frag}} + \tilde{\boldsymbol{U}}\tilde{\boldsymbol{D}}^{\frac{1}{2}}\tilde{\boldsymbol{U}}^\dagger\right)\boldsymbol{\gamma}_{e_1 f} \\ &\quad + \boldsymbol{\gamma}_{e_2 f}^\dagger\boldsymbol{\gamma}_{e_2 f} \\ &= 2\left(\boldsymbol{\gamma}_{e_1 f}^\dagger\boldsymbol{\gamma}_{e_1 f} + \boldsymbol{\gamma}_{e_2 f}^\dagger\boldsymbol{\gamma}_{e_2 f} + \boldsymbol{\gamma}_{e_1 f}^\dagger\tilde{\boldsymbol{U}}\tilde{\boldsymbol{D}}^{\frac{1}{2}}\tilde{\boldsymbol{U}}^\dagger\boldsymbol{\gamma}_{e_1 f}\right), \end{aligned} \tag{5.81}$$

or equivalently,

$$\boldsymbol{V}^\dagger\boldsymbol{V} = 2\boldsymbol{\gamma}_{e_1 f}^\dagger\tilde{\boldsymbol{U}}\tilde{\boldsymbol{D}}^{\frac{1}{2}}\left(\mathbf{1}_{L_{frag}} + \tilde{\boldsymbol{D}}^{\frac{1}{2}}\right)\tilde{\boldsymbol{U}}^\dagger\boldsymbol{\gamma}_{e_1 f}, \tag{5.82}$$

where we readily see that the invertibility of $\boldsymbol{\gamma}_{e_1 f}$ induces that of $\boldsymbol{V}^\dagger \boldsymbol{V}$. Note that the two previous equations were simplified by the use of Eq. (5.80).

In order to compare the present approach with the alternative SVD-based procedure discussed in Section 4.2.2, one can rewrite the HH-t matrix in blocks as follows,

$$\boldsymbol{R} = \begin{bmatrix} \mathbf{1}_{L_{frag}} & \mathbf{0}_{L_{frag}\times(L-L_{frag})} \\ \mathbf{0}_{(L-L_{frag})\times L_{frag}} & \tilde{\boldsymbol{U}} \end{bmatrix} \tag{5.83}$$

$$= \begin{bmatrix} \mathbf{1}_{L_{frag}} & \mathbf{0}_{L_{frag}} & \mathbf{0}_{L_{frag}\times(L-2L_{frag})} \\ \mathbf{0}_{(L-L_{frag})\times L_{frag}} & \boldsymbol{U}_{e\tilde{b}} & \boldsymbol{U}_{e\tilde{\mathcal{E}}} \end{bmatrix}, \tag{5.84}$$

where, according to Eqs. (5.78) and (5.79), the two sub-blocks $\boldsymbol{U}_{e\tilde{b}}$ and $\boldsymbol{U}_{e\tilde{\mathcal{E}}}$ read as

$$\boldsymbol{U}_{e\tilde{b}} = \begin{bmatrix} \mathbf{1}_{L_{frag}} - 2\left(\mathbf{1}_{L_{frag}} + \tilde{\boldsymbol{U}}\tilde{\boldsymbol{D}}^{\frac{1}{2}}\tilde{\boldsymbol{U}}^\dagger\right)\boldsymbol{\gamma}_{e_1 f}\left(\boldsymbol{V}^\dagger\boldsymbol{V}\right)^{-1}\boldsymbol{\gamma}_{e_1 f}^\dagger\left(\mathbf{1}_{L_{frag}} + \tilde{\boldsymbol{U}}\tilde{\boldsymbol{D}}^{\frac{1}{2}}\tilde{\boldsymbol{U}}^\dagger\right) \\ -2\boldsymbol{\gamma}_{e_2 f}\left(\boldsymbol{V}^\dagger\boldsymbol{V}\right)^{-1}\boldsymbol{\gamma}_{e_1 f}^\dagger\left(\mathbf{1}_{L_{frag}} + \tilde{\boldsymbol{U}}\tilde{\boldsymbol{D}}^{\frac{1}{2}}\tilde{\boldsymbol{U}}^\dagger\right) \end{bmatrix} \tag{5.85}$$

and

$$\boldsymbol{U}_{e\tilde{\mathcal{E}}} = \begin{bmatrix} -2\left(\mathbf{1}_{L_{frag}} + \tilde{\boldsymbol{U}}\tilde{\boldsymbol{D}}^{\frac{1}{2}}\tilde{\boldsymbol{U}}^\dagger\right)\boldsymbol{\gamma}_{e_1 f}\left(\boldsymbol{V}^\dagger\boldsymbol{V}\right)^{-1}\boldsymbol{\gamma}_{e_2 f}^\dagger \\ \mathbf{1}_{(L-2L_{frag})} - 2\boldsymbol{\gamma}_{e_2 f}\left(\boldsymbol{V}^\dagger\boldsymbol{V}\right)^{-1}\boldsymbol{\gamma}_{e_2 f}^\dagger \end{bmatrix}. \tag{5.86}$$

The block Householder transformed density matrix reads as

$$\boldsymbol{R}^\dagger\boldsymbol{\gamma}\boldsymbol{R} = \begin{bmatrix} \boldsymbol{\gamma}_{ff} & \boldsymbol{\gamma}_{\tilde{b}f}^\dagger & \boldsymbol{\gamma}_{ef}^\dagger\boldsymbol{U}_{e\tilde{\mathcal{E}}} \\ \boldsymbol{\gamma}_{\tilde{b}f} & \boldsymbol{\gamma}_{\tilde{b}\tilde{b}} & \boldsymbol{\gamma}_{\tilde{\mathcal{E}}\tilde{b}}^\dagger \\ \boldsymbol{U}_{e\tilde{\mathcal{E}}}^\dagger\boldsymbol{\gamma}_{ef} & \boldsymbol{\gamma}_{\tilde{\mathcal{E}}\tilde{b}} & \boldsymbol{U}_{e\tilde{\mathcal{E}}}^\dagger\boldsymbol{\gamma}_{ee}\boldsymbol{U}_{e\tilde{\mathcal{E}}} \end{bmatrix}, \tag{5.87}$$

where

$$\boldsymbol{\gamma}_{\tilde{b}f} = \boldsymbol{U}_{e\tilde{b}}^\dagger\boldsymbol{\gamma}_{ef}, \tag{5.88}$$

$$\boldsymbol{\gamma}_{\tilde{b}\tilde{b}} = \boldsymbol{U}_{e\tilde{b}}^\dagger\boldsymbol{\gamma}_{ee}\boldsymbol{U}_{e\tilde{b}}, \tag{5.89}$$

and

$$\boldsymbol{\gamma}_{\tilde{\mathcal{E}}\tilde{b}} = \boldsymbol{U}_{e\tilde{\mathcal{E}}}^\dagger\boldsymbol{\gamma}_{ee}\boldsymbol{U}_{e\tilde{b}}. \tag{5.90}$$

According to Eqs. (5.77) and (5.86)

$$\begin{aligned} \boldsymbol{\gamma}_{ef}^\dagger\boldsymbol{U}_{e\tilde{\mathcal{E}}} = & -2\boldsymbol{\gamma}_{e_1 f}^\dagger\left(\mathbf{1}_{L_{frag}} + \tilde{\boldsymbol{U}}\tilde{\boldsymbol{D}}^{\frac{1}{2}}\tilde{\boldsymbol{U}}^\dagger\right)\boldsymbol{\gamma}_{e_1 f}\left(\boldsymbol{V}^\dagger\boldsymbol{V}\right)^{-1}\boldsymbol{\gamma}_{e_2 f}^\dagger \\ & +\boldsymbol{\gamma}_{e_2 f}^\dagger - 2\boldsymbol{\gamma}_{e_2 f}^\dagger\boldsymbol{\gamma}_{e_2 f}\left(\boldsymbol{V}^\dagger\boldsymbol{V}\right)^{-1}\boldsymbol{\gamma}_{e_2 f}^\dagger, \end{aligned} \tag{5.91}$$

or equivalently,

$$\begin{aligned}\boldsymbol{\gamma}_{ef}^{\dagger}\boldsymbol{U}_{e\tilde{\mathcal{E}}} =& \Bigg(\boldsymbol{V}^{\dagger}\boldsymbol{V} - 2\boldsymbol{\gamma}_{e_1 f}^{\dagger}\left(\mathbf{1}_{L_{frag}} + \tilde{\boldsymbol{U}}\tilde{\boldsymbol{D}}^{\frac{1}{2}}\tilde{\boldsymbol{U}}^{\dagger}\right)\boldsymbol{\gamma}_{e_1 f} \\ & - 2\boldsymbol{\gamma}_{e_2 f}^{\dagger}\boldsymbol{\gamma}_{e_2 f}\Bigg)\left(\boldsymbol{V}^{\dagger}\boldsymbol{V}\right)^{-1}\boldsymbol{\gamma}_{e_2 f}^{\dagger},\end{aligned} \tag{5.92}$$

thus leading to [See Eq. (5.81)]

$$\boldsymbol{\gamma}_{ef}^{\dagger}\boldsymbol{U}_{e\tilde{\mathcal{E}}} = \mathbf{0}_{L_{frag}\times(L-2L_{frag})}, \tag{5.93}$$

which means that, similarly as in DMET, the impurities are entangled only with the bath spin-orbitals. Note that the $\boldsymbol{V}$ matrix in Eq. (5.38) has been defined for that purpose.

We can now focus on the equivalence of the two formulations. For this, we will use the unitary matrices defined in Eq. (4.40) for the SVD ($\boldsymbol{U}_{eb}$ and $\boldsymbol{U}_{e\mathcal{E}}$) and in Eqs. (5.85) and (5.86) for the block HH-t ($\boldsymbol{U}_{e\tilde{b}}$ and $\boldsymbol{U}_{e\tilde{\mathcal{E}}}$). Note the tilde marks distinguishing them.

Note also that, according to Eqs. (4.49) and (5.93),

$$\begin{aligned}\boldsymbol{U}_{e\tilde{\mathcal{E}}}^{\dagger}\boldsymbol{\gamma}_{ef}\boldsymbol{\gamma}_{ef}^{\dagger}\boldsymbol{U}_{eb} &= \boldsymbol{U}_{e\tilde{\mathcal{E}}}^{\dagger}\boldsymbol{U}_{eb}\boldsymbol{D} \\ &= \left(\boldsymbol{\gamma}_{ef}^{\dagger}\boldsymbol{U}_{e\tilde{\mathcal{E}}}\right)^{\dagger}\boldsymbol{\gamma}_{ef}^{\dagger}\boldsymbol{U}_{eb} \\ &= \mathbf{0}_{(L-2L_{frag})\times L_{frag}},\end{aligned} \tag{5.94}$$

so that

$$\boldsymbol{U}_{e\tilde{\mathcal{E}}}^{\dagger}\boldsymbol{U}_{eb} = \mathbf{0}_{(L-2L_{frag})\times L_{frag}}. \tag{5.95}$$

Note also that, according to Eqs. (5.88) and (5.93),

$$\begin{aligned}\boldsymbol{\gamma}_{ef}^{\dagger}\boldsymbol{U}_{e\mathcal{E}} &= \boldsymbol{\gamma}_{ef}^{\dagger}\left(\boldsymbol{U}_{e\tilde{b}}\boldsymbol{U}_{e\tilde{b}}^{\dagger} + \boldsymbol{U}_{e\tilde{\mathcal{E}}}\boldsymbol{U}_{e\tilde{\mathcal{E}}}^{\dagger}\right)\boldsymbol{U}_{e\mathcal{E}} \\ &= \boldsymbol{\gamma}_{\tilde{b}f}^{\dagger}\boldsymbol{U}_{e\tilde{b}}^{\dagger}\boldsymbol{U}_{e\mathcal{E}}\end{aligned}, \tag{5.96}$$

thus leading to,

$$\boldsymbol{U}_{e\tilde{b}}^{\dagger}\boldsymbol{U}_{e\mathcal{E}} = \left(\boldsymbol{\gamma}_{\tilde{b}f}^{-1}\right)^{\dagger}\boldsymbol{\gamma}_{ef}^{\dagger}\boldsymbol{U}_{e\mathcal{E}} = \mathbf{0}_{L_{frag}\times(L-2L_{frag})}. \tag{5.97}$$

Consequently, bath spin-orbitals build from the SVD (block HH-t) are both orthogonal to environment spin-orbitals obtained from the block HH-t (SVD).

In the last step, we will connect the two transformations,

$$\boldsymbol{U}_{eb}\boldsymbol{T} = \boldsymbol{U}_{e\tilde{b}}, \tag{5.98}$$

or equivalently,

$$\boldsymbol{T} = \boldsymbol{U}_{eb}^{\dagger}\boldsymbol{U}_{e\tilde{b}} \tag{5.99}$$

where $\boldsymbol{T}$ is a linear transformation. Obviously, this transformation within the bath spin-orbital space is well defined only if $\boldsymbol{T}$ is unitary. According to Eq. (5.95) and the fact that $\boldsymbol{R}\boldsymbol{R}^{\dagger} = \mathbf{1}_L$

$$\begin{aligned}\boldsymbol{T}\boldsymbol{T}^{\dagger} &= \boldsymbol{U}_{eb}^{\dagger}\boldsymbol{U}_{e\tilde{b}}\boldsymbol{U}_{e\tilde{b}}^{\dagger}\boldsymbol{U}_{eb} \\ &= \boldsymbol{U}_{eb}^{\dagger}\left(\boldsymbol{U}_{e\tilde{b}}\boldsymbol{U}_{e\tilde{b}}^{\dagger} + \boldsymbol{U}_{e\tilde{\mathcal{E}}}\boldsymbol{U}_{e\tilde{\mathcal{E}}}^{\dagger}\right)\boldsymbol{U}_{eb} \\ &= \boldsymbol{U}_{eb}^{\dagger}\boldsymbol{U}_{eb} = \mathbf{1}_{L_{frag}}.\end{aligned} \tag{5.100}$$

Similarly,

$$\begin{aligned}\boldsymbol{T}^{\dagger}\boldsymbol{T} &= \boldsymbol{U}_{e\tilde{b}}^{\dagger}\boldsymbol{U}_{eb}\boldsymbol{U}_{eb}^{\dagger}\boldsymbol{U}_{e\tilde{b}} \\ &= \boldsymbol{U}_{e\tilde{b}}^{\dagger}\left(\boldsymbol{U}_{eb}\boldsymbol{U}_{eb}^{\dagger} + \boldsymbol{U}_{e\mathcal{E}}\boldsymbol{U}_{e\mathcal{E}}^{\dagger}\right)\boldsymbol{U}_{e\tilde{b}} \\ &= \boldsymbol{U}_{e\tilde{b}}^{\dagger}\boldsymbol{U}_{e\tilde{b}} = \mathbf{1}_{L_{frag}},\end{aligned} \tag{5.101}$$

which is the most important result of this section and proves that the one-electron quantum bath space generated within the (block) HH-t is the same up to an unitary transformation to the one generated with singular value decomposition methodology.

In the following, we will present two expansions of the bath orbital on the Hubbard rings. In Fig. 5.6, we observe that the nearest neighbors of the fragment contribute the most to the bath. Nevertheless, the delocalization of the latter over the lattice can be quite substantial, in particular in the weakly correlated regime. The impact of correlation on the bath varies with the lattice filling. For example, in the quarter-filled 12-site ring, the deviation from the non-interacting bath orbital remains relatively small when entering the strongly correlated regime (see the top panel of Fig. 5.6). This is an important observation which makes the

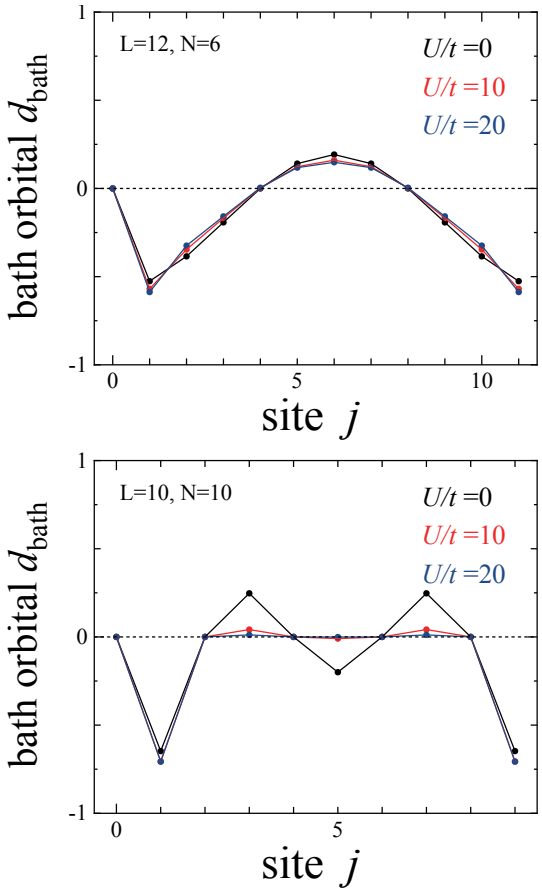

Figure 5.6: Expansion of the exact (ground state) bath orbital on the lattice [See Eq. (5.23)] for quarter-filled 12-site (top panel) and half-filled 10-site (bottom panel) Hubbard rings in various correlation regimes.

use of a mean-field bath in conventional DMET calculations[39] relevant. Interestingly, in the half-filled case, the bath delocalization reduces as correlation increases.

To conclude this section, we have presented two unitary transformations, the (block) Householder ones and observed that interesting properties are retrieved if applied to an idempotent one-electron reduced density matrix. More importantly, we have proved the equivalence between the bath spin-orbitals generated by the singular value decomposition and by the HH-t when the original full system is described by a single Slater determinant, *i.e.* with no explicit treatment of electron correlation. Interestingly, even though it has never been exploited so far, this equivalence is shown to remain valid for a correlated full system when the SVD is directly applied to the (one-electron reduced) density matrix.

Chapter 6

Householder transformed density matrix functional embedding theory

In Householder transformed density matrix functional embedding theory (Ht-DMFET), the goal is to have access to the local properties of the system by the evaluation of the one- and two- electron density matrices with a truncated wave function,

$$\begin{aligned} \langle \Psi_0 | \hat{c}^\dagger_{i\sigma} \hat{c}_{j\sigma} | \Psi_0 \rangle &\approx \left\langle \Psi_0^{\mathcal{C}} \middle| \hat{c}^\dagger_{i\sigma} \hat{c}_{j\sigma} \middle| \Psi_0^{\mathcal{C}} \right\rangle , \\ \langle \Psi_0 | \hat{c}^\dagger_{i\sigma} \hat{c}^\dagger_{j\sigma'} \hat{c}_{l\sigma'} \hat{c}_{k\sigma} | \Psi_0 \rangle &\approx \left\langle \Psi_0^{\mathcal{C}} \middle| \hat{c}^\dagger_{i\sigma} \hat{c}^\dagger_{j\sigma'} \hat{c}_{l\sigma'} \hat{c}_{k\sigma} \middle| \Psi_0^{\mathcal{C}} \right\rangle , \end{aligned} \tag{6.1}$$

where $\Psi_0^{\mathcal{C}}$ is the Householder cluster ground state wave function obtained from the embedding scheme. To that purpose, an exact formulation is derived for a non-interacting model Hamiltonian. On that basis, we construct an approximate embedding scheme for the interacting Hamiltonian. Note that an extension to *Ab initio* Hamiltonian is also presented.

The following presentation is greatly inspired by the paper entitled "Householder transformed density matrix functional embedding theory" [21]. More importantly, as proven in Section 5.3, the orbital space for the quantum bath in this work is similar to that of density matrix embedding theory (DMET). Thus, the following methodology is inspired by DMET and results are reproducible by applying a singular value decomposition (instead of the (block) Householder transformation)

to the one-electron reduced density matrix.

6.1 Exact embedding in the non-interacting case

In the non-interacting (NI) case (*i.e.* $U = 0$), which is equivalent to the mean-field approximation in the uniform Hubbard model, the ground state per-site energy reads [See Eqs. (3.3) and (1.19)]

$$e^{\mathrm{NI}}(n) = -4t\gamma_{10}, \tag{6.2}$$

where we fix the number N of electrons in the lattice and therefore the uniform filling $n = N/L = 2\gamma_{ii}$. Evaluating γ_{10} requires solving the NI problem for the full system, which is computationally affordable for a large number of sites (we considered $L = 400$ in this work). For that purpose, we have to minimize the *total* NI energy

$$E^{\mathrm{NI}} = 2\sum_{i,j=0}^{L-1} h_{ij}\gamma_{ij}, \tag{6.3}$$

where

$$h_{ij} \overset{0<i\leq L-1}{=} -t\left[\delta_{j(i+1)} + \delta_{j(i-1)}\right], \tag{6.4}$$

and $h_{0(L-1)} \equiv \pm t$ (the sign depends on the boundary conditions). In practice, we simply need to diagonalize the hopping matrix $\boldsymbol{h} \equiv \{h_{ij}\}$ and construct the density matrix in the lattice representation from the occupied (orthonormal) eigen-spin-orbitals $|\kappa_\sigma\rangle = \sum_i C_{i\kappa}|\phi_{i\sigma}\rangle$ as follows,

$$\gamma_{ij} = \sum_{\kappa}^{\mathrm{occ.}} C_{i\kappa}C_{j\kappa}. \tag{6.5}$$

We propose in this section to reformulate the NI problem into an embedded one. As such, it is in principle useless. However, when it comes to introducing electron correlation, which is of course our ultimate goal, this reformulation will provide a starting point for the embedding. It will also suggest how the latter can be systematically improved, as discussed further in Section 6.2.

Let us rewritte Eq. (6.3) in the (block-) Householder representation,

$$E^{\mathrm{NI}} = 2\sum_{kl} \tilde{h}_{kl}\tilde{\gamma}_{kl}, \tag{6.6}$$

where

$$\tilde{h}_{kl} = \sum_{ij} R_{ki} h_{ij} R_{jl} \tag{6.7}$$

Note that elements in the Householder representation will systematically written with a tilde mark. Since, in this representation, the (idempotent) density matrix can be split into cluster and environment parts [See Figure 5.2], the same applies to the NI energy:

$$E^{\mathrm{NI}} = E^{\mathrm{NI}}_{\mathcal{C}} + E^{\mathrm{NI}}_{\mathcal{E}}. \tag{6.8}$$

The cluster energy reads

$$E^{\mathrm{NI}}_{\mathcal{C}} = 2 \sum_{k,l=0}^{2N_f-1} \tilde{h}_{kl} \tilde{\gamma}_{kl}, \tag{6.9}$$

or, equivalently,

$$E^{\mathrm{NI}}_{\mathcal{C}} = \left\langle \Phi^{\mathcal{C}} \middle| \hat{h}^{\mathcal{C}} \middle| \Phi^{\mathcal{C}} \right\rangle, \tag{6.10}$$

where $\Phi^{\mathcal{C}}$ is the (single determinant) $N_{\mathcal{C}}$-electron cluster wave function ($N_{\mathcal{C}} = 2N_f$) and the non-interacting Householder cluster Hamiltonian,

$$\hat{h}^{\mathcal{C}} = \sum_{\sigma} \sum_{i,j=0}^{2N_f-1} \tilde{h}_{ij} \hat{d}^{\dagger}_{i\sigma} \hat{d}_{j\sigma}. \tag{6.11}$$

On the other hand, the energy of the environment is an explicit functional of the environment density matrix $\tilde{\gamma}^{\mathcal{E}} \equiv \{\tilde{\gamma}_{ij}\}_{i>2N_f, j>2N_f}$:

$$E^{\mathrm{NI}}_{\mathcal{E}} = 2 \sum_{k,l=2N_f}^{L-1} \tilde{h}_{kl} \tilde{\gamma}_{kl} \equiv 2 \,\mathrm{Tr} \left[\tilde{h}^{\mathcal{E}} \tilde{\gamma}^{\mathcal{E}} \right], \tag{6.12}$$

where Tr denotes the trace. The total ground state NI energy can be reached variationally, in principle exactly, as follows,

$$E^{\mathrm{NI}}_0 = \min_{\boldsymbol{v}} \left\{ E^{\mathrm{NI}}_{\mathcal{C}}[\boldsymbol{v}] + E^{\mathrm{NI}}_{\mathcal{E}}[\boldsymbol{v}] \right\}, \tag{6.13}$$

where

$$E^{\mathrm{NI}}_{\mathcal{C}}[\boldsymbol{v}] = \min_{\Phi^{\mathcal{C}}} \left\langle \Phi^{\mathcal{C}} \middle| \hat{h}^{\mathcal{C}}[\boldsymbol{v}] \middle| \Phi^{\mathcal{C}} \right\rangle, \tag{6.14}$$

and

$$E_{\mathcal{E}}^{\mathrm{NI}}[\boldsymbol{v}] = 2 \min_{\tilde{\gamma}^{\mathcal{E}}} \mathrm{Tr}\left[\tilde{\boldsymbol{h}}^{\mathcal{E}}[\boldsymbol{v}]\tilde{\gamma}^{\mathcal{E}}\right]. \tag{6.15}$$

Dependencies in the Householder vector $\boldsymbol{v}$ have been introduced, for clarity. In order to evaluate the per-site energy [See Eq. (6.2)],

$$\langle\Phi|\hat{t}_{01}|\Phi\rangle = -4t\gamma_{10}. \tag{6.16}$$

we can switch to the Householder representation,

$$\begin{aligned}
\langle\Phi|\hat{t}_{01}|\Phi\rangle &= -4t \sum_{i} R_{1i}\tilde{\gamma}_{i0} \\
&= -4t \sum_{0\leq i\leq 1} R_{1i}\tilde{\gamma}_{i0} \\
&= -4t \sum_{0\leq i\leq 1} R_{1i} \left\langle \Phi^{\mathcal{C}}\middle|\hat{d}_{i\sigma}^{\dagger}\hat{d}_{0\sigma}\middle|\Phi^{\mathcal{C}}\right\rangle \\
&= -4t \sum_{i} R_{1i} \left\langle \Phi^{\mathcal{C}}\middle|\hat{d}_{i\sigma}^{\dagger}\hat{c}_{0\sigma}\middle|\Phi^{\mathcal{C}}\right\rangle,
\end{aligned} \tag{6.17}$$

where we used Eq. (5.22) and the fact that $\hat{d}_{i\sigma}\left|\Phi^{\mathcal{C}}\right\rangle \overset{i\geq 1}{=} 0$, since $\Phi^{\mathcal{C}}$ is constructed within the cluster. We finally recover from Eq. (6.17) the following equality,

$$\begin{aligned}
\langle\Phi|\hat{t}_{01}|\Phi\rangle &= -4t \left\langle \Phi^{\mathcal{C}}\middle|\hat{c}_{1\sigma}^{\dagger}\hat{c}_{0\sigma}\middle|\Phi^{\mathcal{C}}\right\rangle \\
&= \left\langle \Phi^{\mathcal{C}}\middle|\hat{t}_{01}\middle|\Phi^{\mathcal{C}}\right\rangle,
\end{aligned} \tag{6.18}$$

which drastically (and exactly) simplifies the evaluation of non-interacting energies for lattices.

According to Eq. (6.18), the per-site NI energy can be evaluated directly from the cluster, which is obviously a huge simplification of the full-size problem. The exact NI per-site energy is recovered when the minimizing Householder vector $\boldsymbol{v}$ in Eq. (6.13) is employed, thus providing the optimal bath orbital(s). As readily seen from the latter equation, the Householder vector connects the cluster to its environment energy wise. In the present formalism, the optimal cluster (or, equivalently, the optimal bath) minimizes the sum of the cluster and environment energies. At the NI level, Eqs. (6.13)–(6.15) are much more complicated than Eq. (6.5) implementation wise, especially because the Hamiltonian of the environment should in principle be diagonalized for each trial Householder vector.

However, once the full-size NI problem is solved [with Eq. (6.5)], Eqs. (6.13)–(6.15) can be used for describing $N_{\mathcal{C}}$-electron interactions. In the simplest embedding scheme, which is described in the present work, electron correlation is introduced within the cluster while freezing the Householder vector to its NI value. The embedding might then be systematically improved by (i) updating the Householder vector variationally, (ii) describing correlations between the cluster and the environment and, ultimately, (iii) describing correlation within the environment.

To resume, in (block-) Ht-DMFET, the cornerstone is the exact and perfect disentanglement of the Householder cluster and its environment at the NI level, but also the integer number of electrons in the Householder cluster [See Sections 5.1.2 and 5.2.2]. From this, electronic correlation is introduced within the cluster. This approximate embedding scheme is analoguous to DMET[26] with a mean-field description of the full lattice.

6.2 Approximate embedding in the interacting case

For simplicity, we keep on using the Householder vector $\boldsymbol{v}$ evaluated from the NI density matrix of Eq. (6.5). First we need to rewrite the on-site repulsion operator in the (block-) Householder representation [See Eq. (5.20)],

$$U \sum_{i=0}^{L-1} \hat{n}_{i\sigma} \hat{n}_{isigma'} = \sum_{jklm} \tilde{U}_{jklm} \hat{d}^{\dagger}_{j\sigma} \hat{d}_{k\sigma} \hat{d}^{\dagger}_{l\sigma'} \hat{d}_{m\sigma'}, \tag{6.19}$$

where

$$\tilde{U}_{jklm} = U \sum_{i=0}^{L-1} R_{ij} R_{ik} R_{il} R_{im}. \tag{6.20}$$

After projecting onto the cluster, we obtain the following expression for the interacting cluster Hamiltonian:

$$\hat{\mathcal{H}}^{\mathcal{C}} = \hat{h}^{\mathcal{C}} + \sum_{j,k,l,m=0}^{2N_f} \tilde{U}_{jklm} \hat{d}^{\dagger}_{j\sigma} \hat{d}_{k\sigma} \hat{d}^{\dagger}_{l\sigma'} \hat{d}_{m\sigma'} \tag{6.21}$$

where $\hat{h}^{\mathcal{C}}$ is obtained from Eq. (6.11). In the DMET terminology[38,39], the use of the complete embedding Hamiltonian of Eq. (6.21) is referred to as *interacting*

bath (IB) embedding. In this case, the interaction $\tilde{U}_{jklm}$ on the totality of the cluster is taken into account. We should stress that, in the present work, like in regular DMET, the bath orbital (which is described by the operators $\hat{d}^{\dagger}_{i\sigma}$ and $\hat{d}_{i\sigma}$ ($2N_f > i > N_f$) is determined from the density matrix of the full *non-interacting* lattice, according to Eq. (5.23). Therefore, the acronym IB should not be confused with the level of calculation of the bath orbital. In the *non-interacting bath* (NIB) formulation[38,39], only the interaction on the impurity sites are conserved. Note that, in the context of DMET, correlating the bath would require the computation of a correlated many-body wave function for the full system[149] or the introduction of frequency dependencies into the theory[146]. In the present density matrix functional formulation, correlation might be introduced into the bath simply by employing in the (block-) Householder transformation [See Eqs. (5.15) and (5.31)] of a correlated full-system-size density matrix. This can be achieved at a reasonable computational cost[150] with low-level natural orbital functionals (NOFs). Their (sometimes poor [151]) description of strongly correlated energies may then be improved *via* the embedding, thus avoiding the use of more sophisticated NOFs which can be more difficult to converge. In this context, we may actually proceed with successive (block-) Householder transformations since the Householder "impurity+bath" cluster will in principle not be disconnected anymore from its environment. Applying a *second* (block-) Householder transformation to the "bath+buffer+environment" subblock of the (block-) Householder transformed density matrix [See Figure 5.2] would generate a second couple of bath orbital(s). The interacting lattice problem can then be projected onto the enlarged "impurity+two bath orbitals" cluster. Applying further Householder transformations would generate more bath orbitals and, ultimately, make the embedding exact. Interestingly, in EwDMET[146], the enlarged number of bath orbitals is determined from the order to which impurity spectral moments should be reproduced. Note that, within a hybrid NOF/Householder scheme, we will still be able to choose between IB and NIB formulations. In the rest of the (block-) Ht-DMFET embedding scheme, we employ an *uncorrelated* bath approach.

Let us return to the embedding Hamiltonian in Eq. (6.21). We observe in

Fig. 6.1 that the impurity occupation may systematically deviate from the lattice filling n when solving the interacting problem within the cluster. Consequently we introduce and adjust a chemical potential $\tilde{\mu}_i^{\text{frag}}$ on each impurity sites (*i.e.* ad hoc correction), in complete analogy with DMET[39], such that the cluster wave function reads,

$$\Psi^{\mathcal{C}} = \arg\min_{\Psi} \langle \Psi | \hat{\mathcal{H}}^{\mathcal{C}} - \tilde{\mu}_i^{\text{frag}} \sum_{\sigma} \sum_{i}^{N_f - 1} \hat{d}_{i\sigma}^{\dagger} \hat{d}_{i\sigma} | \Psi \rangle \,, \tag{6.22}$$

reproduces the desired occupation n, *i.e.*

$$\left\langle \Psi^{\mathcal{C}} \middle| \sum_{\sigma} \hat{d}_{i\sigma}^{\dagger} \hat{d}_{i\sigma} \middle| \Psi^{\mathcal{C}} \right\rangle \stackrel{!}{=} n. \tag{6.23}$$

where the subscript i refers to the local impurity site we are interested in. Once the

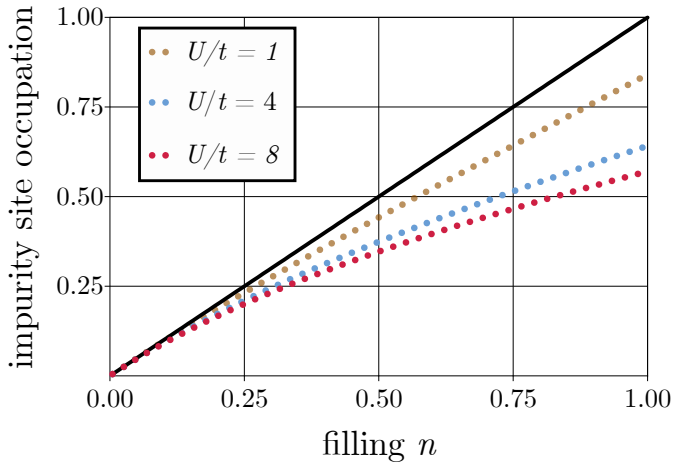

Figure 6.1: Householder cluster's (single) impurity site occupation plotted as a function of the lattice filling n in various correlation regimes for $\tilde{\mu}^{\text{frag}} = 0$ [See Eq. (6.22)] and the non-interacting bath case. The reference black straight line corresponds to the desired situation (which is ultimately reached by adjusting $\tilde{\mu}^{\text{frag}}$) where the embedded impurity occupation matches the lattice filling.

constraint in Eq. (6.23) is fulfilled, we obtain an approximate correlated expression for the per-site energy,

$$e(n) \approx -4t \left\langle \hat{c}_{1\sigma}^{\dagger} \hat{c}_{0\sigma} \right\rangle_{\Psi^{\mathcal{C}}} + U \left\langle \hat{n}_{0\sigma} \hat{n}_{0\sigma'} \right\rangle_{\Psi^{\mathcal{C}}} , \tag{6.24}$$

In the DMET terminology[39], Eqs. (6.22)–(6.24) describe a *single-shot* embedding which has a similar mapping conditions as Density Embedding Theory (DET)[38,40].

6.3 Summary of the embedding scheme

We have described the single-shot embedding of a single impurity site in the particular case of a 1D Hubbard lattice. First we solve the non-interacting problem. In the present work we diagonalize the bare hopping matrix [See Eq. (6.4)] and construct the (idempotent) ground state density matrix of the full lattice for a given and fixed number $N = nL$ of electrons. The latter density matrix gives immediately access to the bath orbital thanks to the Householder transformation [See the expression in Eq. (5.23) but also Eqs. (5.16) and (5.14)]. Then we project the original interacting lattice Hamiltonian of Eq. (3.3) onto the "impurity+bath" many-body subspace, which gives the cluster Hamiltonian expression of Eq. (6.21). At this level, we can decide to keep the interaction in the bath (IB formulation) or to remove it (NIB formulation). Finally, a chemical potential is introduced and adjusted on the embedded impurity to ensure that its occupation matches the lattice filling n [See Eqs. (6.22) and (6.23)]. A correlated per-site energy can then be evaluated from the (interacting) cluster many-body wave function [See Eq. (6.24)].

Let us stress that, at a given level of approximation (we performed a *single-shot* embedding for simplicity but stronger mapping constraints could of course be employed), the IB formulations of Ht-DMFET and standard DMET are formally equivalent. Indeed, for a non-interacting (or mean-field) lattice, the bath orbitals constructed from the Householder transformation and the Schmidt decomposition are identical, as shown in Section 5.3. As a result, when projecting the lattice interactions onto the "impurity+bath" cluster, both approaches will lead to the same embedding Hamiltonian [the one in Eq. (6.21)]. Note also that the Householder transformation can in principle be substituted for the Schmidt decomposition when constructing hole and particle bath states in EwDMET [See Eqs. (25) and (26) in Ref.[152]]. In this case, we would need to construct density matrices for cationic and anionic systems [See Eq. (10) in Ref.[153]].

6.4 Results

6.4.1 Homogeneous 1D Hubbard model

For the (large $L = 400$) uniform Hubbard ring with the hopping parameter set to $t = 1$, periodic/antiperiodic boundary conditions have been used when $\frac{N}{2}$ is odd/even in order to remove pathological degeneracies from the N-electron full-size non-interacting calculation. Comparison is made with the Bethe Ansatz (BA) results which are exact in the thermodynamic limit[35]. We note that the single-impurity DMET results presented in Ref.[26] were obtained without the interaction in the bath. Multiple-impurity block Ht-DMFET calculations have been performed and the correlated embedded cluster problem has been solved numerically using a full configuration interaction method developed in the laboratory.

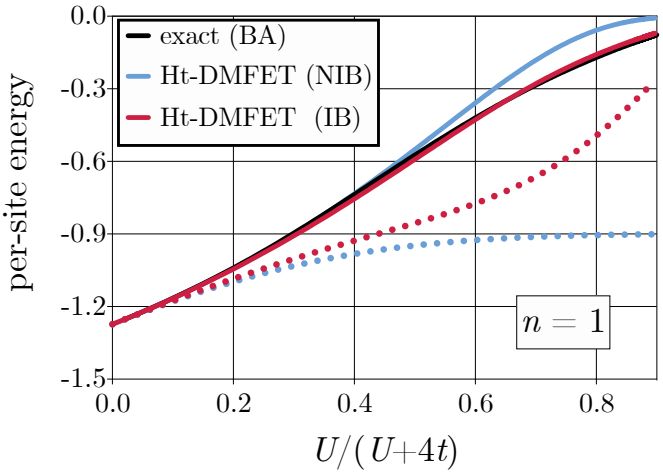

Figure 6.2: (Single-impurity) Ht-DMFET per-site energy plotted as a function of the interaction strength at half-filling. Results obtained for $\tilde{\mu}^{\text{frag}} = 0$ (dotted lines), those with an adjusted chemical potential are shown (full lines). Interaction in the bath results are shown for analysis purposes. Comparison is made with the exact Bethe Ansatz (BA) result.

First we discuss the importance of having a chemical potential $\tilde{\mu}^{\text{frag}}$ which will restore the desired occupation number on the impurity site. It is illustrated in the calculation of per-site energies in Fig. 6.2 for a simple case, a single impurity

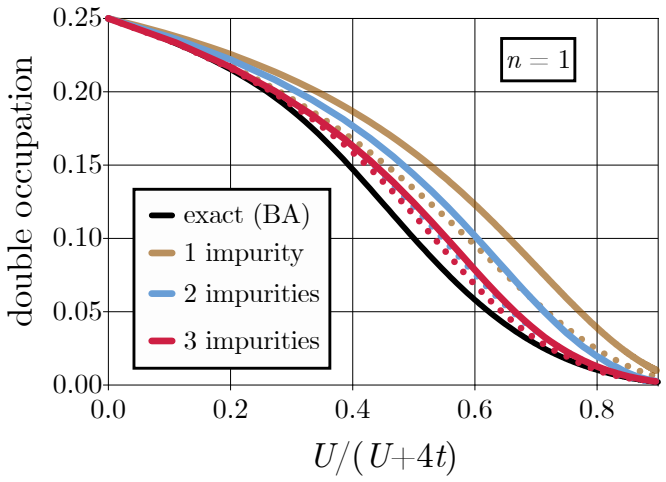

Figure 6.3: Ht-DMFET impurity site double occupation $\langle \hat{n}_{0\sigma}\hat{n}_{0\sigma'}\rangle_{\Psi^c}$ plotted as a function of the interaction strength at half-filling ($n = 1$). Comparison is made with the exact Bethe Ansatz (BA) result. Non-interacting bath (NIB) results in full lines are shown for analysis purposes.

at half-filled lattice. Once a proper $\tilde{\mu}^{\text{frag}}$ value is employed (which will be the case in the rest of the discussion), thus ensuring that the filling and the impurity occupation match, the error becomes substantial in the strongly correlated regime only if the interaction in the bath is neglected. We note that, in the latter case, we reproduce the single-impurity DMET results of Ref.[26], as expected from the analysis in Section. 5.3. The agreement with the BA results is almost perfect in all correlation regimes once the interaction in the bath is restored. This success may be related to the fact that, like in our approximate Ht-DMFET scheme, the true (correlated) Householder cluster contains exactly two electrons in the half-filled case, as a consequence of the hole-particle symmetry. Nevertheless, even though the interaction in the bath improves on the impurity double occupation, the error remains substantial when electron correlation is strong, as shown in Fig. 6.3. In order to further reduce the error, more impurities should be introduced into the cluster[26]. Therefore, the success of the present (single-impurity) Ht-DMFET at half-filling relies also on error cancellations in the evaluation of the (total) per-site energy.

Away from half-filling, the performance of (single-impurity) Ht-DMFET deteriorates as U/t increases, as shown in Fig. 6.4, probably because fluctuations in

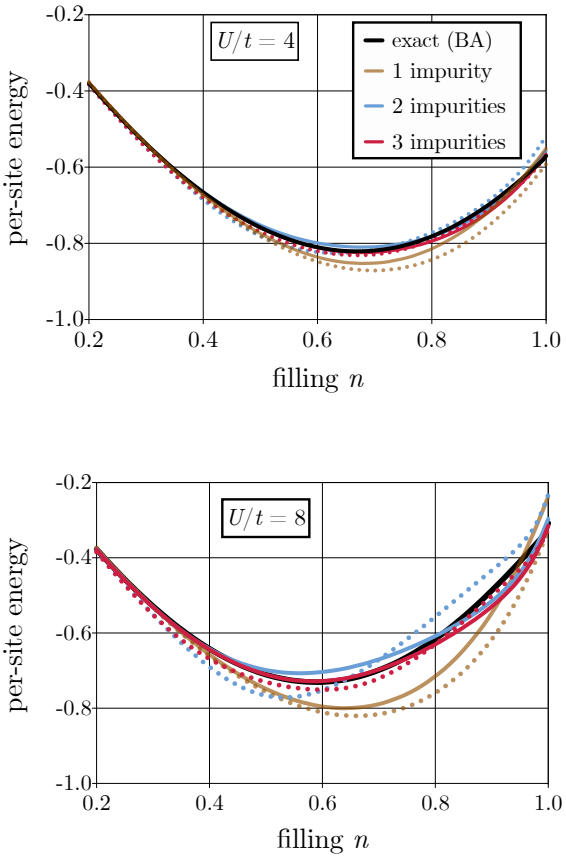

Figure 6.4: Ht-DMFET per-site energies plotted as a function of the lattice filling n for various correlation regimes, $U/t = 4$ and $U/t = 8$. Results obtained with a single and multiple impurityies are shown as (colored) solid lines. The dotted lines corresponds to the non-interacting bath (NIB) case. Comparison is made with the exact Bethe Ansatz (BA) results (black solid lines).

the number of electrons within our ("single impurity+single bath") cluster are not allowed in our approximate embedding. As discussed in Section 5.1.3, away from half-filling, the cluster becomes an open subsystem as soon as U/t deviates from zero. Surprisingly, in this density regime, per-site energies are in better agreement with the BA values when the interaction in the bath is neglected. Again, in the latter case, we recover the single-impurity DMET results of Ref.[26]. As expected[26,38] and shown in the bottom panel of Fig. 6.4, the results dramatically improve when several impurities are embedded, even at the simplest NIB level of approximation.

Finally, we investigate in Fig. 6.5 the density-driven Mott–Hubbard transition *via*

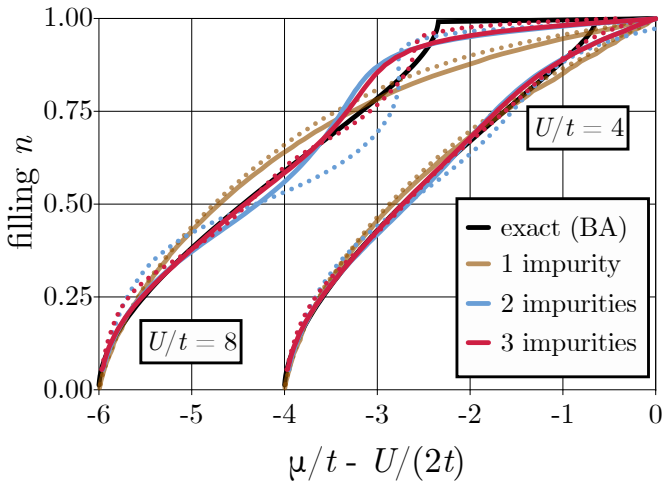

Figure 6.5: Lattice filling plotted, *via* the relation $\mu \equiv \mu(n) = \partial e(n)/\partial n$, as a function of the (lattice) chemical potential μ at the Ht-DMFET level of calculation for various correlation regimes. Non-interacting bath (NIB) results are shown as solid lines while interacting-bath (IB) results are in dotted lines. Comparison is made with the exact Bethe Ansatz (BA) results.

the evaluation of the density-functional $\mu(n) = \partial e(n)/\partial n$ chemical potential from the Ht-DMFET energy expression of Eq. (6.24). As expected from Ref.[26], at the single-impurity level, there is no density-driven Mott-Hubbard transition when the interaction in the bath is neglected. Restoring the interaction in the bath has actually no impact on the transition. This failure relies on a closed two-electron "single impurity+single bath" cluster. Already at the NIB level of approximation, embedding several impurities substantially improves the results. Nevertheless, even in this case, the gap remains closed. Interestingly, the transition is better described at the multiple-impurity level when the interactions in the bath are taken into account. Indeed, for three impurities, the filling n is almost on top of the exact results. This could be explained by the environment of the local impurity which tends to be similar to the original full system.

We have observed that the Ht-DMFET approach systematically improves the description of the local properties when the number of impurities is increased. Among all, it has shown particularly good results for the description of the

density-driven Mott-Hubbard transition which is an explicit demonstration of the efficiency of this embedding scheme.

Finally, if we just see in the Householder transformation an equivalent construction of bath orbitals such as in the singular value decomposition applied in DMET, it becomes clear that, by complete analogy with the latter, Ht-DMFET can be extended to more general Hamiltonians like, for example, quantum chemical ones written in a localized orbital basis. This will be the purpose of the next Section.

6.4.2 Hydrogen ring

In this section, the application of the Ht-DMFET using block-Householder is extended to the context of molecular systems. To do so, an embedding calculation is realized to determine the ground state energy of an hydrogen ring with 10 atoms. The system's geometry is shown in the left plot of Fig. 6.6. The realization of a

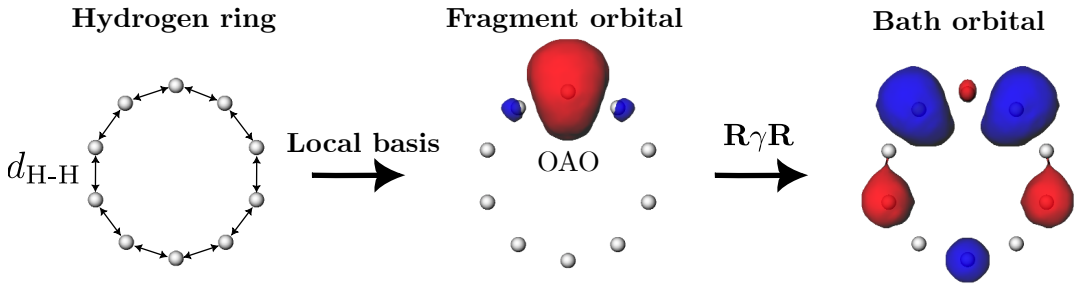

Figure 6.6: **Left:** hydrogen ring geometry used in our simulation with the interatomic distance $d_{\text{H-H}}$. **Middle:** associated local Orthogonal Atomic Orbital basis used to define molecular impurities. **Right:** shape of a bath orbital for the specific case of a single-orbital impurity.

quantum embedding on a chemical system is a bit more involved in practice. In this case, the localization of orbitals is an important pre-requisite for the definition of local molecular impurities. To build these orbitals, the first steps consist in realizing a (cheap) mean-field calculation over the whole chemical system (*e.g.* Hartree-Fock) to obtain a set of N_{occ} orthogonal occupied molecular orbital $\{|\phi_i^{\text{OCC}}\rangle\}_{i=1}^{N_{occ}}$ built as

a linear combination of atomic orbitals such that

$$\left|\phi_i^{\mathrm{OCC}}\right\rangle = \sum_{\mu}^{\mathrm{AOs}} [\mathbf{C}_{\mathrm{AO}}^{\mathrm{OCC}}]_{\mu i} \left|\chi_\mu^{\mathrm{AO}}\right\rangle, \tag{6.25}$$

where $\mathbf{C}_{\mathrm{AO}}^{\mathrm{OCC}}$ is the so-called MO coefficient matrix and $\{|\chi_\mu\rangle\}$ is the set of non-orthogonal atomic orbitals of the systems (original basis-set). Starting from this, we then express all occupied MOs into an orthogonal basis of local MOs. In practice, many methods exist to generate such basis. In this work, for sake of simplicity we choose to carry out calculations on hydrogen systems using a minimal basisset (i.e. STO-6G). This makes it possible to build symmetrically Orthogonalized Atomic Orbital (OAO) as a local orthogonal basis (also known as the Lowdin orbitals see Refs[154,155,156]). The resulting OAOs are designed to be as close as possible to the original AOs of any chemical system (in our case the 1s AOs of the hydrogen atoms). The OAOs are defined such as

$$\left|\overline{\chi}_l^{\mathrm{OAO}}\right\rangle = \sum_{\mu}^{\mathrm{AOs}} [\mathbf{S}^{-\frac{1}{2}}]_{\mu l} \left|\chi_\mu^{\mathrm{AO}}\right\rangle, \tag{6.26}$$

where the matrix $\mathbf{S}$ encodes the overlap between the different AOs of the system such as

$$[\mathbf{S}]_{\mu\nu} = \int d\mathbf{r} \chi_\mu(\mathbf{r}) \chi_\nu(\mathbf{r}).$$

Thanks to their locality, the OAOs will be assumed to play the role the molecular impurities in our case. Once the impurity orbitals are created, we then express the occupied MOs in this new orthogonal local basis

$$\left|\phi_l^{\mathrm{OCC}}\right\rangle = \sum_{p}^{\mathrm{OAOs}} [\mathbf{C}_{\mathrm{OAO}}^{\mathrm{OCC}}]_{pl} \left|\overline{\chi}_p^{\mathrm{OAO}}\right\rangle, \tag{6.27}$$

where we have

$$\mathbf{C}_{\mathrm{OAO}}^{\mathrm{OCC}} = \mathbf{S}^{\frac{1}{2}} \mathbf{C}_{\mathrm{AO}}^{\mathrm{OCC}}. \tag{6.28}$$

Note that we have here a positive sign as an exponent. Considering this, we compute the 1-RDM of the mean-field wave function $|\Phi\rangle$ and express the latter in the OAO basis such that

$$[\boldsymbol{\gamma}]_{pq} = \langle\Phi| \hat{c}_p^\dagger \hat{c}_q |\Phi\rangle \equiv 2\mathbf{C}_{\mathrm{OAO}}^{\mathrm{OCC}} (\mathbf{C}_{\mathrm{OAO}}^{\mathrm{OCC}})^\dagger. \tag{6.29}$$

We then choose a given impurity (i.e. the OAO associated with a given hydrogen atom). We then build the Householder transformation based on the shape of 1-RDM

expressed in the OAO basis to make it block-diagonal

$$\begin{aligned}\tilde{\boldsymbol{\gamma}} &= \mathbf{R}\boldsymbol{\gamma}\mathbf{R} \\ &= 2\mathbf{C}_{\text{HH-t}}^{\text{OCC}}(\mathbf{C}_{\text{HH-t}}^{\text{OCC}})^{\dagger},\end{aligned} \tag{6.30}$$

with

$$\mathbf{C}_{\text{HH-t}}^{\text{OCC}} = \mathbf{R}\mathbf{C}_{\text{OAO}}^{\text{OCC}}. \tag{6.31}$$

The resulting Householder-transformed 1-RDM will exhibit two blocks: one describing a Householder cluster encoding interaction between the impurities and their effective bath orbitals, the second block encodes information about interactions between occupied MOs which are totally disconnected from the cluster.

The Householder MO basis can be straightforwardly obtained and expressed in the OAO basis such that

$$\left|\phi_l^{\text{HH-t}}\right\rangle = \sum_m [\mathbf{R}]_{ml} \left|\phi_m^{\text{OAO}}\right\rangle, \tag{6.32}$$

which naturally can be expressed in the original AO basis such that

$$\left|\phi_l^{\text{HH-t}}\right\rangle = \sum_m [\mathbf{C}_{\text{AO}}^{\text{HH-t}}]_{\mu l}, \left|\phi_\mu^{\text{AO}}\right\rangle \tag{6.33}$$

with $\mathbf{C}_{\text{AO}}^{\text{HH-t}} = \mathbf{S}^{-\frac{1}{2}}\mathbf{R}$. As an illustration, we show in Fig. 6.7 the structure of the cluster orbitals for a hydrogen ring consisting of $N_A = 10$ atoms in total. Similarly

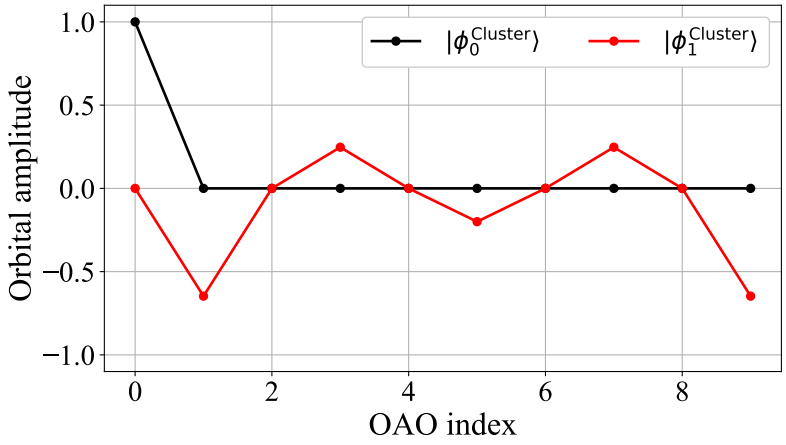

Figure 6.7: Cluster orbitals amplitudes in the OAO basis.

to the previous observations realized in the case of the Hubbard model [See bottom

panel of Fig. 5.6], there are two types of cluster orbitals: the impurity is unchanged by the transformation and remains localized on the first OAO and the bath orbital which is delocalized over the rest of the OAOs with a non-zero amplitude only on odd indices (and a null amplitude on the first OAO). The spatial extension of the Householder orbitals can also be appreciated in real space as shown in the middle and right plots of Fig. 6.6. In the middle, the impurity orbital is the OAO localized on the reference atom. On the right, the bath orbital which is delocalized all across the system. We see here the important role played by the two first neighbours of the reference atom around which the wave function exhibits the largest amplitudes. The wave function amplitude decays progressively as we get away from the original reference atom. Note that any other orbital forming the so-called "environment" of the effective Householder cluster extends over the OAOs of the system but never on the first OAO (not shown here).

With the creation of the cluster orbitals, one can set up its associated local active-space Hamiltonian. To do so, we start from the full second-quantized Hamiltonian of the chemical system and we express the latter in the Householder orbitals basis which yields three distinct contributions

$$\hat{\mathcal{H}} = \hat{\mathcal{H}}^{\mathcal{C}} + \hat{\mathcal{H}}^{\mathcal{E}} + \Delta\hat{\mathcal{H}}. \tag{6.34}$$

The two first Hamiltonians $\hat{\mathcal{H}}^{\mathcal{C}}$ and $\hat{\mathcal{H}}^{\mathcal{E}}$ define the one- and two-electron contributions which are respectively attached to either the Householder cluster, or its environment solely. They are defined such that

$$\hat{\mathcal{H}}^{\mathcal{C}} = \sum_{pq}^{\mathcal{C}} h_{pq}\hat{c}_p^\dagger\hat{c}_q + \frac{1}{2}\sum_{pqrs}^{\mathcal{C}} g_{pqrs}\hat{c}_p^\dagger\hat{c}_q^\dagger\hat{c}_s\hat{c}_r, \tag{6.35}$$

and

$$\hat{\mathcal{H}}^{\mathcal{E}} = \sum_{pq}^{\mathcal{E}} h_{pq}\hat{c}_p^\dagger\hat{c}_q + \frac{1}{2}\sum_{pqrs}^{\mathcal{E}} g_{pqrs}\hat{c}_p^\dagger\hat{c}_q^\dagger\hat{c}_s\hat{c}_r. \tag{6.36}$$

The last contribution in Eq. 6.34 encodes the environment/cluster interaction occurring when electrons are exchanged between both sub-systems. It is defined as

$$\Delta\hat{\mathcal{H}} = \sum_{pq}^{\mathcal{E}\text{-}\mathcal{C}} h_{pq}\hat{c}_p^\dagger\hat{c}_q + \frac{1}{2}\sum_{pqrs}^{\mathcal{E}\text{-}\mathcal{C}} g_{pqrs}\hat{c}_p^\dagger\hat{c}_q^\dagger\hat{c}_s\hat{c}_r. \tag{6.37}$$

At this step, we use the interacting bath approach where we project the full Hamiltonian according to the usual CAS-CI method. In this case, the active space is defined by the cluster MOs (impurities + bath orbitals) which yield an embedding Hamiltonian such as

$$\hat{\mathcal{H}}^{\mathcal{C}}_{\text{emb}} = \hat{\mathcal{H}}^{\mathcal{C}} + \hat{h}^{\text{eff}} + E^{\mathcal{E}}_{\text{MF}}, \tag{6.38}$$

where the term $E^{\mathcal{E}}_{\text{MF}}$ encodes the mean-field-like energy obtained from the frozen doubly-occupied environment orbitals,

$$E^{\text{MF}}_{\text{frozen}} = 2 \sum_{i}^{occ. \in \mathcal{E}} h_{ii} + \frac{1}{2} \sum_{ij}^{occ. \in \mathcal{E}} (2g_{iijj} - g_{ijji}), \tag{6.39}$$

The operator $\hat{h}^{\text{eff}}$ defined by

$$\hat{h}^{\text{eff}} = \sum_{pq}^{\mathcal{C}} h^{\text{eff}}_{pq} \hat{c}^{\dagger}_{p} \hat{c}_{q}, \text{ with } h^{\text{eff}}_{pq} = \sum_{i}^{occ. \in \mathcal{E}} (2g_{pqii} - g_{piiq}), \tag{6.40}$$

represents an effective one-body potential which encodes the interaction of the frozen electrons in the environment $\mathcal{E}$ with the active space electrons (living in the Householder cluster).

In practice, due to the summation over all the impurities composing the molecule, one discards the mean-field energy contribution $E^{\text{MF}}_{\text{frozen}}$ from the cluster Hamiltonian. This is made in order to avoid double counting when summing all the local energy contributions obtained from each impurity.

In order to check the equivalence of the Householder transformation with the singular value decomposition [See Section 5.3], the single-shot DMET scheme for molecular systems is followed.[39,61] The bath is treated in the so-called interacting picture and a democratic partitioning of the local cluster contributions is used to produce an estimation of the global ground state energy. A chemical potential μ_{glob} is introduced to correct the total number of electrons in the systems such as

$$\hat{\mathcal{H}}^{\mathcal{C}}_{\text{emb}} \leftarrow \hat{\mathcal{H}}^{\mathcal{C}}_{\text{emb}} - \mu_{glob} \sum_{i \in \text{ impurities}} \hat{n}_i. \tag{6.41}$$

This implies that we minimize the cost function

$$\text{CF}(\mu_{glob}) = \left(N_{elec} - \sum_{\mathcal{C}} \sum_{i \in \text{ impurities}} \gamma^{\mathcal{C}}_{ii}(\mu_{glob}) \right)^2, \tag{6.42}$$

in order to retrieve the same number of electrons when considering all the impurities.

Following this scheme, embedding calculations using Block-Householder in Ht-DMFET on the H_{10} hydrogen system were conducted. In Fig. 6.8, results obtained for the embedding of molecular impurities composed of one and two neighbour Hydrogen atoms (*i.e.* OAOs) are shown with respective orange and blue dashed curves. For comparison, exact FCI calculations are also shown (dashed-line black curve) with Hartree-Fock energies (full-line black curve). The left panel shows the resulting potential energy surfaces (PES) whereas the right panel shows the percentage of correlation energies recovered by Ht-DMFET as a function of the interatomic distance $d_{\text{H-H}}$. As readily seen with the PESs, for both sizes of impurity, the Ht-DMFET energies follow the FCI results very closely along the whole dissociation curve (the FCI curve is almost indistinguishable). In similar way to DMET, the evolution of the percentage of correlation energy recovered shows that the Ht-DMFET method is non-variational (as the orange curves goes beyond the 100% of correlation energy). This is expected due to the way the energy is computed here (as explained in Ref.[39,61]). In practice, no real improvement of the embedding quality is observed when increasing the number of impurity site in the Block-Householder partitioning. This is essentially related to the intrinsic single shot-nature of Ht-DMFET.

To conclude, similar in spirit to DMET, a (static and zero-temperature) (block) Householder transformed density matrix functional embedding theory (Ht-DMFET) has been derived. The theory has been applied to the 1D Hubbard model and an hydrogen ring. In the non-interacting case, the formal reduction of the full system to a $2L_f$-electron cluster is exact. Thanks to the Householder transformation, the bath orbitals can be determined (analytically) from the density matrix of the (full) system. Starting from the exact non-interacting and *closed* Householder cluster, correlation can be introduced straightforwardly by Householder transforming (and projecting onto the cluster) the on-site two-electron repulsion operator, which is defined in the real space representation. For the Hubbard lattice at half-filling ($n = 1$), the resulting (approximate) Ht-DMFET per-site energies are in almost

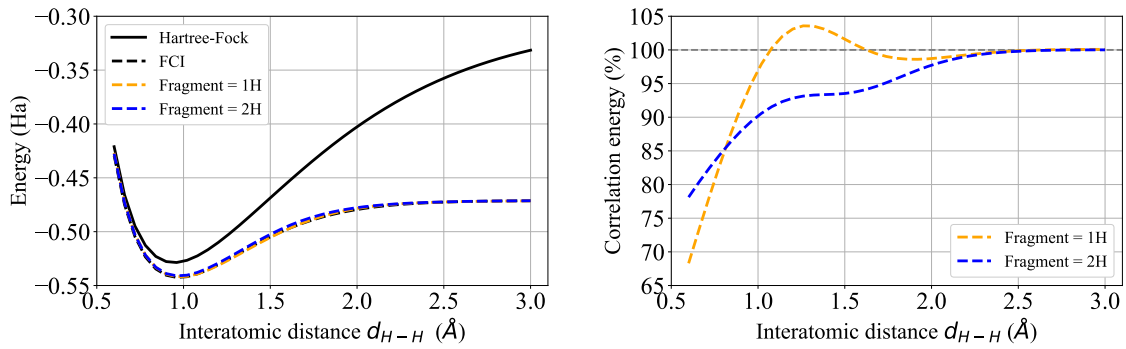

Figure 6.8: Energy of a ring composed of 10 hydrogen as a function of the regular interatomic distance d_{H-H}. Comparison of Ht-DMFET energies with FCI (dashed black curve) and Hartree-Fock (full-line black curve). **Left:** the PES dissociation curve obtained with the embedding of one and two-atom impurities (orange and blue curves) compared to the exact FCI results (black curve). **Right:** percentage of correlation energy recovered with both sizes of impurity (this energy is the difference between Hartree-Fock and FCI calculations).

perfect agreement with the Bethe Ansatz (BA) results in all correlation regimes provided that *(i)* a chemical potential is introduced on the impurity site, like in DMET, thus ensuring that the correct filling is reproduced, and *(ii)* the interaction in the bath is taken into account. The good performance of Ht-DMFET in this case can be partly related to the fact that, at half-filling, the true (correlated) Householder cluster contains exactly $2L_f$ electrons, as a consequence of the hole-particle symmetry. Away from half-filling, the deviation from the BA results becomes substantial in the strongly correlated regime. The results dramatically improve increasing the number of impurities to embed. In the latter case, a block Householder transformation is employed[37]. Description of the density-driven Mott-Hubbard transition is almost retrieved by embedding three impurities at the interacting bath level. This result is interesting for the future as it proves that Ht-DMFET is able to capture non-trivial properties coming from strongly correlated materials. A multiple impurity implementation of Ht-DMFET applied to an *Ab initio* Hamiltonian has also been presented. This approach recovers results obtained in DMET[61] and ensure the similarity proven in Section 5.3. In the light of recent advances in DMET and related approaches, several extensions of the present

work can already be foreseen[157,158,143,149].

Interestingly, we observed that the density mapping conditions was crucial in order to retrieve significant results. It is known that in DMET, the mapping of the cluster density matrix has representability problems[159]. Consequently, applying the Householder transformation to the Kohn-Sham density matrix would make the approach formally exact. Moreover, introducing an orbital occupation mapping constraints in a self-consistency loop, like in DET[38] or SDE[160], would make complete sense in this context. This new paradigm is the purpose of the next section.

Chapter 7

Local potential functional embedding theory

In the present embedding scheme, we circumvent the ill-defined density matrix mapping conditions of DMET by an in-principle-exact combination of KS-DFT with Ht-DMFET for the one-dimensional (1D) Hubbard lattice and develop a self-consistent loop, between the original lattice and the Householder cluster, based on a density mapping which has been proven to be crucial in order to retrieve meaningful results [See section 6]. For that purpose, we use the density-matrix functional Householder transformation. On the basis of well-identified density-functional approximations, we propose and implement a *local potential functional embedding theory* (LPFET) where the Hxc potential is evaluated self-consistently in the lattice by "learning" from the embedding cluster at each iteration of the optimization process. LPFET can be seen as a flavor of KS-DFT where no density functional is actually used or a static and zero temperature version of the two-site DMFT[161] where instead of updating the self-energy Σ from the impurity problem, the Hxc potential is updated from the reduced-in-size Householder cluster. Note that the following section is greatly inspired by the paper entitled *"local potential functional embedding theory: a self-consistent flavor of density functional theory for lattices without density functionals"*[162].

By analogy with Ht-DMFET, various quantum embedding strategies will be discussed in the following within the simple but nontrivial uniform 1D Hubbard

model. The corresponding lattice Hamiltonian (for a L-site ring) reads as

$$\hat{H} = \hat{T} + \hat{U} + v_{\text{ext}}\hat{N}, \tag{7.1}$$

where the two-electron repulsion operator $\hat{U}$ is identical to Eq. (3.2) and the kinetic energy operator is defined as in Eq. (3.1). We will systematically use periodic boundary conditions, *i.e.*, $\hat{c}^{\dagger}_{L\sigma} \equiv \hat{c}^{\dagger}_{0\sigma}$ for convenience. Since the lattice is uniform, the local external potential (which would correspond to the nuclear potential in a conventional quantum chemical calculation) operator is proportional to the electron counting operator [See the last term on the right-hand side of Eq. (7.1)],

$$\hat{N} = \sum_{i=0}^{L-1} \sum_{\sigma=\uparrow,\downarrow} \hat{n}_{i\sigma}. \tag{7.2}$$

The uniform value of the external potential can be rewritten as

$$v_{\text{ext}} = -\mu, \tag{7.3}$$

where the chemical potential μ controls the number of electrons N or, equivalently, the uniform density $n = N/L$ in the lattice. In this case, $\hat{H}$ is actually a (zero-temperature) grand canonical Hamiltonian.

It is important to underline that unlike in the exact reformulation of the theory proposed in LPFET and where the chemical potential μ controls the density of the uniform lattice, the total number of electrons is *fixed* to the value N in Ht-DMFET. In other words, the uniform density is set to $n = N/L$ and μ is an arbitrary constant (that could be set to zero). The following derivations will be developed for a single impurity but extensions to multiple impurity is possible but require more involved developments.

7.1 Non-interacting embedding Hamiltonian

Let us first recall concisely the particular case of a non-interacting ($U = 0$) lattice for which Ht-DMFET is exact [See Section 6.1]. As it will be applied later on to the auxiliary KS lattice, it is important to highlight the key features of the non-interacting embedding.

As the Householder cluster is strictly disconnected from its environment in the non-interacting case, it is exactly described by the two-electron ground state $\left|\Phi^{\mathcal{C}}\right\rangle$ of the Householder-transformed hopping operator (that we refer to as kinetic energy operator from now on, like in DFT for lattices[163]) projected onto the cluster, *i.e.*,

$$\hat{\mathcal{T}}^{\mathcal{C}} \left|\Phi^{\mathcal{C}}\right\rangle = \mathcal{E}_{\mathrm{s}}^{\mathcal{C}} \left|\Phi^{\mathcal{C}}\right\rangle, \tag{7.4}$$

where, according to Eqs. (3.1) and (5.20),

$$\hat{\mathcal{T}}^{\mathcal{C}} = \sum_{ij} \sum_{\sigma=\uparrow,\downarrow} t_{ij} \sum_{k,l=0}^{1} R_{ik} R_{jl} \hat{d}^{\dagger}_{k\sigma} \hat{d}_{l\sigma}. \tag{7.5}$$

For convenience, we will separate in $\hat{\mathcal{T}}^{\mathcal{C}}$ the physical per-site kinetic energy operator [See Eq. (3.1)],

$$\hat{t}_{01} = -t \sum_{\sigma=\uparrow,\downarrow} \left(\hat{c}^{\dagger}_{0\sigma} \hat{c}_{1\sigma} + \hat{c}^{\dagger}_{1\sigma} \hat{c}_{0\sigma} \right), \tag{7.6}$$

from the correction induced (within the cluster) by the Householder transformation:

$$\hat{\tau}^{\mathcal{C}} = \hat{\mathcal{T}}^{\mathcal{C}} - \hat{t}_{01}. \tag{7.7}$$

Note that, since $t_{00} = 0$, $\hat{\tau}^{\mathcal{C}}$ can be expressed more explicitly as follows,

$$\begin{aligned}
\hat{\tau}^{\mathcal{C}} &= \sum_{\sigma=\uparrow,\downarrow} \left(\sum_{ij} R_{i1} R_{j0} t_{ij} \right) \left[\hat{d}^{\dagger}_{0\sigma} \hat{d}_{1\sigma} + \hat{d}^{\dagger}_{1\sigma} \hat{d}_{0\sigma} \right] \\
&\quad + \sum_{\sigma=\uparrow,\downarrow} \left(\sum_{ij} R_{i1} R_{j1} t_{ij} \right) \hat{d}^{\dagger}_{1\sigma} \hat{d}_{1\sigma} - \hat{t}_{01} \\
&= \sum_{\sigma=\uparrow,\downarrow} \left(\sum_{i} R_{i1} t_{i0} \right) \left[\hat{c}^{\dagger}_{0\sigma} \hat{d}_{1\sigma} + \hat{d}^{\dagger}_{1\sigma} \hat{c}_{0\sigma} \right] \\
&\quad + \sum_{\sigma=\uparrow,\downarrow} \left(\sum_{ij} R_{i1} R_{j1} t_{ij} \right) \hat{d}^{\dagger}_{1\sigma} \hat{d}_{1\sigma} - \hat{t}_{01} \\
&= \sum_{\sigma=\uparrow,\downarrow} t_{10} \left[\hat{c}^{\dagger}_{0\sigma} \hat{d}_{1\sigma} + \hat{d}^{\dagger}_{1\sigma} \hat{c}_{0\sigma} \right] \\
&\quad - 2\mathrm{v}_1 \sum_{\sigma=\uparrow,\downarrow} \left(\sum_{i} \mathrm{v}_i t_{i0} \right) \left[\hat{c}^{\dagger}_{0\sigma} \hat{d}_{1\sigma} + \hat{d}^{\dagger}_{1\sigma} \hat{c}_{0\sigma} \right] \\
&\quad + \sum_{\sigma=\uparrow,\downarrow} \left(\sum_{ij} R_{i1} R_{j1} t_{ij} \right) \hat{d}^{\dagger}_{1\sigma} \hat{d}_{1\sigma} - \hat{t}_{01},
\end{aligned} \tag{7.8}$$

thus leading to

$$\begin{aligned}\hat{\tau}^{\mathcal{C}} = & 2t\mathrm{v}_1 \sum_{\sigma=\uparrow,\downarrow} \sum_{k\geq 1} \mathrm{v}_k \left[\hat{c}^{\dagger}_{0\sigma}\hat{c}_{k\sigma} + \hat{c}^{\dagger}_{k\sigma}\hat{c}_{0\sigma}\right] \\ & - 2\mathrm{v}_1 \sum_{\sigma=\uparrow,\downarrow} \left(\sum_i \mathrm{v}_i t_{i0}\right) \left[\hat{c}^{\dagger}_{0\sigma}\hat{d}_{1\sigma} + \hat{d}^{\dagger}_{1\sigma}\hat{c}_{0\sigma}\right] \\ & + 4\left(\sum_{ij} \mathrm{v}_i\mathrm{v}_j\left(\mathrm{v}_1^2 - \delta_{j1}\right) t_{ij}\right) \sum_{\sigma=\uparrow,\downarrow} \hat{d}^{\dagger}_{1\sigma}\hat{d}_{1\sigma},\end{aligned} \tag{7.9}$$

where we used Eqs. (5.15) and (5.23), as well as the fact that $t_{11} = 0$ and $t_{10} = -t$. Note that, when no Householder transformation is performed (*i.e.*, when $\mathrm{v}_i = 0$ for $0 \leq i \leq L-1$), the bath site simply corresponds to the nearest neighbor ($i = 1$) of the impurity in the lattice [See Eq. (5.23)] and, as readily seen from Eqs. (7.7) and (7.9), the non-interacting cluster's Hamiltonian $\hat{\mathcal{T}}^{\mathcal{C}}$ reduces to $\hat{t}_{01}$.

Unlike in the interacting case, which is discussed in Section 7.2, it is unnecessary to introduce an additional potential on the embedded impurity in order to ensure that it reproduces the correct lattice filling [See Figure 6.1],

$$\left\langle \Phi^{\mathcal{C}} \middle| \hat{c}^{\dagger}_{0\sigma}\hat{c}_{0\sigma} \middle| \Phi^{\mathcal{C}} \right\rangle = \left\langle \Phi^{\mathcal{C}} \middle| \hat{d}^{\dagger}_{0\sigma}\hat{d}_{0\sigma} \middle| \Phi^{\mathcal{C}} \right\rangle = n/2. \tag{7.10}$$

This constraint is automatically fulfilled when Householder transforming the kinetic energy operator $\hat{T}$ of the full lattice, thanks to the local potential contribution on the bath [See the last term on the right-hand side of Eq. (7.9)]. Interestingly, the true (non-interacting in this case) per-site energy of the lattice can be determined solely from $\Phi^{\mathcal{C}}$. Indeed, according to Eqs. (6.17) and (6.18) , the per-site kinetic energy can be evaluated from the lattice ground state wave function Φ as follows,

$$\begin{aligned}\langle \Phi | \hat{t}_{01} | \Phi \rangle &= -4t\gamma_{10} \\ &= \left\langle \Phi^{\mathcal{C}} \middle| \hat{t}_{01} \middle| \Phi^{\mathcal{C}} \right\rangle,\end{aligned} \tag{7.11}$$

which facilitates the evaluation of non-interacting energies for lattices.

7.2 Approximate interacting embedding

The simplest (approximate) extension of Ht-DMFET to interacting electrons consists in introducing the on-impurity-site two-electron repulsion operator $\hat{U}_0$ into the

non-interacting Householder cluster's Hamiltonian of Eq. (7.4), by analogy with DMET[26]. In such a (standard) scheme, the interaction is treated *on top* of the non-interacting embedding. Unlike in the non-interacting case, it is necessary to introduce a chemical potential $\tilde{\mu}^{\text{frag}}$ on the embedded impurity in order to ensure that it reproduces the correct lattice filling N/L [See Eqs. (6.22),(6.23) and Fig. 6.1], *i.e.*,

$$\langle \hat{n}_0 \rangle_{\Psi^{\mathcal{C}}} = N/L, \tag{7.12}$$

where the two-electron cluster's ground state wave function $\Psi^{\mathcal{C}}$ fulfills the following interacting Schrödinger equation:

$$\left(\hat{\mathcal{T}}^{\mathcal{C}} + \hat{U}_0 - \tilde{\mu}^{\text{frag}} \hat{n}_0\right) \left|\Psi^{\mathcal{C}}\right\rangle = \mathcal{E}^{\mathcal{C}} \left|\Psi^{\mathcal{C}}\right\rangle . \tag{7.13}$$

The physical per-site energy (from which we remove the chemical potential contribution) is then evaluated as follows:

$$(E + \mu N)/L \underset{\text{Ht}-\text{DMFET}}{\approx} \left\langle \Psi^{\mathcal{C}} \middle| \hat{t}_{01} + \hat{U}_0 \middle| \Psi^{\mathcal{C}} \right\rangle . \tag{7.14}$$

We will show in the following that, once it has been merged with KS-DFT, Ht-DMFET can be made formally exact. For clarity, we start with reviewing briefly KS-DFT for lattice Hamiltonians in Section 7.3. A multi-determinantal extension of the theory based on the interacting Householder cluster's wave function is then proposed in Section 7.4.

7.3 KS-DFT for uniform lattices

According to the Hohenberg–Kohn (HK) variational principle[66], which is applied in this work to lattice Hamiltonians, the ground state energy of the full lattice can be determined as follows,

$$E = \min_{n} \left\{ F(n) + v_{\text{ext}} n L \right\}, \tag{7.15}$$

where the HK density functional reads as

$$F(n) = \langle \Psi(n) | \hat{T} + \hat{U} | \Psi(n) \rangle , \tag{7.16}$$

and $|\Psi(n)\rangle$ is the lattice ground state with uniform density profile $n \overset{0 \leq i < L}{=} \langle \Psi(n) | \hat{n}_i | \Psi(n) \rangle$. Strictly speaking, $F(n)$ is a function of the site occupation n,

hence the name *site occupation functional theory* often given to DFT for lattices. Note that the ground state energy E is in fact a (zero-temperature) grand canonical energy since a change in uniform density n induces a change in the number $N = nL$ of electrons. In the thermodynamic $N \to +\infty$ and $L \to +\infty$ limit, with N/L fixed to n, one can in principle describe *continuous* variations in n with a pure-state wave function $\Psi(n)$. The derivations that follow will be based on this assumption. If we introduce the per-site analog of the HK functional,

$$f(n) = F(n)/L = \langle \Psi(n) | \hat{t}_{01} + \hat{U}_0 | \Psi(n) \rangle \,, \tag{7.17}$$

and use the notation of Eq. (7.3), then Eq. (7.15) becomes

$$E/L \equiv E(\mu)/L = \min_n \{ f(n) - \mu n \} \,, \tag{7.18}$$

and the minimizing density $n(\mu)$ fulfills the following stationarity condition:

$$\mu = \left. \frac{\partial f(n)}{\partial n} \right|_{n=n(\mu)} . \tag{7.19}$$

In the conventional KS formulation of DFT, the per-site HK functional is decomposed as follows,

$$f(n) = t_{\rm s}(n) + e_{\rm Hxc}(n), \tag{7.20}$$

where

$$t_{\rm s}(n) = \langle \Phi(n) | \hat{t}_{01} | \Phi(n) \rangle = \frac{1}{L} \langle \Phi(n) | \hat{T} | \Phi(n) \rangle \,, \tag{7.21}$$

is the (per-site) analog for lattices of the non-interacting kinetic energy functional, and the Hxc density functional reads as

$$e_{\rm Hxc}(n) = \frac{U}{4} n^2 + e_{\rm c}(n), \tag{7.22}$$

where $e_{\rm c}(n)$ is the exact (per-site) correlation energy functional of the interacting lattice. The (normalized) density-functional lattice KS determinant $\Phi(n)$ fulfills the (non-interacting) KS equation

$$\left(\hat{T} - \mu_{\rm s}(n) \hat{N} \right) | \Phi(n) \rangle = \mathcal{E}_{\rm s}(n) \, | \Phi(n) \rangle \,, \tag{7.23}$$

so that [See Eq. (7.21)]

$$\begin{aligned}\frac{\partial t_{\rm s}(n)}{\partial n} &= \frac{2}{L}\left\langle \frac{\partial\Phi(n)}{\partial n}\middle|\hat{T}\middle|\Phi(n)\right\rangle \\ &= \frac{2\mu_{\rm s}(n)}{L}\left\langle \frac{\partial\Phi(n)}{\partial n}\middle|\hat{N}\middle|\Phi(n)\right\rangle \\ &= \frac{\mu_{\rm s}(n)}{L}\frac{\partial(nL)}{\partial n} \\ &= \mu_{\rm s}(n),\end{aligned} \tag{7.24}$$

since $\langle\Phi(n)|\hat{N}|\Phi(n)\rangle = N = nL$. Thus we recover from Eqs. (7.19) and (7.20) the well-known relation between the physical and KS chemical potentials:

$$\mu_{\rm s}(n(\mu)) \equiv \mu_{\rm s} = \mu - v_{\rm Hxc}, \tag{7.25}$$

where the density-functional Hxc potential reads as $v_{\rm Hxc} = v_{\rm Hxc}(n(\mu))$ with

$$v_{\rm Hxc}(n) = \frac{\partial e_{\rm Hxc}(n)}{\partial n}. \tag{7.26}$$

Note that the exact non-interacting density-functional chemical potential can be expressed analytically as follows[164]:

$$\mu_{\rm s}(n) = -2t\cos\left(\frac{\pi}{2}n\right). \tag{7.27}$$

Capelle and coworkers[164] have designed a local density approximation (LDA) to $e_{\rm Hxc}(n)$ on the basis of exact Bethe Ansatz (BA) solutions[35] (the functional is usually referred to as BALDA). Even though BALDA can be extended to higher dimensions[165], there is no general strategy for constructing (localized) orbital-occupation functional approximations, thus preventing direct applications to quantum chemistry[166], for example. Turning ultimately to a potential-functional theory, as proposed in Section 7.5, is appealing in this respect. With this change of paradigm, which is the second key result of this method, the Hxc energy and potential become implicit functionals of the density, and they can be evaluated from a (few-electron) correlated wave function through a quantum embedding procedure.

7.4 Density-functional interacting cluster

We propose in this section an alternative formulation of DFT based on the interacting Householder cluster introduced in Section 7.2. For that purpose, we consider

the following *exact* decomposition,

$$f(n) = f^{\mathcal{C}}(n) + \overline{e}_{\rm c}(n), \tag{7.28}$$

where the Householder cluster HK functional

$$f^{\mathcal{C}}(n) = \left\langle \Psi^{\mathcal{C}}(n) \middle| \hat{t}_{01} + \hat{U}_0 \middle| \Psi^{\mathcal{C}}(n) \right\rangle, \tag{7.29}$$

is evaluated from the two-electron cluster density-functional wave function $\Psi^{\mathcal{C}}(n)$, and $\overline{e}_{\rm c}(n)$ is the complementary correlation density functional that describes the missing correlation effects of the interacting bath and the Householder cluster's environment on the embedded impurity. Note that, according to Section 7.2, $\left|\Psi^{\mathcal{C}}(n)\right\rangle$ fulfills the following Schrödinger-like equation,

$$\hat{\mathcal{H}}^{\mathcal{C}}(n) \left|\Psi^{\mathcal{C}}(n)\right\rangle = \mathcal{E}^{\mathcal{C}}(n) \left|\Psi^{\mathcal{C}}(n)\right\rangle, \tag{7.30}$$

where (we use the same notations as in Section 7.2)

$$\hat{\mathcal{H}}^{\mathcal{C}}(n) \equiv \hat{\mathcal{T}}^{\mathcal{C}}(n) + \hat{U}_0 - \tilde{\mu}^{\rm frag}(n)\, \hat{n}_0, \tag{7.31}$$

and

$$\hat{\mathcal{T}}^{\mathcal{C}}(n) \equiv \hat{t}_{01} + \hat{\tau}^{\mathcal{C}}(n). \tag{7.32}$$

The dependence in n of the (projected-onto-the-cluster) Householder-transformed kinetic energy operator $\hat{\mathcal{T}}^{\mathcal{C}}(n)$ comes from the fact that the KS lattice density matrix $\boldsymbol{\gamma}(n) \equiv \langle \Phi(n) | \hat{c}^{\dagger}_{i\sigma} \hat{c}_{j\sigma} | \Phi(n) \rangle$ (on which the Householder transformation is based) is, like the KS determinant $\Phi(n) \equiv \Phi^{\mathcal{C}}(n) \Phi_{\rm core}(n)$ of the lattice, a functional of the uniform density n. On the other hand, for a given uniform lattice density n, the local potential $-\tilde{\mu}^{\rm frag}(n)$ is adjusted on the embedded impurity such that the interacting cluster reproduces n, *i.e.*,

$$\left\langle \Psi^{\mathcal{C}}(n) \middle| \hat{n}_0 \middle| \Psi^{\mathcal{C}}(n) \right\rangle = n. \tag{7.33}$$

Interestingly, on the basis of the two decompositions in Eqs. (7.20) and (7.28), and Eq. (7.29), we can relate the exact Hxc functional to the density-functional Householder cluster as follows,

$$e_{\rm Hxc}(n) \;\; = \left\langle \Psi^{\mathcal{C}}(n) \middle| \hat{t}_{01} + \hat{U}_0 \middle| \Psi^{\mathcal{C}}(n) \right\rangle - t_{\rm s}(n) + \overline{e}_{\rm c}(n), \tag{7.34}$$

where, as shown in Eq. (6.18), the per-site non-interacting kinetic energy can be determined exactly from the two-electron cluster's part $\Phi^{\mathcal{C}}(n)$ of the KS lattice determinant $\Phi(n)$, *i.e.*,

$$t_{\rm s}(n) = \left\langle \Phi^{\mathcal{C}}(n) \middle| \hat{t}_{01} \middle| \Phi^{\mathcal{C}}(n) \right\rangle , \tag{7.35}$$

thus leading to the final expression

$$e_{\rm Hxc}(n) = \left\langle \Psi^{\mathcal{C}}(n) \middle| \hat{t}_{01} + \hat{U}_0 \middle| \Psi^{\mathcal{C}}(n) \right\rangle - \left\langle \Phi^{\mathcal{C}}(n) \middle| \hat{t}_{01} \middle| \Phi^{\mathcal{C}}(n) \right\rangle + \overline{e}_{\rm c}(n). \tag{7.36}$$

Note that, according to Eqs. (7.4) and (7.7), $\Phi^{\mathcal{C}}(n)$ fulfills the KS-like equation

$$\left(\hat{t}_{01} + \hat{\tau}^{\mathcal{C}}(n)\right) \left| \Phi^{\mathcal{C}}(n) \right\rangle = \mathcal{E}_{\rm s}^{\mathcal{C}}(n) \left| \Phi^{\mathcal{C}}(n) \right\rangle , \tag{7.37}$$

where the Householder transformation ensures that $\left\langle \Phi^{\mathcal{C}}(n) \middle| \hat{n}_0 \middle| \Phi^{\mathcal{C}}(n) \right\rangle = n$ [See Eq. (7.10)].

We will now establish a clearer connection between the KS lattice system and the Householder cluster *via* the evaluation of the Hxc density-functional potential in the lattice. According to Eqs. (7.26) and (7.36), the latter can be expressed as follows,

$$\begin{aligned} v_{\rm Hxc}(n) = 2 \left\langle \frac{\partial \Psi^{\mathcal{C}}(n)}{\partial n} \middle| \hat{t}_{01} + \hat{U}_0 \middle| \Psi^{\mathcal{C}}(n) \right\rangle \\ - 2 \left\langle \frac{\partial \Phi^{\mathcal{C}}(n)}{\partial n} \middle| \hat{t}_{01} \middle| \Phi^{\mathcal{C}}(n) \right\rangle + \frac{\partial \overline{e}_{\rm c}(n)}{\partial n}, \end{aligned} \tag{7.38}$$

or, equivalently [See Eqs. (7.30), (7.33), and (7.37)],

$$\begin{aligned} v_{\rm Hxc}(n) = \tilde{\mu}^{\rm frag}(n) - 2 \left\langle \frac{\partial \Psi^{\mathcal{C}}(n)}{\partial n} \middle| \hat{\tau}^{\mathcal{C}}(n) \middle| \Psi^{\mathcal{C}}(n) \right\rangle \\ + 2 \left\langle \frac{\partial \Phi^{\mathcal{C}}(n)}{\partial n} \middle| \hat{\tau}^{\mathcal{C}}(n) \middle| \Phi^{\mathcal{C}}(n) \right\rangle + \frac{\partial \overline{e}_{\rm c}(n)}{\partial n}. \end{aligned} \tag{7.39}$$

If we introduce the following bi-functional of the density,

$$\tau_{\rm c}^{\mathcal{C}}(n,\nu) = \left\langle \Psi^{\mathcal{C}}(\nu) \middle| \hat{\tau}^{\mathcal{C}}(n) \middle| \Psi^{\mathcal{C}}(\nu) \right\rangle - \left\langle \Phi^{\mathcal{C}}(\nu) \middle| \hat{\tau}^{\mathcal{C}}(n) \middle| \Phi^{\mathcal{C}}(\nu) \right\rangle , \tag{7.40}$$

which can be interpreted as a kinetic correlation energy induced within the density-functional cluster by the Householder transformation and the interaction on the impurity, we obtain the final *exact* expression

$$v_{\rm Hxc}(n) = \tilde{\mu}^{\rm frag}(n) - \left. \frac{\partial \tau_{\rm c}^{\mathcal{C}}(n,\nu)}{\partial \nu} \right|_{\nu=n} + \frac{\partial \overline{e}_{\rm c}(n)}{\partial n}, \tag{7.41}$$

which is the first key result of this method.

Before turning Eq. (7.41) into a practical self-consistent embedding method (See Section 7.5), let us briefly discuss its physical meaning and connection with Ht-DMFET. As pointed out in Section 7.1, the (density-functional) operator $\hat{\tau}^{\mathcal{C}}(n)$ is an auxiliary correction to the true per-site kinetic energy operator $\hat{t}_{01}$ which originates from the Householder-transformation-based embedding of the impurity. It is not physical and its impact on the impurity chemical potential $\tilde{\mu}^{\text{frag}}(n)$, which is determined in the presence of $\hat{\tau}^{\mathcal{C}}(n)$ in the cluster's Hamiltonian [See Eqs. (7.30)-(7.32)], should be removed when evaluating the Hxc potential of the true lattice, hence the minus sign in front of the second term on the right-hand side of Eq. (7.41). Finally, the complementary correlation potential $\partial\overline{e}_{\text{c}}(n)/\partial n$ is in charge of recovering the electron correlation effects that were lost when considering an (impurity-only) interacting cluster that is disconnected from its environment. We should stress at this point that, in Ht-DMFET (which is equivalent to DMET or DET when a single impurity is embedded), the following density-functional approximation is made:

$$\overline{e}_{\text{c}}(n) \underset{\text{Ht}-\text{DMFET}}{\approx} 0, \tag{7.42}$$

so that the physical density-functional chemical potential is evaluated as follows,

$$\mu(n) \underset{\text{Ht}-\text{DMFET}}{\approx} \frac{\partial f^{\mathcal{C}}(n)}{\partial n}. \tag{7.43}$$

Interestingly, even though it is never computed explicitly in this context, the corresponding (approximate) Hxc potential simply reads as

$$v_{\text{Hxc}}(n) \underset{\text{Ht}-\text{DMFET}}{\approx} \frac{\partial (f^{\mathcal{C}}(n) - t_{\text{s}}(n))}{\partial n}, \tag{7.44}$$

or, equivalently [See Eqs. (7.41) and (7.42)],

$$v_{\text{Hxc}}(n) \underset{\text{Ht}-\text{DMFET}}{\approx} \tilde{\mu}^{\text{frag}}(n) - \left.\frac{\partial \tau_{\text{c}}^{\mathcal{C}}(n,\nu)}{\partial \nu}\right|_{\nu=n}. \tag{7.45}$$

Therefore, Ht-DMFET can be seen as an approximate formulation of KS-DFT where the Hxc potential is determined solely from the density-functional Householder cluster. As illustrated in Fig. 6.4, the approximation of Eq. (7.42) leads, for example, to

a substantial underestimation of the per-site energy, except in the vicinity of half filling where the energy is overestimated. Describing the electron repulsion in the bath (not considered in the present work, for simplicity) lowers the energy even further, thus leading to accurate results only at half filling, because of error cancellations. Most importantly, Eq. (7.42) implies that Ht-DMFET neglects the fluctuations in the electron number within the Householder cluster [See Eqs. (7.28)-(7.30)]. Consequently, as further discussed in section 6.4, Ht-DMFET at the single impurity level is unable to describe the opening of the gap at half filling.

7.5 Local potential functional embedding theory

Until now the Householder transformation has been described as a functional of the uniform density n or, more precisely, as a functional of the KS density matrix, which is itself a functional of the density. If we opt for a potential-functional reformulation of the theory, as suggested in the following, the Householder transformation becomes a functional of the KS chemical potential $\mu_{\rm s}$ instead, and, consequently, the Householder correction to the per-site kinetic energy operator within the cluster [See Eq. (7.32)] is also a functional of $\mu_{\rm s}$:

$$\hat{\tau}^{\mathcal{C}}(n) \to \hat{\tau}^{\mathcal{C}}(\mu_{\rm s}). \tag{7.46}$$

Similarly, the interacting cluster's wave function becomes a bi-functional of the KS *and* interacting embedded impurity chemical potentials:

$$\Psi^{\mathcal{C}}(n) \to \Psi^{\mathcal{C}}\left(\mu_{\rm s}, \tilde{\mu}^{\rm frag}\right). \tag{7.47}$$

In the exact theory, for a given chemical potential value μ in the true interacting lattice, both the KS lattice and the embedded impurity reproduce the interacting lattice density $n(\mu)$, *i.e.*,

$$n(\mu) = n^{\rm KS}_{\rm lattice}\left(\mu - v_{\rm Hxc}\right) = n^{\mathcal{C}}\left(\mu - v_{\rm Hxc}, \tilde{\mu}^{\rm frag}\right), \tag{7.48}$$

where

$$n^{\rm KS}_{\rm lattice}(\mu_{\rm s}) \equiv \langle \hat{n}_0 \rangle_{\hat{T}-\mu_{\rm s}\hat{N}}, \tag{7.49}$$

and

$$\begin{aligned} n^{\mathcal{C}}\left(\mu_{\rm s},\tilde{\mu}^{\rm frag}\right) &= \langle \hat{n}_0 \rangle_{\Psi^{\mathcal{C}}\left(\mu_{\rm s},\tilde{\mu}^{\rm frag}\right)} \\ &\equiv \langle \hat{n}_0 \rangle_{\hat{t}_{01}+\hat{\tau}^{\mathcal{C}}(\mu_{\rm s})+\hat{U}_0-\tilde{\mu}^{\rm frag}\hat{n}_0}\,, \end{aligned} \tag{7.50}$$

with, according to Eq. (7.41),

$$\begin{aligned} \tilde{\mu}^{\rm frag} &= \tilde{\mu}^{\rm frag}(n(\mu)) \\ &= v_{\rm Hxc} - \left[\frac{\partial \overline{e}_{\rm c}(\nu)}{\partial \nu} - \frac{\partial \tau_{\rm c}^{\mathcal{C}}(n(\mu),\nu)}{\partial \nu}\right]_{\nu=n(\mu)}. \end{aligned} \tag{7.51}$$

The density constraint of Eq. (7.48) combined with Eq. (7.51) allows for an in-principle-exact evaluation of the Hxc potential $v_{\rm Hxc}$. Most importantly, these two equations can be used for designing an alternative (and self-consistent) embedding strategy on the basis of well-identified density-functional approximations. Indeed, in Ht-DMFET, the second term on the right-hand side of Eq. (7.51) is simply dropped, for simplicity [See Eq. (7.42)]. If, in addition, we neglect the Householder kinetic correlation density-bi-functional potential correction $\partial \tau_{\rm c}^{\mathcal{C}}(n,\nu)/\partial\nu$ [last term on the right-hand side of Eq. (7.51)], we obtain from Eq. (7.48) the following self-consistent equation,

$$n^{\rm KS}_{\rm lattice}\left(\mu - \tilde{v}_{\rm Hxc}\right) = n^{\mathcal{C}}\left(\mu - \tilde{v}_{\rm Hxc}, \tilde{v}_{\rm Hxc}\right), \tag{7.52}$$

from which an approximation $\tilde{v}_{\rm Hxc} \equiv \tilde{v}_{\rm Hxc}(\mu)$ to the Hxc potential can be determined. Eq. (7.52) is the second main result of this method. Since $\tilde{v}_{\rm Hxc}$ is now the to-be-optimized quantity on which the embedding fully relies, we refer to the approach as *local potential functional embedding theory* (LPFET), in which the key density-functional approximation that is made reads as

$$v_{\rm Hxc}(n) \underset{\rm LPFET}{\approx} \tilde{\mu}^{\rm frag}(n). \tag{7.53}$$

The approach is graphically summarized in Fig. 7.1. In order to verify that the first HK theorem[66] still holds at the LPFET level of approximation, let us assume that two chemical potentials μ and $\mu+\Delta\mu$ lead to the same density. If so, the converged Hxc potentials should differ by $\tilde{v}_{\rm Hxc}\left(\mu+\Delta\mu\right) - \tilde{v}_{\rm Hxc}(\mu) = \Delta\mu$, so that both calculations give the same KS chemical potential value [See Eq. (7.25)]. According to Eqs. (7.52) and (7.53), it would imply that two different values of the interacting

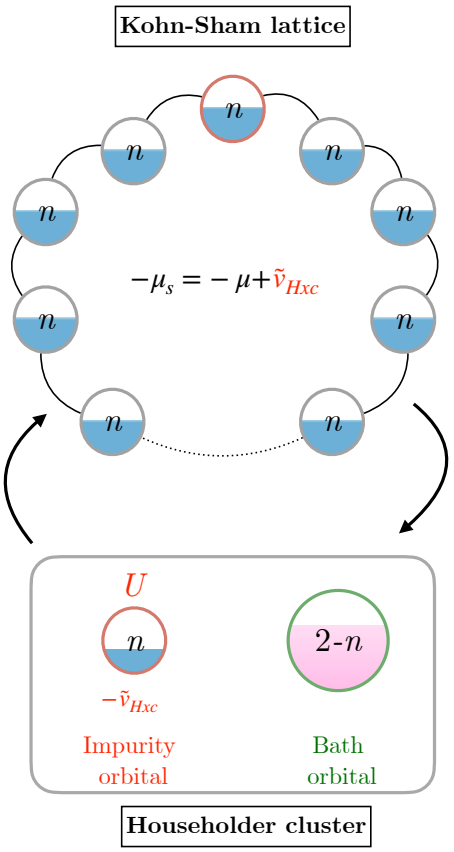

Figure 7.1: Graphical representation of the LPFET procedure. Note that the *same* Hxc potential $\tilde{v}_{\text{Hxc}}$ is used in the KS lattice and the embedding Householder cluster. It is optimized self-consistently in order to fulfill the density constraint of Eq. (7.52). See text for further details.

embedded impurity chemical potential can give the same density, which is impossible[163]. Therefore, when convergence is reached in Eq. (7.52), we can generate an approximate map

$$\mu \to n(\mu) \underset{\text{LPFET}}{\approx} n^{\text{KS}}_{\text{lattice}}\left(\mu - \tilde{v}_{\text{Hxc}}\right) = \langle \hat{n}_0 \rangle_{\Psi^{\mathcal{C}}(\mu - \tilde{v}_{\text{Hxc}}, \tilde{v}_{\text{Hxc}})} \,, \tag{7.54}$$

and compute approximate per-site energies as follows,

$$\frac{E(\mu)}{L} + \mu n(\mu) \underset{\text{LPFET}}{\approx} \left\langle \hat{t}_{01} + \hat{U}_0 \right\rangle_{\Psi^{\mathcal{C}}(\mu - \tilde{v}_{\text{Hxc}}, \tilde{v}_{\text{Hxc}})} \,, \tag{7.55}$$

since the approximation in Eq. (7.42) is also used in LPFET, as discussed above.

Note that Ht-DMFET (which is equivalent to DMET) and LPFET use the same per-site energy expression [See Eq. (7.14)], which is a functional of the

interacting cluster's wave function. In both approaches, the latter and the non-interacting lattice share the same density. Therefore, if the per-site energy or the double occupation $\langle \hat{n}_{0\sigma}\hat{n}_{0\sigma'}\rangle$ were plotted as functions of the (converged) lattice filling n, as it is usually done in the literature[26], both methods would give exactly the same results. The reason is that, at convergence of the LPFET algorithm, the density constraint of Eq. (7.52) should be fulfilled, exactly like in Ht-DMFET [See Eqs. (7.12) and (7.13)]. However, if properties were plotted as functions of the chemical potential value μ in the true interacting lattice, LPFET and Ht-DMFET would give different results, simply because the densities obtained (for a given μ value) with the two methods would be different. Indeed, as shown in Section 7.4, Ht-DMFET can be viewed as an approximation to KS-DFT where the Hxc density-functional potential of Eq. (7.45) is employed. As readily seen from Eq. (7.53), the LPFET and Ht-DMFET Hxc potentials differ by the Householder kinetic correlation potential (which is neglected in LPFET). If the corresponding KS densities were the same then the Hxc potential, the Householder transformation, and, therefore, the chemical potential on the interacting embedded impurity would be the same, which is impossible according to Eqs. (7.45) and (7.53). In summary, differences in properties between LPFET and Ht-DMFET are directly related to differences in density. This is the reason why, in order to compare the two methods, we will restrict ourselves to the computation of chemical-potential-density maps (See Section 7.8).

7.6 Comparison with SDE

At this point we should stress that LPFET is very similar to the SDE approach of Mordovina *et al.*[160]. The major difference between SDE and LPFET (in addition to the fact that LPFET has a clear connection with a formally exact density-functional embedding theory based on the Householder transformation) is that no KS construction is made within the cluster. Instead, the Hxc potential is directly updated in the KS lattice, on the basis of the correlated embedded impurity density. This becomes

even more clear when rewriting Eq. (7.52) as follows,

$$\tilde{v}_{\mathrm{Hxc}} = \mu - \left[n^{\mathrm{KS}}_{\mathrm{lattice}}\right]^{-1} \left(n^{\mathcal{C}}\left(\mu - \tilde{v}_{\mathrm{Hxc}}, \tilde{v}_{\mathrm{Hxc}}\right)\right), \tag{7.56}$$

where $\left[n^{\mathrm{KS}}_{\mathrm{lattice}}\right]^{-1} : n \rightarrow \mu_{\mathrm{s}}(n)$ is the inverse of the non-interacting chemical-potential-density map. A practical advantage of such a procedure (which remains feasible since the full system is treated at the non-interacting KS level only) lies in the fact that the KS construction within the cluster is automatically (and exactly) generated by the Householder transformation, once the density has been updated in the KS lattice (See Eq. (7.10) and the comment that follows). Most importantly, the density in the KS lattice and the density of the non-interacting KS embedded impurity (which, unlike the embedded *interacting* impurity, is not used in the actual calculation) will match *at each iteration* of the Hxc potential optimization process, as it should when convergence is reached. If, at a given iteration, the KS construction were made directly within the cluster, there would always be a "delay" in density between the KS lattice and the KS cluster, which would only disappear at convergence. Note that, when the latter is reached, the (approximate) Hxc potential of the lattice should match the one extracted from the cluster, which is defined in SDE as the difference between the KS cluster Hamiltonian and the one-electron part of the interacting cluster's Hamiltonian[160], both reproducing the density of the KS lattice. Therefore, according to Eqs. (7.31), (7.32) and (7.37), the converged Hxc potential will simply correspond to the chemical potential on the interacting embedded impurity, exactly like in LPFET [See Eq. (7.53)].

Note finally that the simplest implementation of LPFET, as suggested by Eq. (7.56), can be formally summarized as follows:

$$\begin{aligned} \tilde{v}^{(i+1)}_{\mathrm{Hxc}} &= \mu - \left[n^{\mathrm{KS}}_{\mathrm{lattice}}\right]^{-1} \left(n^{\mathcal{C}}\left(\mu - \tilde{v}^{(i)}_{\mathrm{Hxc}}, \tilde{v}^{(i)}_{\mathrm{Hxc}}\right)\right), \\ \tilde{v}^{(i=0)}_{\mathrm{Hxc}} &= 0. \end{aligned} \tag{7.57}$$

A complete description of the algorithm is given in the next section.

7.7 LPFET algorithm

The LPFET approach introduced in Section 7 aims at computing the interacting chemical-potential-density $\mu \rightarrow n(\mu)$ map through the self-consistent optimization

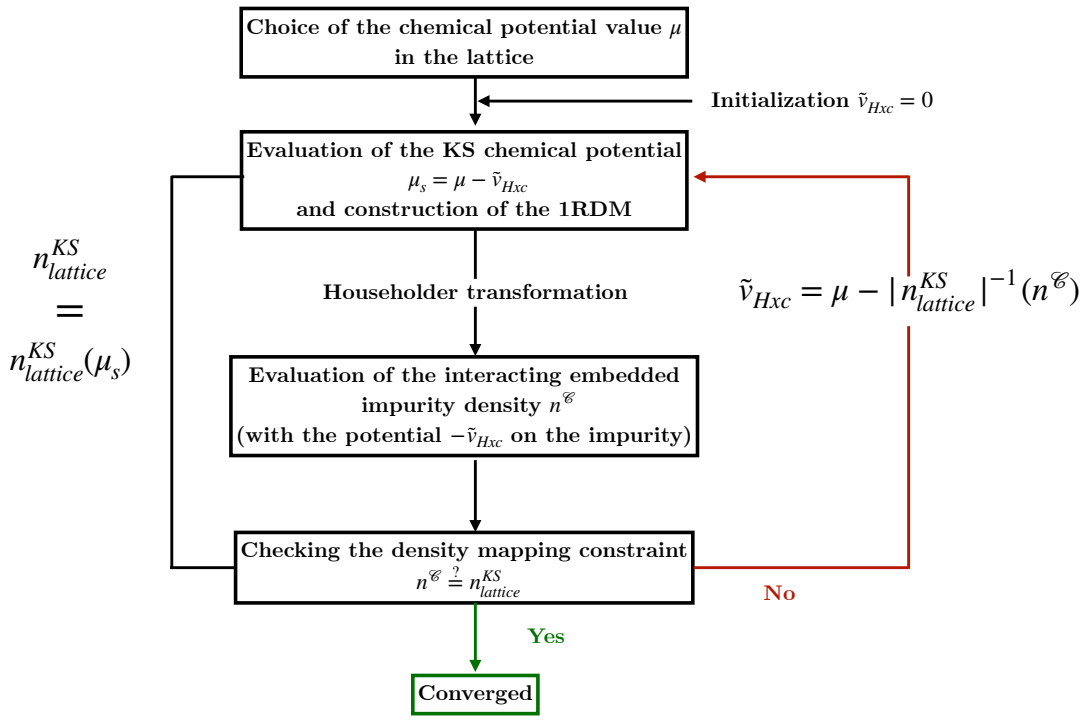

Figure 7.2: Schematics of the LPFET algorithm. The (one-electron reduced) density matrix of the KS lattice is referred to as the 1RDM. See text for further details.

of the uniform Hxc potential. A schematics of the algorithm is provided in Fig. 7.2. It can be summarized as follows.

1. We start by diagonalizing the one-electron Hamiltonian (*i.e.*, the hopping in the present case) matrix $\boldsymbol{t} \equiv t_{ij}$ [See Eq. (6.4)]. Thus we obtain the "molecular" spin-orbitals and their corresponding energies. We fix the chemical potential of the interacting lattice to some value μ and (arbitrarily) initialize the Hxc potential to $\tilde{v}_{\text{Hxc}} = 0$. Therefore, at the zeroth iteration, the KS chemical potential μ_{s} equals μ.

2. We occupy all the molecular spin-orbitals with energies below $\mu_{\text{s}} = \mu - \tilde{v}_{\text{Hxc}}$ and construct the corresponding density matrix (in the lattice representation). The latter provides the uniform KS density (denoted $n^{\text{KS}}_{\text{lattice}}$ in Fig. 7.2) and the embedding Householder cluster Hamiltonian [See Eq. (7.13)] in which the impurity chemical potential is set to $\tilde{\mu}^{\text{frag}} = \tilde{v}_{\text{Hxc}}$ [See Eq. (7.53)].

3. We solve the interacting Schrödinger equation for the two-electron House-

holder cluster and deduce the occupation of the embedded impurity (which is denoted $n^{\mathscr{C}}$ in Fig. 7.2). This can be done analytically since the Householder cluster is an asymmetric Hubbard dimer[21].

4. We verify that the density in the KS lattice $n^{\rm KS}_{\rm lattice}$ and the occupation of the interacting embedded impurity $n^{\mathscr{C}}$ match (a convergence threshold has been set to 10^{-4}). If this is the case, the calculation has converged and $n^{\mathscr{C}}$ is interpreted as (an approximation to) the density $n(\mu)$ in the true interacting lattice. If the two densities do not match, the Hxc potential $\tilde{v}_{\rm Hxc}$ is adjusted in the KS lattice such that the latter reproduces $n^{\mathscr{C}}$ [See Eq. (7.57)] or, equivalently, such that the KS lattice contains $Ln^{\mathscr{C}}$ electrons. We then return to step 2.

7.8 Results and discussion

In the following, LPFET is applied to a uniform Hubbard ring with a large $L = 1000$ number of sites in order to approach the thermodynamic limit. We recall that periodic boundary conditions have been used. The hopping parameter is set to $t = 1$. As explained at the end of Section 7, plotting Ht-DMFET (which is equivalent to DMET or DET) and LPFET properties such as the per-site energy or the double occupation as functions of the (converged) lattice filling n would give exactly the same results. On the other hand, the two methods are expected to give different chemical-potential-density $\mu \to n(\mu)$ maps since they rely on different density-functional approximations [See Eqs. (7.45) and (7.53)]. We focus in the following on the self-consistent computation of this map at the LPFET level of theory. Comparison will be made with Ht-DMFET and the exact BA results.

As illustrated by the strongly correlated results of Figs. 7.3 and 7.4, the LPFET self-consistency loop converges smoothly in few iterations. The same observation is made in weaker correlation regimes (not shown). The deviation in density between the KS lattice and the embedded impurity is drastically reduced after the first iteration (See Figure 7.3). This is also reflected in the large variation of the Hxc

potential from the zeroth to the first iteration (See Figure 7.4). It originates from the fact that, at the zeroth iteration, the Hxc potential is set to zero in the lattice while, in the embedding Householder cluster, the interaction on the impurity site is "turned on". As shown in Fig. 7.3, the occupation of the interacting embedded impurity is already at the zeroth iteration a good estimate of the self-consistently converged density. A few additional iterations are needed to refine the result. The

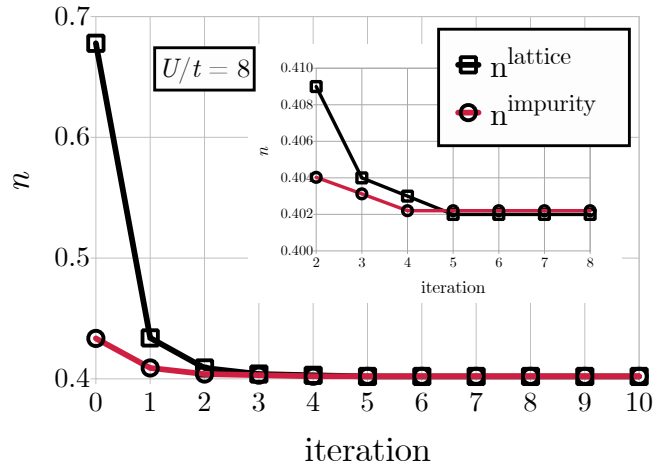

Figure 7.3: Comparison of the KS lattice and embedded impurity densities at each iteration of the LPFET calculation. The interaction strength and chemical potential values are set to $U/t = 8$ and $\mu/t = -0.97$, respectively. As shown in the inset, convergence is reached after five iterations.

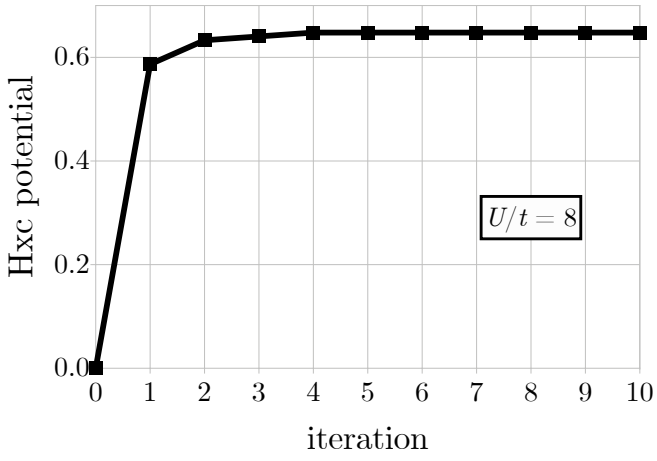

Figure 7.4: Convergence of the LPFET Hxc potential for $U/t = 8$ and $\mu/t = -0.97$.

converged LPFET densities are plotted in Fig. 7.5 as functions of the chemical potential μ in various correlation regimes. The non-interacting $U/t = 0$ curve describes the KS lattice at the zeroth iteration of the LPFET calculation. Thus we can visualize, as U/t deviates from zero, how much the KS lattice learns from the interacting two-electron Householder cluster. Interestingly, this scheme can be related to the well known DMFT [See Section 4.2.1]. We recall that in the latter, the unsolvable many-body lattice problem is mapped onto an impurity problem that can be solved numerically. More precisely, the local self-energy of the lattice $\Sigma(\omega)$ [See Eq. (4.19)] which contains all the many-body effects is self-consistently approximated by the resolution of the SIAM. For that purpose, the variables to match are the local Green's function of the lattice $G_{loc}(\omega)$ [See equation (4.21)] and the one of the impurity $G_{imp}(\omega)$ [See equation (4.18)] and at convergence the hybridization function $\Delta(\omega)$ [See Eq. (4.17)] representing the exchange of electrons between the impurity and the bath and thus allowing for electron fluctuations on the impurity is fixed. By analogy, in LPFET approach, the many-body effects represented by the local and frequency-independent Hxc potential $\tilde{v}_{Hxc}(n)$ [See Eq. 7.53] are self-consistently updated by learning from the interacting Householder cluster. The mapping condition is between the lattice density $n^{KS}_{lattice}(\mu - \tilde{v}_{Hxc})$ and the occupation number of the impurity orbital in the cluster $n^{\mathcal{C}}(\mu - \tilde{v}_{Hxc}, \tilde{v}_{Hxc})$ [See Eq. (7.52)] and at convergence the hopping parameter $\tilde{t}_{01}(\mu - \hat{v}_{Hxc})$ [See Eq. (7.11)] is fixed. Thus, LPFET can be seen as a static and zero-temperature version of two-site DMFT[161] where the analogy between the ingredients of the two theories can be summarized as follows,

$$\begin{aligned} \Sigma(\omega) &\longleftrightarrow \tilde{v}_{Hxc}(n), \\ G_{loc}(\omega) \overset{!}{=} G_{imp}(\omega) &\longleftrightarrow n^{KS}_{lattice}(\mu - \tilde{v}_{Hxc}) \overset{!}{=} n^{\mathcal{C}}(\mu - \tilde{v}_{Hxc}, \tilde{v}_{Hxc}), \\ \Delta(\omega) &\longleftrightarrow \tilde{t}_{01}(\mu - \tilde{v}_{Hxc}). \end{aligned} \tag{7.58}$$

LPFET is actually quite accurate (even more than Ht-DMFET $\equiv$ DET $\equiv$ DMET here, probably because of error cancellations) in the low filling regime. Even though LPFET deviates from Ht-DMFET when electron correlation is strong, as expected, their chemical-potential-density maps are quite similar. This is an indication that neglecting the Householder kinetic correlation potential contribution to the Hxc potential, as done in LPFET, is not a crude approximation, even in the strongly

correlated regime. As expected[26,21], LPFET and Ht-DMFET poorly perform when approaching half filling. Like the well-established single-site DMFT (See Figure 7 of Ref.[167]), they are unable to describe the density-driven Mott–Hubbard transition (*i.e.*, the opening of the gap). As discussed in Ref.[21], this might be related to the fact that, in the exact theory, the Householder cluster is not disconnected from its environment and it contains a fractional number of electrons, away from half filling, unlike in the (approximate) Ht-DMFET and LPFET schemes. In the language of KS-DFT, modeling the gap opening is equivalent to modeling the derivative discontinuity in the density-functional correlation potential $v_{\mathrm{c}}(n) = \mu(n) - \mu_{\mathrm{s}}(n) - \frac{U}{2}n$ at half filling. As clearly shown in Fig. 7.6, Ht-DMFET and LPFET do not reproduce this feature. In the language of the exact density-functional embedding theory derived in Section 7.3 , both Ht-DMFET and LPFET approximations neglect the complementary density-functional correlation energy $\overline{e}_{\mathrm{c}}(n)$ that is induced by the interacting bath and the environment of the (closed) density-functional Householder cluster. As readily seen from Eq. (7.41), it should be possible to describe the density-driven Mott–Hubbard transition with a single statically embedded impurity, provided that we can model the derivative discontinuity in $\partial\overline{e}_{\mathrm{c}}(n)/\partial n$ at half filling. This is obviously a challenging task that is usually bypassed by embedding more impurity[26,21]. The missing correlation effects might also be recovered by applying a multi-reference Görling–Levy-type perturbation theory on top of the correlated cluster calculation[21].

To conclude, an in-principle-exact density-functional reformulation of the Ht-DMFET[21] has been derived for the uniform 1D Hubbard Hamiltonian with a single embedded impurity. On that basis, an approximate LPFET has been proposed and implemented. Ht-DMFET is reinterpreted in this context as an approximation to DFT where the complementary density-functional correlation energy $\overline{e}_{\mathrm{c}}(n)$ induced by the interacting bath and the environment of the (closed) embedding "impurity+bath" cluster is neglected. LPFET neglects, in addition, the kinetic correlation effects induced by the Householder transformation on the impurity chemical potential. We have shown that combining the two approximations is equivalent to approximating the latter potential with the Hxc potential of the full lattice. Thus an approximate Hxc potential can be determined *self-consistently* for a given choice

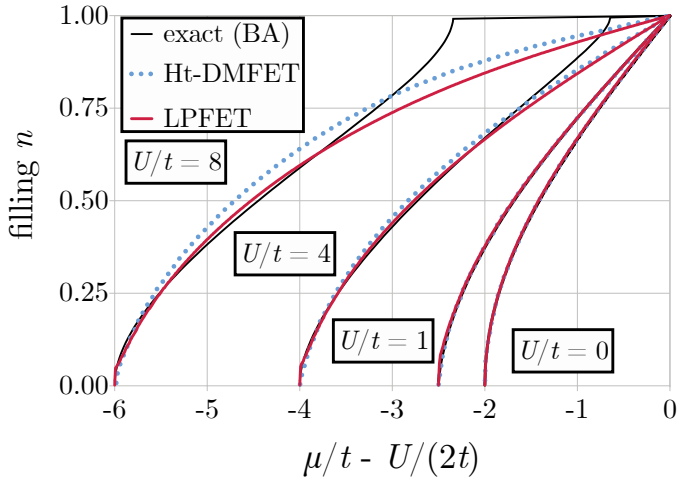

Figure 7.5: Converged LPFET densities (red solid lines) plotted as functions of the chemical potential μ in various correlation regimes. Comparison is made with the exact BA (black solid lines) and Ht-DMFET (blue dotted lines) results. In the latter case, the chemical potential is evaluated *via* the numerical differentiation of the density-functional Ht-DMFET per-site energy [See Eqs. (7.29) and (7.43)]. The non-interacting ($U = 0$) chemical-potential-density map [See Eq. (7.27)] is shown for analysis purposes.

of external (chemical in the present case) potential in the true interacting lattice. The self-consistency loop, which does not exist in regular single impurity version of DMET or DET[146], emerges naturally in LPFET from the exact density constraint, *i.e.*, by forcing the KS lattice and interacting embedded impurity densities to match. In this context, the energy becomes a functional of the Hxc potential. In this respect, LPFET can be seen as a flavor of KS-DFT where no density functional is used. LPFET is very similar to SDE[160]. The two approaches essentially differ in the optimization of the potential. In LPFET, no KS construction is made within the embedding cluster, unlike in SDE. Instead, the Hxc potential is directly updated in the lattice. As a result, the KS cluster (which is not used in the actual calculation) can be automatically generated with the correct density by applying the Householder transformation to the KS lattice Hamiltonian. Note that, like Ht-DMET, DMET or SDE, LPFET is in principle applicable to quantum chemical Hamiltonians written in a localized molecular orbital basis.

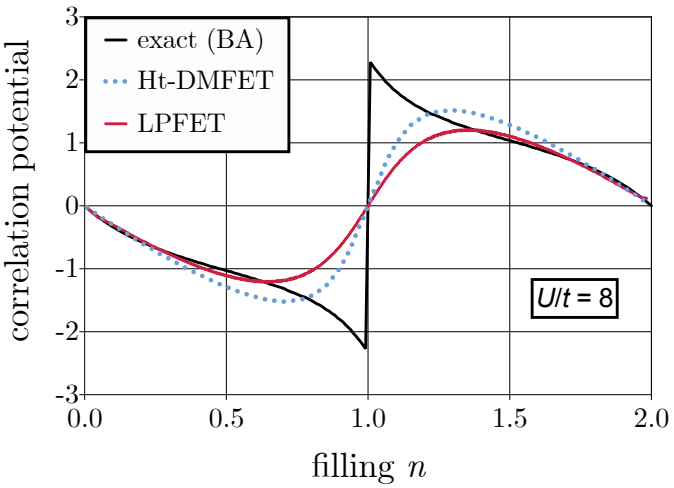

Figure 7.6: Correlation potential $v_{\mathrm{c}}(n) = \mu(n) - \mu_{\mathrm{s}}(n) - \frac{U}{2}n$ plotted as a function of the lattice filling n at the Ht-DMFET (blue dashed line) and LPFET (red solid line) levels of approximation for $U/t = 8$. Comparison is made with the exact BA correlation potential (black solid line).

Chapter 8

Density matrix interpolation variational ansatz

The purpose of this section is to introduce a work that has been realized in a very specific embedding case, namely the embedding of a single fragment in the 1D homogeneous Hubbard model within the RDMFT framework. While this work has not been published, it provides an interesting proof of concept regarding the description of the density-driven Mott-Hubbard transition [See Figure 3.1].

In the density matrix interpolation variational ansatz (DIVA), a single-site Householder transformed formulation of RDMFT for the 1D homogeneous Hubbard model [See Eq. (3.3)] is combined with a linear interpolation approximation between a non-interacting and strictly correlated density matrix. This approach provides an interesting proof of concept as it is possible to reproduce of the density-driven Mott-Hubbard transition with an open two-site system.

8.1 Construction of the two-level interaction functional

In this embedding approach, we will focus on a specific interaction energy functional $W^{2L}[\gamma]$ developed by W. Töws and G. M. Pastor[168] which is derived especially for strongly correlated systems. More precisely, it is an approximation to the interaction

functional of the Anderson dimer [See Figure 3.2] and will replace the bi-electronic repulsion in our embedding cluster system. It reads,

$$W^{2L}(U,\gamma_{ff},\gamma_{ss},\gamma_{sf}) = U\Big(\frac{\gamma_{ff}}{2} - \frac{\gamma_{sf}^2/4}{min\{\frac{N_e}{2}, 2-N_e\} - \sqrt{\gamma_{ff}\gamma_{ss}-\gamma_{sf}^2}}\Big), \tag{8.1}$$

where γ_{ff}, γ_{ss} denote the diagonal elements of the the 2×2 spin-summed density matrix of the Anderson dimer and γ_{sf} is the off-diagonal element.

The idea is to apply the single fragment embedding and describe the cluster with W^{2L}. For that purpose, we consider the general expression for the homogeneous Hubbard Hamiltonian [See Eq. (3.3)],

$$\hat{H} = -t \sum_{\sigma=\uparrow,\downarrow} \sum_{i=0}^{L-1} \Big(\hat{c}_{i\sigma}^{\dagger}\hat{c}_{(i+1)\sigma} + \text{H.c.}\Big) + U \sum_{i=0}^{L-1} \hat{n}_{i\uparrow}\hat{n}_{i\downarrow}. \tag{8.2}$$

The exact ground state energy can be obtained variationally as follows,

$$E(U) \;=\; \min_{\gamma} \left\{ -4t \sum_{\langle i,j \rangle} \gamma_{ij} + W\left[U,\gamma\right] \right\}, \tag{8.3}$$

where the interaction functional reads,

$$W\left[\boldsymbol{U},\boldsymbol{\gamma}\right] = \min_{\Psi\to\boldsymbol{\gamma}} \left\{ \sum_i U_i \left\langle \Psi | \hat{n}_{i\uparrow}\hat{n}_{i\downarrow} | \Psi \right\rangle \right\} \tag{8.4}$$

Note that,

$$W\left[\boldsymbol{U},\boldsymbol{\gamma}\right] = \sum_i U_i \frac{\partial W\left[\boldsymbol{U},\boldsymbol{\gamma}\right]}{\partial U_i}. \tag{8.5}$$

and one can immediately obtain the per-site energy expression (*e.g.* site 0) as,

$$e(U) = \min_{\boldsymbol{\gamma}} \left\{ -4t\gamma_{10} + U_0 \left.\frac{\partial W\left[\boldsymbol{U},\boldsymbol{\gamma}\right]}{\partial U_0}\right|_{U_0=U}, \right\} \tag{8.6}$$

where the second part of the r.h.s. is the decomposition of interaction functional according to Hellmann-Feynman theorem. Let us now consider the Householder transformed expression for the interaction functional. The Householder cluster is

composed of the fragment site ($\hat{c}^\dagger_{0\sigma} = \hat{d}^\dagger_{0\sigma}$) and the bath site ($\hat{d}^\dagger_{1\sigma} = \sum_i R_{i1}\hat{c}^\dagger_{i\sigma}$) [See Eqs. (5.22) and (5.23)]. We can decompose the interaction functional into two contributions as follows,

$$W\left[U,\boldsymbol{\gamma}\right] = W^{\text{frag}}\left[U_0,\boldsymbol{\gamma}\right] + \overline{W}\left[U,\boldsymbol{\gamma}\right], \tag{8.7}$$

where

$$W^{\text{frag}}\left[U_0,\boldsymbol{\gamma}\right] = U_0 \min_{\hat{\Gamma}^{\mathcal{C}}\to\tilde{\boldsymbol{\gamma}}^{\mathcal{C}}} \text{Tr}\left[\hat{\Gamma}^{\mathcal{C}}\hat{n}_{0\uparrow}\hat{n}_{0\downarrow}\right]. \tag{8.8}$$

The minimization in Eq. (8.8) is performed over the cluster grand-canonical ensemble density matrix operators $\hat{\Gamma}^{\mathcal{C}} = \sum_I \lambda_I \left|\Psi^{\mathcal{C}}_I\right\rangle\left\langle\Psi^{\mathcal{C}}_I\right|$ that reproduce the cluster sector $\tilde{\boldsymbol{\gamma}}^{\mathcal{C}}$ of the Householder transformed density matrix $\tilde{\boldsymbol{\gamma}}$. This constraint can be written formally as follows,

$$\text{Tr}\left\{\hat{\Gamma}^{\mathcal{C}}\hat{d}^\dagger_{i\sigma}\hat{d}_{j\sigma}\right\} = \tilde{\gamma}_{ij}, \;\; 0 \leq i,j \leq 1. \tag{8.9}$$

Note that $\tilde{\boldsymbol{\gamma}}^{\mathcal{C}}$ is in principle *not* pure-state representable since the number of electrons within the Householder cluster might be fractional in the exact (correlated) theory. According to the constrained search expression in Eq. (8.8), the minimizing cluster wave functions $\Psi^{\mathcal{C}}_I$ are eigenfunctions of a two-site cluster Hamiltonian,

$$\hat{H}^{\mathcal{C}} = U_0\hat{n}_{0\uparrow}\hat{n}_{0\downarrow} + \sum_\sigma \sum_{i,j=0}^{1} \tilde{t}_{ij}\hat{d}^\dagger_{i\sigma}\hat{d}_{j\sigma}, \tag{8.10}$$

which is nothing but a two-level Anderson Hamiltonian[168]. As a result, an exact-for-two-electrons analytical expression (in terms of $\tilde{\boldsymbol{\gamma}}^{\mathcal{C}}$) can be derived for the fragment functional $W^{\text{frag}}\left[U_0,\boldsymbol{\gamma}\right]$[168],

$$W^{\text{frag}}\left[U_0,\boldsymbol{\gamma}\right] \approx W^{\text{2L}}\left(U = U_0, \gamma_{ff}, \gamma_{ss}, \gamma_{sf}\right), \tag{8.11}$$

where, with the notations of Ref.[168], $\gamma_{ff} = 2\tilde{\gamma}_{00}$, $\gamma_{ss} = 2\tilde{\gamma}_{11}$, and $\gamma_{sf} = 2\tilde{\gamma}_{10}$, thus leading to the simplified notation

$$W^{\text{frag}}\left[U_0,\boldsymbol{\gamma}\right] \equiv W^{\text{2L}}\left(U = U_0, 2\tilde{\boldsymbol{\gamma}}^{\mathcal{C}}\right) = U_0 W^{\text{2L}}\left(U = 1, 2\tilde{\boldsymbol{\gamma}}^{\mathcal{C}}\right). \tag{8.12}$$

and thus the form taken in Eq. (8.1),

$$W^{\text{2L}}\left(U,\gamma_{ff},\gamma_{ss},\gamma_{sf}\right) = U\left(\frac{\gamma_{ff}}{2} - \frac{\gamma^2_{sf}/4}{\min\left\{\frac{N^{\mathcal{C}}}{2}, 2-\frac{N^{\mathcal{C}}}{2}\right\} - \sqrt{\gamma_{ff}\gamma_{ss}-\gamma^2_{sf}}}\right), \tag{8.13}$$

where we remind the reader that $N^{\mathcal{C}} = \gamma_{ff} + \gamma_{ss}$.

Regarding the complementary density matrix functional of Eq. (8.7), it contains contributions from both the bath and the Householder environment,

$$\overline{W}\left[U,\gamma\right] = \overline{W}^{\text{bath}}\left[U,\gamma\right] + \overline{W}^{\mathcal{E}}\left[U,\gamma\right], \tag{8.14}$$

where

$$\overline{W}^{\text{bath}}\left[U,\gamma\right] = \text{Tr}\left[\hat{\Gamma}_0^{\mathcal{C}}\left[\gamma\right]\hat{U}^{\mathcal{C}}\right] - W^{\text{frag}}\left[U_0,\gamma\right], \tag{8.15}$$

$\hat{\Gamma}_0^{\mathcal{C}}\left[\boldsymbol{\gamma}\right]$ is the minimizing density matrix operator in Eq. (8.8) and $\hat{U}^{\mathcal{C}}$ is the projection of the interaction operator onto the many-body Hilbert space of the Householder cluster.

By inserting Eq. (8.7) into Eq. (8.6) we obtain the following exact expression for the per-site energy,

$$e(U) = \min_{\gamma}\left\{-4t\gamma_{10} + W^{\text{2L}}\left(U, 2\tilde{\boldsymbol{\gamma}}^{\mathcal{C}}\right) + U\frac{\partial\overline{W}\left[U,\gamma\right]}{\partial U_0}\bigg|_{U_0=U}\right\}. \tag{8.16}$$

Note that in first approximation, the last term of the r.h.s. will be neglected and one ends up with an approximated per-site energy expression,

$$e(U) \approx \min_{\gamma}\left\{-4t\gamma_{10} + W^{\text{2L}}\left(U, 2\tilde{\boldsymbol{\gamma}}^{\mathcal{C}}\right)\right\}. \tag{8.17}$$

8.2 Density matrix interpolation variational ansatz

In this work, we are still describing a singlet ground state and denote, for simplicity, $\boldsymbol{\gamma} \equiv \gamma_{ij} = \left\langle \hat{c}_{i\uparrow}^{\dagger}\hat{c}_{j\uparrow}\right\rangle = \left\langle \hat{c}_{i\downarrow}^{\dagger}\hat{c}_{j\downarrow}\right\rangle$ the spin up and down one-electron reduced density matrices.

The *density matrix variational interpolation* is in fact a linear interpolation approximation (LIA) connecting the mean-field density matrix to a strictly correlated one,

$$\boldsymbol{\gamma} \to \boldsymbol{\gamma}(\alpha) = (1-\alpha)\boldsymbol{\gamma}^{(0)} + \alpha\,\frac{n}{2}\mathbf{1}, \tag{8.18}$$

where $0 \leq \alpha \leq 1$, $\boldsymbol{\gamma}^{(0)}$ is the (idempotent) mean-field approximation to the exact 1RDM, $n = N/L$, and $\mathbf{1}$ is the identity matrix.

Note that $\boldsymbol{\gamma}(\alpha)$ and $\boldsymbol{\gamma}^{(0)}$ share the same Householder transformation. Moreover, even though $\boldsymbol{\gamma}(\alpha)$ loses its idempotency as soon as α differs from zero, the Householder cluster and environment sectors remain disconnected for any value of α. If we neglect the environment contribution to the interaction energy, the per-site energy expression in Eq. (8.17) becomes

$$e^{\mathrm{LIA}}(U) = \min_{\alpha} \left\{ -4t(1-\alpha)\gamma_{10}^{(0)} + W^{\mathrm{2L}}\left(U, 2\tilde{\boldsymbol{\gamma}}^{\mathcal{C}}(\alpha)\right) \right\}. \tag{8.19}$$

One can now evaluate the density matrix elements in Eq. (8.18) in the Householder representation,

$$\tilde{\gamma}_{00}(\alpha) \;=\; \gamma_{00}(\alpha) = \frac{n}{2}, \tag{8.20}$$

and

$$\begin{aligned} \tilde{\gamma}_{11}(\alpha) &= (1-\alpha)\left(1-\frac{n}{2}\right) + \alpha\frac{n}{2} \\ &= 1 - \alpha + (2\alpha - 1)\frac{n}{2} \\ &= 1 - \frac{n}{2} + \alpha\,(n-1)\,. \end{aligned} \tag{8.21}$$

Moreover, since $\tilde{\boldsymbol{\gamma}}^{(0)\mathcal{C}}$ is a ground state one-electron (per-spin) idempotent density matrix, it comes

$$\tilde{\gamma}_{10}(\alpha) = (1-\alpha)\sqrt{\frac{n}{2}\left(1-\frac{n}{2}\right)}, \tag{8.22}$$

where we used the following relation for a symmetric idempotent matrix,

$$\tilde{\gamma}_{00}^2 + \tilde{\gamma}_{10}^2 = \tilde{\gamma}_{00}. \tag{8.23}$$

Note that the total number of electrons in the Householder cluster is in principle fractional,

$$N^{\mathcal{C}}(\alpha) = 2 \times (\tilde{\gamma}_{00} + \tilde{\gamma}_{11}) = 2 + 2\alpha\,(n-1)\,. \tag{8.24}$$

Finally, we can rewrite the per-site energy of Eq. (8.19) as,

$$e^{\mathrm{LIA}}(U) = \min_{\alpha}\Big\{ (1-\alpha)\, t_{\mathrm{s}}(n) + U d^{\mathrm{2L}}(\alpha) \Big\}, \tag{8.25}$$

where $t_s(n)$=-4$t$sin($\pi n/2$)/π in the thermodynamic limit and, for $n \leq 1$ and using Eqs. (8.13),(8.20),(8.21),(8.22),(8.20) and (8.24) one ends up with the following completely analytical expression,

$$d^{\mathrm{2L}}(\alpha) = \frac{n}{2} = -\frac{1}{4}\frac{(1-\alpha)^2 n(2-n)}{M^{\mathcal{C}}(\alpha) - \sqrt{n\,(N^{\mathcal{C}}(\alpha)-n) - (1-\alpha)^2 n\,(2-n)}}, \tag{8.26}$$

where

$$M^{\mathcal{C}}(\alpha) = \min\left\{\frac{N^{\mathcal{C}}(\alpha)}{2}, 2 - \frac{N^{\mathcal{C}}(\alpha)}{2}\right\} = 1 + \alpha\,(n-1)\,. \tag{8.27}$$

In the case where we decide to restrict the cluster to have 2 electrons, *i.e.*,

$$N^{\mathcal{C}}(\alpha) \to 2, \;\; M^{\mathcal{C}}(\alpha) \to 1, \tag{8.28}$$

it comes, for $N/L \leq 1$,

$$d_{2\mathrm{e}}^{2\mathrm{L}}(\alpha) = \frac{n}{2} - \frac{(1-\alpha)^2 n\,(2-n)}{4\left(1 - \sqrt{\alpha(2-\alpha)n\,(2-n)}\right)}. \tag{8.29}$$

Note that in the half-filled case (n=1), the two-electron and open cluster LIA are equivalent.

8.3 Results

The first observation is related to the number of electrons within the cluster. In the DIVA approach, we will evaluate the behavior of the fragment site with two physically different environment. In the first case that we will refer to as the *closed cluster*, the number of electrons within the cluster is fixed to $N_{\mathcal{C}} = 2$. On the other hand, this constraint will not be applied and is referred to as *open cluster*. This flexibility is observed in Fig. 8.1 where the charge fluctuation increases with the on-site electronic repulsion parameter U. Similarly as in Fig. 5.3, the cluster contains exactly two electrons at half-filling as a consequence of the particle-hole symmetry.

Finally, we investigate in Fig. 8.2 the density-driven Mott–Hubbard transition [See Section 3.1 and Fig. 3.1] *via* the evaluation of the density-functional $\mu(n) = \partial e(n)/\partial n$ chemical potential from the DIVA energy expression of Eq. (8.19). Interestingly, at the single fragment level of embedding, there is a gap opening when the number of electrons within the Householder cluster is not fixed. This first interesting result is of great importance as it provides a simple explanation of the failure of DMET[26], DET[38] or Ht-DMFET[21] [See Section 6] to reproduce the gap with a single embedded fragment subsystem. Indeed, charge fluctuations should

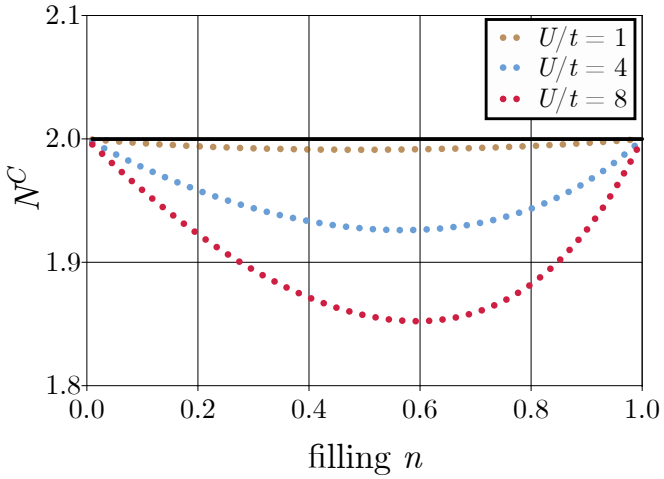

Figure 8.1: Number of electrons within the Householder cluster as a function of the lattice filling n in the *open cluster* DIVA approach for different regime of correlation U/t.

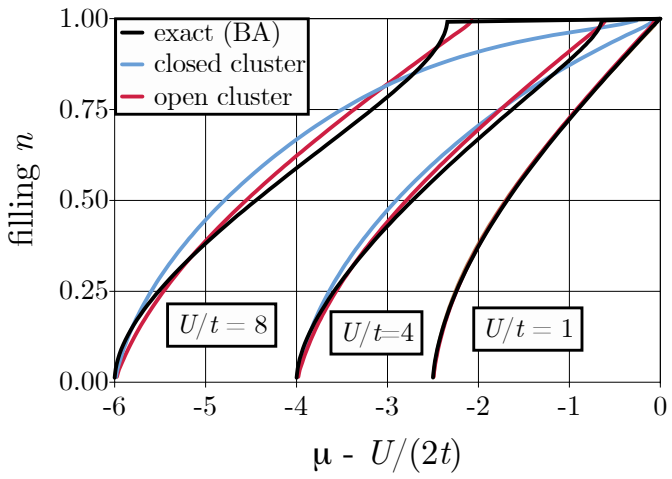

Figure 8.2: Lattice filling plotted, *via* the relation $\mu \equiv \mu(n) = \partial e(n)/\partial n$, as a function of the (lattice) chemical potential μ at the DIVA level of calculation for various correlation regimes. Comparison is made with the exact Bethe Ansatz (BA) results.

be present within the reduced-in-size embedding subsystem in order to correctly describing this feature[21].

To conclude this chapter, we observed through a very specific embedding case

that the density-driven Mott-Hubbard transition is only dependent on the charge fluctuation occuring within the fragment site and is not related to the strictly disentangled block structure of the density matrix. While this result allows us to clearly point out the successes and failures of our previous embedding schemes, it is hard to identify a way to extrapolate our linear interpolation approximation to an *Ab intio* calculation.

Conclusions

In this manuscript, we presented several embedding scheme that we developed and implemented in order to treat strongly correlated systems in both quantum chemistry and condensed matter physics. In the following a brief recap of the main outcomes are presented.

To begin, the Householder transformation played a central role in all the embedding schemes that we developed: Ht-DMFET, LPFET and DIVA.
The first interesting result is related to the construction of the quantum bath. It is determined analytically from the density matrix of the full system. Interestingly, this construction is not restricted to non-interacting or mean-field density matrix and allows to connect the embedding to the RDMFT. While this approach has not been investigated during the present thesis, describing the full system at the non-interacting or mean-field level (*i.e.* idempotent density matrix) leads to an exact and strict disentanglement between fragment and bath orbitals (*i.e.* cluster) from the cluster's environment. More importantly, the cluster is composed by a fixed number of spin-orbitals. Consequently, similarly as in DMET, the initial description has been rewritten as a CASCI problem where the active space is composed by the fragment and bath spin-orbitals while the core and virtual spin-orbitals are the occupied and unoccupied spin-orbitals of the cluster's environment, respectively. Thus, FCI have been applied within the reduced-in-size system.
Interestingly, we proved that the quantum bath obtained within DMET (using SVD) live in the same space as the ones obtained with the Householder transformation. In other words, the SVD used in DMET can be replaced by the Householder transformation. Further investigation are left for future work.

Similar in spirit to DMET, a (static and zero-temperature) Householder transformed density matrix functional embedding theory (Ht-DMFET) has been derived. The theory has been applied to the 1D Hubbard model and extended to an *Ab initio* Hamiltonian where identical results as DMET were recovered. As expected, the results dramatically improve when a larger number of fragments is embedded thanks to the block Householder transformation was employed. The density-driven Mott-Hubbard transition is almost recover in the case of three fragments. This can be explained by an enhanced charge fluctuation on the fragment spin-orbital as explicitely proven in DIVA.

Then, an in-principle-exact density-functional reformulation of the recently proposed Ht-DMFET has been derived for the uniform 1D Hubbard Hamiltonian with a single embedded fragment. On that basis, an approximate *local potential functional embedding theory* (LPFET) has been proposed and implemented. Ht-DMFET, which is equivalent to DMET or DET in the particular case of a single fragment, is reinterpreted in this context as an approximation to DFT. An approximate Hxc potential can be determined *self-consistently* for a given choice of chemical potential in the true interacting lattice. The self-consistency loop, which does not exist in regular single fragment version of DMET or DET, emerges naturally in LPFET from the exact density constraint, *i.e.*, by forcing the KS lattice and interacting embedded fragment densities to match. In this context, the energy becomes a functional of the Hxc potential. In this respect, LPFET can be seen as a flavor of KS-DFT where no density functional is used. LPFET is very similar to SDE. Interestingly, conceptual analogies have been made with two-sites DMFT. Note that, like DMET or SDE, LPFET is in principle applicable to quantum chemical Hamiltonians written in a localized molecular orbital basis. Work is in progress in that direction

To conclude, new ideas and *in-principle-exact* embedding strategies have been explored in order to describe accurately strongly correlated systems. From model to *Ab initio* Hamiltonian, promising results have been obtained and need now to be applied on a larger scale. The block Householder transformation is a simple and

accessible numerical method which can be used in various context of embedding. Naturally, different questions may arise motivated by these results. For example, it would be interesting to investigate how correlated 1-RDM could be used in practice in Ht-DMFET and LPFET. This would imply to find way to circumvent the problem of non-integer charge in the cluster and thus to re-adapt the block Householder method to more general case of matrices (and potentially also the embedding method). Still on block Householder, another interesting path would be investigate the use of this method to generate a partitioning based on other type of matrices (*i.e.* different from the density matrix). To stick to the single-particle level one could think of the Fock-Matrix, or in a many-body perspective one could try to apply Householder on the two-electron reduced density matrix (2RDM). Finally, in the light of recent advances in DMET and related approaches, several extensions of the present work can already be foreseen.

To conclude, an original and analytical way of performing embedding has been developed during this thesis. While it has been applied on model and Hamiltonian in order to verify its potential towards strongly correlated systems, it is still an exciting and challenging task to extend it to *Ab initio* Hamiltonian. This naturally constitutes a remarkable challenge for the future.

Bibliography

[1] Suss-Fink, G.; Meister, G. *Advances in Organometallic Chemistry*; Elsevier, 1993; Vol. 35; pp 41–134.

[2] Hill, C. L.; Prosser-McCartha, C. M. Homogeneous catalysis by transition metal oxygen anion clusters. *Coordination Chemistry Reviews* **1995**, *143*, 407–455.

[3] Kostas, I. D. Recent advances on P, N-containing ligands for transition-metal homogeneous catalysis. *Current Organic Synthesis* **2008**, *5*, 227–249.

[4] Widegren, J. A.; Finke, R. G. A review of the problem of distinguishing true homogeneous catalysis from soluble or other metal-particle heterogeneous catalysis under reducing conditions. *Journal of Molecular Catalysis A: Chemical* **2003**, *198*, 317–341.

[5] Boudart, M. Heterogeneous catalysis by metals. *Journal of Molecular Catalysis* **1985**, *30*, 27–38.

[6] Van Santen, R. A.; Neurock, M. Concepts in theoretical heterogeneous catalytic reactivity. *Catalysis Reviews* **1995**, *37*, 557–698.

[7] Williams, R. Role of transition metal ions in biological processes. *Royal Institute of Chemistry, Reviews* **1968**, *1*, 13–38.

[8] Ge, E. J.; Bush, A. I.; Casini, A.; Cobine, P. A.; Cross, J. R.; DeNicola, G. M.; Dou, Q. P.; Franz, K. J.; Gohil, V. M.; Gupta, S., *et al.* Connecting copper and cancer: from transition metal signalling to metalloplasia. *Nature Reviews Cancer* **2022**, *22*, 102–113.

[9] Bleackley, M. R.; MacGillivray, R. T. Transition metal homeostasis: from yeast to human disease. *Biometals* **2011**, *24*, 785–809.

[10] Krieger, G.; Martinelli, L.; Zeng, S.; Chow, L.; Kummer, K.; Arpaia, R.; Sala, M. M.; Brookes, N.; Ariando, A.; Viart, N., *et al.* Charge and Spin Order Dichotomy in NdNiO 2 Driven by the Capping Layer. *Physical Review Letters* **2022**, *129*, 027002.

[11] Pacchioni, G. Nickelates enter the scene. *Nature Reviews Materials* **2020**, *5*, 171–171.

[12] Maeno, Y.; Hashimoto, H.; Yoshida, K.; Nishizaki, S.; Fujita, T.; Bednorz, J.; Lichtenberg, F. Superconductivity in a layered perovskite without copper. *Nature* **1994**, *372*, 532–534.

[13] Cava, R. J.; Batlogg, B.; Krajewski, J.; Rupp, L.; Schneemeyer, L.; Siegrist, T.; VanDover, R.; Marsh, P.; Peck, W.; Gallagher, P., *et al.* Superconductivity near 70 K in a new family of layered copper oxides. *Nature* **1988**, *336*, 211–214.

[14] Tokura, Y.; Arima, T. New classification method for layered copper oxide compounds and its application to design of new high Tc superconductors. *Japanese Journal of Applied Physics* **1990**, *29*, 2388.

[15] Chahara, K.-i.; Ohno, T.; Kasai, M.; Kozono, Y. Magnetoresistance in magnetic manganese oxide with intrinsic antiferromagnetic spin structure. *Applied Physics Letters* **1993**, *63*, 1990–1992.

[16] Moritomo, Y.; Asamitsu, A.; Kuwahara, H.; Tokura, Y. Giant magnetoresistance of manganese oxides with a layered perovskite structure. *Nature* **1996**, *380*, 141–144.

[17] Tokura, Y.; Tomioka, Y.; Kuwahara, H.; Asamitsu, A.; Moritomo, Y.; Kasai, M. Origins of colossal magnetoresistance in perovskite-type manganese oxides. *Journal of Applied Physics* **1996**, *79*, 5288–5291.

[18] Mott, N. F. Metal-insulator transition. *Reviews of Modern Physics* **1968**, *40*, 677.

[19] Yang, Z.; Ko, C.; Ramanathan, S., *et al.* Oxide electronics utilizing ultrafast metal-insulator transitions. *Annual Review of Materials Research* **2011**, *41*, 337–367.

[20] Ruzmetov, D.; Senanayake, S. D.; Narayanamurti, V.; Ramanathan, S. Correlation between metal-insulator transition characteristics and electronic structure changes in vanadium oxide thin films. *Physical Review B* **2008**, *77*, 195442.

[21] Sekaran, S.; Tsuchiizu, M.; Saubanère, M.; Fromager, E. Householder-transformed density matrix functional embedding theory. *Physical Review B* **2021**, *104*, 035121.

[22] Hohenberg, P.; Kohn, W. Inhomogeneous electron gas. *Physical Review* **1964**, *136*, B864.

[23] Kohn, W.; Sham, L. J. Self-consistent equations including exchange and correlation effects. *Physical Review* **1965**, *140*, A1133.

[24] Georges, A.; Kotliar, G. Hubbard model in infinite dimensions. *Physical Review B* **1992**, *45*, 6479.

[25] Georges, A.; Kotliar, G.; Krauth, W.; Rozenberg, M. J. Dynamical mean-field theory of strongly correlated fermion systems and the limit of infinite dimensions. *Reviews of Modern Physics* **1996**, *68*, 13.

[26] Knizia, G.; Chan, G. K.-L. Density matrix embedding: A simple alternative to dynamical mean-field theory. *Physical Review Letters* **2012**, *109*, 186404.

[27] Knizia, G.; Chan, G. K.-L. Density matrix embedding: A strong-coupling quantum embedding theory. *Journal of Chemical Theory and Computation* **2013**, *9*, 1428–1432.

[28] Coleman, A. J. Structure of fermion density matrices. *Reviews of modern Physics* **1963**, *35*, 668.

[29] Smith, D. W. N-representability problem for fermion density matrices. II. The first-order density matrix with N even. *Physical Review* **1966**, *147*, 896.

[30] Gilbert, T. L. Hohenberg-Kohn theorem for nonlocal external potentials. *Physical Review B* **1975**, *12*, 2111.

[31] Levy, M. Universal variational functionals of electron densities, first-order density matrices, and natural spin-orbitals and solution of the v-representability problem. *Proceedings of the National Academy of Sciences of the United States of America* **1979**, *76*, 6062–6065.

[32] Valone, S. M. A one-to-one mapping between one-particle densities and some n-particle ensembles. *The Journal of Chemical Physics* **1980**, *73*, 4653–4655.

[33] Valone, S. M. Consequences of extending 1-matrix energy functionals from pure–state representable to all ensemble representable 1 matrices. *The Journal of Chemical Physics* **1980**, *73*, 1344–1349.

[34] Hubbard, J. Electron correlations in narrow energy bands. *Proceedings of the Royal Society of London. Series A. Mathematical and Physical Sciences* **1963**, *276*, 238–257.

[35] Lieb, E. H.; Wu, F.-Y. *Exactly Solvable Models of Strongly Correlated Electrons*; World Scientific, 1994; pp 9–12.

[36] Householder, A. S. Unitary triangularization of a nonsymmetric matrix. *Journal of the ACM (JACM)* **1958**, *5*, 339–342.

[37] Rotella, F.; Zambettakis, I. Block Householder transformation for parallel QR factorization. *Applied Mathematics Letters* **1999**, *12*, 29–34.

[38] Bulik, I. W.; Scuseria, G. E.; Dukelsky, J. Density matrix embedding from broken symmetry lattice mean fields. *Physical Review B* **2014**, *89*, 035140.

[39] Wouters, S.; Jiménez-Hoyos, C. A.; Sun, Q.; Chan, G. K.-L. A practical guide to density matrix embedding theory in quantum chemistry. *Journal of Chemical Theory and Computation* **2016**, *12*, 2706–2719.

[40] Bulik, I. W.; Chen, W.; Scuseria, G. E. Electron correlation in solids via density embedding theory. *The Journal of Chemical Physics* **2014**, *141*, 054113.

[41] Löwdin, P.-O. Quantum theory of many-particle systems. III. Extension of the Hartree-Fock scheme to include degenerate systems and correlation effects. *Physical Review* **1955**, *97*, 1509.

[42] Helgaker, T.; Jorgensen, P.; Olsen, J. *Molecular electronic-structure theory*; John Wiley & Sons, 2014.

[43] Steglich, F.; Geibel, C.; Gloos, K.; Olesch, G.; Schank, C.; Wassilew, C.; Loidl, A.; Krimmel, A.; Stewart, G. R. Heavy fermions: Typical phenomena and recent developments. *Journal of Low Temperature Physics* **1994**, *95*, 3–22.

[44] Steglich, F.; Stockert, O.; Wirth, S.; Geibel, C.; Yuan, H.; Kirchner, S.; Si, Q. Routes to heavy-fermion superconductivity. Journal of Physics: Conference Series. 2013; p 012028.

[45] Koelling, D.; Dunlap, B.; Crabtree, G. f-electron hybridization and heavy-fermion compounds. *Physical Review B* **1985**, *31*, 4966.

[46] Pierloot, K. The CASPT2 method in inorganic electronic spectroscopy: from ionic transition metal to covalent actinide complexes. *Molecular Physics* **2003**, *101*, 2083–2094.

[47] Roos, B. O.; Lindh, R.; Malmqvist, P.-Å.; Veryazov, V.; Widmark, P.-O. New relativistic ANO basis sets for transition metal atoms. *The Journal of Physical Chemistry A* **2005**, *109*, 6575–6579.

[48] Roca-Sanjuán, D.; Aquilante, F.; Lindh, R. Multiconfiguration second-order perturbation theory approach to strong electron correlation in chemistry and photochemistry. *Wiley Interdisciplinary Reviews: Computational Molecular Science* **2012**, *2*, 585–603.

[49] Singh, S. K.; Eng, J.; Atanasov, M.; Neese, F. Covalency and chemical bonding in transition metal complexes: An ab initio based ligand field perspective. *Coordination Chemistry Reviews* **2017**, *344*, 2–25.

[50] Singh, S. K.; Atanasov, M.; Neese, F. Challenges in multireference perturbation theory for the calculations of the g-tensor of first-row transition-metal

complexes. *Journal of Chemical Theory and Computation* **2018**, *14*, 4662–4677.

[51] Liechtenstein, A.; Katsnelson, M.; Gubanov, V. Exchange interactions and spin-wave stiffness in ferromagnetic metals. *Journal of Physics F: Metal Physics* **1984**, *14*, L125.

[52] Liechtenstein, A.; Katsnelson, M.; Gubanov, V. Local spin excitations and Curie temperature of iron. *Solid State Communications* **1985**, *54*, 327–329.

[53] Liechtenstein, A. I.; Katsnelson, M.; Antropov, V.; Gubanov, V. Local spin density functional approach to the theory of exchange interactions in ferromagnetic metals and alloys. *Journal of Magnetism and Magnetic Materials* **1987**, *67*, 65–74.

[54] Katsnelson, M.; Lichtenstein, A. First-principles calculations of magnetic interactions in correlated systems. *Physical Review B* **2000**, *61*, 8906.

[55] Himmetoglu, B.; Floris, A.; De Gironcoli, S.; Cococcioni, M. Hubbard-corrected DFT energy functionals: The LDA+ U description of correlated systems. *International Journal of Quantum Chemistry* **2014**, *114*, 14–49.

[56] Anisimov, V.; Kondakov, D.; Kozhevnikov, A.; Nekrasov, I.; Pchelkina, Z.; Allen, J.; Mo, S.-K.; Kim, H.-D.; Metcalf, P.; Suga, S., *et al.* Full orbital calculation scheme for materials with strongly correlated electrons. *Physical Review B* **2005**, *71*, 125119.

[57] Lechermann, F.; Georges, A.; Poteryaev, A.; Biermann, S.; Posternak, M.; Yamasaki, A.; Andersen, O. Dynamical mean-field theory using Wannier functions: A flexible route to electronic structure calculations of strongly correlated materials. *Physical Review B* **2006**, *74*, 125120.

[58] Amadon, B.; Lechermann, F.; Georges, A.; Jollet, F.; Wehling, T.; Lichtenstein, A. Plane-wave based electronic structure calculations for correlated materials using dynamical mean-field theory and projected local orbitals. *Physical Review B* **2008**, *77*, 205112.

[59] Nielsen, M. A.; Chuang, I. Quantum computation and quantum information. 2002.

[60] Ekert, A.; Knight, P. L. Entangled quantum systems and the Schmidt decomposition. *American Journal of Physics* **1995**, *63*, 415–423.

[61] Wouters, S.; Jiménez-Hoyos, C. A.; Chan, G. K.-L. Five years of density matrix embedding theory. *arXiv preprint arXiv:1605.05547* **2016**,

[62] Hunter, G. Conditional probability amplitudes in wave mechanics. *International Journal of Quantum Chemistry* **1975**, *9*, 237–242.

[63] Slater, J. C. The theory of complex spectra. *Physical Review* **1929**, *34*, 1293.

[64] Roothaan, C. C. J. New developments in molecular orbital theory. *Reviews of Modern Physics* **1951**, *23*, 69.

[65] Hall, G. The molecular orbital theory of chemical valency VIII. A method of calculating ionization potentials. *Proceedings of the Royal Society of London. Series A. Mathematical and Physical Sciences* **1951**, *205*, 541–552.

[66] Hohenberg, P.; Kohn, W. Inhomogeneous Electron Gas. *Physical Review* **1964**, *136*, B864–B871, Publisher: American Physical Society.

[67] Lieb, E. H. Density Functionals for Coulomb Systems. *International Journal of Quantum Chemistry* **1983**, *XXIV*, 243–277.

[68] Harriman, J. E. Orthonormal orbitals for the representation of an arbitrary density. *Physical Review A* **1981**, *24*, 680.

[69] Lieb, E. H. *Inequalities*; Springer, 2002; pp 269–303.

[70] Perdew, J. P.; Zunger, A. Self-interaction correction to density-functional approximations for many-electron systems. *Physical Review B* **1981**, *23*, 5048.

[71] Tsuneda, T.; Hirao, K. Self-interaction corrections in density functional theory. *The Journal of Chemical Physics* **2014**, *140*, 18A513.

[72] Becke, A. D. A new mixing of Hartree–Fock and local density-functional theories. *The Journal of Chemical Physics* **1993**, *98*, 1372–1377.

[73] Perdew, J. P.; Burke, K.; Ernzerhof, M. Generalized gradient approximation made simple. *Physical Review Letters* **1996**, *77*, 3865.

[74] Perdew, J. P.; Ernzerhof, M.; Burke, K. Rationale for mixing exact exchange with density functional approximations. *The Journal of Chemical Physics* **1996**, *105*, 9982–9985.

[75] Heyd, J.; Scuseria, G. E.; Ernzerhof, M. Hybrid functionals based on a screened Coulomb potential. *The Journal of Chemical Physics* **2003**, *118*, 8207–8215.

[76] Henderson, T. M.; Janesko, B. G.; Scuseria, G. E. Range separation and local hybridization in density functional theory. *The Journal of Physical Chemistry A* **2008**, *112*, 12530–12542.

[77] Rubtsov, A.; Katsnelson, M.; Lichtenstein, A. Dual fermion approach to non-local correlations in the Hubbard model. *Physical Review B* **2008**, *77*, 033101.

[78] Pernal, K.; Giesbertz, K. J. *Density-Functional Methods for Excited States*; Springer, 2015; pp 125–183.

[79] Altunbulak, M.; Klyachko, A. The Pauli principle revisited. *Communications in Mathematical Physics* **2008**, *282*, 287–322.

[80] Anderson, P. W. Localized magnetic states in metals. *Physical Review* **1961**, *124*, 41.

[81] Kondo, J. Resistance minimum in dilute magnetic alloys. *Progress of Theoretical Physics* **1964**, *32*, 37–49.

[82] Galpin, M. R.; Logan, D. E. Anderson impurity model in a semiconductor. *Physical Review B* **2008**, *77*, 195108.

[83] Bergfield, J. P.; Liu, Z.-F.; Burke, K.; Stafford, C. A. Bethe ansatz approach to the kondo effect within density-functional theory. *Physical Review Letters* **2012**, *108*, 066801.

[84] Liu, Z.-F.; Bergfield, J. P.; Burke, K.; Stafford, C. A. Accuracy of density functionals for molecular electronics: The Anderson junction. *Physical Review B* **2012**, *85*, 155117.

[85] Liu, Z.-F.; Burke, K. Density functional description of Coulomb blockade: Adiabatic versus dynamic exchange correlation. *Physical Review B* **2015**, *91*, 245158.

[86] Zawadzki, K.; Oliveira, L. N. How sharply does the Anderson model depict a single-electron transistor? *The European Physical Journal B* **2018**, *91*, 1–10.

[87] Caffarel, M.; Krauth, W. Exact diagonalization approach to correlated fermions in infinite dimensions: Mott transition and superconductivity. *Physical Review Letters* **1994**, *72*, 1545.

[88] Zgid, D.; Chan, G. K.-L. Dynamical mean-field theory from a quantum chemical perspective. *The Journal of Chemical Physics* **2011**, *134*, 094115.

[89] Rozenberg, M.; Zhang, X.; Kotliar, G. Mott-Hubbard transition in infinite dimensions. *Physical Review Letters* **1992**, *69*, 1236.

[90] Rubtsov, A. N.; Savkin, V. V.; Lichtenstein, A. I. Continuous-time quantum Monte Carlo method for fermions. *Physical Review B* **2005**, *72*, 035122.

[91] Fuhrmann, A.; Heilmann, D.; Monien, H. From Mott insulator to band insulator: A dynamical mean-field theory study. *Physical Review B* **2006**, *73*, 245118.

[92] Werner, P.; Comanac, A.; De'Medici, L.; Troyer, M.; Millis, A. J. Continuous-time solver for quantum impurity models. *Physical Review Letters* **2006**, *97*, 076405.

[93] Haule, K. Quantum Monte Carlo impurity solver for cluster dynamical mean-field theory and electronic structure calculations with adjustable cluster base. *Physical Review B* **2007**, *75*, 155113.

[94] García, D. J.; Hallberg, K.; Rozenberg, M. J. Dynamical mean field theory with the density matrix renormalization group. *Physical Review Letters* **2004**, *93*, 246403.

[95] Karski, M.; Raas, C.; Uhrig, G. S. Single-particle dynamics in the vicinity of the Mott-Hubbard metal-to-insulator transition. *Physical Review B* **2008**, *77*, 075116.

[96] Gordon, R. G.; Kim, Y. S. Theory for the forces between closed-shell atoms and molecules. *The Journal of Chemical Physics* **1972**, *56*, 3122–3133.

[97] Rae, A. A theory for the interactions between closed shell systems. *Chemical Physics Letters* **1973**, *18*, 574–577.

[98] Kim, Y. S.; Gordon, R. Unified theory for the intermolecular forces between closed shell atoms and ions. *The Journal of Chemical Physics* **1974**, *61*, 1–16.

[99] Senatore, G.; Subbaswamy, K. Density dependence of the dielectric constant of rare-gas crystals. *Physical Review B* **1986**, *34*, 5754.

[100] Cortona, P. Self-consistently determined properties of solids without band-structure calculations. *Physical Review B* **1991**, *44*, 8454.

[101] Wesolowski, T. A.; Warshel, A. Frozen density functional approach for ab initio calculations of solvated molecules. *The Journal of Physical Chemistry* **1993**, *97*, 8050–8053.

[102] Jacob, C. R.; Neugebauer, J. Subsystem density-functional theory. *Wiley Interdisciplinary Reviews: Computational Molecular Science* **2014**, *4*, 325–362.

[103] Gomes, A. S. P.; Jacob, C. R. Quantum-chemical embedding methods for treating local electronic excitations in complex chemical systems. *Annual Reports Section" C"(Physical Chemistry)* **2012**, *108*, 222–277.

[104] Elliott, P.; Burke, K.; Cohen, M. H.; Wasserman, A. Partition density-functional theory. *Physical Review A* **2010**, *82*, 024501.

[105] Wesolowski, T. A.; Weber, J. Kohn-Sham equations with constrained electron density: an iterative evaluation of the ground-state electron density of interacting molecules. *Chemical physics letters* **1996**, *248*, 71–76.

[106] Elliott, P.; Cohen, M. H.; Wasserman, A.; Burke, K. Density functional partition theory with fractional occupations. *Journal of Chemical Theory and Computation* **2009**, *5*, 827–833.

[107] Huang, C.; Pavone, M.; Carter, E. A. Quantum mechanical embedding theory based on a unique embedding potential. *The Journal of Chemical Physics* **2011**, *134*, 154110.

[108] Huang, C.; Carter, E. A. Potential-functional embedding theory for molecules and materials. *The Journal of Chemical Physics* **2011**, *135*, 194104.

[109] Wesołowski, T. A. Embedding a multideterminantal wave function in an orbital-free environment. *Physical Review A* **2008**, *77*, 012504.

[110] Govind, N.; Wang, Y.; Da Silva, A.; Carter, E. Accurate ab initio energetics of extended systems via explicit correlation embedded in a density functional environment. *Chemical physics letters* **1998**, *295*, 129–134.

[111] Govind, N.; Wang, Y. A.; Carter, E. A. Electronic-structure calculations by first-principles density-based embedding of explicitly correlated systems. *The Journal of Chemical Physics* **1999**, *110*, 7677–7688.

[112] Klüner, T.; Govind, N.; Wang, Y. A.; Carter, E. A. Prediction of electronic excited states of adsorbates on metal surfaces from first principles. *Physical Review Letters* **2001**, *86*, 5954.

[113] Klüner, T.; Govind, N.; Wang, Y. A.; Carter, E. A. Periodic density functional embedding theory for complete active space self-consistent field and configuration interaction calculations: Ground and excited states. *The Journal of Chemical Physics* **2002**, *116*, 42–54.

[114] Manby, F. R.; Stella, M.; Goodpaster, J. D.; Miller III, T. F. A simple, exact density-functional-theory embedding scheme. *Journal of chemical theory and computation* **2012**, *8*, 2564–2568.

[115] Lee, S. J.; Welborn, M.; Manby, F. R.; Miller III, T. F. Projection-based wavefunction-in-DFT embedding. *Accounts of chemical research* **2019**, *52*, 1359–1368.

[116] Graham, D. S.; Wen, X.; Chulhai, D. V.; Goodpaster, J. D. Robust, accurate, and efficient: quantum embedding using the Huzinaga level-shift projection

operator for complex systems. *Journal of Chemical Theory and Computation* **2020**, *16*, 2284–2295.

[117] Huo, P.; Uyeda, C.; Goodpaster, J. D.; Peters, J. C.; Miller III, T. F. Breaking the correlation between energy costs and kinetic barriers in hydrogen evolution via a cobalt pyridine-diimine-dioxime catalyst. *ACS Catalysis* **2016**, *6*, 6114–6123.

[118] Bennie, S. J.; van der Kamp, M. W.; Pennifold, R. C.; Stella, M.; Manby, F. R.; Mulholland, A. J. A projector-embedding approach for multiscale coupled-cluster calculations applied to citrate synthase. *Journal of Chemical Theory and Computation* **2016**, *12*, 2689–2697.

[119] Barnes, T. A.; Kaminski, J. W.; Borodin, O.; Miller III, T. F. Ab initio characterization of the electrochemical stability and solvation properties of condensed-phase ethylene carbonate and dimethyl carbonate mixtures. *The Journal of Physical Chemistry C* **2015**, *119*, 3865–3880.

[120] Libisch, F.; Huang, C.; Liao, P.; Pavone, M.; Carter, E. A. Origin of the energy barrier to chemical reactions of O 2 on Al (111): Evidence for charge transfer, not spin selection. *Physical Review Letters* **2012**, *109*, 198303.

[121] Goodpaster, J. D.; Barnes, T. A.; Manby, F. R.; Miller III, T. F. Accurate and systematically improvable density functional theory embedding for correlated wavefunctions. *The Journal of Chemical Physics* **2014**, *140*, 18A507.

[122] Kotliar, G.; Vollhardt, D. Strongly correlated materials: Insights from dynamical mean-field theory. *Physics Today* **2004**, *57*, 53–60.

[123] Held, K. Electronic structure calculations using dynamical mean field theory. *Advances in Physics* **2007**, *56*, 829–926.

[124] Hettler, M.; Mukherjee, M.; Jarrell, M.; Krishnamurthy, H. Dynamical cluster approximation: Nonlocal dynamics of correlated electron systems. *Physical Review B* **2000**, *61*, 12739.

[125] Kotliar, G.; Savrasov, S. Y.; Pálsson, G.; Biroli, G. Cellular dynamical mean field approach to strongly correlated systems. *Physical Review Letters* **2001**, *87*, 186401.

[126] Potthoff, M.; Aichhorn, M.; Dahnken, C. Variational cluster approach to correlated electron systems in low dimensions. *Physical Review Letters* **2003**, *91*, 206402.

[127] Lichtenstein, A.; Katsnelson, M.; Kotliar, G. Finite-temperature magnetism of transition metals: An ab initio dynamical mean-field theory. *Physical Review Letters* **2001**, *87*, 067205.

[128] Maier, T.; Jarrell, M.; Pruschke, T.; Hettler, M. H. Quantum cluster theories. *Reviews of Modern Physics* **2005**, *77*, 1027.

[129] Leonov, I.; Poteryaev, A.; Anisimov, V.; Vollhardt, D. Electronic correlations at the α- γ structural phase transition in paramagnetic iron. *Physical Review Letters* **2011**, *106*, 106405.

[130] Leonov, I.; Poteryaev, A.; Anisimov, V.; Vollhardt, D. Calculated phonon spectra of paramagnetic iron at the α-γ phase transition. *Physical Review B* **2012**, *85*, 020401.

[131] Tremblay, A.-M.; Kyung, B.; Sénéchal, D. Pseudogap and high-temperature superconductivity from weak to strong coupling. Towards a quantitative theory. *Low Temperature Physics* **2006**, *32*, 424–451.

[132] Maier, T.; Jarrell, M.; Pruschke, T.; Keller, J. d-wave superconductivity in the Hubbard model. *Physical Review Letters* **2000**, *85*, 1524.

[133] Maier, T. A. Superconductivity in striped and multi-Fermi-surface Hubbard models: From the cuprates to the pnictides. *Journal of Superconductivity and Novel Magnetism* **2012**, *25*, 1307–1311.

[134] Sordi, G.; Sémon, P.; Haule, K.; Tremblay, A.-M. Strong coupling superconductivity, pseudogap, and Mott transition. *Physical Review Letters* **2012**, *108*, 216401.

[135] Sénéchal, D.; Day, A.; Bouliane, V.; Tremblay, A.-M. Resilience of d-wave superconductivity to nearest-neighbor repulsion. *Physical Review B* **2013**, *87*, 075123.

[136] Jiang, M.; Hähner, U. R.; Schulthess, T. C.; Maier, T. A. d-wave superconductivity in the presence of nearest-neighbor Coulomb repulsion. *Physical Review B* **2018**, *97*, 184507.

[137] Zhang, G.; Gorelov, E.; Sarvestani, E.; Pavarini, E. Fermi surface of Sr 2 RuO 4: spin-orbit and anisotropic Coulomb interaction effects. *Physical Review Letters* **2016**, *116*, 106402.

[138] Zhang, G.; Pavarini, E. Mott transition, spin-orbit effects, and magnetism in Ca 2 RuO 4. *Physical Review B* **2017**, *95*, 075145.

[139] Zhang, G.; Pavarini, E. Higgs mode and stability of x y-orbital ordering in Ca 2 RuO 4. *Physical Review B* **2020**, *101*, 205128.

[140] Sun, C.; Ray, U.; Cui, Z.-H.; Stoudenmire, M.; Ferrero, M.; Chan, G. K.-L. Finite-temperature density matrix embedding theory. *Physical Review B* **2020**, *101*, 075131.

[141] Kretchmer, J. S.; Chan, G. K.-L. A real-time extension of density matrix embedding theory for non-equilibrium electron dynamics. *The Journal of Chemical Physics* **2018**, *148*, 054108.

[142] Mitra, A.; Pham, H. Q.; Pandharkar, R.; Hermes, M. R.; Gagliardi, L. Excited states of crystalline point defects with multireference density matrix embedding theory. *The Journal of Physical Chemistry Letters* **2021**, *12*, 11688–11694.

[143] Tran, H. K.; Van Voorhis, T.; Thom, A. J. Using SCF metadynamics to extend density matrix embedding theory to excited states. *The Journal of Chemical Physics* **2019**, *151*, 034112.

[144] Qiao, J.; Jie, Q. Density matrix embedding theory of excited states for spin systems. *Computer Physics Communications* **2021**, *261*, 107712.

[145] Gunst, K.; Wouters, S.; De Baerdemacker, S.; Van Neck, D. Block product density matrix embedding theory for strongly correlated spin systems. *Physical Review B* **2017**, *95*, 195127.

[146] Sriluckshmy, P.; Nusspickel, M.; Fertitta, E.; Booth, G. H. Fully algebraic and self-consistent effective dynamics in a static quantum embedding. *Physical Review B* **2021**, *103*, 085131.

[147] Wilkinson, J. *Handbook for Automatic Computation, Volume II, Linear Algebra*; Springer-Verlag New York, 1971.

[148] Rotella, F.; Borne, P. *Théorie et pratique du calcul matriciel*; Editions technip, 1995; Vol. 6.

[149] Hermes, M. R.; Gagliardi, L. Multiconfigurational self-consistent field theory with density matrix embedding: The localized active space self-consistent field method. *Journal of Chemical Theory and Computation* **2019**, *15*, 972–986.

[150] Giesbertz, K. J. Avoiding the 4-index transformation in one-body reduced density matrix functional calculations for separable functionals. *Physical Chemistry Chemical Physics* **2016**, *18*, 21024–21031.

[151] Mitxelena, I.; Piris, M.; Rodríguez-Mayorga, M. On the performance of natural orbital functional approximations in the Hubbard model. *Journal of Physics: Condensed Matter* **2017**, *29*, 425602.

[152] Fertitta, E.; Booth, G. H. Energy-weighted density matrix embedding of open correlated chemical fragments. *The Journal of Chemical Physics* **2019**, *151*, 014115.

[153] Fertitta, E.; Booth, G. H. Rigorous wave function embedding with dynamical fluctuations. *Physical Review B* **2018**, *98*, 235132.

[154] Löwdin, P.-O. On the non-orthogonality problem connected with the use of atomic wave functions in the theory of molecules and crystals. *The Journal of Chemical Physics* **1950**, *18*, 365–375.

[155] Carlson, B.; Keller, J. M. Orthogonalization procedures and the localization of Wannier functions. *Physical Review* **1957**, *105*, 102.

[156] Mayer, I. On Löwdin's method of symmetric orthogonalization. *International Journal of Quantum Chemistry* **2002**, *90*, 63–65.

[157] Zheng, B.-X.; Chan, G. K.-L. Ground-state phase diagram of the square lattice Hubbard model from density matrix embedding theory. *Physical Review B* **2016**, *93*, 035126.

[158] Fan, Z.; Jie, Q.-l. Cluster density matrix embedding theory for quantum spin systems. *Physical Review B* **2015**, *91*, 195118.

[159] Tsuchimochi, T.; Welborn, M.; Van Voorhis, T. Density matrix embedding in an antisymmetrized geminal power bath. *The Journal of Chemical Physics* **2015**, *143*, 024107.

[160] Mordovina, U.; Reinhard, T. E.; Theophilou, I.; Appel, H.; Rubio, A. Self-consistent density-functional embedding: A novel approach for density-functional approximations. *Journal of Chemical Theory and Computation* **2019**, *15*, 5209–5220.

[161] Potthoff, M. Two-site dynamical mean-field theory. *Physical Review B* **2001**, *64*, 165114.

[162] Sekaran, S.; Saubanère, M.; Fromager, E. Local Potential Functional Embedding Theory: A Self-Consistent Flavor of Density Functional Theory for Lattices without Density Functionals. *Computation* **2022**, *10*, 45.

[163] Senjean, B.; Nakatani, N.; Tsuchiizu, M.; Fromager, E. Site-occupation embedding theory using Bethe ansatz local density approximations. *Physical Review B* **2018**, *97*, 235105.

[164] Lima, N.; Silva, M.; Oliveira, L.; Capelle, K. Density functionals not based on the electron gas: Local-density approximation for a luttinger liquid. *Physical Review Letters* **2003**, *90*, 146402.

[165] Vilela, L.; Capelle, K.; Oliveira, L. N.; Campo, V. L. Approximate expression for the ground-state energy of the two-and three-dimensional Hubbard model at arbitrary filling obtained from dimensional scaling. *Journal of Physics: Condensed Matter* **2019**, *31*, 455601.

[166] Fromager, E. On the exact formulation of multi-configuration density-functional theory: electron density versus orbitals occupation. *Molecular Physics* **2015**, *113*, 419–434.

[167] Kotliar, G.; Savrasov, S. Y.; Haule, K.; Oudovenko, V. S.; Parcollet, O.; Marianetti, C. Electronic structure calculations with dynamical mean-field theory. *Reviews of Modern Physics* **2006**, *78*, 865.

[168] Töws, W.; Pastor, G. Lattice density functional theory of the single-impurity Anderson model: Development and applications. *Physical Review B* **2011**, *83*, 235101.

Abstract

The present thesis aims at developing and implementing novel and *in-principle-exact* embedding methodologies at the interface between chemistry and physics. Towards an accurate description of strongly correlated molecules and materials, the quantum embedding will be applied to the *Hubbard model*, and then generalized to *Ab initio* molecular Hamiltonian. We will verify if *density matrix embedding theory* (DMET) can be made formally exact and systematically improvable while preserving a single-particle quantum partitioning picture. More precisely, we will rewrite the embedding as a functional of the density matrix, thus bypassing the Schmidt decomposition of the reference (correlated or not) full-system wave function. Then, we will clarify the connections between DMET and the *in-principle-exact* theories that are *density functional theory* (DFT) and *reduced density matrix functional theory* (RDMFT). On that basis, alternative flavors of DMET will be explored.

Résumé

L'objectif de cette thèse est le développement et l'implémentation de nouvelles méthodes dites d'embedding à l'intersection entre la chimie et la physique. Afin de pourvoir une description précise des molécules et matériaux fortement corrélés, l'embedding quantique sera appliqué au modèle d'Hubbard et généralisé à des Hamiltonien moléculaires *Ab initio*. Nous vérifierons si la *density matrix embedding theory* (DMET) peut être rendu formellement exacte et améliorée tout en préservant la nature orbitalaire de notre partitionnement quantique. Plus précisément, nous réécrirons notre approche d'embedding comme étant une fonctionnelle de la matrice densité à un corps, contournant ainsi la décomposition de Schmidt de la fonction d'onde de référence (corrélée ou non) décrivant le système dans son intégralité. Enfin, nous clarifierons les parallèles entre la DMET et les théories *en principe exactes* que sont la *density functional theory* (DFT) et la *reduced density matrix functional theory* (RDMFT). Sur cette base, plusieurs alternatives de la DMET seront explorées.